| AD NUMBER |
| --- |
| AD368603 |
| CLASSIFICATION CHANGES |
| TO: unclassified |
| FROM: confidential |
| LIMITATION CHANGES |
| TO:<br>Approved for public release, distribution unlimited |
| FROM:<br>Distribution authorized to U.S. Gov't. agencies and their contractors; Administrative/Operational Use; DEC 1965. Other requests shall be referred to Rocket Propulsion Lab., AFSC, Edwards AFB, CA. |
| AUTHORITY |
| AFRPL ltr, 7 May 1973; AFRPL ltr, 7 May 1973 |

# SECURITY MARKING

**The classified or limited status of this report applies to each page, unless otherwise marked.**
**Separate page printouts MUST be marked accordingly.**

THIS DOCUMENT CONTAINS INFORMATION AFFECTING THE NATIONAL DEFENSE OF THE UNITED STATES WITHIN THE MEANING OF THE ESPIONAGE LAWS, TITLE 18, U.S.C., SECTIONS 793 AND 794. THE TRANSMISSION OR THE REVELATION OF ITS CONTENTS IN ANY MANNER TO AN UNAUTHORIZED PERSON IS PROHIBITED BY LAW.

**NOTICE:** When government or other drawings, specifications or other data are used for any purpose other than in connection with a definitely related government procurement operation, the U. S. Government thereby incurs no responsibility, nor any obligation whatsoever; and the fact that the Government may have formulated, furnished, or in any way supplied the said drawings, specifications, or other data is not to be regarded by implication or otherwise as in any manner licensing the holder or any other person or corporation, or conveying any rights or permission to manufacture, use or sell any patented invention that may in any way be related thereto.

(Unclassified Title)

# MANEUVERING SATELLITE PROPULSION SYSTEM DEMONSTRATION

TECHNICAL DOCUMENTARY REPORT NO. AFRPL-TR-65-127
DECEMBER 1965

FINAL REPORT - PART III
FOR PERIOD MAY 1964 THROUGH JULY 1965

Rocket Propulsion Laboratory
Research and Technology Division
Air Force Systems Command
Edwards Air Force Base, California





Program Structure No. 750G
BPSN No. 6299, Task No. 305803

(Prepared Under Contract No. AF04(611)-8183 by
The Bell Aerosystems Company, Buffalo 5, New York

## NOTICES

This material contains information affecting the national defense of the United States within the meaning of the espionage laws, Title 18. U.S.C.: Sect. 793 and 794, the transmission or revelation of which in any manner to an unauthorized person is prohibited by law.

Each paragraph, table, and illustration of this report is marked individually to indicate the appropriate security classifications: (C) indicates that the material is Confidential; (U) indicates that the material is Unclassified.

(Unclassified Title)

# MANEUVERING SATELLITE PROPULSION SYSTEM DEMONSTRATION

TECHNICAL DOCUMENTARY REPORT NO. AFRPL-TR-65-127
DECEMBER 1965

FINAL REPORT - PART III
FOR PERIOD MAY 1964 THROUGH JULY 1965

Rocket Propulsion Laboratory
Research and Technology Division
Air Force Systems Command
Edwards Air Force Base, California



Program Structure No. 750C
BPSN No. 6299, Task No. 305803

(Prepared Under Contract No. AF04(611)-8183 by
The Bell Aerosystems Company. Buffalo 5. New York

(This Foreword is Unclassified)

## (U) FOREWORD

(U) Presented in this report is the work accomplished by the Bell Aerosystems Company during the period May 1964 through May 1965 for the Air Force Rocket Propulsion Laboratory, Research and Technology Division, Edwards Air Force Base, California, under Contract AF04(611)-8183. The program was directed toward the feasibility demonstration of an advanced thrust chamber cooling concept.

(U) The contractor's secondary report number is 8173-S33009.

(U) Principal contributors to the report were:

| | |
|---|---|
| J. Germano | H. Lucas |
| W. Pearson | L. Baker |
| M. Chazen | E. Dolega |
| C. Schmidt | S. Kerho |
| N. Fitzsimmons | F. King |

(This Abstract is Unclassified)

## (U) ABSTRACT

(U) This document presents the exploratory development work accomplished in the design, fabrication and testing of advanced rocket engine components for a high energy propellant space maneuvering vehicle. The exploratory development effort consisted of a series of critical experiments to determine operational capabilities of high temperature material and coating in fluorine rich and HF environments, the feasibility of a wide range throttling concept utilizing mixed phase propellants, and the feasibility of an advanced thrust chamber cooling concept.

(U) This document has been reviewed and is approved.

# (U) CONTENTS

## (U) CONTENTS (CONT)

## (U) ILLUSTRATIONS

## (U) ILLUSTRATIONS (CONT)

## (U) ILLUSTRATIONS (CONT)

## (U) ILLUSTRATIONS (CONT)

## (U) ILLUSTRATIONS (CONT)

## (U) TABLES

# SECTION 1

## (C) INTRODUCTION

(C) Bell Aerosystems Company has demonstrated the feasibility of obtaining a throttling engine for a Maneuvering Satellite Vehicle with high performance over the complete throttling range on Contract AF04(611)-8183. To accomplish this, Bell investigated the two-stage combustion concept in an adiabatic wall thrust chamber with the propellant combination of $N_2O_4$ and 50% $N_2H_4$-50% UDMH. This concept utilizes oxidizer rich and fuel rich gas generators to provide reactive gases that are injected into the combustion chamber through a mixer assembly where these gases further react at the optimum mixture ratio to obtain high performance.

(C) Initial studies performed in 1961 indicated that earth storable propellants were desirable for long term space missions of intercept, rendezvous and inspection. Although high energy cryogenic propellant combinations provide higher engine performance, the long term (one year) space residence time resulted in lower vehicle performance with the high energy propellants. The earth storable propellant combination of $N_2O_4$ and 50% $N_2H_4$-50% UDMH was chosen because of high vehicle performance for long term space missions and also for the advanced development status of this propellant combination.

(C) A review of the mission requirements performed in 1964 indicated that space missions of interest could be performed within a space residence time of 14 days. With the reduced residence time and the advances during the past two years in the development of engines and components utilizing high energy propellant combinations, a program utilizing these high energy propellants could be undertaken with a high degree of confidence to develop a thrust modulated propulsion system for space missions which will provide for maximum performance.

(U) Bell Aerosystems Company undertook a program to determine the feasibility of throttling a thrust chamber assembly utilizing the adiabatic wall cooling concept with the high energy propellant combination of fluorine and a hydrazine blend. Throttling of the engine was accomplished with a fixed orifice injector.

(U) To provide design information for the adiabatic wall cooling concept, a program of critical experiments was performed to determine the capability of materials and coating (for compatibility with the HF product of combustion) to be used in the fabrication of the adiabatic wall cooled thrust chamber. A program was also conducted where the feasibility of a throttling concept utilizing mixed phase propellants was demonstrated.

(U) An advanced thrust chamber cooling concept designated adiabatic wall cooling was conducted. The program culminated in the demonstration of the feasibility and durability of this advanced cooling concept.

## SECTION 2

## (U) SUMMARY

(C) A program of design, fabrication, and test was performed to demonstrate the feasibility of thrust chamber components and concepts for application to a deep throttling (12.5:1) liquid fluorine/BA1014* thrust chamber rated at 65 psia chamber pressure and weight mixture ratio of 1.8. The original thrust chamber concept consisted of an adiabatic wall thrust chamber with a two-stage combustion injector utilizing fuel rich and oxidizer rich gas generators. Fuel rich gas generators using these propellants had been successfully tested under previous programs. Therefore, demonstration of a feasible oxidizer rich gas generator was required prior to injector fabrication. This requirement necessitated that materials evaluation be performed at temperatures between 1500 and 2000° F in a fluorine rich atmosphere. A fluorine injection concept consisting of heat exchange to the initially subcooled liquid with subsequent two-phase expansion through a fixed area injector was demonstrated. Cold flow and fire tests were performed at sea level to verify the feasibility of this concept. This injection technique precludes the requirement of a fluorine rich gas generator. Materials testing was performed to facilitate the design and fabrication of a 3750-lb thrust adiabatic wall thrust chamber intended for operation at optimum thrust chamber mixture ratio with wall temperatures in excess of 3000° F. A fixed area injector with provision for fuel rich gas generator gas injection at the periphery of the chamber was designed, fabricated, and tested. This injector was used to test the adiabatic wall thrust chamber. A summary of the major tasks performed during the program is presented in the following paragraphs.

### 1. (U) Gas Generator Materials Program

(U) A materials literature search and sample compatibility test program was performed to determine uncoated and coated materials for application to the oxidizer rich, $F_2$/BA1014 gas generator. Tests performed in a fluorine rich environment at elevated temperatures indicated that uncoated TD Nickel and Haynes 25 alloy were applicable to temperatures above 1500° F, yet below 2000° F. Haynes 25 alloy with an iron-aluminum coating and TD Nickel with an aluminum-silicon-chrome coating were also found to be satisfactory at temperatures above 1500° F but below 2000° F.

---

* The BA1014 fuel is the Bell Aerosystems Company designation given to the following blend:

| | |
|---|---|
| Monomethylhydrazine, $CH_3N_2H_3$: | 1 mol (24% by weight) |
| Hydrazine Hydrate, $N_2H_4$-$H_2O$: | 1 mol (26% by weight) |
| Hydrazine, $N_2H_4$: | 3 mol (50% by weight) |

2. (C) Fluorine Rich Gas Generator

(C) A fluorine gas generator feasibility program was performed utilizing various gas generator injector design configurations. Haynes 25 chamber inserts were used during these gas generator assembly tests. The configurations tested included a fixed area oxidizer, variable area fuel helical design rated at 25:1 weight mixture ratio. Also tested was a fixed area triplet design, and fixed area fuel modifications of the original helical injector design. Durability was the basic problem encountered during the test and, as a result, the decision was made to terminate further oxidizer rich gas generator testing and perform adiabatic wall thrust chamber feasibility testing with a fixed area injector with provision for injection of fuel rich gases at the wall barrier.

3. (U) Thrust Chamber Materials Program

(U) An extensive materials evaluation test program was performed to allow design of the adiabatic wall thrust chamber. Four potential chamber materials, including pure tungsten, tantalum-tungsten, columbium alloy SCb-291, and graphite were tested as chamber inserts in a 200-lb $F_2$/BA1014 thrust chamber while operating over a mixture ratio range of 0.8 to 2.2. Two tungsten chamber inserts coated externally with a silicide coating for high emittance and to preclude exterior oxidation were successfully tested through the brittle temperature transition. Maximum wall temperature during these tests was 3920°F. A graphite sleeve with a tungsten retainer was tested to measured temperatures of 2950°F. A heat transfer analysis indicated that the maximum internal graphite temperature was 3410°F. Only minor erosion occurred during the 100 psia chamber pressure test while operating at a 1.96 mixture ratio for 100 seconds. A tantalum-tungsten chamber section coated with an external silicide oxidation resistant coating of high emissivity was tested successfully for 100 seconds at 2.06 mixture ratio with a maximum measured temperature of 2900°F. Heat transfer analysis indicated that maximum internal wall temperature was 3240°F. Successful tests were performed on the columbium thrust chamber sections with wall temperatures in excess of 2900°F. Streaking occurred, resulting in a maximum temperature of 3450°F. However, the alloy with aluminide inside coating and silicide external coating met the design requirements of the adiabatic wall chamber. This series of tests proved the potential of the tungsten, tantalum-tungsten, graphite, and SCb-291 columbium alloy as materials for the adiabatic wall thrust chamber.

4. (C) Adiabatic Wall Thrust Chamber

(C) A program was performed to demonstrate the feasibility of an advanced thrust chamber cooling concept using the high energy propellant combination of fluorine/BA1014. This concept utilizes a refractory thrust chamber and a refractory liner within the thrust chamber to direct the coolant gases to the nozzle or any other portion of the thrust chamber which requires cooling. Thrust chamber materials evaluation provided data that refractory materials could be utilized in the environment produced from the combustion products of fluorine/BA1014.

(C) The objects of the program were to demonstrate that this cooling concept (adiabatic wall cooling) was feasible. Program goals generated at the initiation of the program were: (1) provide high performance - 95% of theoretical c*; (2) demonstrate durability of the hardware - 120 seconds of continuous operation; and (3) throttle the engine over a 2:1 thrust range.

(C) The program has achieved a theoretical c* of 94% at rated chamber pressure (≈ 70 psia) and 93% at the minimum chamber pressure level (≈ 35 psia); throttling over 2:1 chamber pressure was achieved, and the feasibility and durability of the concept has been demonstrated. At the minimum chamber pressure condition (≈35 psia), 137 seconds of continuous operation was demonstrated, and at the rated chamber pressure condition (≈ 70 psia), 115 seconds continuous operation was demonstrated.

5. (U) Mixed Phase Injection

(U) A program of fabrication, test and analysis was performed to demonstrate the feasibility of the mixed phase fluorine injection concept. A series of cold flow tests was performed at sea level using an existing fixed area injector. Subcooled fluorine liquid was heated and partially vaporized by a gaseous nitrogen annular heat exchanger. Stable, high injector pressure drop was demonstrated during the two-phase fluorine tests performed over an 8:1 weight flow rate range. Hot tests were performed with the 200-lb water cooled thrust chamber used in the chamber materials compatibility test program. During these sea level tests performed with $F_2$/BA1014, high fluorine pressure drop was experienced. During low chamber pressure operation, combustion induced instability occurred while injecting liquid fluorine and two-phase fluorine. High fuel injection velocity was not maintained during these tests; therefore, combustion efficiency decreased as chamber pressure was reduced. However, the feasibility of this simple, nonmechanical fluorine injection system was demonstrated, and is believed to represent a stable, high performance injection system for deep throttling operation when fuel side throttling provides controlled, high energy injection. An analysis of test data was made to correlate measured fluorine flow rate with compressible, two-phase theories. In general, the theories underpredicted the actual flow rate. However, closer agreement was made using separated phase relations as compared to homogeneous (fog) flow representations of the two-phase fluid.

# SECTION 3

# (U) GAS GENERATOR MATERIALS PROGRAM

## A. (U) GENERAL

(U) The feasibility of operation of the two-stage combustion concept required the knowledge of reliable operation of an oxidizer rich (fluorine) gas generator and a fuel rich (BA-1014) gas generator with the propellant combination of fluorine and a hydrazine blend (BA-1014). Since Bell Aerosystems Company had successfully and reliably operated fuel rich gas generators with this propellant combination, only the feasibility of operation of an oxidizer rich gas generator with this combination had to be determined. The feasibility of operating an oxidizer rich gas generator with this propellant combination was predicated upon the availability of material and coatings for use in a fluorine rich environment. Therefore, a literature survey was conducted, and the application of chemical and metallurgical background information was used to select materials for potential use in this environment. A screening test was conducted to determine the compatibility of these materials and coatings with fluorine at elevated temperatures.

## B. (U) TECHNICAL DISCUSSION

### 1. (U) Literature Survey

(U) A literature survey was conducted to determine the maximum temperature limitations for operation of materials and coatings in a fluorine rich environment as applicable to the operation of an oxidizer rich gas generator. Predicated upon the results of this literature survey, and application of theoretical chemical and metallurgical information in conjunction with heat transfer analyses, materials and coatings were tested in a laboratory screening test program to determine their compatibility with fluorine at elevated temperatures. The results of the literature survey are summarized in the following paragraphs.

#### a. (U) Reports Investigated

(U) A total of seven reports was investigated:

"Materials of Construction for Handling Fluorine,"
Earl L. White and Frederick W. Fink, Battelle
Memorial Institute

"Corrosion by Fluorine and Fluorine Compounds,"
Ralph Landan, Corrosion V8, (1952)

"Fluorine Corrosion," W.R. Meyers and W.B. Delong,
Chemical Engineering Progress, Vol. 44, (1948)

(U) "Corrosion of Metals in Fluorine and Hydrofluoric Acid, "
G.C. Whitaker, Corrosion V6, (1950)

"Corrosion of Materials in the Presence of Fluorine at Elevated Temperatures," Martin T. Steindler and Richard C. Vogel, Argonne National Laboratory, ANL 5662.

"The Fluorination of Metallic Titanium,"
M. J. Steindler, D. V. Steidl, and R. K. Steunenberg, Argonne National Laboratory, ANL 6002.

"Ignition of Several Metals in Fluorine,"
Thomas W. Goodwin and Carl F. Lorenzo,
Fenn College

b. (U) Discussion

(U) The corrosion mechanism of fluorine gas with materials resulted in compounds which were volatile at elevated temperatures and other compounds which were not volatile at elevated temperatures. Corrosion problems occured primarily because fluorine is the most electronegative element and, consequently, will react with any element (even $O_2$ and $Cl_2$) other than noble gases. It was anticipated that the only materials which will not react with fluorine are fluoride compounds in their highest valence state.

(U) The products formed by the reaction of various materials with fluorine determined their corrosion behavior. Table I lists the fluorine compounds which are gas or liquid at low temperatures. The reaction of fluorine with these materials resulted in the formation of volatile compounds. The reaction products separated from the reaction surface and the continuation of the reaction occurred until one of the reactants was completely exhausted.

(U) Table II lists the various materials, formed by the reaction of fluorine, which have high melting or sublimation points, and did not volatilize at elevated temperatures. The postulation was proposed that a coating would act as a barrier when formed on the base metal with this type of reaction.

(U) If such a coating were adherent and nonporous, protection would be afforded against further attack by fluorine. However, this formation of a protected film on the surface of the base metal was complicated by such factors as sublimation, heats of reaction, thermal conductivity, fluxing, etc., of various reaction products. Another factor which could not be overlocked was the mechanical action of erosion, since the rate of corrosion was increased by exposing fresh unprotected base material.

(U) The heat of reaction was found to be significantly greater for a reaction of fluorine with a base material than the heat of reaction with oxygen or

TABLE I

(U) SELECTED FLUORINE COMPOUNDS WITH LOW SUBLIMATION OR MELTING POINTS

| Below 70°F | | Between 70°F and 600°F |
|---|---|---|
| $OF_2$ | $ClF_3$ | $SbF_5$ |
| $NF_3$ | HF | $SbF_3$ |
| $CF_4$ | $AsF_5$ | $MoF_6$ |
| $BF_3$ | $TeF_6$ | $NbF_5$ |
| $PF_3$ | $SeF_6$ | $TaF_5$ |
| $PF_5$ | WF | $SnF_6$ |
| $SF_6$ | $OF_6$ | $VF_5$ |
| $SiF_4$ | | |

TABLE II

(U) SELECTED FLUORINE COMPOUNDS WITH HIGH SUBLIMATION OR MELTING POINTS

| Between 600°F and 1500°F | | Above 1500°F |
|---|---|---|
| AgF | $PbF_4$ | $CrF_2$ |
| $AgF_2$ | $ThF_4$ | $CuF_2$ |
| $BiF_3$ | $BeF_2$ | $FeF_2$ |
| $BiF_5$ | $MnF_2$ | $CoF_2$ |
| $CrF_3$ | $LiF_2$ | $CoF_3$ |
| $CrF_4$ | $ZnF_2$ | $AlF_3$ |
| $PbF_2$ | | $MgF_2$ |

(U) chlorine. This can be demonstrated comparatively as follows:

| | |
|---|---|
| $F_2 + Ni = NiF_2$ | $\Delta H = 283{,}000$ BTU/lb mole $F_2$ |
| $Cl_2 + Ni = NiCl_2$ | $\Delta H = 135{,}000$ BTU/lb mole $Cl_2$ |
| $O_2 + 2\,Ni = 2\,NiO$ | $\Delta H = 210{,}000$ BTU/lb mole $O_2$ |

From the corrosion standpoint, the extreme reactivity of fluorine with its high heat of reaction and similarity in chemical behavior to oxygen and chlorine suggested a number of generalized conclusions such as:

(1) (U) All metals were potentially vulnerable to reaction by fluorine. Metals offering superior resistance to oxidation might also resist fluorine, as was shown by the fact that Ni resisted oxidation better than iron and was successfully used in a fluorine environment.

(2) (U) In the presence of fluorine, chlorine and oxygen were replaced by fluorine to form a fluoride in the presence of fluorine.

(3) (U) Contaminants, particularly organic in nature, may react so rapidly in a system containing fluorine that a secondary effect such as ignition and combustion will occur.

(U) Ignition temperature of materials in a fluorine gas were measured by Goodwin and Lorenzo for six metals and two alloys by electrically heating metal wires in a chamber containing fluorine. The temperatures were calculated based on current and voltage readings using resistivity-temperature data. The results of the experiments by Goodwin and Lorenzo in obtaining ignition temperature are tabulated in Table III. In the case of aluminum, it was reasonable that the metal either melted before ignition or ignited at a temperature near the melting point which was supported by two observations. The observations indicated that little or no evidence of reaction or corrosion occurred and the maximum temperature at failure was found to be above the melting point. The reason for the difference in the maximum temperature of failure and melting point for pure aluminum was attributed to the uncertainty of the resistivity in temperature characteristics near the melting point and the extreme difficulty in evaluating a distance because of the minor amount of apparent corrosion. It was believed that the original aluminum oxide film sufficiently slowed down the reaction to the point that ignition could not begin.

(U) The ability for a substance to react spontaneously upon exposure under fluorine was found to be dependent upon conditions of exposure. The most important parameters affecting these conditions were:

(1) (U) Initial temperature and pressure of the environment of the substance.

## TABLE III

## (U) IGNITION POINT OF METALS IN FLUORINE

| Material (Metal) | Diameter Used (inches) | Length (inches) | Est "d" (inches) | Ignition Temp (°F) | Average Ign Temp |
|---|---|---|---|---|---|
| Aluminum | 0.010 | 4 & 8 | 0.562 | - | * |
| Copper | 0.0123 | 12 | 1 - 1/4 | 1335 | 1280 |
| | | 12 | | 1190 | |
| | | 12 | | 1238 | |
| | | 10 | | 1238 | |
| | | 10 | | 1380 | |
| Iron | 0.014 | 6 | 0.225 | 1250 | 1238 |
| | | 6 | | 1230 | |
| | | 8 | | 1230 | |
| | | 8 | | 1250 | |
| Molybdenum | 0.0149 | 4 | 0.25 | 395 | 402 |
| | | 4 | | 381 | |
| | | 5 | | 352 | |
| | | 5 | | 408 | |
| | | 5 | | 352 | |
| Monel | 0.010 | 4 | 0.218 | 816 | 744 |
| | | 4 | | 795 | |
| | | 6 | | 658 | |
| | | 6 | | 712 | |
| Nickel | 0.0155 | 6 | 0.25 | 2130 | 2080 |
| | | 6 | | 2010 | |
| | | 6 | | 2220 | |
| | | 7 1/2 | | 2190 | |
| | | 7 1/2 | | 2210 | |
| | | 6 | | 1980 | |
| Stainless Steel (302) | 0.020 | 6 | 0.125 | 1382 | 1256 |
| | | 6 | | 1470 | |
| | | 8 | | 1130 | |
| | | 8 | | 1058 | |
| Tungsten | 0.0153 | 2 1/2 | 9/32 | 446 | 539 |
| | | 2 1/2 | | 564 | |
| | | 4 | | 474 | |
| | | 5 | | 500 | |

*Metal either melts before ignition or ignites at a temperature near the melting point.

(2) (U) The thermal conductivity of the substance if the material is solid in nature.

(3) (U) The particle size or exposed surface area with respect to the mass of substance exposed.

(4) (U) Kinetic or static exposure.

c. (U) Corrosion Rates

(U) The corrosion rates of various metallic and ceramic materials by gaseous fluorine is shown in Tables IV through XI.

(U) The results of the literature survey indicated that nickel was the best material since it exhibited the lowest corrosion rate in fluorine. Haynes 25 offered a similar characteristic. Monel was satisfactory as a material for use to 1100°F and copper to 930°F. No data on materials operating in a fluorine environment above 1400°F was found during the literature survey.

2. (U) Fluorine Material Evaluation

(U) Metallurgical screening tests were conducted to evaluate the compatibility of various materials in gaseous fluorine over a temperature range of 1500 to 2000°F. Selection of materials for these tests was based upon the results of the literature survey and material believed to be metallurgically and/or chemically suitable.

a. (U) Test Setup

(U) An exposure chamber of uncemented stacked insulating (fire) bricks was utilized with copper buss bars installed in opposite sides of the chamber as the means of heating the specimens by electrical resistance. The specimens were placed across the buss bars and bolted down to complete the circuit. The temperature of the specimen was measured by an optical pyrometer. A metal shroud with a window was installed over the entire exposure chamber to act as a barrier against oxidation due to the air environment surrounding the setup and to contain the brick chamber in case of any malfunction. A tubular manifold located parallel to and directly above the specimen was used to inject helium as a purge and fluorine as the environment for 60 seconds duration (test cell limitation). In addition, the space between the metal shroud and the brick chamber was continuously purged during the tests to prevent any air from entering to complicate any possible reactions. Schematics of the test chamber and system are shown in Figures 1 and 2.

b. (U) Materials Selected

(U) Specimens of preselected materials and coatings in the form of tensile bars were exposed to gaseous fluorine at temperatures from 1500 to 2000°F

## TABLE IV

## (U) CORROSION RATES OF IRON AND MILD STEEL EXPOSED TO GASEOUS FLUORINE

| Material | Corrosion Rates (mil/year) according to Temp. (°F) | | | | | | | | | |
|---|---|---|---|---|---|---|---|---|---|---|
| | 0<br>100 | 100<br>200 | 200<br>300 | 400<br>500 | 500<br>600 | 600<br>700 | 700<br>800 | 800<br>900 | 900<br>1000 | 1000<br>1100 |
| Armco, iron | | 0.7 | | | | | | | 132,000 | |
| Armco, iron | | | Nil | 24.0 | 108 | 96 | 288 | 3600 | 139,000 | |
| Low Si, iron (0.004% Si) | | | | | | | | | | |
| High Si, iron (0.780% Si) | | | | | | | | | | |
| Iron | | | | | | A* | | | | |
| Steel, low carbon | 3.3 | | | | | 394 | | | | |
| Steel, low carbon | 6.0 | | | | | 403 | | | | |
| SAE 1010 | | <0.1 | | | | | | | | |
| SAE 1030 (Trace Si) | | 24 | 96 | 180 | 238,000 | | | | | |
| SAE 1030 (Trace Si) | | | | 6480 | | | | | | |
| Steel (0.007% Si) | | Nil | 192 | 144 | 89,000 | | | | | |
| Steel (0.007% Si) | | | | 3600 | | | | | | |
| SAE 1015 (0.070% Si) | | | | | | | | | | |
| Music Wire (0.130% Si) | | | | | | | | | | |
| SAE 1030 (0.180% Si) | | | | | | | | | | |
| SAE 1020 (0.220% Si) | | | | 18,000 | | | | | | |
| SAE 1020 (0.220% Si) | | 456 | 5760 | 6480 | | | | | | |

*A, little or no attack

## TABLE V

## (U) CORROSION RATES OF STAINLESS STEELS EXPOSED TO GASEOUS FLUORINE

| Material | Corrosion Rates (mil/year) according to Temp. (°F) | | | | | | | | | | | |
|---|---|---|---|---|---|---|---|---|---|---|---|---|
| | 0 100 | 100 200 | 200 300 | 300 400 | 400 500 | 500 600 | 600 700 | 700 800 | 800 900 | 900 1000 | 1000 1100 | 1300 1400 |
| Type 304 | 1.3 | | | | 6.8 | | 1500 | | | | | |
| Type 304 | 2.0 | | | | 5.5 | | 1600 | | | | | |
| Type 309 Nb | | | | Nil | Nil | 900 | 5500 | 8000 | | | | |
| Type 310 | | | | Nil | Nil | 372 | 4250 | 6730 | | | | |
| Type 347 | 2.7 | | | | 4.2 | | | 4266 | | | | |
| Type 347 | 2.7 | | | | 3.5 | | | 4230 | | | | |
| Type 347 | | | | Nil | 1740 | 2550 | 6200 | 9450 | | | | |
| Type 430 | | | | 8.4 | Nil | 3060 | 936 | 936 | | | | |

## TABLE VI

## (U) CORROSION RATES OF COPPER AND COPPER ALLOYS EXPOSED TO GASEOUS FLUORINE

Corrosion Rates (mil/year) according to Temp. (°F)

| Material | 0 100 | 100 200 | 200 300 | 300 400 | 400 500 | 500 600 | 600 700 | 700 800 | 800 900 | 900 1000 | 1000 1100 | 1300 1400 |
|---|---|---|---|---|---|---|---|---|---|---|---|---|
| Copper ETP | Nil | | | | 12.3 | | 324 | | | 245 | | |
| Copper ETP | Nil | | | | 2.0 | | 26.9 | | | 219 | | |
| Copper | | | | | | | | | | | 110 | 750 |
| Copper (de-oxidized) | | | | | | | | 1920 | | 1440 | | |
| Copper (sheet) | | | | | | | | | | 2440 | | |
| Copper (foil) | | Nil | | | | | | | | | | |
| Copper (wool) | | | Burned | | | | | | | | | |
| Copper | | | | | | | | A* | | | | |
| Brass 70-30 | | Nil | | | | | | | | | | |
| Brass Type 243 | 10.5 | | | 15.8 | | | 394 | | | 3890 | | |
| Brass Type 243 | 24.5 | | | 24.5 | | | 368 | | | 3811 | | |
| Brass, Red | Nil | | | | 5.1 | | | 71.8 | | 394 | | |
| Brass, Red | Nil | | | | 6.1 | | | 70.1 | | 408 | | |
| Bronze | | Nil | | | | | | | | | | |
| Copper-Nickel | | Nil | | | | | | | | | | |

A*, Little or No Attack

## TABLE VII

## (U) CORROSION RATES OF ALUMINUM AND ALUMINUM ALLOYS EXPOSED TO GASEOUS FLUORINE

| Material | Corrosion Rates (mil/year) According to Temp. (°F) | | | | | | | | | | | |
|---|---|---|---|---|---|---|---|---|---|---|---|---|
| | 0 | 100 | 200 | 300 | 400 | 500 | 600 | 700 | 800 | 900 | 1000 | 1100 |
| | 100 | 200 | 300 | 400 | 500 | 600 | 700 | 800 | 900 | 1000 | 1100 | 1200 |
| Aluminum (Sheet) | | | | | | | | | | 480 | | 720 |
| Aluminum 2S | | | | | | | | Nil | Nil | 13.0 | | 216 |
| Aluminum | | | | | | | A* | | | | | |
| Aluminum | <5 | <5 | | <5 | <5 | <20 | <20 | | | | | |
| Aluminum (foil) | | | | Nil | | | | | | | | |
| Type 1100 H14 | Nil | | | Nil | | | 6.6 | | | 1820 | | |
| Type 1100 H14 | Nil | | | Nil | | | 5.6 | | | | | |
| Type 2024-T3 | Nil | | | Nil | | | Nil | | | 34.2 | | |
| Type 2024-T3 | Nil | | | | | | Nil | | | 24.5 | | |
| Type 3003 H14 | 1.9 | | | 1.0 | | | Nil | | | 22.8 | | |
| Type 3003 H14 | Nil | | | Nil | | | Nil | | | 19.3 | | |
| Type 5154 H34 | Nil | | | Nil | | | Nil | | | 6.8 | | |
| Type 5154 H34 | Nil | | | Nil | | | Nil | | | 8.8 | | |

*A, little or no attack

TABLE VIII

(U) CORROSION RATES MAGNESIUM AND MAGNESIUM ALLOYS EXPOSED TO GASEOUS FLUORINE

| | Corrosion Rates (mil/year) According to Temp. (°F) | | | | | | | | | | | | |
|---|---|---|---|---|---|---|---|---|---|---|---|---|---|
| | 0 | 100 | 200 | 300 | 400 | 500 | 600 | 700 | 800 | 900 | 1000 | 1100 | 1200 |
| Material | 100 | 200 | 300 | 400 | 500 | 600 | 700 | 800 | 900 | 1000 | 1100 | 1200 | 1300 |
| Magnesium M 1A | Nil | | | | Nil | | | 5.9 | | 31.5 | | | |
| Magnesium M 1A | Nil | | | | 1.9 | | | Nil | | | | | |
| Magnesium | | | | | | | A* | | | | | | |
| Magnesium HZ81C-76 | Nil | | | | 1.3 | | | 13.1 | | | 39.4 | | |
| Magnesium HK31A-H24 | 7.4 | | | 11.4 | | | 9.6 | | | 20.1 | | | |
| Magnesium HK31A-H24 | 3.7 | | | 1.8 | | | 3.7 | | | 20.1 | | | |
| MA (1.2 Mn) | | Nil | | | | | | | | | | | |
| FS-1.1 (3% Al, 1% Zn, 0.2% Mn) | | Nil | | | | | | | | | | | |
| J-1H (3% Al, 0.7% Zn, 0.2% Mn) | | Nil | | | | | | | | | | | |
| Dow Metal G | | | | Nil | Nil | Nil | | | | | | | |

*A, little or no attack

## TABLE IX

## (U) CORROSION RATES OF NICKEL AND NICKEL ALLOYS EXPOSED TO GASEOUS FLUORINE

| | Corrosion Rates (mil/year) According to Temp. (°F) | | | | | | | | | | | | | |
|---|---|---|---|---|---|---|---|---|---|---|---|---|---|---|
| Material | 0 100 | 100 200 | 200 300 | 300 400 | 400 500 | 500 600 | 600 700 | 700 800 | 800 900 | 900 1000 | 1000 1100 | 1100 1200 | 1200 1300 | 1300 1400 |
| "A" Nickel | 1.0 | | | 3.8 | | | | Nil | | | 25.4 | | | |
| "A" Nickel | 1.0 | | | 2.8 | | | | 2.8 | | | 23.7 | | | |
| "A" Nickel | | | | | | | | | | | 4.4 | | 59.0 | 353 |
| "A" Nickel | | | | | | | | | | | | 0.3 | | |
| "L" Nickel | 1.0 | | | | 1.8 | | | 1.8 | | | 20.1 | | | |
| "L" Nickel | 3.8 | | | | 4.6 | | | 1.0 | | | 20.1 | | | |
| "D" Nickel | | | | | | | | | | | | 2.0 | | |
| Nickel (Sheet) | | | | | | | | | | 72 | | | 1200 | |
| Nickel | | | | | | | | 8.4 | 22.8 | 61.2 | | 348 | 192 | |
| Nickel | | | | | | | | | | | | | 408 | |
| Nickel (foil) | Nil | Nil | | | | | | | | | | | | |
| Nickel (electrolyte) | | | | | | | | | | | | Nil | | |
| Nickel (electrolyte) | | | | | | | | | | | | Nil | | |
| Nickel (low carbon) | | | | | | | | | | | | 0.3 | | |
| Duranickel | | | | | | | | | | | | 0.8 | | |
| Monel | 1.9 | | | 1.0 | | | Nil | | | | 28.9 | | | |
| Monel | 2.0 | | | Nil | | | Nil | | | | 30.7 | | | |
| Monel (sheet) | | | | | | | | | | 24.0 | | | 2400 | |
| Monel | | | | | | | | | | | | | 410 | 2900 |
| Monel | | | | | | | | | | | | Nil | | |
| Monel (tube) | | | Nil | | | | | | | | | | | |
| Monel (welded) | | Nil | | | | | | | | | | | | |
| "K" Monel | | | | | | | | | | | | 1.2 | | |
| Monel (cast) | 3.0 | | | 1.0 | | | | 3.9 | | 42.9 | | | | |
| Inconel | 1.7 | | | Nil | | | 75.3 | | | 3451 | | | | |
| Inconel | Nil | | | Nil | | | 79.7 | | | | | | | |
| Inconel | | | | | | | 45.6 | 115 | 74.4 | | 2040 | 1560 | | |
| Inconel | | | | | | | | | | | | 6120 | | |
| Inconel | | | | | | | | | | | 3200 | | 7100 | 24,000 |
| Inconel | | | | | | | | | | | | | | 26,000 |
| Inconel | | | | | | | | | | | | 5.9 | | |

## TABLE X

## (U) CORROSION RATES OF TITANIUM AND TITANIUM ALLOYS EXPOSED TO GASEOUS FLUORINE

| | Corrosion Rates (mil/year) According to Temp. (°F) | | | | | | | | | |
|---|---|---|---|---|---|---|---|---|---|---|
| Material | 0<br>50 | 50<br>100 | 100<br>150 | 150<br>200 | 200<br>250 | 250<br>300 | 300<br>350 | 350<br>400 | 400<br>450 | 450<br>500 |
| A-55 | | 4.5 | | | | | 73.6 | 1790 | | |
| A-55 | | 6.8 | | | | | 74.5 | 1890 | | |
| Ti 75A | | 4.4 | | | | | | | | |
| Ti 75A | | 5.1 | | | | | | | | |
| Ti 75A | | 5.2 | | | | | | | | |
| Ti 75A | | 2.4 | 0.5 | 0.5 | 0.2 | | | | | |
| Ti 75A | | 1.9 | 1.5 | 1.4 | 0.2 | | | | | |
| Ti 75A | | | | Nil | | | | | | |
| Ti 75A | | | | Nil | | | | | | |
| Ti 6Al 4Y | | 2.8 | 0.7 | 3.2 | 0.5 | | | | | |
| Ti 6Al 4Y | | | | 4.7 | Nil | | | | | |
| Ti 6Al 4Y | | | | Nil | | | | | | |
| Ti 6Al 4Y | | | | 2.2 | | | | | | |
| B 120 VCA | | Nil | | | | | Nil | 45.6 | 333 | 1148 |
| B 120 VCA | | Nil | | | | | Nil | 44.7 | | |
| B 120 VCA | | | | | | | | 85.0 | | |
| B 120 VCA | | | | | | | | 85.0 | | |
| B 120 VCA | | 12.1 | 0.5 | 0.4 | 0.2 | | | | | |
| B 120 VCA | | | | 1.1 | Nil | | | | | |
| B 120 VCA | | | | 1.8 | | | | | | |
| B 120 VCA | | | | 0.1 | | | | | | |
| Ti 16V 2.5 Al | | 3.1 | 0.8 | 0.7 | 1.7 | 0.4 | | | | |
| Ti 16V 2.5 Al | | | | | 2.3 | 0.2 | | | | |
| Ti 16V 2.0 Al | | 3.7 | 3.0 | 1.1 | Nil | | | | | |
| Ti 8 Mn | | 3.7 | 3.0 | 1.1 | 3.2 | 2.0 | | | | |
| Ti 8 Mn | | | | | 0.1 | 0.7 | | | | |
| Ti 8 Mn | | | | | 0.1 | | | | | |

## TABLE XI

## (U) CORROSION RATES OF VARIOUS METALS EXPOSED TO GASEOUS FLUORINE

| | Corrosion Rate (mil/year) According to Temp. (°F) | | | | | | | |
|---|---|---|---|---|---|---|---|---|
| | 0 | 100 | 200 | 300 | 400 | 500 | 600 | 700 |
| Material | 100 | 200 | 300 | 400 | 500 | 600 | 700 | 800 |
| Zirconium | 2.0 | | | 24.5 | | | 8200 | |
| Zirconium | 1.0 | | | 28.9 | | | 7499 | |
| Zirconium | | | | | | | C | |
| Zirconium | | | | B | | | | |
| Zircaloy 2 | 3.0 | | | 16.6 | | | 7660 | |
| Zircaloy 2 | 6.0 | | | 24.5 | | | | |
| Tantalum | 12.3 | | CR | | | | | |
| Tantalum | 13.1 | | CR | | | | | |
| Chromium Plate | | | | Nil | | | | |
| Thorium | | | | | | | A | |
| Silver Solder (Flux) | A | | | | | | | |
| Silver Solder (Flux) | B | | | | | | | |
| Silver Solder (Flux) | A | | | | | | | |
| Silver Solder (Flux) | B | | | | | | | |
| Uranium | B | | | | | C | | |
| Uranium | C | | | | | | | |
| Platinum | | | | | | | | B or C |
| Platinum | | | | | | | | B or C |
| Tin | | | | B | | | | |

*A, little or no attack; B, attack but no burning;

C, burning, CR, complete reaction.

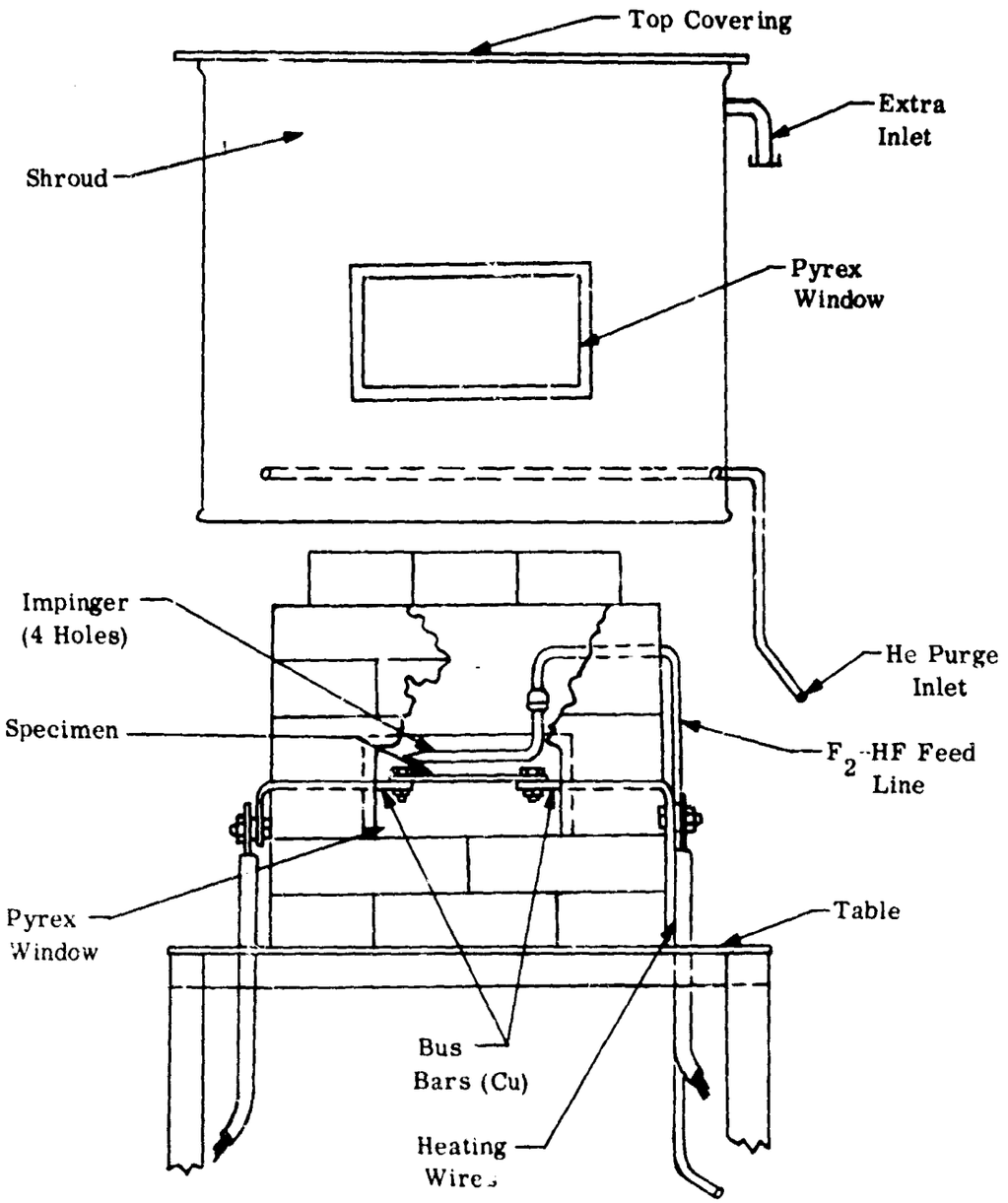


Figure 1. (U) Cell 3B-S Test Chamber

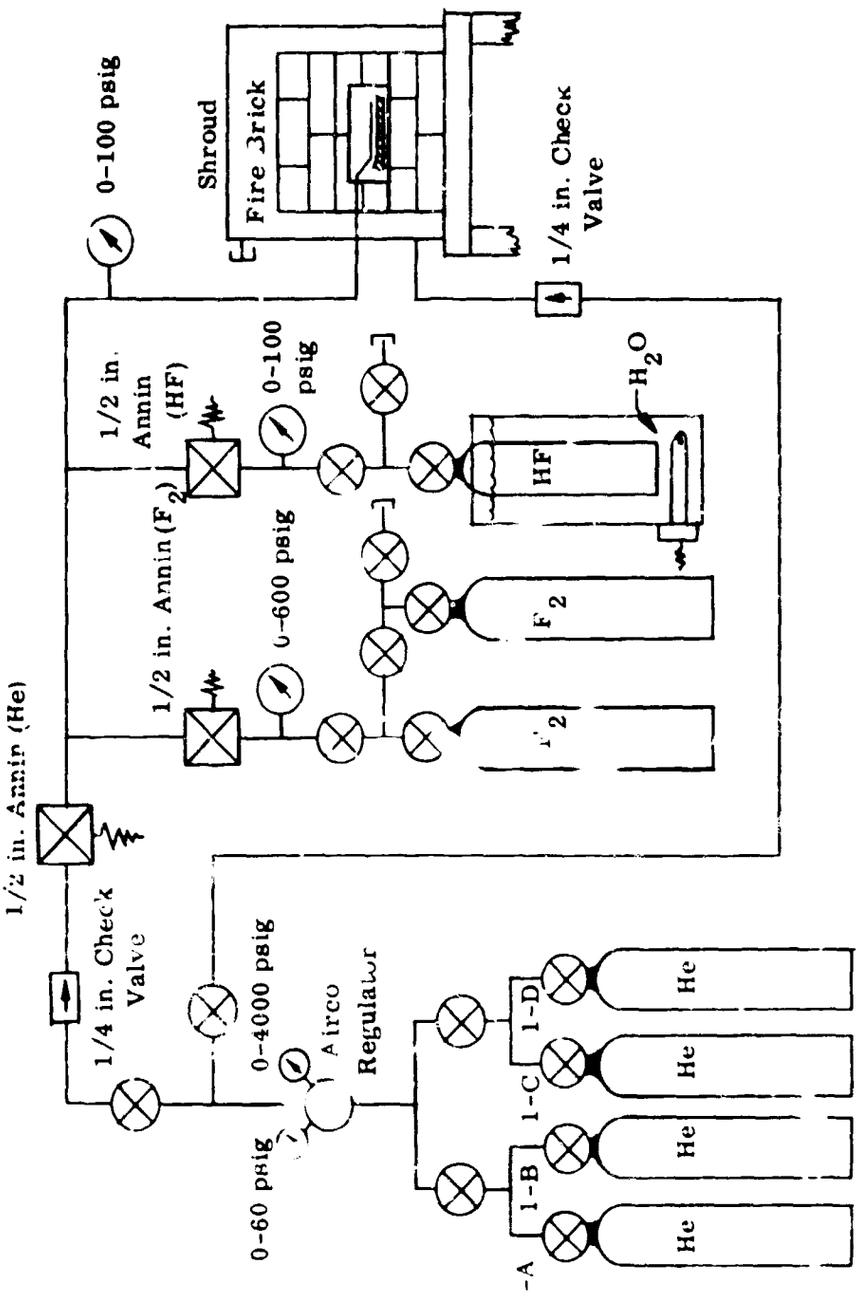


Figure 2. (U) Cell 3B-S Material Compatibility Test System Schematic

(U) to determine their resistance to corrosive attack by gaseous fluorine for 60 seconds duration. The following materials were selected for evaluation:

(1) (U) Uncoated Materials

TD Nickel
L-605 Alloy (Haynes 25)
Pure Tantalum
Pure Tungsten
Columbium Alloy (Cb-1Zr)
Graphite (plain)

(2) (U) Coated Materials

Haynes 25 coated with a multiple element coating rich in iron and aluminum (C-12)

TD Nickel coated with an aluminum-silicon-chrome coating (SUE-2)

Columbium coated with modified aluminide coating
Columbium coated with modified silicide coating
Tantalum coated with modified aluminide coating
Tantalum coated with modified silicide coating

c. (U) Test Results

(U) The test program was conducted to evaluate the compatibility of materials and coatings with gaseous fluorine at elevated temperatures (1500 to 2000° F). The results are summarized in the following paragraphs and in Table XII.

(1) (U) Uncoated Materials

(a) (U) TD Nickel was satisfactorily tested at 1500° F but reacted with the fluorine and melted at 2000° F. Therefore, the limiting temperature of operation in a fluorine rich environment, predicated upon these results, was in excess of 1500° F but below 2000° F.

(b) (U) Haynes 25 was satisfactorily tested for the maximum duration of the test cycle at 1500° F but reacted with fluorine and melted at 2000° F. Therefore, the limiting temperature of operation in a fluorine rich environment, predicated upon these test results, was in excess of 1500° F but below 2000° F.

(c) (U) Pure tantalum was tested at 1500° F but resulted in immediate reaction and burned through. Therefore, the indication was given that tantalum is unsatisfactory for use in a fluorine rich environment at elevated temperatures.

TABLE XII

(U) RESULTS OF FLUORINE MATERIAL EVALUATION

| Material | Coating | Test Temp. °F | Length of Test sec. | % Wt Change | Remarks |
|---|---|---|---|---|---|
| TD Nickel | - | 1550 | 50 | +0.06 | Test ceased at 50 sec due to equipment malfunction. Slight discoloration after test but no visible precipitate. |
| TD Nickel | - | 1510 | 30 | +0 04 | Test ceased at 30 sec due to equipment malfunction. |
| TD Nickel | - | 1960 | 11 | -10.0 | Vigorous reaction with glow of white light and specimen melted. |
| Haynes 25 | - | 1500 | 60 | +0.02 | Discoloration only (darkened). |
| Haynes 25 | - | 1510 | 60 | -0.01 | Discoloration only (darkened). |
| Haynes 25 | - | 2010 | 4.75 | -28.0 | Specimen burned through. Light precipitate noted. |
| Tantalum | - | 1460 | 9.5 | -10.1 | Immediate reaction with very bright glow and dense smoke. White precipitate resulted. |
| Tantalum | - | 1480 | 13.75 | -11.6 | Immediate reaction with very bright glow and dense smoke. White precipitate resulted. |
| Tungsten | - | 1640 | 29.5 | - | Extremely difficult to heat. During heating specimen glowed and then immediate reaction resulted with a bright yellow glow and heavy smoke. |

(U) TABLE XII (CONT)

| Material | Coating | Test Temp. °F | Length of Test sec | % Wt Change | Remarks |
|---|---|---|---|---|---|
| Columbium | - | 1525 | 60 | -27.0 | Immediate reaction and bright glow with white-yellow precipitate. |
| Columbium | - | 1540 | 60 | -32.0 | Immediate reaction and bright glow with white-yellow precipitate. |
| Columbium | - | 1980 | 18 | -6.5 | Immediate reaction with white-yellow precipitate and specimen burned through. |
| Columbium | - | 1990 | - | -18.0 | Immediate reaction with white-yellow precipitate and specimen burned through. |
| Graphite | - | 1500 | - | - | Instant reaction with white light and violent combustion. |
| Haynes 25 | C-12 | 1540 | 60 | - | Discoloration only. |
| Haynes 25 | C-12 | 1700 | 5.25 | -12.0 | Specimen reacted with bright orange color and gave appearance of melting. |
| Haynes 25 | C-12 | 2010 | 3 | -33.1 | Specimen reacted with bright orange color and gave appearance of melting. |
| TD Nickel | SUE-2 | 1530 | 60 | - | Slight discoloration only. |
| TD Nickel | SUE-2 | 1760 | 5 | - | Specimen burned through. |
| TD Nickel | SUE-2 | 1600 | 60 | - | Slight discoloration only. |
| TD Nickel | SUE-2 | 1630 | 60 | - | Slight discoloration only. |

(U) TABLE XII (CONT)

| Material | Coating | Test Temp. °F | Length of Test sec | % Wt Change | Remarks |
|---|---|---|---|---|---|
| Columbium | Modified Aluminide | Ambient | 60 | 0.07 | No visible reaction, but dense smoke resulted. Specimen unaffected. |
| Columbium | Modified Aluminide | 1450 | 60 | -2.0 | Bright orange glow and dense smoke with heavy white-yellow precipitate. |
| Columbium | Modified Aluminide | 1460 | 34 | -25.0 | Bright orange glow and dense smoke with heavy white-yellow precipitate. |
| Columbium | Modified Aluminide | 1900 | 6.75 | -15.0 | Instantaneous reaction with white glow and dense smoke. Specimen burned through. |
| Columbium | R508C | Ambient | 60 | 0 | |
| Columbium | R508C | 1450 | 44.5 | -23.0 | Bright glow and dense smoke with white precipitate. Specimen burned through. |
| Tantalum | Modified Aluminide | 1550 | 60 | -12.0 | Silver precipitate with glow. Specimen broke. |
| Tantalum | Modified Aluminide | 1600 | 32 | -31.2 | Immediate reaction with white glow and dense smoke with white precipitate. |
| Tantalum | Modified Aluminide | 1920 | 5.75 | -10.2 | Immediate reaction with white glow and dense smoke with white precipitate. Specimen burned through. |
| Tantalum | Pfaudler Silicide | Ambient | 60 | - | Slight discoloration. |

(U) TABLE XII (CONT)

| Material | Coating | Test Temp. °F | Length of Test sec | % Wt Change | Remarks |
|---|---|---|---|---|---|
| Tantalum | Pfaudler Silicide | 1475 | 60 | - | Immediate reaction with blinding glow and dense smoke with heavy white precipitate. Specimen broke. |
| Tantalum | Pfaulder Silicide | 1470 | 50 | - | Immediate reaction with blinding glow and dense smoke with heavy white precipitate. Specimen broke. |
| Tantalum | Pfaudler Silicide | 1960 | 6.8 | - | Immediate reaction with blinding glow and dense smoke with heavy white precipitate. Specimen broke. |
| Tantalum | Pfaudler Silicide | 1975 | 49 | - | Immediate reaction with blinding glow and dense smoke with heavy white precipitate. Specimen broke. |
| Tantalum | G.T. and E. R508C | Ambient | 60 | - | Slight white precipitate |
| Tantalum | G.T. and E. R508C | 1560 | 60 | -21.7 | Bright glow and dense smoke with white-yellow precipitate. |
| Tantalum | G.T. and E. R508C | 1530 | 8.0 | -6.2 | Specimen burned through. |
| Tantalum | G.T. and E. R508C | 1970 | 5.0 | -5.6 | Instantaneous reaction with white glow and dense smoke. Specimen burned through. |
| Tantalum | G.T. and E. R508C | 1990 | 5.8 | -6.5 | Instantaneous reaction with white glow and dense smoke. Specimen burned through. |

(d) (U) Tungsten was tested at a temperature of 1600°F but reacted during this test. This indicated that tungsten was unsatisfactory for operation in a fluorine rich environment at elevated temperatures.

(e) (U) Columbium was tested at 1500°F and reacted with the fluorine resulting in a white-yellow precipitate although the maximum duration of the test cycle was accomplished. Testing at 2000°F resulted in a burnthrough caused by reaction with fluorine. Therefore, the indication was given that columbium is unsatisfactory as a material for use in a fluorine environment at elevated temperatures (1500 to 2000°F).

(f) (U) Graphite was tested at 1500°F in a fluorine rich environment but an instantaneous reaction occurred and the test chamber was damaged. This indicated that graphite is unsatisfactory as a material for use in a fluorine rich environment at elevated temperatures.

(2) (U) Coated Materials

(a) (U) Haynes 25 was satisfactorily tested with a C-12 multiple element coating, rich in iron and aluminum, at 1500°F for the maximum duration of the test cycle. Testing with the same material at 1700°F resulted in a reaction with the fluorine with the indication of melting occurring during the reaction. A similar result occurred when testing at 2000°F. Therefore, the limiting temperature of operation of Haynes 25 with the C-12 coating was found to be in excess of 1500°F but below 1700°F and did not appear to be any different than the base material itself.

(b) (U) TD Nickel coated with an aluminum-silicide-chrome coating (SUE-2) was satisfactorily tested at 1500, 1600 and 1630°F for the duration of the test cycle and indicated only a slight discoloration. Testing of the same material at 1760°F resulted in a burnthrough of the sample in five seconds. Therefore, the TD Nickel coated with the SUE-2 coating resulted in a limiting temperature of operation in a fluorine rich environment in excess of 1630°F but below 1760°F. A test was also satisfactorily conducted in an HF environment with this material and coating for the maximum duration of the test cycle at a temperature of 1750°F with no resulting discoloration.

(c) (U) Columbium coated with a modified aluminide coating was tested at 1500°F and reacted with the fluorine, although the reaction took 30 to 60 seconds to complete. Testing at 1900°F resulted in an instantaneous reaction with the fluorine and the specimen burned through after approximately seven seconds. Therefore, the modified aluminide coating on columbium is not satisfactory for operation in a fluorine rich environment between 1500 and 1900°F.

(d) (U) Columbium coated with the R508C silicide coating (GT&E) was tested at 1500°F and reacted with fluorine and burned through. Therefore, this material is not satisfactory for operation in a fluorine rich environment at elevated temperatures.

(e) (U) Tantalum coated with a modified aluminide coating was tested at 1550°F for the maximum duration of the test cycle but reacted with the fluorine to form a white precipitate. Testing at 1600°F resulted in a reaction to form a white precipitate. Similar results occurred when tested at 1900°F. Therefore, this material was not found to be satisfactory for operation in a fluorine rich environment at elevated temperatures.

(f) (U) Tantalum coated with the Pfaudler silicide coating was tested at 1500°F for the maximum duration of the test cycle but a reaction occurred causing a heavy white precipitate on the specimen. The specimen broke at the completion of the test. Testing of the same material at 2000°F resulted in a reaction and burned through the sample. However, the thicker the coating, the more protection offered. Therefore, tantalum coated with the Pfaudler silicide coating is not satisfactory for operation in a fluorine rich environment at elevated temperatures.

(U) Tantalum coated with the R508C silicide coating (GT&E) was tested at 1500°F but reacted with the fluorine to form a yellow-white precipitate. Testing of the same material at 2000°F resulted in an instantaneous reaction and a burnthrough of the sample. Therefore, tantalum coated with the GT&E silicide coating is unsatisfactory for operation in a fluorine rich environment at elevated temperature.

(3) (U) X-ray diffraction experiments were conducted on many of the tested specimens to determine the mode of reactions and an attempt to ascertain the mode of protection of the material. Table XIII summarizes the results of the X-ray diffraction experiments.

(4) (U) Conclusions

(U) The results of the tests conducted to determine the materials compatible with a fluorine rich environment at elevated temperatures indicate that TD Nickel and Haynes 25 have the capability of operation in excess of 1500°F but below 2000°F. Haynes 25 coated with the C-12 coating and TD Nickel coated with the SUE-2 coating have the capability of operation in a fluorine rich environment in excess of 1500°F but below 2000°F.

## TABLE XIII

## (U) X-RAY DIFFRACTION RESULTS

| Specimen | 1500°F | 2000°F | Standards – Remarks |
|---|---|---|---|
| Tartalum (bare) | $Ta_2O_5 + TaF_3$ | $Ta_2O_5 + TaF_3$ | |
| Columbium (bare) | $Nb\ F_3 + NbO_2$ | $Nb\ F_3 + NbO_2$ | |
| T.D. Nickel (bare) | $Ni + NiF_2 + Ni + ThO_2$ | $ThO_2 + Ni + NiF_2$ | Ran base material pattern subtracted pattern |
| L-605 (bare) | Base material + $NiF_2$ Trace NiO | Base material + $NiF_2$ | Ran standard material pattern and subtracted base material peaks |
| Ta + Aluminide coating | $AlF_3$ | $Ta_2O_5 + TaF_3$ | |
| Cb + Aluminide coating | $AlF_3$ | $NbO_2 + NbF_3$ | |
| L-605-C-12 coating | $NiF_2 + Al_3Ni_2 + Cr$ | $NiF_2 + Al_3Ni_2 + Cr\ AlF_3$ | $Al_3Ni_2$+Cr |
| Tantalum Pfaudler | $Ta_2O_5$+$TaF_3$ | $Ta_2O_5$+$TaF_3$ | |
| Columbium Pfaudler | $NbO_2 + NbF_3$ | $NbO_2 + NbF_3$ | |
| TD Nickel SUE No. 2 | | | Coating vendor did not return specimen in time to test. |

SECTION 4

(C) FLUORINE RICH GAS GENERATOR

A. (U) GENERAL

(U) Critical experiments were conducted on full-scale oxidizer rich gas generators to determine the feasibility of operation in a fluorine rich environment. The purpose of these tests was to define whether or not there were major oxidizer rich gas generator development problems associated with the high energy propellant combination of liquid fluorine and a hydrazine blend (BA-1014). The major problems anticipated were the ability of using fluorine to cool the gas generator wall without reacting fluorine with the wall material, and to define and obtain wall temperatures compatible with materials presently available for construction of the generator. This information was required to design the two-stage combustion injector for use with the advanced (adiabatic wall) thrust chamber.

B. (C) TECHNICAL DISCUSSION

1. (C) Design Analysis

(U) Analyses of theoretical propellant performance were accomplished over the gamut of oxidizer rich, fuel rich, and stoichiometric mixture ratio regimes for the propellant combination of liquid fluorine and a hydrazine blend (BA-1014). The results of the theoretical characteristic velocity (c*) and combustion temperature are shown in Figures 3 and 4 over the complete mixture ratio band of 0.04 to 30 for equilibrium conditions. In addition, the effect of 50% dissociation of ammonia at the fuel rich mixture ratio regime is also shown in these figures.

(C) Based upon the results of the theoretical propellant performance information, the gas side wall temperatures were analyzed for operation with a fluorine rich gas generator at a chamber pressure of 100 psia which is compatible with the two-stage combustion injector operating at a final chamber pressure of 65 psia. This analysis incorporated the effect of combustion efficiency and mixture ratio and was predicated upon an emissivity of the wall approaching zero, which is based upon a shiny surface. The method used in the calculations is described in the following paragraphs.

(U) The heat transfer coefficient and combustion temperature utilized was based upon data obtained by the free-stream properties of the combustion gases. Utilizing the basic heat transfer equation of heat input equals heat output, the equation can be written:

$$q/a = \frac{T_c - T_{wg}}{1/h_g} = \sigma \epsilon T_{wg}^4$$

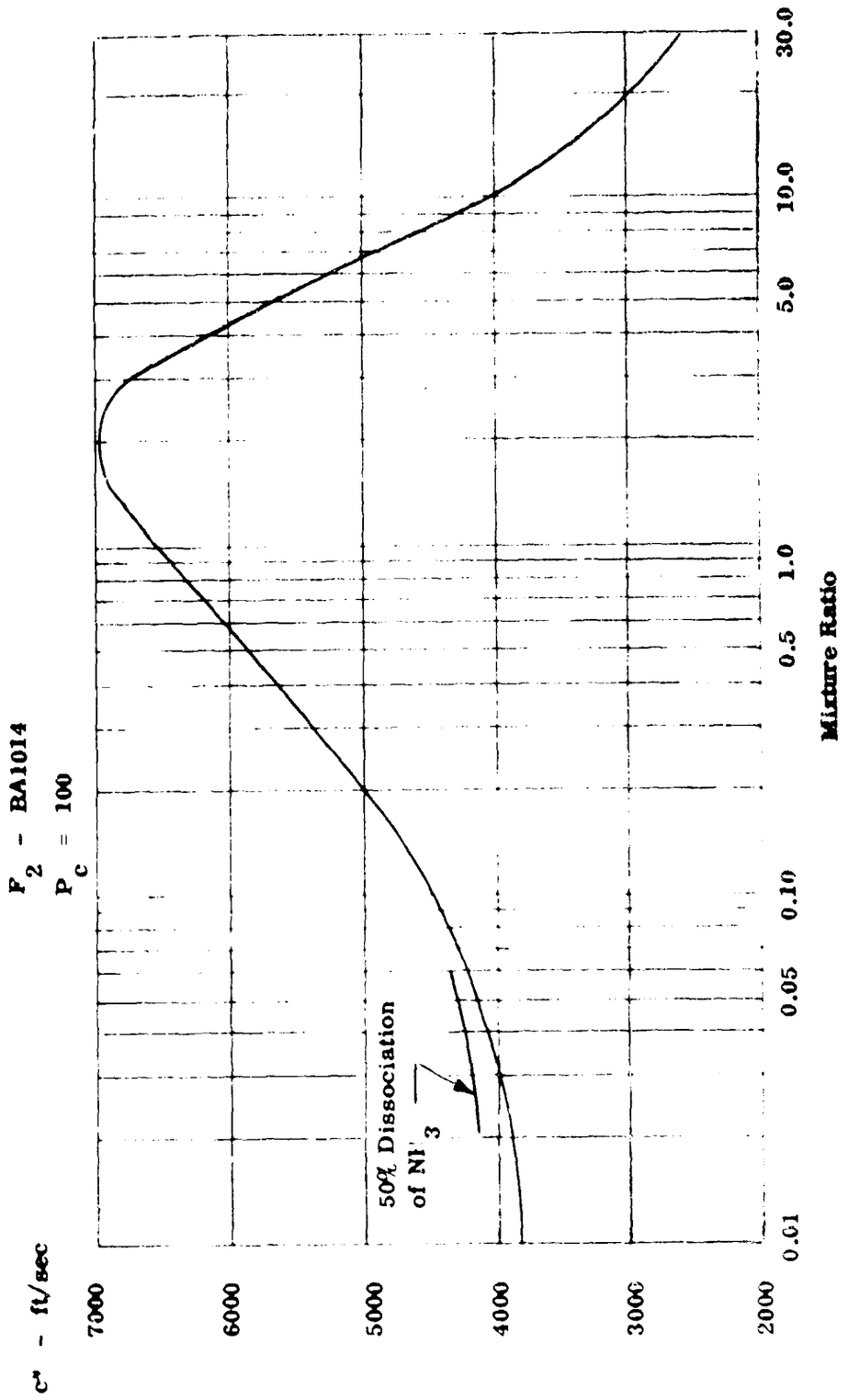


Figure 3. (U) Characteristic Velocity versus Mixture Ratio

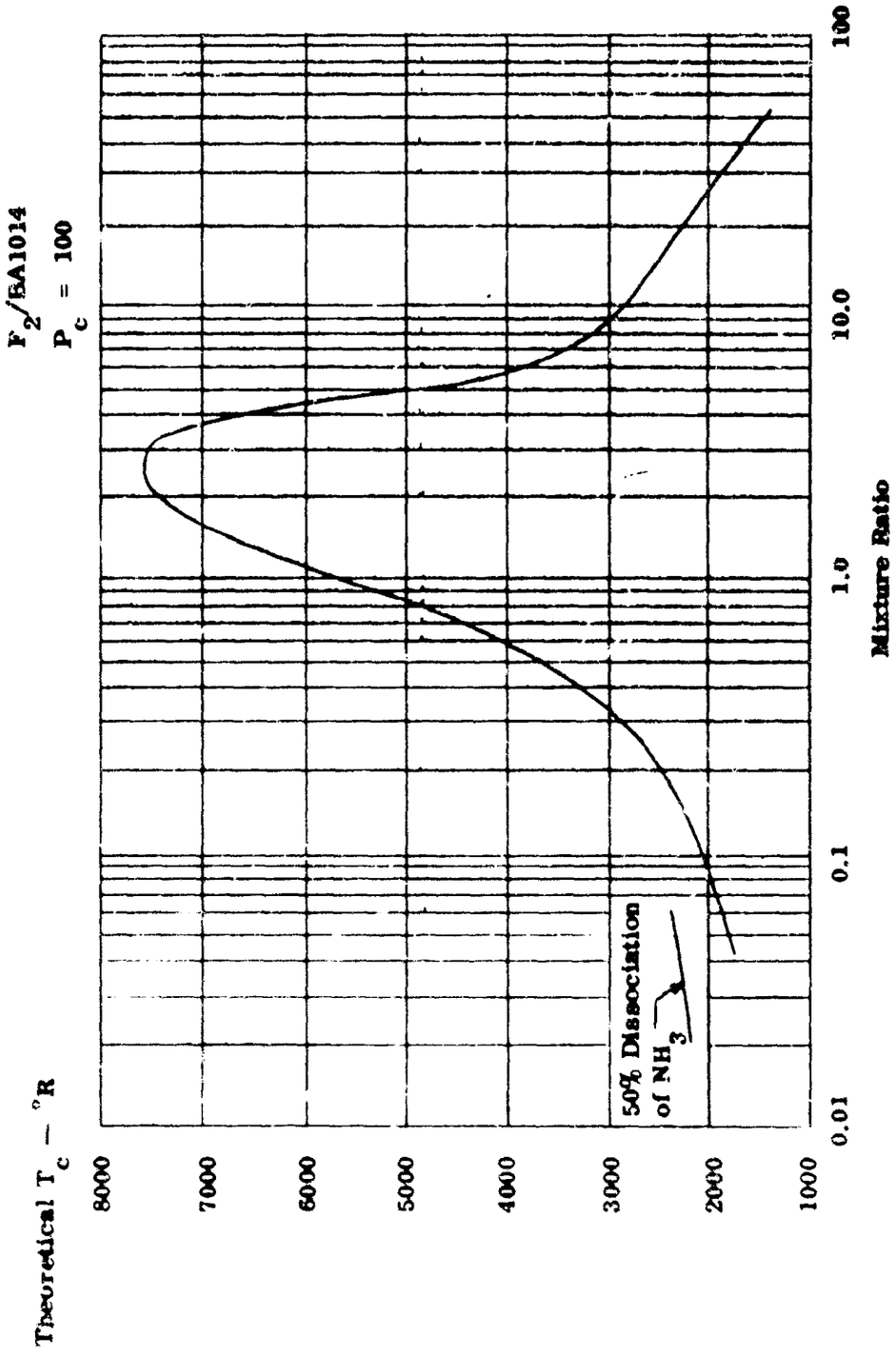


Figure 4. (U) Combustion Temperature versus Mixture Ratio



CONFIDENTIAL

(This page is Unclassified)

(U) where: $q/a$ = heat flux

$T_c$ = actual combustion temperature

$T_{wg}$ = gas side wall temperature

$\sigma$ = Stefan-Boltzmann constant

$\epsilon$ = emissivity

Figure 5 shows the results of this analysis. Based upon the results of the $N_2O_4$/50% $N_2H_4$ + 50% UDMH program, it was anticipated that the oxidizer rich gas generator would operate at a combustion efficiency of approximately 65%. Therefore, the initial mixture ratio was tentatively selected as 25 which would result in a gas side wall temperature of 450°F. Based upon materials currently available, this would allow for localized temperatures significantly higher than the average gas side wall temperature resulting from a nonuniform combustion process and would still allow the reliable operation of a fluorine rich gas generator operating at a mixture ratio as high as 40. This would result in a gas side wall temperature of 250°F predicated upon a 65% combustion efficiency which would allow an even greater margin of safety for localized temperature resulting from nonuniform combustion process. Should the combustion efficiency approach 80%, a gas side wall temperature of 860°F would result based upon operation at a mixture ratio of 25 or 590°F based upon operation at a mixture ratio of 40. Therefore analyses indicated that operation of an oxidizer rich gas generator at a mixture ratio between 25 and 40 would result in reliable operation based upon the low resulting temperatures indicated by theoretical heat transfer analyses.

2. (C) Design and Fabrication

(C) Two oxidizer rich gas generator configurations were initially selected to demonstrate the feasibility of operation of a fluorine rich gas generator. One type was a typical triplet injector consisting of a primary combustion zone and a wall barrier zone to provide a curtain of fuel to mask the wall from the hot gas primary zone. Figure 6 shows this injector which is similar in design to other generator configurations tested at Bell Aerosystems. This injector was designed for a primary combustion zone mixture ratio of 10 and an overall mixture ratio of 40 to allow for reduction of wall temperatures based upon the analysis previously discussed. This injector was designed utilizing baffles in both the fuel and oxidizer manifolds for uniform distribution of propellants. The injector was fabricated from 304 stainless steel.

(C) A second injector configuration was composed of helical jet geometry. This injector, shown in Figure 7, consists of a series of 36 oxidizer orifices located at the outer periphery and injected in a helical arrangement. A Bendix spring-loaded pintle injection nozzle, shown in Figure 8, was located in the center to provide a conical spray of fuel. This injector was designed for an overall mixture ratio of 25, but has the capability of operating a mixture ratios up to 40 to allow for lower wall temperatures as discussed in the previous analysis. This injector was fabricated from

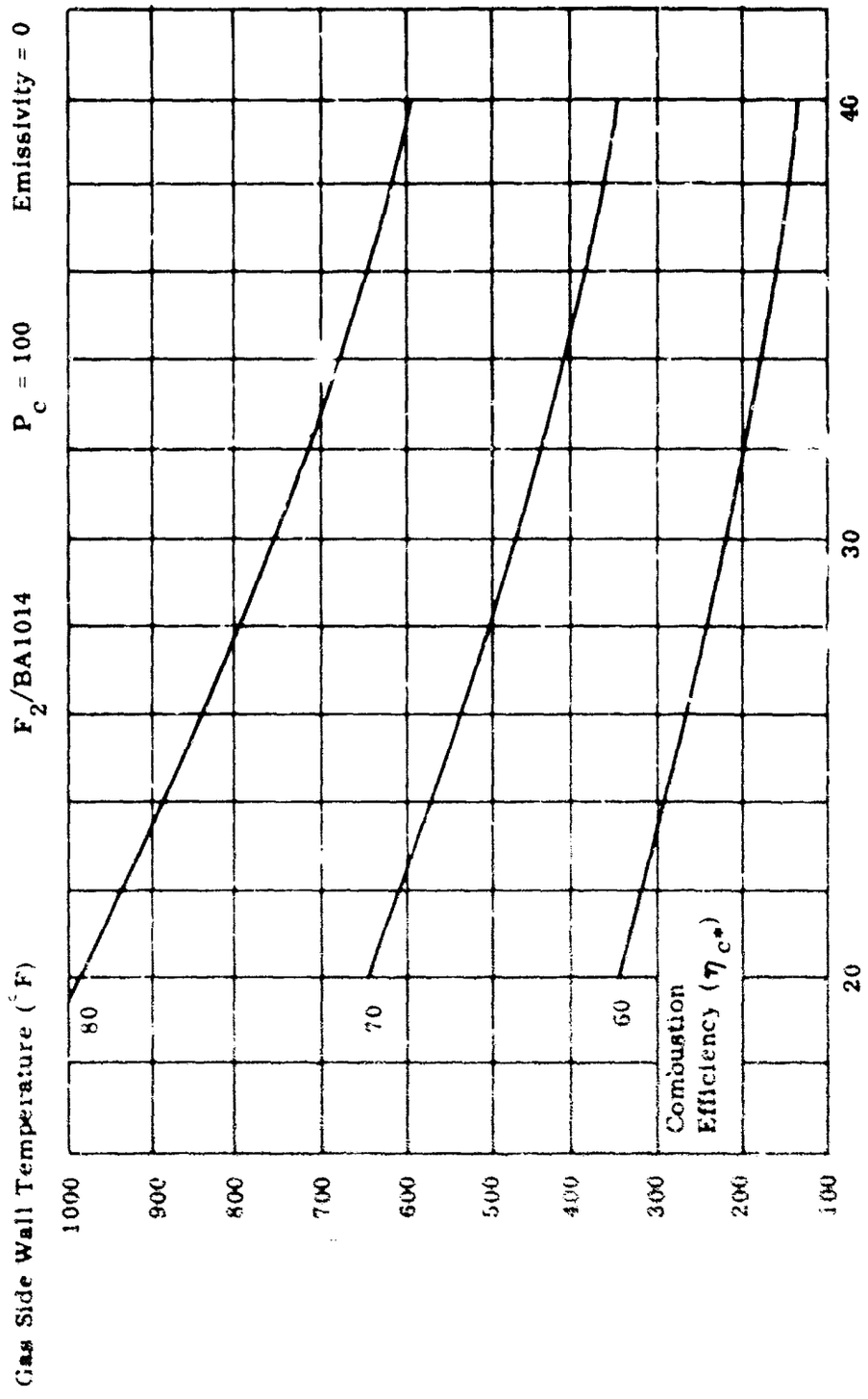


Figure 5. (U) Theoretical Wall Temperature, Oxidizer Rich Gas Generator

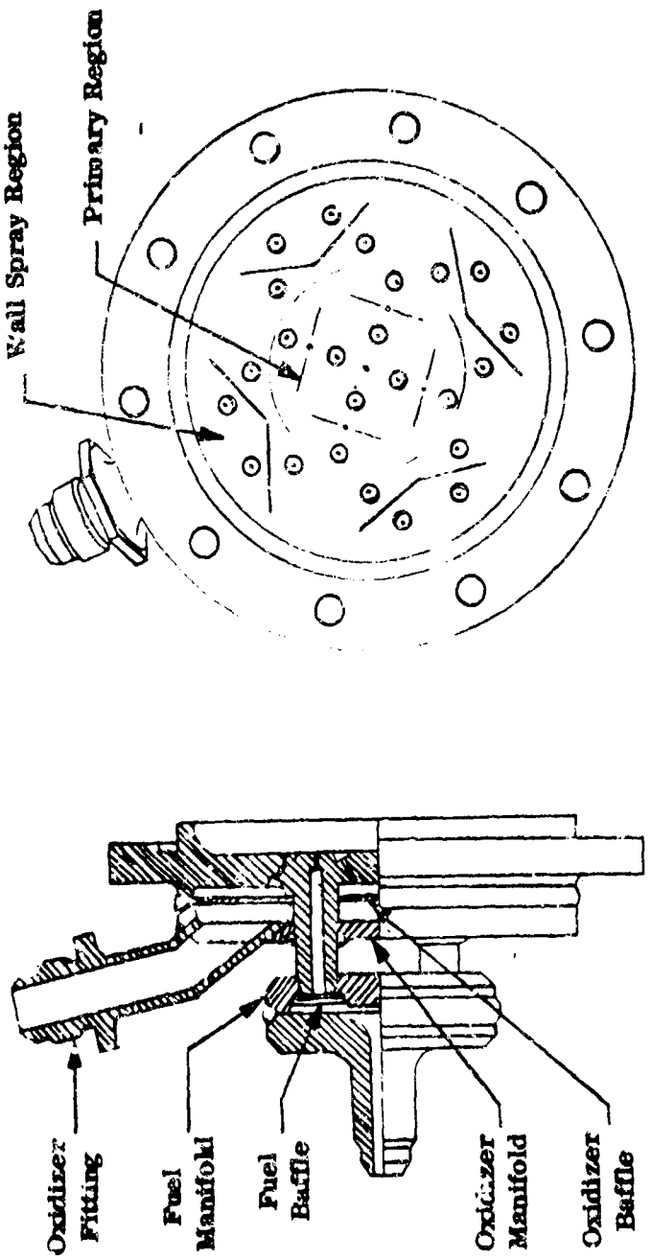


Figure 6. (U) Oxidizer Rich Gas Generator Injector S/N-1

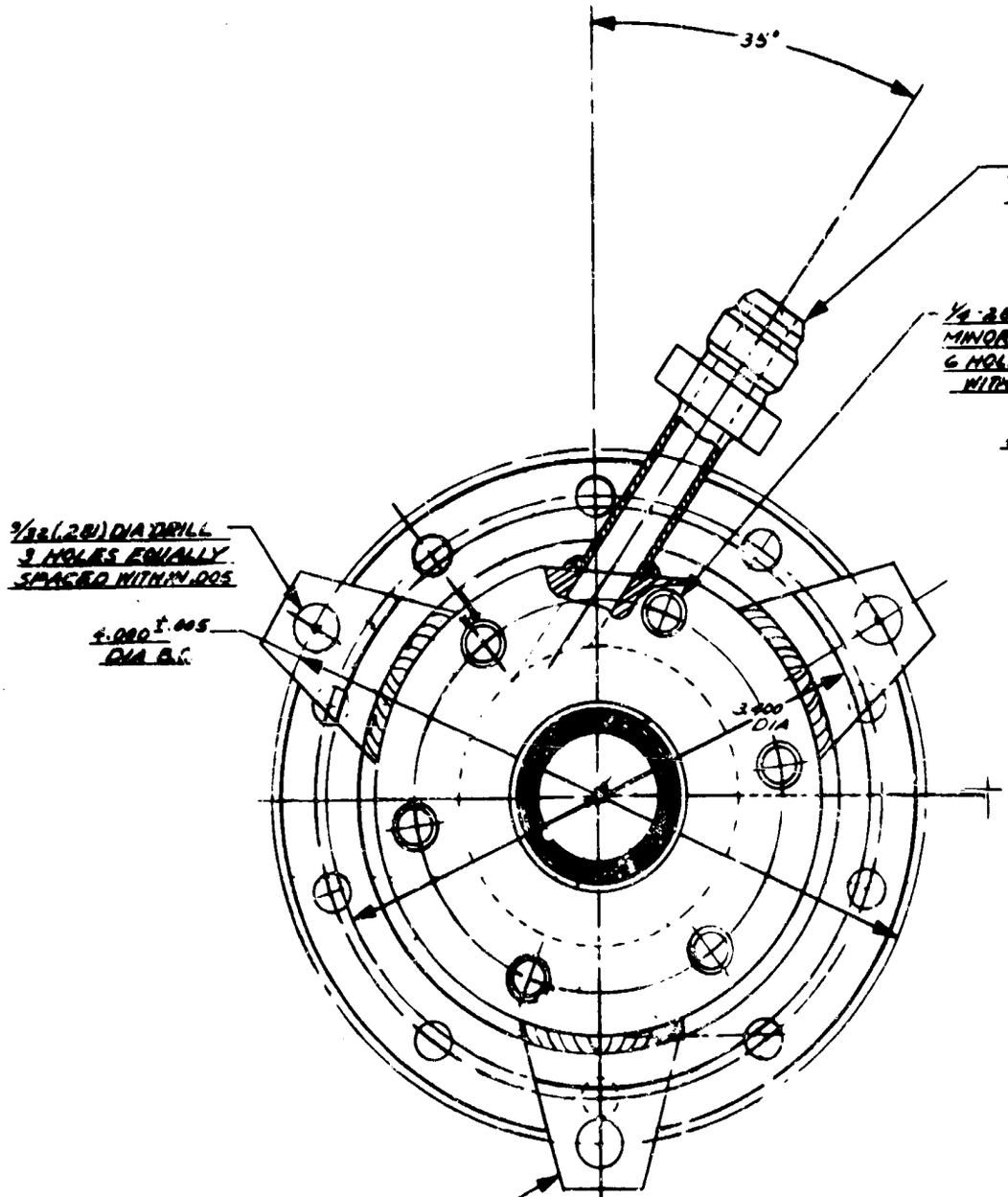
35°
8173-473003-1
FITTING
1/4-28 UNF-3B THRU
MINOR DIA .2113 +.002 -.003
6 HOLES EQUALLY SPACED
WITHIN .003
8173-473004-5
OX MANIFOLD
9/32 (.281) DIA DRILL
3 HOLES EQUALLY
SPACED WITHIN .005
4.000 ±.005
DIA B.C.
.266 DIA
(TYP)
3.400
DIA
.765 ±.010
DIA
8173-473004-1
ORIFICE PLATE
-3
-5
-7 LUG
3 REQ'D

Fi

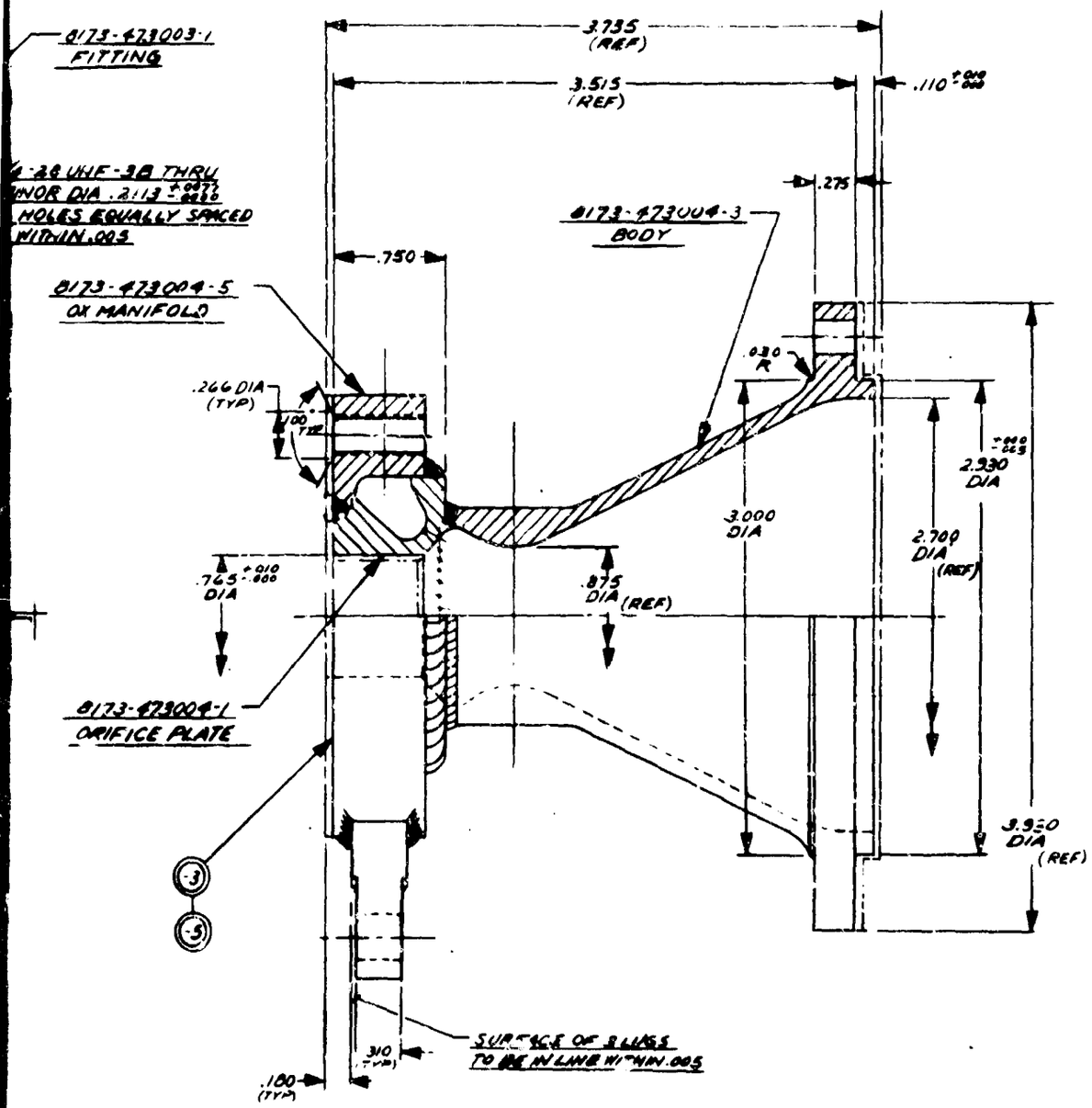


2

Figure 7. (U) 8173-473005 ORGG Conical Injector, Assembly of - S/N-2

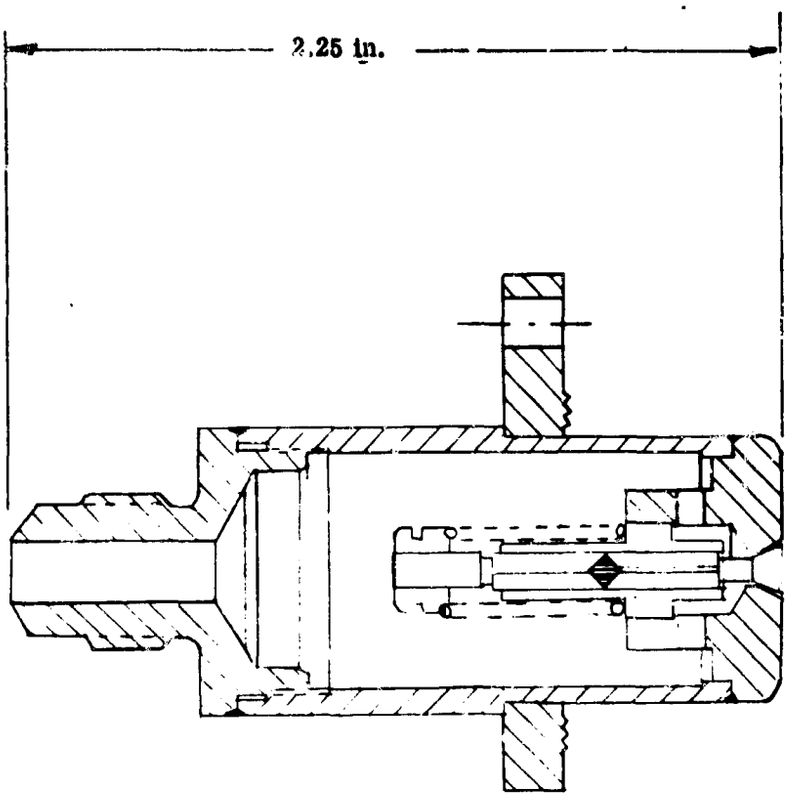


Figure 8. (U) Bendix Spring-Loaded Pintle Injection Nozzle

(C) 304 stainless steel and had a coverging-diverging section to obtain the proper combustion geometry. The convergent-divergent section was fabricated from Haynes 25 and welded to the stainless injector to obtain an injector assembly.

(U) Uncooled chamber sections were designed and fabricated to allow testing with combustion volume to mass flow ratios ranging from 8.6 to 30.0 $in.^3$/lb/sec to evaluate performance, stability and heat transfer characteristics.

3. (C) Test

(C) The oxidizer rich gas generator assembly consisted of the injector assembly bolted to a chamber section fabricated for Haynes 25 and bolted to an aluminum water cooled segmented nozzle. The test setup is shown in Figure 9. The water cooled nozzle was utilized to prevent potentially high wall temperatures resulting from high velocity combustion gases flowing through a sonic nozzle. This potentially high temperature condition would not be applicable once the generator was installed in a mixer assembly as the pressure drop from the generator to the mixer would range between 20 psi and 40 psi. The water cooled nozzle not only would provide heat transfer information for use in the design of the mixer, but also would indicate the degree of nonuniform combustion resulting with the particular injector.

(C) Nine tests were conducted on the various oxidizer rich gas generator configurations with the following results:

(a) (C) Two tests were conducted with the helical injector incorporating the Bendix variable area injection nozzle (sping-loaded pintle design) as shown in Figure 10. The tests were conducted in a chamber designed to give a volume of propellant to mass flow ratio of 15 $in.^3$/lb/sec with the following results:

(1) (C) The first test (1AW-601) was terminated after 4.3 seconds due to the ground safety chamber pressure switch automatically terminating the test. Chamber pressure was initially obtained and then decayed. Post-test inspection of the injection nozzle indicated that the injection nozzle was stuck in the closed position and would not open with a 60 psi pressure drop across the nozzle. Normal cracking pressure is 15 psi. The test data indicated performance of 68% combustion efficiency at a mixture ratio of 35.4 and a chamber pressure of 99.2 psia.

(2) (C) The injection nozzle was replaced and another test (1AW-602) was conducted but terminated after 8.0 seconds. Post-test inspection revealed a burnthrough of the conical section of the injector at the minimum diameter area (33% of the circumferential area). The test data taken at five seconds indicated a combustion efficiency of 67.5% at a mixture ratio of 39.4 and a chamber pressure of 94.5 psia. Post-test flow check of the injection nozzle indicated nonreproducible spray characteristics.

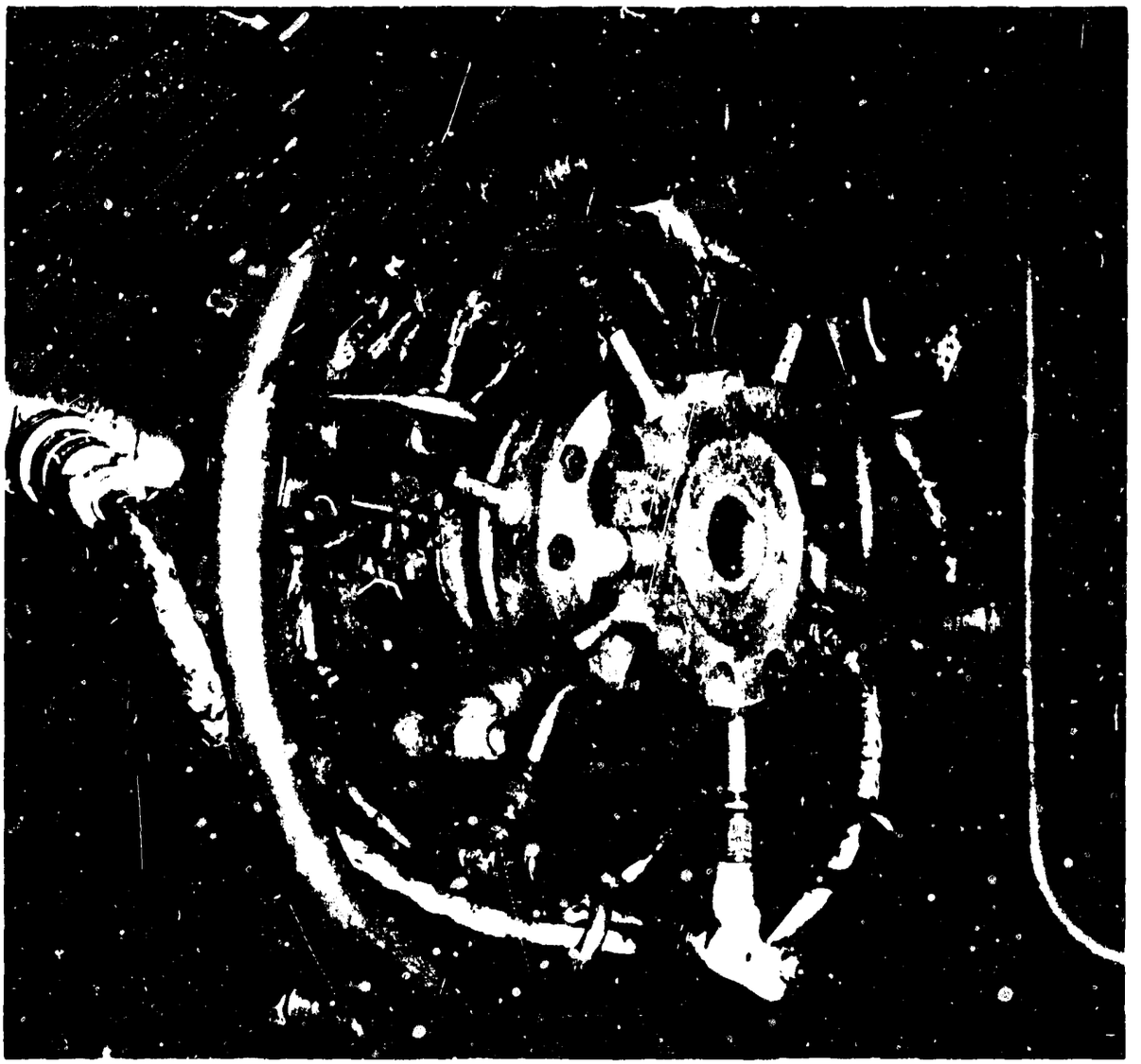

Figure 9. (U) Oxidizer Rich Gas Generator Test Setup

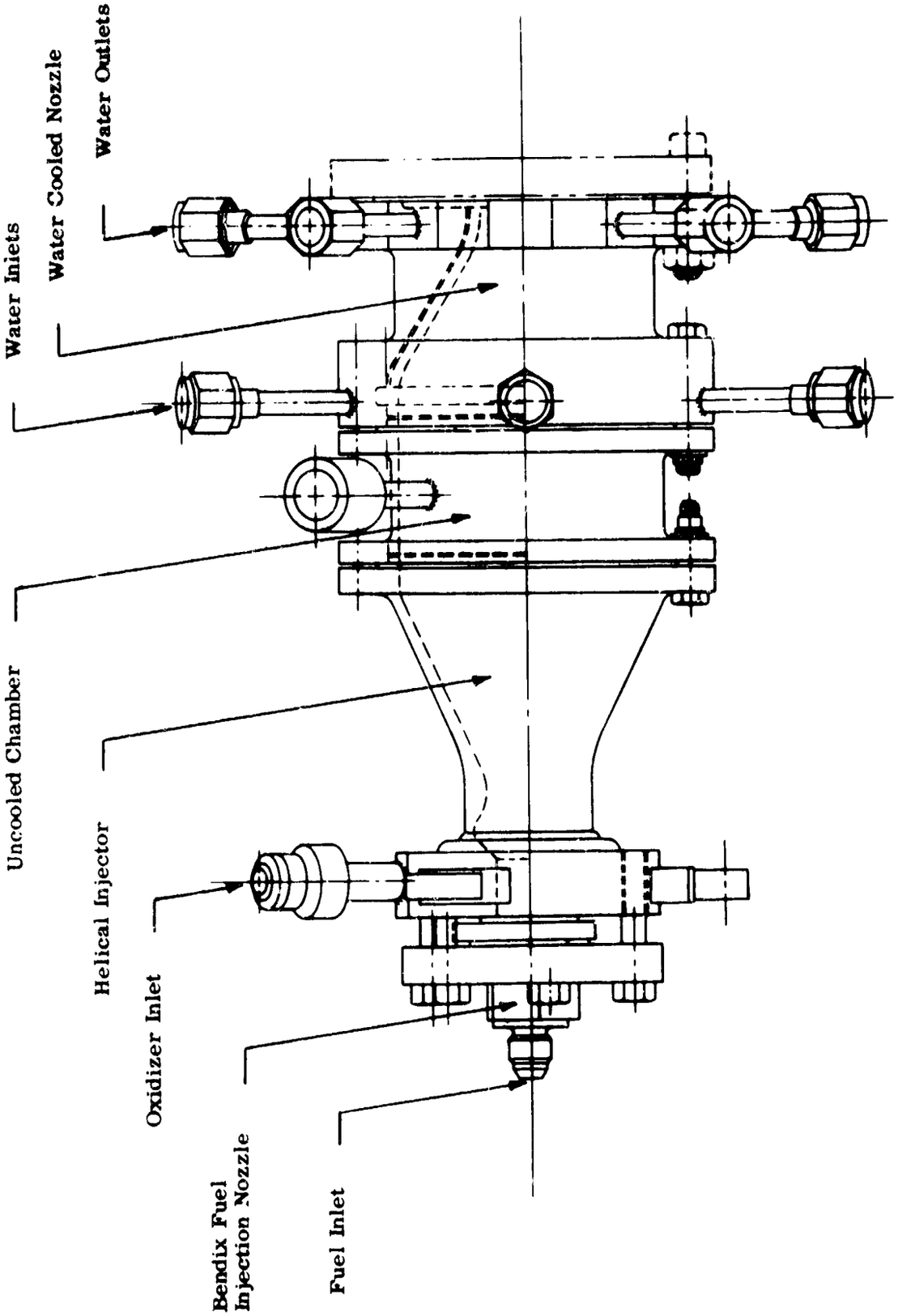


Figure 10. (U) Oxidizer Rich Gas Generator Assembly

(3) (C) The conclusions reached from these tests were that the Bendix injection nozzle cycled during the tests since it was dynamically unstable in the system utilized for testing and its nonreproducibility apparently caused the burnout. The tests conducted were not deemed conclusive in demonstrating the feasibility or infeasibility of operating a fluorine rich gas generator.

(4) (C) The following recommendation for redesign and additional testing were undertaken:

(a) (C) Design, fabricate and test a fixed orifice conical spray for use with the helical injector to determine the feasibility of operation of this type of oxidizer rich gas generator.

(b) (C) Design, fabricate and test a fixed orifice plug (single fuel stream) to replace the conical spray for use with the helical injector to determine the degree of combustion and feasibility of operation of a durable oxidizer rich gas generator with the propellant combination of $F_2$/BA-1014.

(b) (C) Two tests were conducted with the triplet injector incorporating four triplets and eight oxidizer barrier doublets. The results of these tests are summarized as follows:

(1) (C) A five-second test (1AW-603) was conducted as a checkout firing to determine the performance of this injector configuration using a 19.2 $in.^3/lb/sec$ volume of propellant to mass flow ratio. Performance during this test indicated a combustion efficiency of 91% at a mixture ratio of 34.3 and a chamber pressure of 130.7 psia. Post-test observation revealed that the $F_2$ test line just downstream from the stand valve (Annin) cracked and burned through (1/2 inch length) and revealed four holes (1/4 inch by 1/2 inch) located 45° to the triplets as shown in Figure 11 in an area of 0.5 to 0.7 inch downstream from the flange of the chamber where it is attached to the injector. A review of the data indicated the following:

(a) (U) The signal to close the fuel valve was given at 4.97 seconds and the fuel flow reached zero at 6.57 seconds based on the flowmeter data.

(b) (U) The oxidizer inlet pressure decay was initiated at 5.17 seconds and reached zero at 6.67 seconds even though the oxidizer stand valve signal to close was not given until 6.99 seconds and purge pressure was only 50 psi.

(c) (U) The oxidizer position indicator indicated the valve closed at 7.69 seconds.

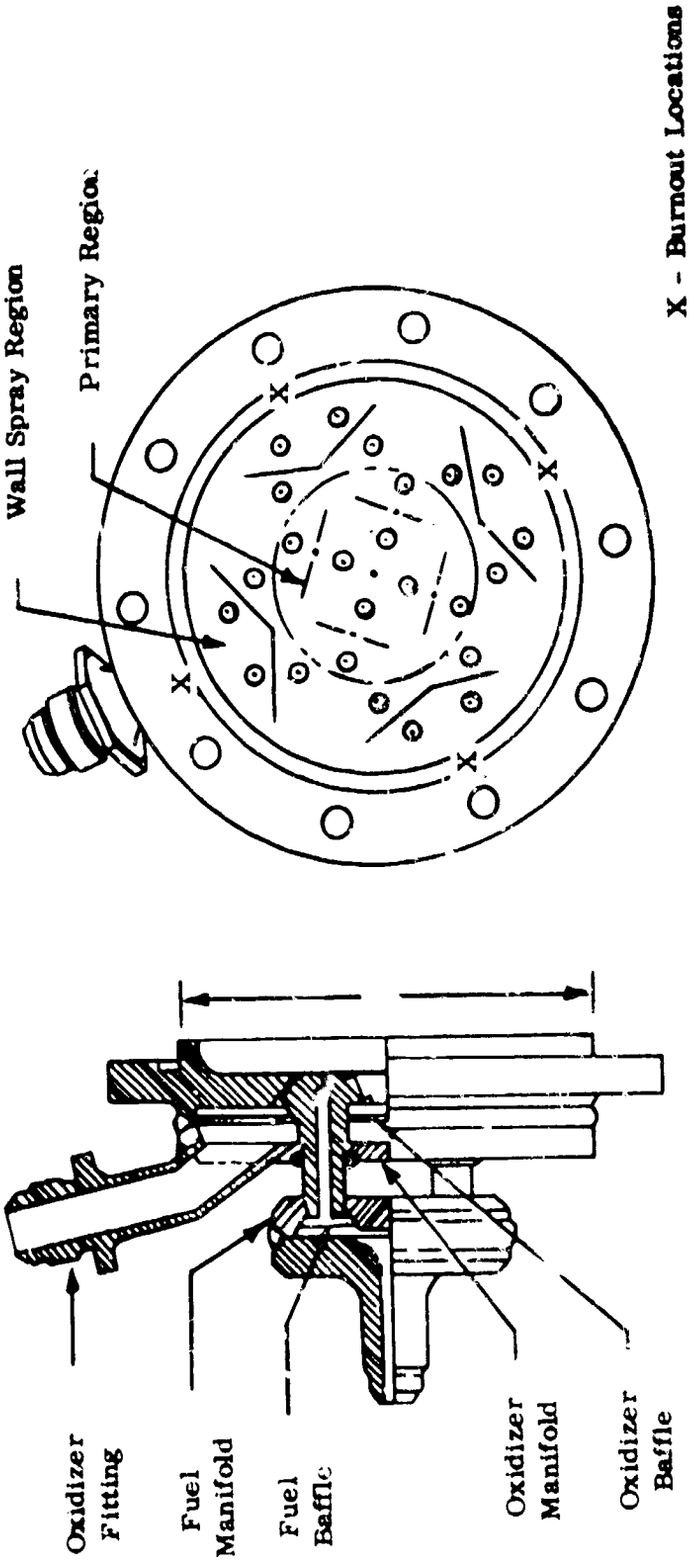


Figure 11. (U) Oxidizer Rich Gas Generator Injector - S/N-1

(d) (U) The skin temperatures rose sharply between 6.0 and 6.5 seconds but were less than 1300°F in all cases.

(e) (U) A review of the shutdown transients indicated the mixture ratio was 12 assuming liquid $F_2$ flow between 6.0 and 6.5. As gaseous $F_2$ flow occurred, this ratio was significantly less and in any case approached the high temperature regime which was the cause of the burnthrough.

(f) (U) The run was stable.

(g) (U) All material used for the $F_2$ line was 347 stainless steel which was cleaned, passivated, and freon leak checked twice (100 psi).

(h) (U) The purge dome pressure was 60 psi during the test and the oxidizer in-line pressure was 280 psia prior to shutdown.

(i) (U) Conclusions - The test liquid $F_2$ line broke apparently due to stresses caused by contraction in conjunction with fabrication at approximately five to six seconds which caused mixture ratios resulting in high combustion temperatures and caused the burnthrough of the oxidizer rich gas generator which occurred between six and seven seconds.

(j) (U) Recommendations for redesign and additional tests:

(1) (U) Redesign the test line to allow for more contraction to minimize built-in stresses.

(2) (U) Fabricate a new test chamber section

(3) (U) Test the injector in the presently available short chamber.

(c) (C) An intended 120-second test (1AW-604) was terminated at 5.2 seconds due to high skin temperatures. This test was conducted with a 10.7 $in.^3/lb/sec$ volume of propellant to mass flow ratio chamber with an indicated performance of 85.4% combustion efficiency at a mixture ratio of 34.4 and a chamber pressure of 122.7 psia. Post-test inspection revealed the entire chamber section between two flanges completely burned. A review of the data indicated the following:

(1) (U) The burnout came at 4.6 seconds.

(2) (U) The mixture ratio during the start transient was always greater than 34.

(3) (U) The fuel stand valve failed to close and full fuel flow remained for 5.20 seconds after the command to shutdown which allowed the mixture ratios to approach the stoichiometric regime during the period of operation.

(4) (U) The maximum skin temperature during the test was 1850°F.

(5) (U) The oxidizer side of the injector increased its pressure drop by 20 psi, thus indicating there was probably some gas in the injector.

(6) (U) Conclusions - It appeared that this injector did not have the capability of operation as an oxidizer rich gas generator at a mixture ratio of 34 and a chamber pressure of 123 psia in an uncooled Haynes 25 chamber (uncoated). The triplet was too powerful for the barrier doublets under these conditions.

(d) (C) Five tests were conducted with the helical injector using various fuel plugs to replace the Bendix injection nozzle. Figure 12 shows the helical injector spray pattern in water flow test. The results of this series of tests are summarized as follows:

(1) (C) The helical injector with a fixed orifice fuel plug (0° conical angle) was tested for 3.6 seconds (1AW-605). The test was terminated due to a frozen fuel line. The volume of propellant to mass flow ratio for this test was 8.6 $in.^3/lb/sec$.

(2) (C) Test (1AW-606) was conducted as a repeat of the previous test with chamber pressure reaching 20 psia and allowing a great deal of combustion to occur outside of the nozzle.. There was no indication of high temperature in the gas generator.

(3) (C) Test (1AW-607) was conducted using the short chamber bolted to the injector and nozzle to yield 15 $in.^3/lb/sec$ of propellant volume to mass flow ratio. However, similar results occurred as in the previous test.

(4) (C) The single orifice fuel plug was replaced with a fixed orifice conical (40° angle) fuel spray and the helical injector was tested with the short chamber for 5.3 seconds (1AW-608) indicating no problems. The propellant volume to mass flow ratio utilized for this test was 15 $in.^3/lb/sec$. Performance during this test was 77% combustion efficiency with a mixture ratio of 35.0 and a chamber pressure of 110.6 psia.

(5) (C) A scheduled 120-second test (1AW-609) was attempted but terminated after 8.8 seconds due to a burnthrough of approximately 2/3 of the conical section of the helical injector and, in addition, two small holes burned through the chamber. The performance during this test was 75.4% combustion efficiency at a mixture ratio of 35.1 and a chamber pressure of 107.4 psia. The conclusion drawn from this

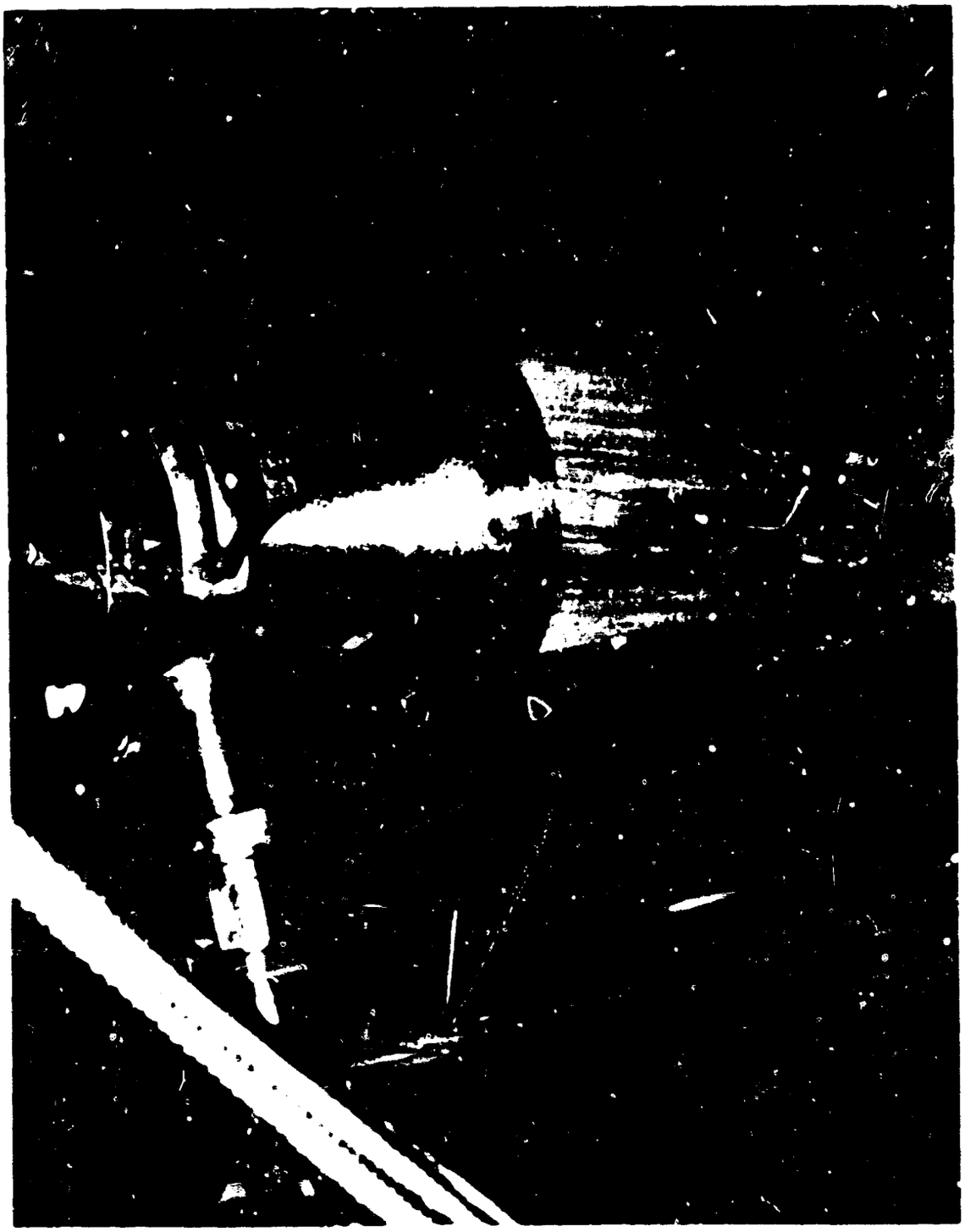

Figure 12. (C) Helical Injector Spray Pattern

(C) test was that the 40° conical fuel spray angle was too great and, therefore, a reduced conical angle was required to operate this type of oxidizer rich gas generator.

(e) (C) Summary of Oxidizer Rich Gas Generator Tests

The results of the fluorine (oxidizer) rich gas generator tests indicated the following:

(1) (C) The helical injector using the Bendix nozzle (conical spray) was not adequate because the nozzle was dynamically unstable in the system utilized for testing.

(2) (C) The helical injector using a 40° angle conical fuel spray (fixed orifice) was not adequate because the angle was too great.

(3) (C) The helical injector using a 0° angle fuel spray allowed combustion to occur downstream from the nozzle.

(4) (C) The triplet injector was not adequate because the triplets were too powerful for the barrier doublets in the particular design.

4. (C) Conclusions and Recommendations

(C) As a result of the helical injector testing conducted, the recommendation was made to utilize this injector configuration with a conical angle fuel spray ranging from 5 to 20° predicated upon the fact that a 0° conical angle fuel spray was successful although it gave low combustion efficiency and the 40° conical angle fuel spray resulted in a burnthrough of the generator. It may be well to point out that high gas generator performance is not required in the two-stage combustion concept but the fact that combustion occurred outside the nozzle in the 0° angle fuel spray tests may present problems due to impingement of high temperature gases on the thrust chamber wall. In addition, it was recommended to:

(a) (C) Utilize a triplet injector which strictly has a series of triplets without any barrier doublets.

(b) (C) Utilize a triplet injector with the primary core mixture ratio operating at a lower temperature than the tested configuration and utilize the oxidizer barrier doublets.

(c) (C) Utilize a four oxidizer on one fuel injector with no barrier doublets to completely mask the fuel.

(C) Predicated upon the successful results of other gas generator injector programs utilizing high energy propellants at BAC, it was also recommended that a coaxial injector be evaluated for a fluorine rich gas generator.

# SECTION 5

# (U) THRUST CHAMBER MATERIALS PROGRAM

## A. (U) GENERAL

(U) Critical experiments were conducted to substantiate the assumptions made that high temperature materials are compatible with main core products of combustion and fuel rich products of combustion from the propellant combination of fluorine and a hydrazine blend (BA-1014). The material limitations of each section of the adiabatic wall thrust chamber were determined to design the thrust chamber with adequate cooling for operation with these high energy propellants. This program, which was divided into two sections, is discussed in the following paragraphs.

## B. (U) TECHNICAL DISCUSSION

(U) A literature survey was conducted to determine the maximum operational limitations for materials and coatings for use on an adiabatic wall thrust chamber using the propellant combination of fluorine and BA-1014. Based upon these results and the application of chemical and metallurgical theory and background information, in addition to thermodynamic heat flux analyses, materials and coatings were recommended for use on an adiabatic wall thrust chamber.

(U) Thrust chamber tests at a subscale level were conducted to determine the operational limitations of materials and coatings for use in fuel rich environments and main core environments with the high energy propellant combination of fluorine and BA-1014. This information was utilized in the design of the adiabatic wall thrust chamber.

### 1. (U) Literature Survey

(U) A literature survey was conducted to determine the availability of materials and coatings and their operational limitations for use with adiabatic wall thrust chambers with the propellant combination of fluorine and BA-1014. Based upon these results and the application of theoretical, chemical and metallurgical background information in addition to thermodynamic heat flux analyses, materials and coatings were recommended for use as an adiabatic wall thrust chamber. A review of the literature survey is summarized as follows:

a. (U) Feasibility Investigation of Uncooled Thrust Chamber and Nozzle Designs - Second Quarterly Progress Report, January 30, 1962, by E.P. Bartlett, et al, Aeronutronics Corp.

(U) A study was conducted to determine the feasibility of using lightweight uncooled thrust chambers in corrosive liquid propellant systems for long duration (120 seconds maximum and 360 seconds accumulated time) firings to

(U) withstand high temperatures (5500 to 7500°F) and chamber pressure (50 to 500 psia). $F_2/H_2$ was the propellant system utilized. An analytical screening phase considered the equilibrium behavior of tungsten, graphite, and refractory carbides, nitrides and oxides in the combustion products of $F_2/H_2$ over the previously discussed operating conditions. A 125-lb $F_2/H_2$ thrust chamber was used for screening the materials. The work was conducted with ablatives and various inserts with the result that graphite and tungsten showed excellent compatibility in an HF environment.

b. (U) Thermal Protection of Uncooled Rocket Thrust Chambers - Special Report January 31, 1961, E.P. Bartlett et al, Aeronutronics Corp.

(U) Information was presented in the report to aid the designer in the selection of materials and the sizing of liner thickness required for thermal protection of uncooled rocket thrust chambers. The data presented were mostly for ablative materials such as selected referenced plastics (nylon-phenolic, fiberglass-phenolic and refrasil-phenolic) in addition to two slowly or nonablating refractories such as pyrolytic graphite and polycrystalline graphite insulated with porous carbon. The data were obtained from small-scale experimental thrust chambers using $O_2$/RP-1 and $F_2/H_2$ propellant systems; the data were then extrapolated by means of several theoretical analyses.

c. (U) Study Program of Improved Thrust Chamber Cooling Methods, Final Report by W. Kaufman et al, Aeronutronics Corp., January 31, 1961

(U) This report evaluated refractory and ablative liners for thermal protection of uncooled thrust chambers. The operating conditions were 5800°F nominal combustion temperature with the propellant combination of $O_2$/RP-1 and 7000°F or greater nominal flame temperature with the propellant combination of $F_2/H_2$.

d. (U) Study of Improved Thrust Chamber Cooling Methods Final Report, January 30, 1960, J. Neustein et al, Aeronutronics Corp.

(U) This report experimentally evaluated materials for thermal protection of thrust chambers primarily concerning correlation with ablation theory.

e. (U) Feasibility Investigation of Uncooled Thrust Chamber and Nozzle Designs, Third Quarterly Report, April 30, 1962 by E.P. Bartlett et al, Aeronutronics Corp.

(U) This report primarily discussed the results of 12 test firings conducted on nine nozzles incorporating graphite and tungsten inserts. The total duration accumulated was 12 minutes with low throat erosion in most cases. In addition, 11 tests were conducted on seven thrust chambers with an accumulated duration of 12 minutes.

f. (U) Feasibility Investigation of Uncooled Thrust Chamber and Nozzle Designs, Fourth Quarterly Progress Report, July 30, 1961, E.P. Bartlett et al, Aeronutronics Corp.

(U) Predicated upon the results of screening tests which were conducted during this report period, four uncooled thrust chamber designs were selected for design development. These thrust chambers incorporated throat inserts of free standing pyrolytic graphite, high density graphite, high density graphite using a graphite insulation, and carbon/phenolic.

g. (U) Feasibility Investigation of Uncooled Thrust Chamber and Nozzle Designs, Final Quarterly Progress Report, November 19, 1962, E.P. Bartlett et al, Aeronutronics Corp.

(U) Analyses were performed and small scale screening tests were conducted which indicated the most promising throat inserts were tungsten and high density graphites with the most promising design concepts being radiation cooled and insulated. The most promising nozzle design employing radiation cooling utilized edge grain pyrolytic graphite washers with a chamber of high density graphite insulated with a pyrolytic graphite sleeve.

h. (U) Applied Research for Advanced Cooled Nozzles, Second Quarterly Report, December 15, 1962, W.H. Armour et al, Aeronutronics Corp.

(U) This work was directed toward an advancement in the design of high energy solid rocket nozzles using advanced propellants of the aluminized and $NF_2$ types.

i. (U) Miscellaneous Information

(U) The Marquardt Corporation reported that a tantalum (10% tungsten) alloy and pure tungsten have withstood 3000°F with the propellant combination of chlorine trifluoride and 75% $N_2H_4$/25% MMH whereas pyrolytic graphite showed some slight erosion under the same conditions and the same propellant combination. In addition, a silicide coating was destroyed during the same conditions.

(U) The following conclusions apply to coatings of columbium in a 3000°F environment of fluoride/hydrazine:

(1) (U) Conventional and diffusion coatings can be applied via chemical chamber deposition.

(2) (U) The initial problem is to find a compound which is not appreciably affected by hydrogen fluoride at 3000°F under repeated temperature cycling and exposure.

(3) (U) Nonmetallics which can sustain the effects of an oxidizer (fluorine) for periods greater than 10 hours at 3000°F may reasonably be considered as candidate materials.

(4) (U) Mixtures of oxides and high melting fluorides could lead to interesting possibilities for protection of columbium. Columbium forms a number of complex oxyfluorides about which little is known.

(5) (U) In addition to chemical coating deposition, electrophoretic deposition may be an additional technique for the initial deposition for the large group of materials.

(6) (U) Composite materials also deserve consideration.

2. (U) Thrust Chamber Materials Evaluation

a. (U) Design Analysis

(U) Thrust chamber tests will be conducted at the subscale level to determine the operational limitations of materials and coatings for use in an adiabatic wall thrust chamber design in both fuel rich and main core environments with the propellant combination of fluorine/BA-1014.

(U) Heat transfer analyses were conducted to determine the wall temperatures for testing the various materials utilizing company R&D hardware available at the 200-lb thrust level. An existing injector allowed operation of a fluorine/BA-1014 propellant combination over a mixture ratio range of 0.7 to 2.4. Figure 13 shows the injector available for use on this program. Heat transfer analyses were conducted based upon the same method discussed in Section 4. Figure 14 shows the results of the heat transfer analysis predicated upon a 0.65 wall emissivity for both a 90% and 95% combustion efficiency at a chamber pressure of 100 psia. The 0.65 emissivity is predicated upon the utilization of a silicide coating on the exterior surface.

(U) Similar analyses were conducted on the fuel rich regime based upon the results of the theoretical propellant performance analysis and the method of heat transfer analysis shown in Section 4. The results of this analysis are shown in Figure 15 over a mixture ratio range of 0.04 to 0.10 for combustion efficiencies ranging from 50 to 90% and predicated upon a wall emissivity approaching zero. Based upon the results of the $N_2O_4$/50-50 program, it was anticipated the combustion efficiency would result in approximately 85% of theoretical predicated upon 50% dissociation of ammonia. Based upon this combustion efficiency, operation of the fuel rich gas generator at a mixture ratio of 0.1 would result in a gas side wall temperature of 1350°F. Should nonuniform combustion occur, as would result at localized temperatures significantly above this value, the mixture ratio could be decreased to

Figure 13. (U) Injector for Use with Fluorine/BA1014 Fuel Blend

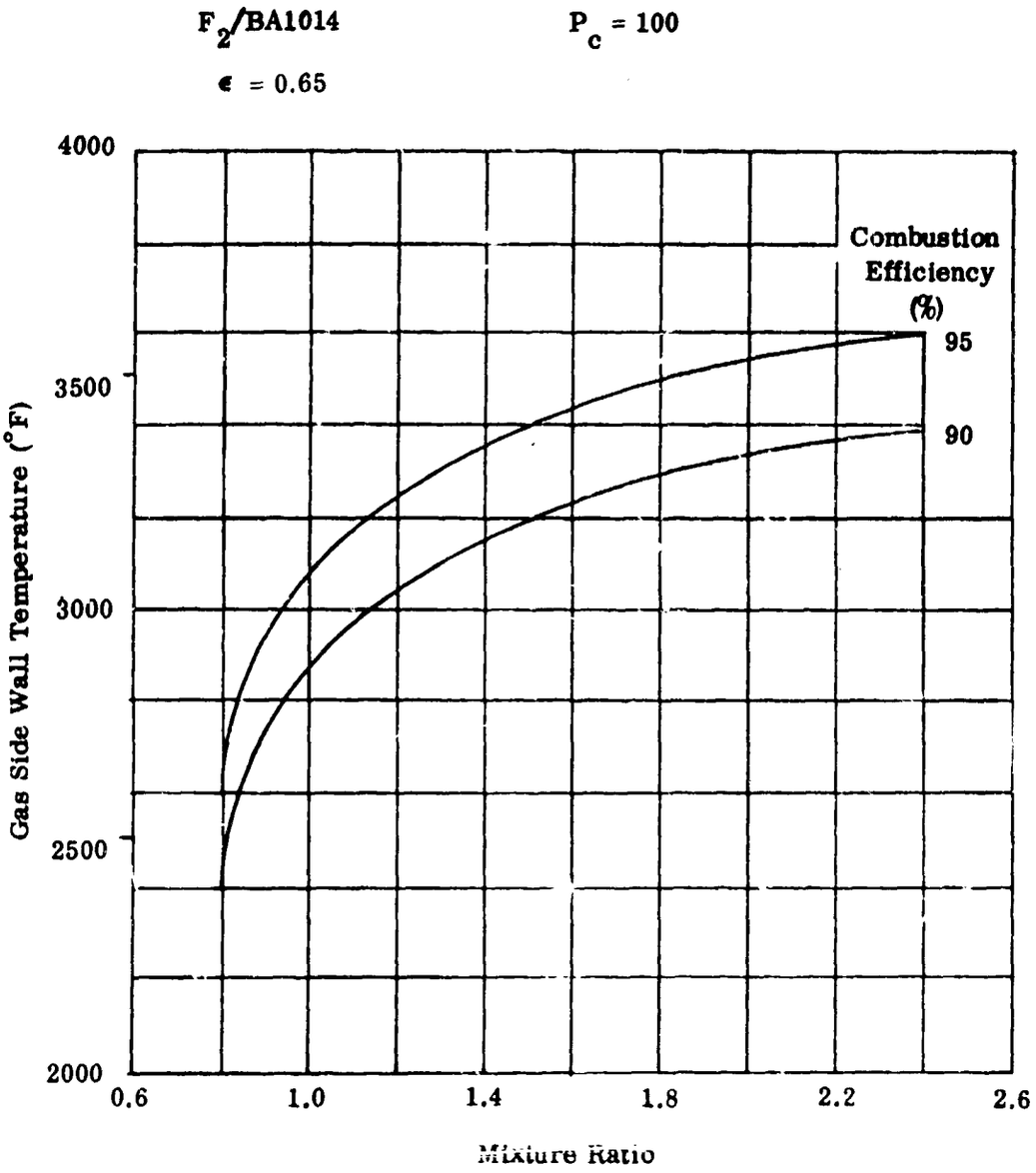


Figure 14. (U) Theoretical Wall Temperature versus Mixture Ratio

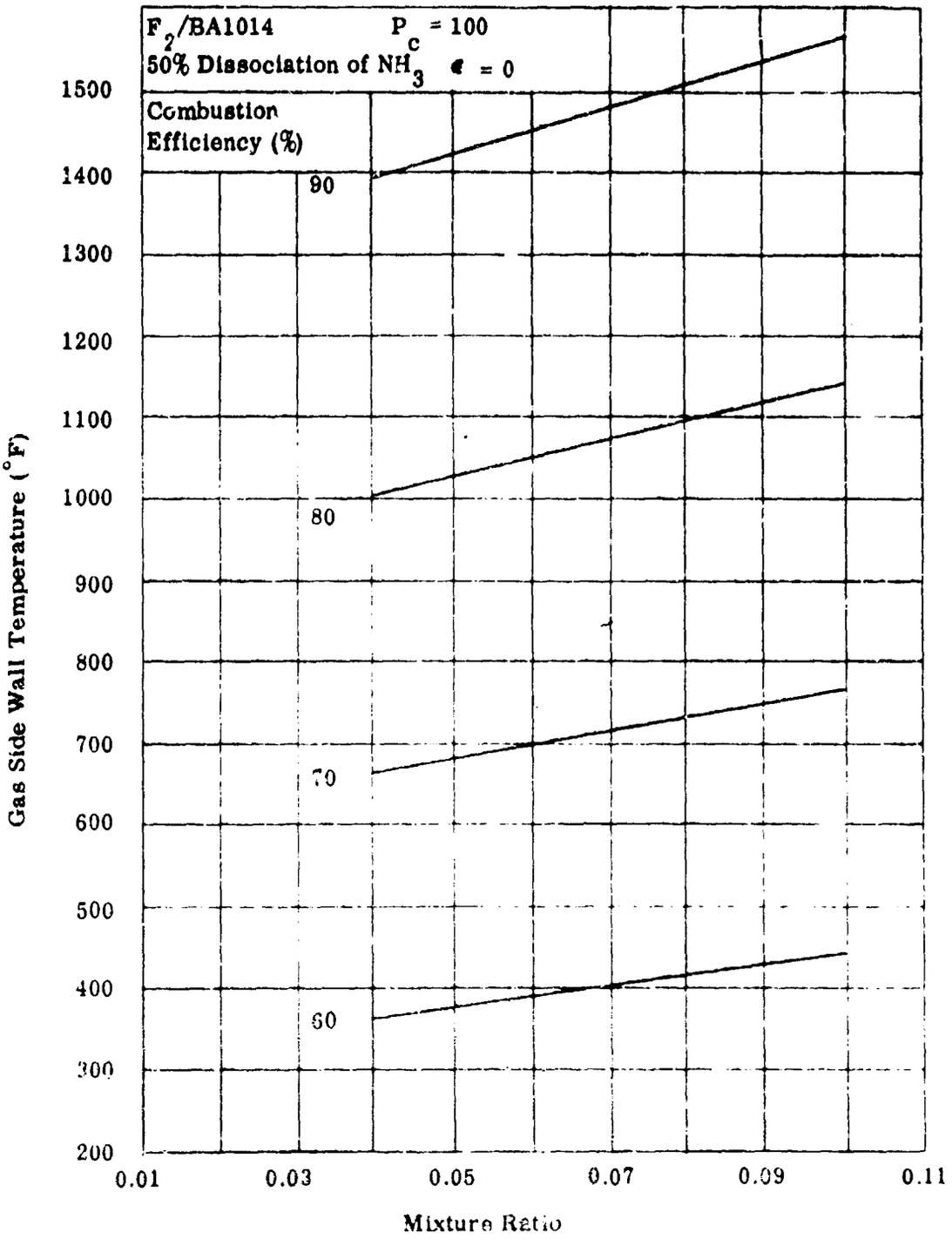


Figure 15. (U) Theoretical Wall Temperature versus Mixture Ratio, Fuel Rich Gas Generator

(U) 0.04 which would result in a gas side wall temperature of 1200°F and would allow for more reliable operation as nonuniform combustion occurs.

b. (U) Design and Fabrication

(U) Thrust chamber tests were conducted on three materials to determine their operational limitations for use in adiabatic wall thrust chamber design with the propellant combination of fluorine/BA-1014. Therefore, radiation cooled chamber sections of pure tungsten, columbium (SCb-291) alloy and graphite cylinders housed in a tungsten retainer were designed as shown in Figure 16.

(U) A contract was signed with Super-Temp Corporation to fabricate the tungsten chamber sections and the tungsten retainer by spinning from wrought material. However, Super-Temp was unable to spin the part to the configuration shown in Figure 17. Therefore, the part was fabricated from pressed and sintered material with the wall thickness increased to 0.25 inch. However, the part as received from Super-Temp was 0.22 inch. The tungsten chamber was then coated externally with a silicide coating to protect from oxidation from the surrounding air environment and to allow for high emittance ($\epsilon$ = 0.65) to dissipate the heat by radiation. No internal coating was utilized on the tungsten parts in order to determine the compatibility with the main core products of combustion and from the fuel rich products of combustion.

(U) Super-Temp Corporation fabricated two SCb-291 columbium alloy chamber sections as shown in Figure 18 by spinning from wrought material. The parts were then coated with a silicide coating externally to protect against oxidation from the surrounding air environment and to allow for high emittance ($\epsilon$ = 0.65) and was coated internally with an aluminide coating to protect the columbium from the products of combustion.

(U) Two graphite cylinders were also fabricated by Super-Temp Corporation and were tested with a tungsten retainer which was coated externally with a silicide coating. No coating was used internally.

c. (U) Test Results

(U) The high temperature material sections were assembled with an injector and installed between a water cooled chamber section and a water cooled nozzle section as shown in Figure 19. The water cooled chamber section was utilized to eliminate the injector effects to allow for homogeneous combustion gas at uniform temperatures. The water cooled nozzle was utilized to obtain nozzle heat rejection to aid in the design of the adiabatic wall thrust chamber. Tests were conducted at a chamber pressure of 100 psia at the 200-lb thrust level over a mixture ratio range varying from 0.8 to 2.2.

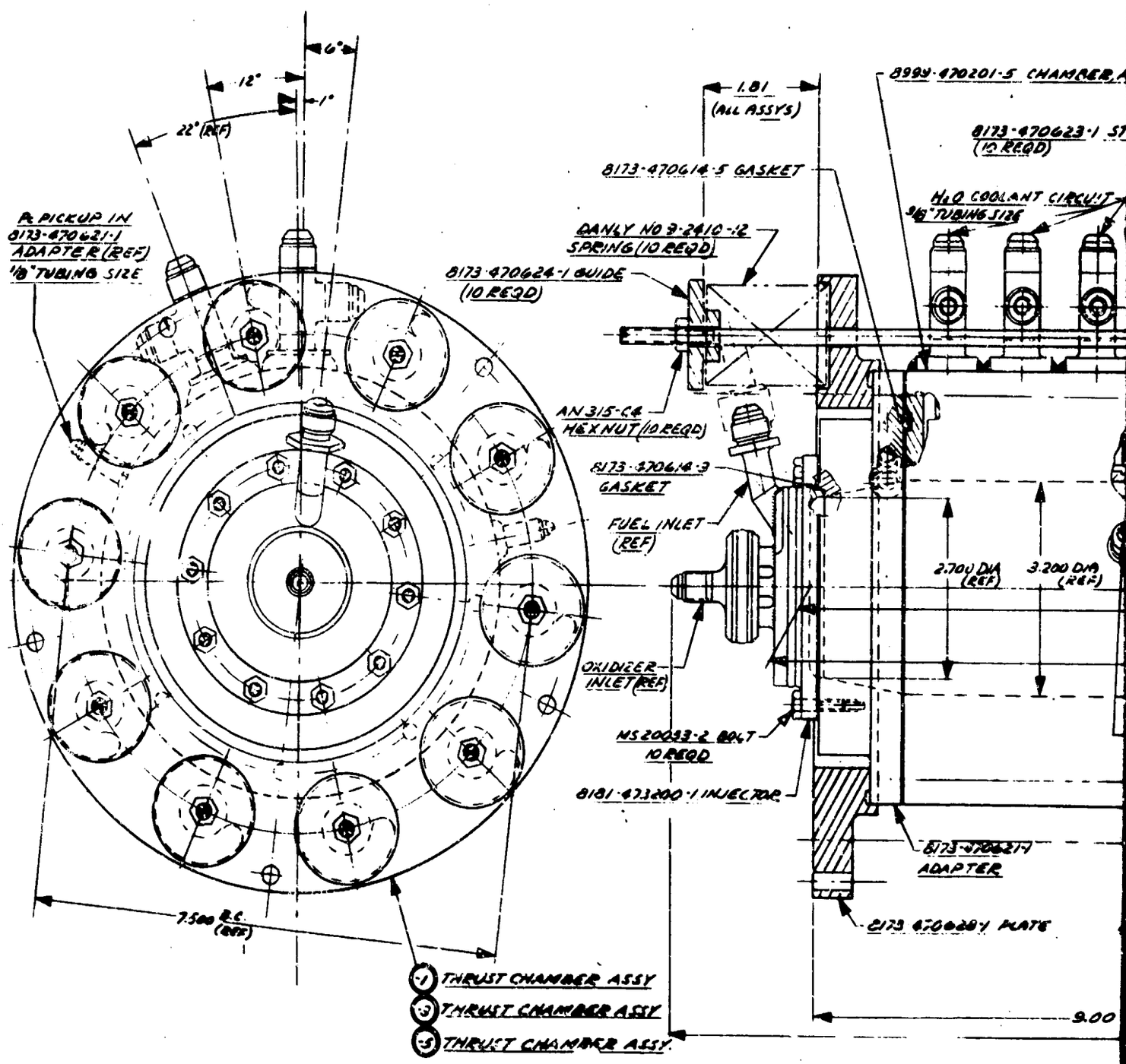
6°
12°
1°
22° (REF)
P, PICKUP IN
8173-470621-1
ADAPTER (REF)
1/8" TUBING SIZE
1.81
(ALL ASSYS)
8173-470614-5 GASKET
8173-470623-1 ST
(10 REQD)
H2O COOLANT CIRCUIT
3/16" TUBING SIZE
DANLY NO 3-2410-12
SPRING (10 REQD)
8173-470624-1 GUIDE
(10 REQD)
AN 315-C4
HEX NUT (10 REQD)
8173-470614-3
GASKET
FUEL INLET
(REF)
2.700 DIA
(REF)
3.200 DIA
(REF)
OXIDIZER
INLET (REF)
MS 20033-2 BOLT
10 REQD
8181-473200-1 INJECTOR
8173-470621-1
ADAPTER
8173-470628-1 PLATE
7.500 B.C.
(REF)
-1 THRUST CHAMBER ASSY
-3 THRUST CHAMBER ASSY
-5 THRUST CHAMBER ASSY
9.00

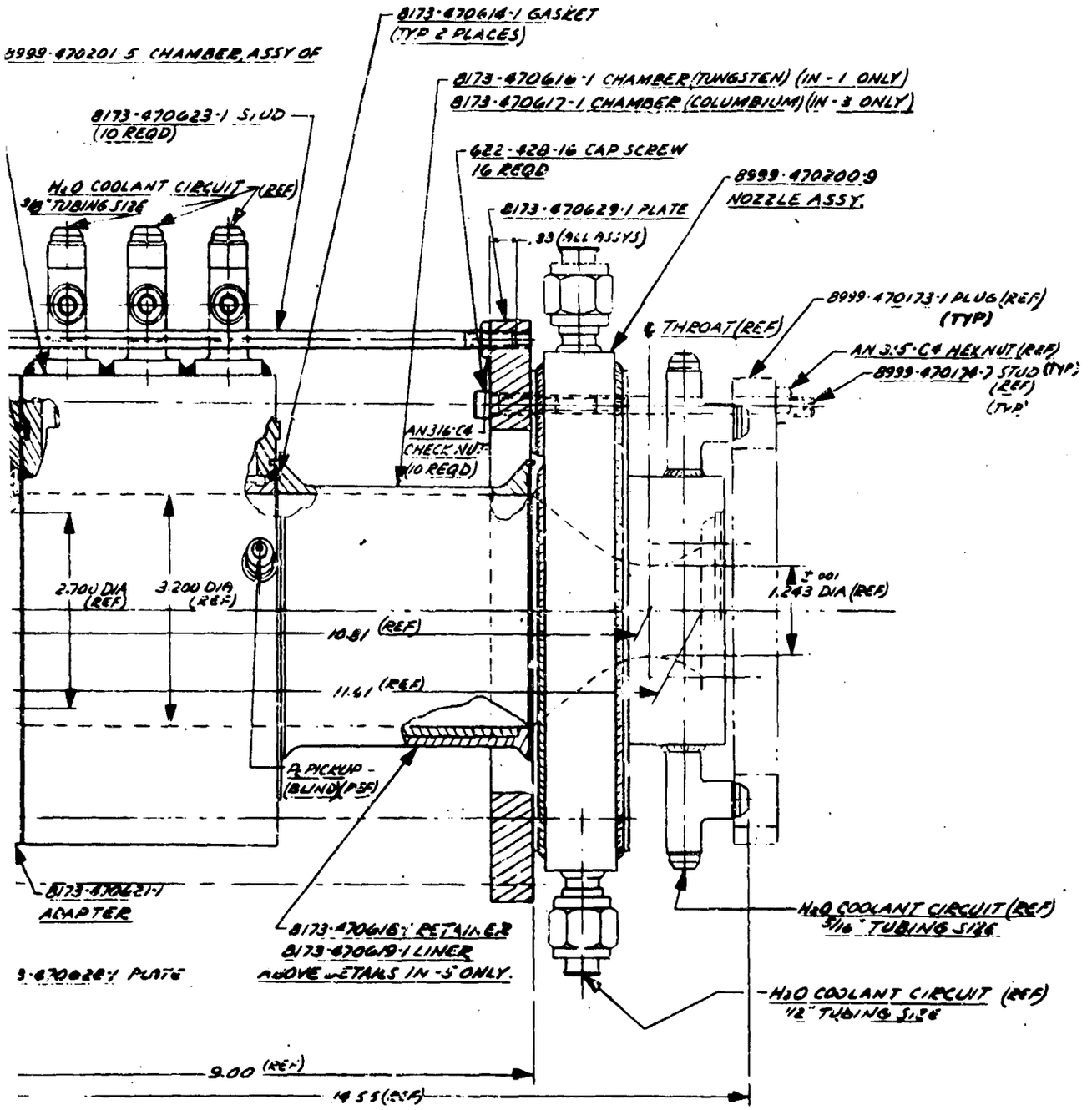


Figure 16. (U) 8173-470625 200-lb Thrust Chamber Assembly Materials Evaluation

2

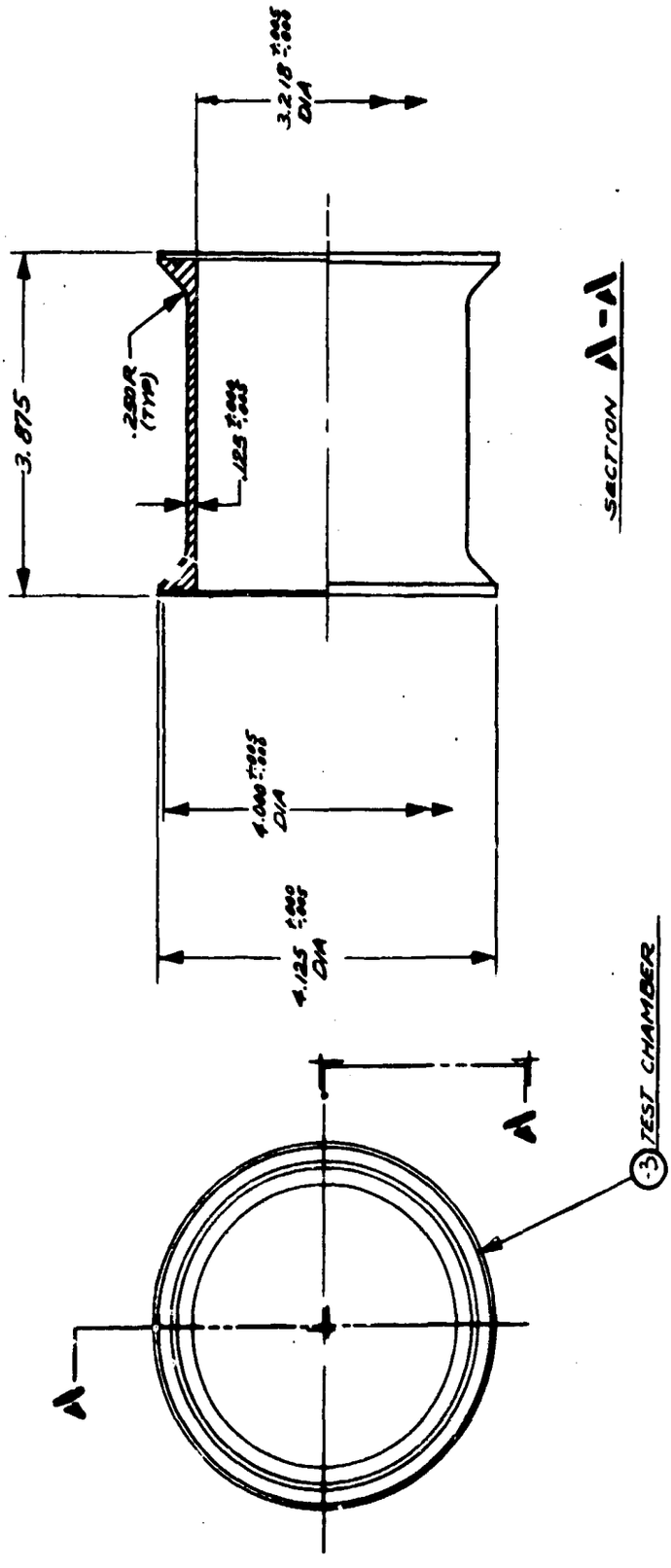


Figure 17. (U) 8173-470616 Tungsten Test Chamber – Radiation Cooled Section

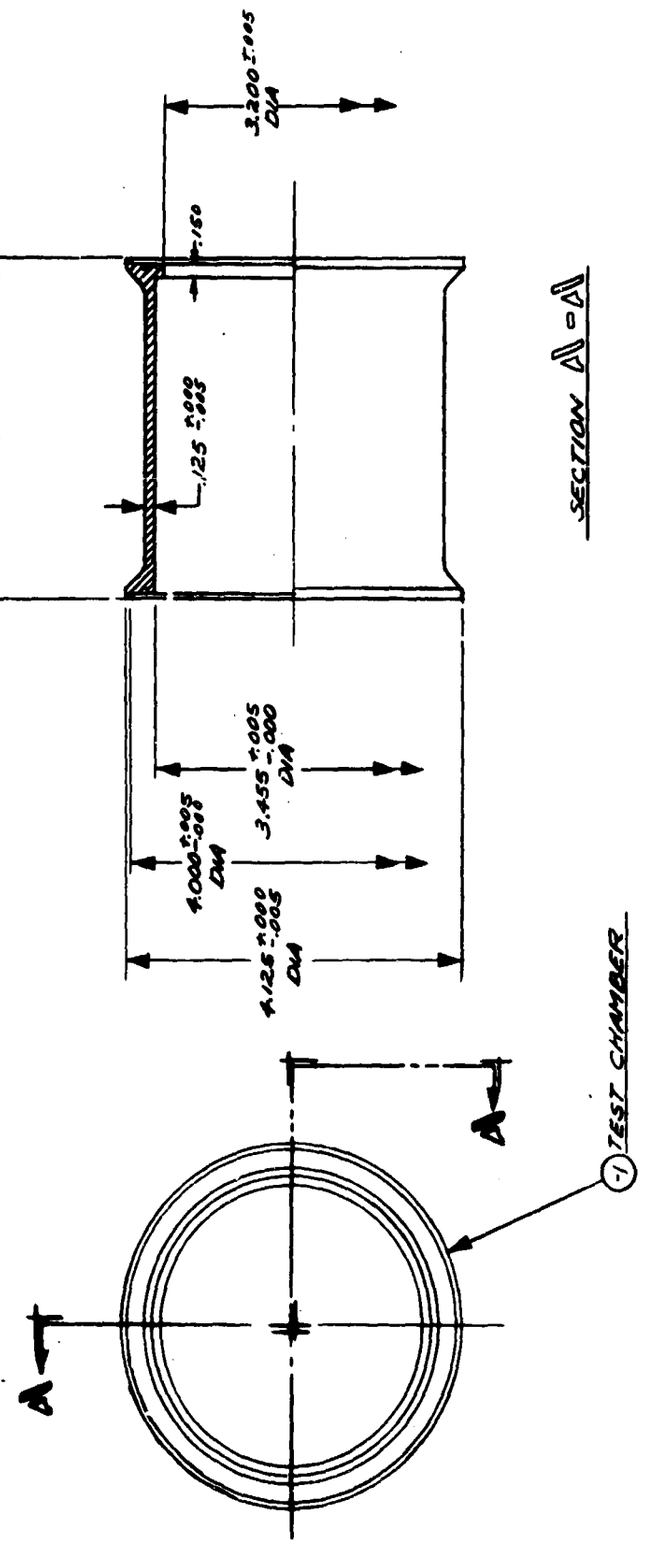


Figure 18. (U) 8173-470617 SCb-291 Test Chamber – Radiation Cooled Section

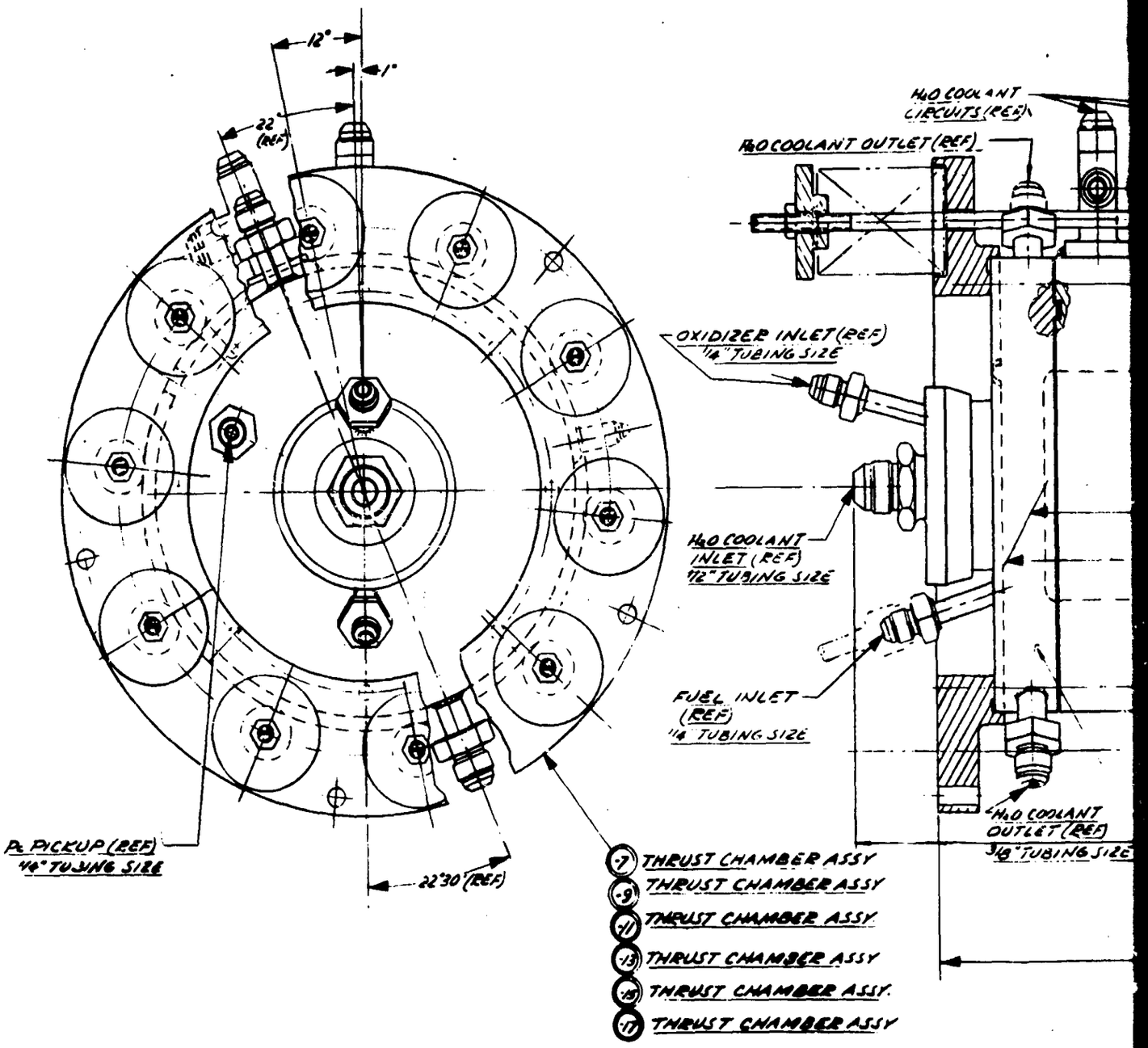


Figure 19. (U) 8173-470625 200-lb Thrust Chamber Assembly Materials Evaluation

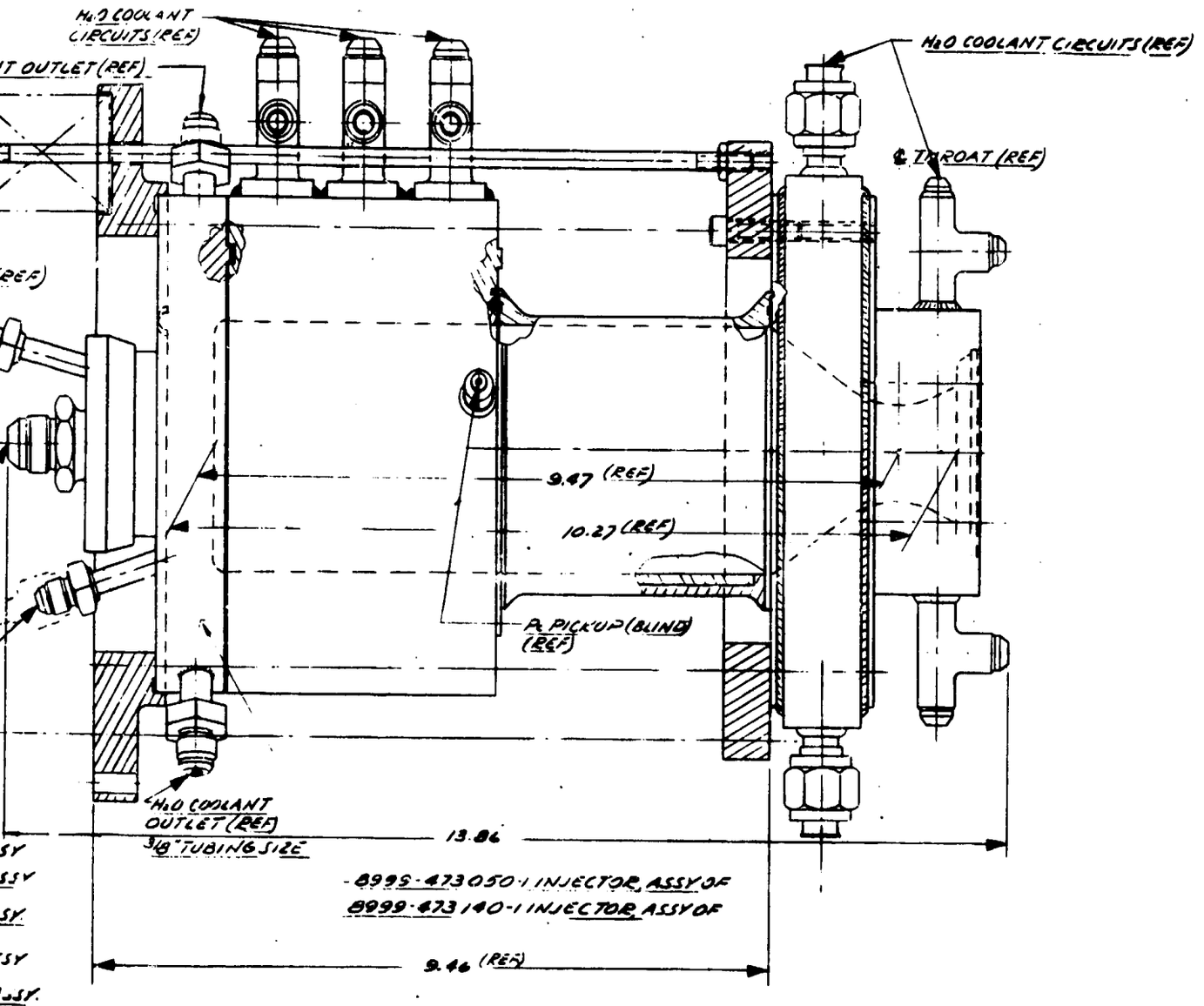
H₂O COOLANT CIRCUITS (REF)
H₂O COOLANT CIRCUITS (REF)
T OUTLET (REF)
℄ THROAT (REF)
9.47 (REF)
10.27 (REF)
Pc PICKUP (BLIND) (REF)
H₂O COOLANT OUTLET (REF) 3/8" TUBING SIZE
13.86
8999-473050-1 INJECTOR ASSY OF
8999-473140-1 INJECTOR ASSY OF
9.46 (REF)

2

(1) (U) Tungsten Chamber Test Results

(U) The literature survey indicated tungsten was a candidate material for use with the products of combustion of $F_2$/BA-1014. Therefore, a series of tests was conducted to determine the compatibility of tungsten including thermal shock characteristics.

(U) Predicated upon a series of discussions with various people at Aeronutronics, General Electric Company, Sylvania, and Fansteel Metallurgical Corporation regarding the thermal shock characteristics of tungsten, it was decided to subject the first tungsten chamber to a short duration test using an uncooled heat sink nozzle (see Figure 20) to determine the thermal shock characteristics of the tungsten in this firing condition. The results of this test (1AW-618) which was a five-second test, indicated a combustion efficiency of 95.7% at a mixture ratio of 0.927 and a chamber pressure of 97.0 psia. The maximum chamber skin temperature during the test was 204°F and rose to 953°F after shutdown due to heat soakback. Since the ductile to brittle transition temperature range of this material is approximately 600°F, this test indicated that the tungsten did go through this regime of operation and, therefore, the test was suitable to determine the thermal shock characteristics of this material. Post-test inspection of the chamber revealed a crack in the chamber at the flange end as shown in Figure 21.

(U) The second tungsten chamber (S/N 2) was fire tested in a 100-second test (1AW-619) at a mixture ratio of 0.99 at a chamber pressure of 99 psia with a resulting combustion efficiency of 95.3%. No detrimental effects were encountered on this chamber. The maximum temperature during the test was 2758°F which is shown in a time history of the skin temperature in Figure 22. It may be noted that the difference between the outside and inside wall temperatures was approximately 10°F due to the high thermal conductivity of the tungsten.

(U) Predicated upon the success of the previous test, an attempted 100-second test (1AW-620) was conducted at a mixture ratio of 1.5 with a tungsten chamber S/N 2 but was terminated after 21.7 seconds due to the following reasons:

(a) (U) A velbestos gasket was used at the chamber end, and the indication was given that the tungsten cylinder bottomed against the water cooled chamber and, therefore, induced stresses to the flange which caused cracks in this area. A review of the movies taken during this test indicated that cracking occurred either prior to or during the initial transient start of the test, since hot cracked areas were indicated within the first few seconds of the test.

(b) (U) Post-test inspection of the chamber revealed that the water cooled chamber had two pinhole leaks which allowed water leakage internally into the chamber.

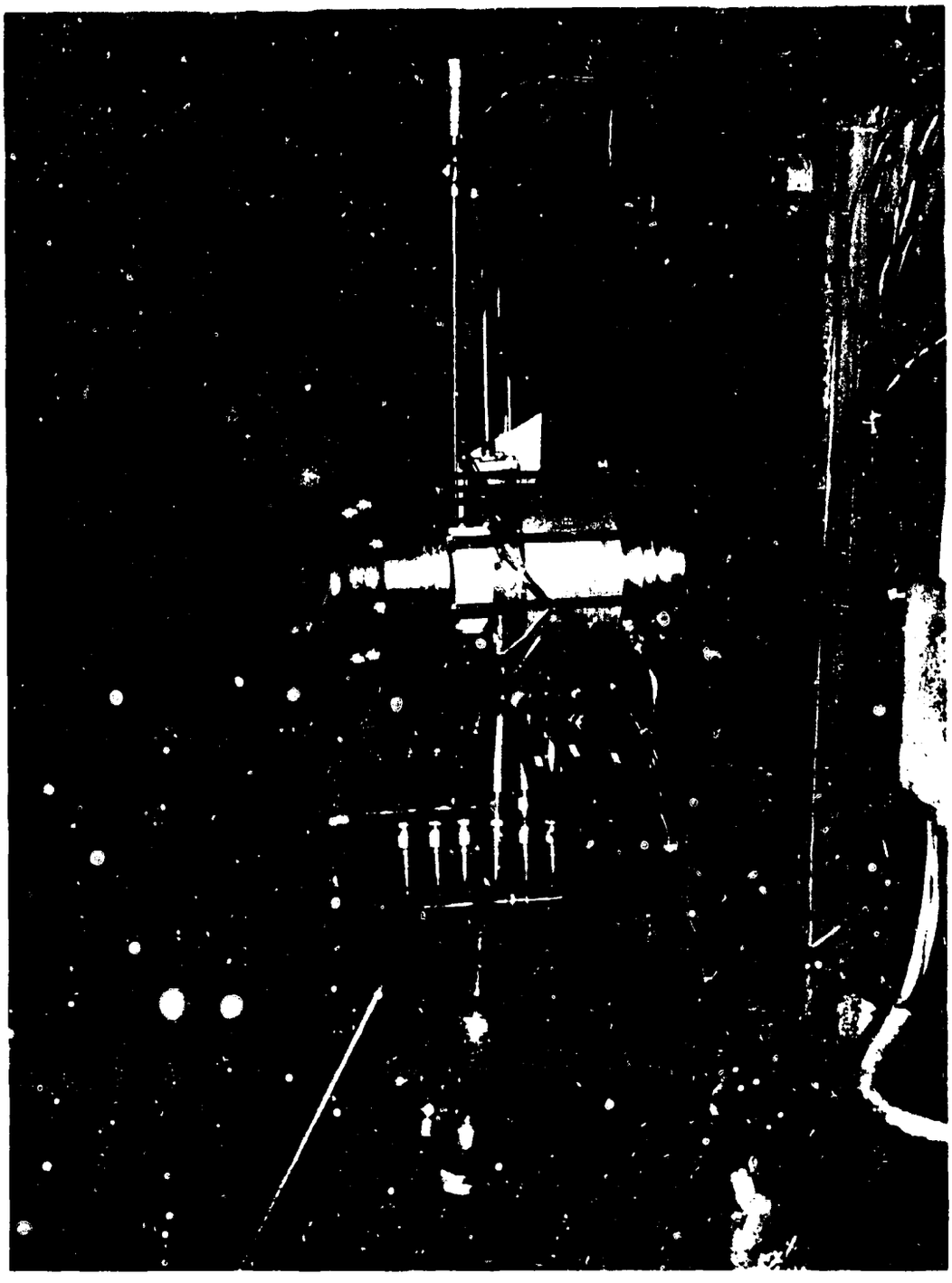

Figure 20. (U) Tungsten Chamber Test Setup

Figure 21. (U) Tungsten Chamber (Post-Fire)

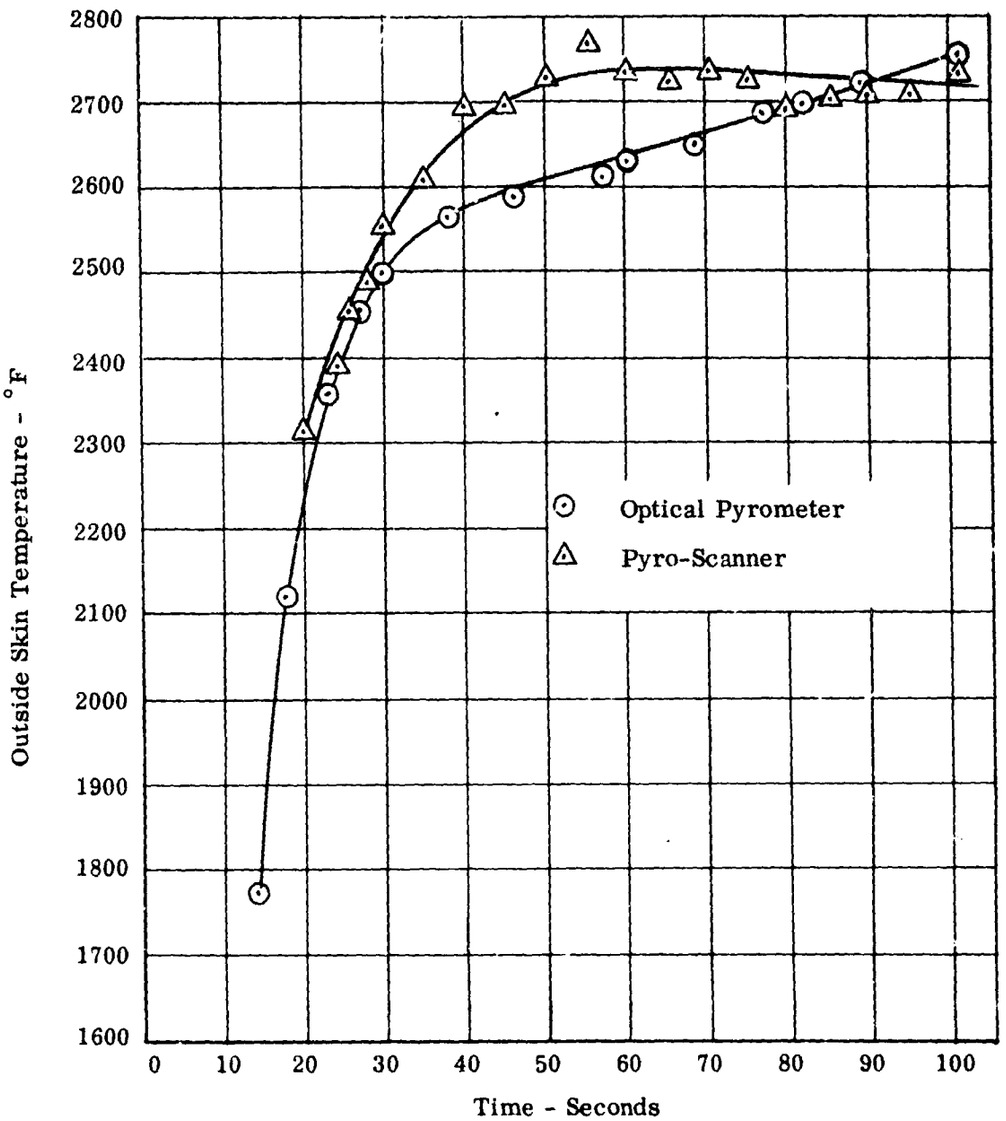


Figure 22. (U) Time History of Outside Temperature of Tungsten Chamber 1AW-619

(c) (U) In addition, post-test inspection revealed a small hole (1/8 inch by 1/4 inch) as shown in Figure 23 (12:00 o'clock looking from nozzle end) occurred at the chamber end which appeared to be caused by an impingement of the water stream on the tungsten chamber which caused thermal shock. A crack was noted on two sides adjacent to this hole, and a crack was also noted approximately 30° from the hole in the clockwise direction looking from the nozzle end as shown in Figure 24. A cracked area was also noted 180° from the hole as shown in Figures 25 through 27. Opposite this cracked area some minor erosion occurred as shown in Figure 28, which was in line with one chamber water leak.

(d) (U) Predicated upon the results of the post-test inspection, a metallurgical investigation was conducted to determine whether the cracks were induced by thermal shock or induced by mechanical stresses and whether or not the hole was caused by oxidation. The results of the metallurgical investigation revealed the following:

(1) (U) Cracking occurred either prior to or during the initial stages of firing since the cracks were completely discolored from heat or gas flow. However, the discoloration did not resemble a tungsten oxide or fluoride but discoloration due to heat only.

(2) (U) The crack (B) which occurred approximately 30° to the hole shown in Figure 24 indicated a brittle fractured surface as shown in Figure 29. This would indicate that the failure occurred prior to reaching the ductile-brittle transition temperature Examination of this crack indicated that cracking started at the thinner edge of the lip of the flange and progressed inward to the notch formed at the root of the flange. The crack then progressed in two directions from the flange root. Metallurgical investigations of this crack revealed a filling of the cracked area with the tungsten disilicide coating which was applied externally to the chamber as shown in Figure 30.

(3) (U) Metallurgical investigation of the area around the hole (A) as shown in Figures 23 and 24 indicated the cracks adjacent to the hole were filled with the tungsten disilicide coating which was applied externally (see Figure 31). The appearance of this coating in the cracks indicated that the cracking occurred early in the firing cycle and the coating filled the cracks after it became molten. The fact that the coating filled the cracks completely without voids indicated that the cracks were not

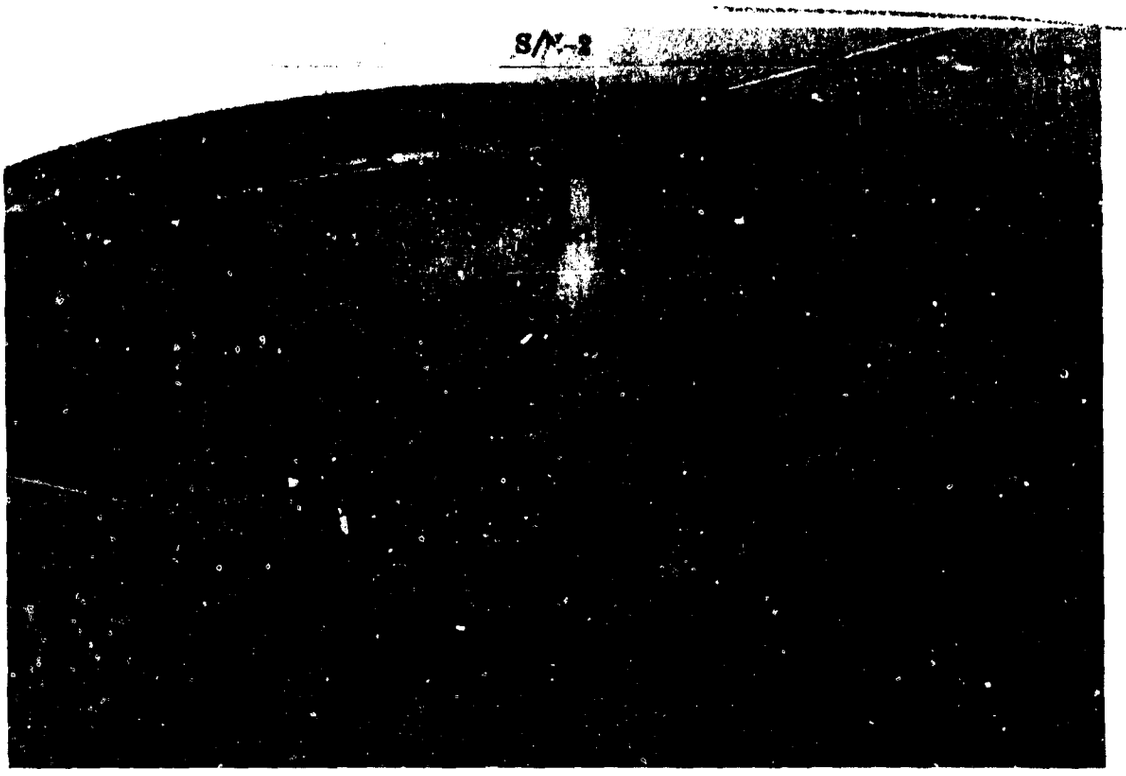


Figure 23. (U) Post-Test Observation of Tungsten Chamber After Test 1AW-620

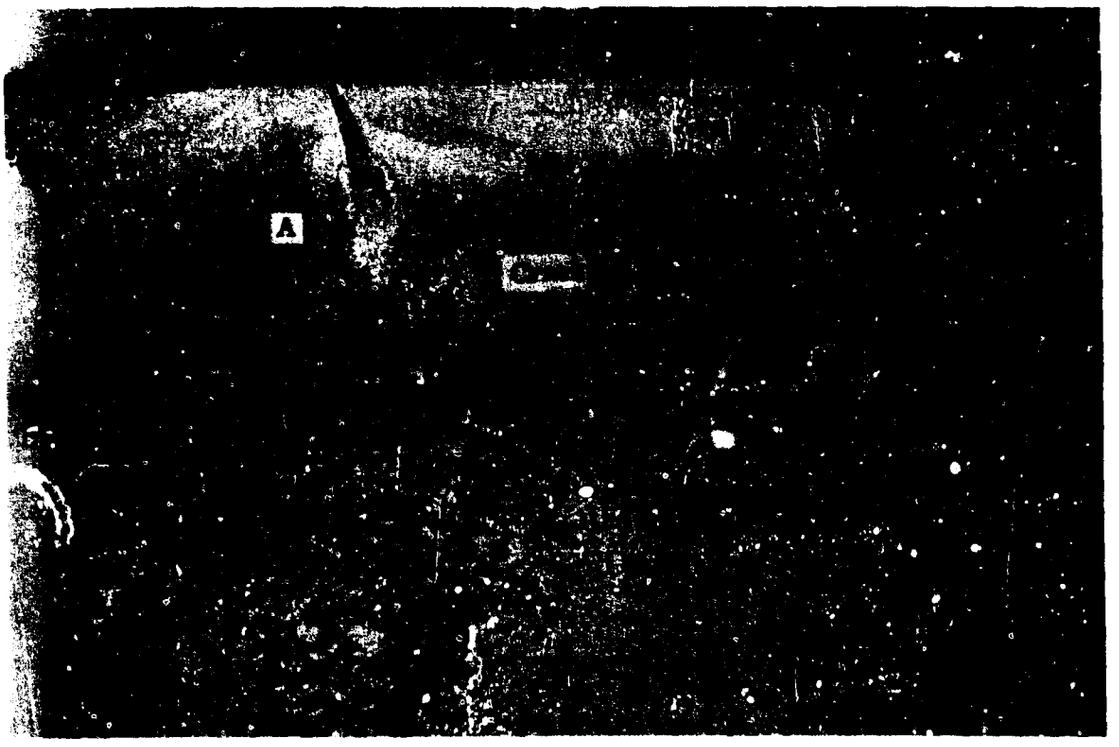


Figure 24. (U) Post-Test Observation of Tungsten Chamber After Test 1AW-620

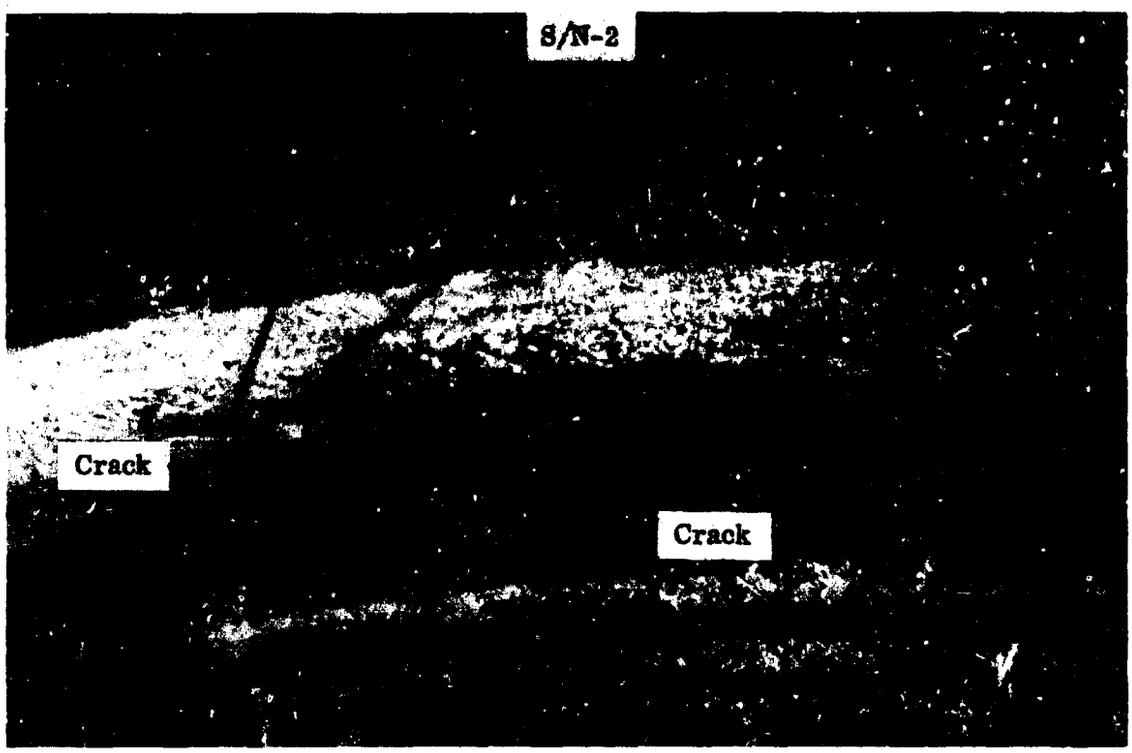


Figure 25. (U) Cracks in Tungsten Chamber After Test 1AW-620

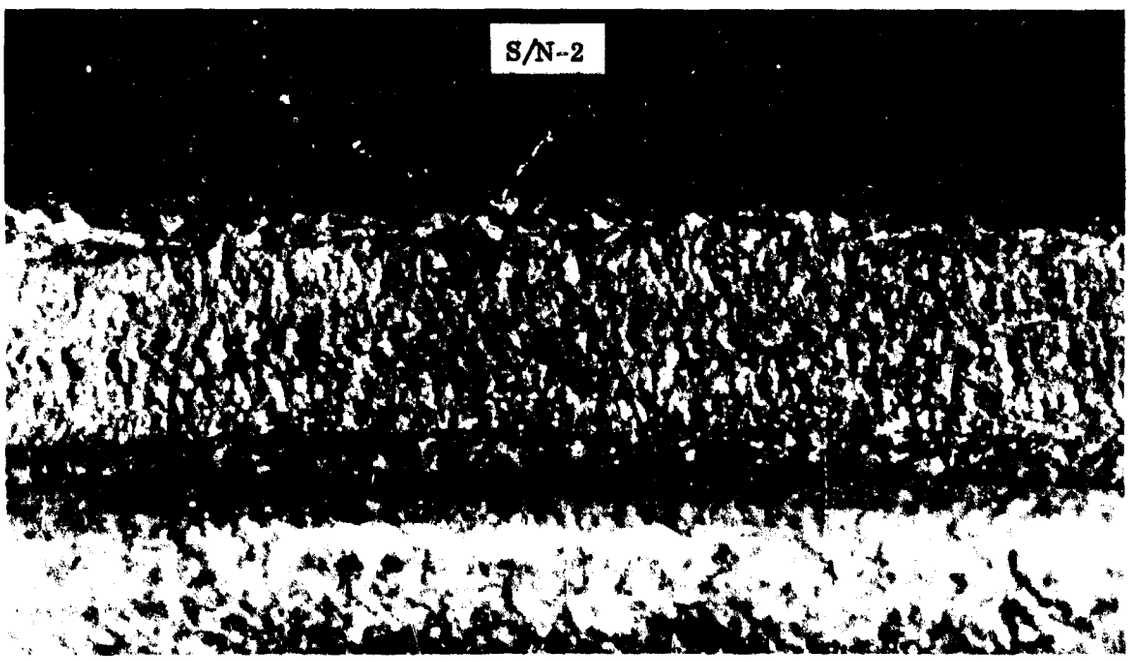


Figure 26. (U) Cracks inTungsten Chamber After Test 1AW-620

Figure 27. (U) Cracks in Tungsten Chamber After Test 1AW-620

S/N-2

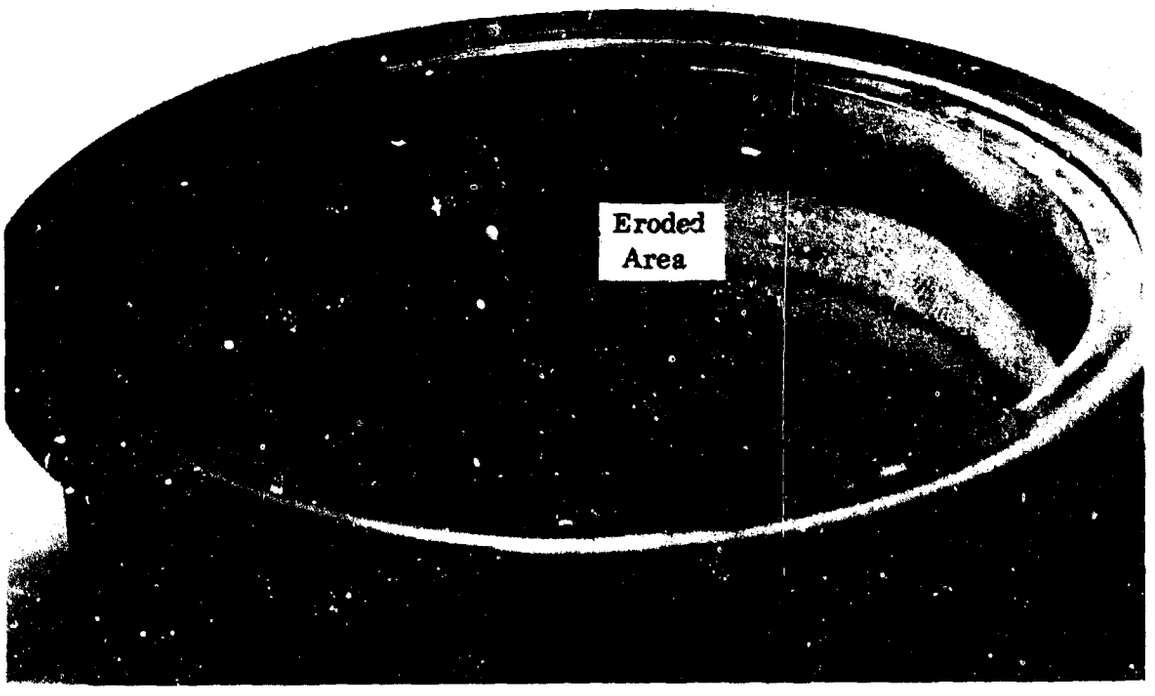


Figure 28. (U) Local Eroded Area After Test 1AW-620


Figure 29. (U) Brittle Fractured Surface

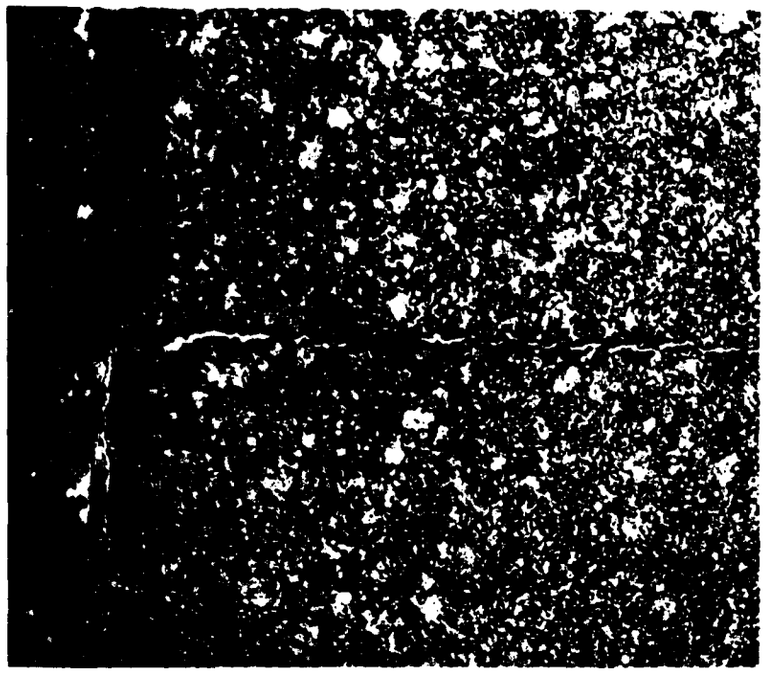

Figure 30. (U) Crack Filled with Silicide Coating - Area B

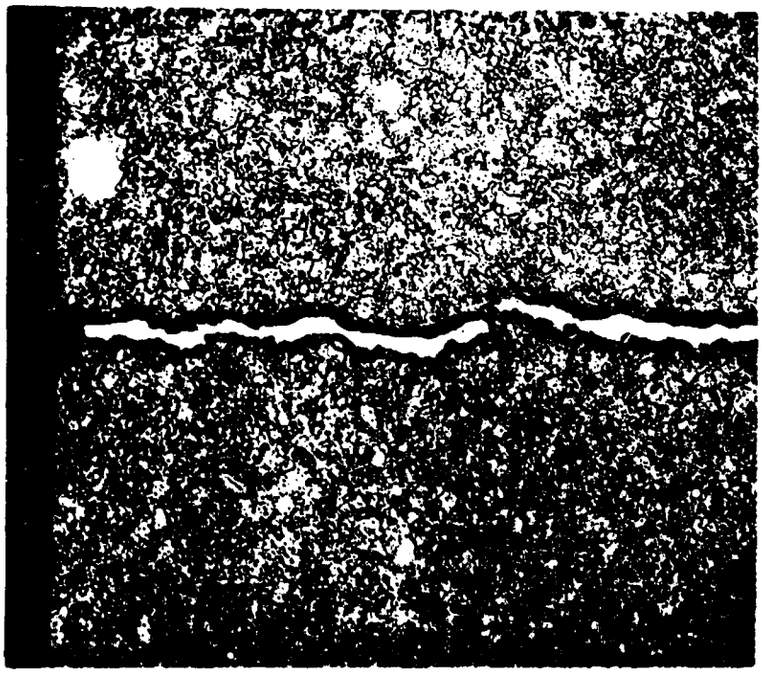

Figure 31. (U) Crack Filled with Silicide Coating - Area A

(U) present in the coating cycle. The appearance of the radius on the edges of the crack indicated that the crack was filled by capillary action after heatup. An examination of the area around the eroded hole shown in Figures 23 and 24 indicated that the cracks adjacent to the hole occurred first and allowed a gas leakage path which caused the hole as the cracks opened up. Examination of the microstructure of this area (see Figures 32 and 33) revealed possible grain boundary melting which was not clearly evident by photomicrographs.

(4) (U) An examination of the microstructure of the eroded area which is shown in Figure 28 indicated a small change in the structure indicating the possibility of some grain growth (see Figure 34).

(5) (U) The cracks along the flange approximately 180° from the hole appeared to be due to machining at the root of the flange. This was caused by the notched sensitivity of the material and the recommendation is that no sharp corners should be utilized on parts made of tungsten.

(6) (U) As a result of the metallurgical investigation, the major cracking of the tungsten chamber section was determined to be caused by the thermal shock induced on this part during the test.

(U) The first tungsten chamber was repaired by Super-Temp Corporation by welding the cracked area. The silicide coated area which was removed locally in the welded area was painted with a chromic oxide coating to protect against oxidation and allow for high emittance ( $\epsilon = 0.67$). This chromic oxide (melting point of 2800°F) was utilized to expedite the test realizing that the chromic oxide would melt. A 100-second duration test (1AW-623) was conducted at a mixture ratio of 2.2 and a chamber pressure of 91 psia with a resultant combustion efficiency of 83.3%. The results of this test indicated a maximum skin temperature of 3920°F as shown in Figure 35. Figures 36 and 37 show the chamber after the test. Cracking of the flange occurred at the end where the repair welding was conducted and the chromic oxide melted as indicated by the external surface of the chamber. However, no change occurred on the tungsten chamber internally.

(U) As a result of the tests conducted on the tungsten chambers, the conclusion can be reached that tungsten is susceptible to thermal shock. However, tungsten has the capability of operating to temperatures in excess of 3900°F with the products of combustion of fluorine/BA-1014 over a mixture ratio range of 1.0 to 2.2. As a result of these tests, tungsten is a candidate material for use in the adiabatic wall thrust chamber design as a liner, but care must be taken to design against thermal shock.

Figure 32. (U) Microstructure of Area Around Hole Shown in Figure 23

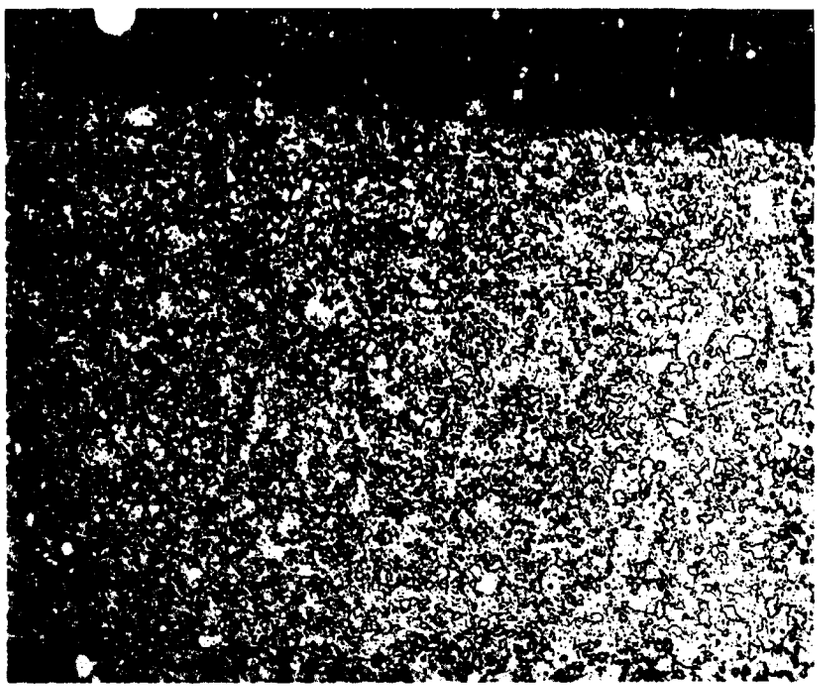

Figure 33. (U) Microstructure Around Eroded Hole

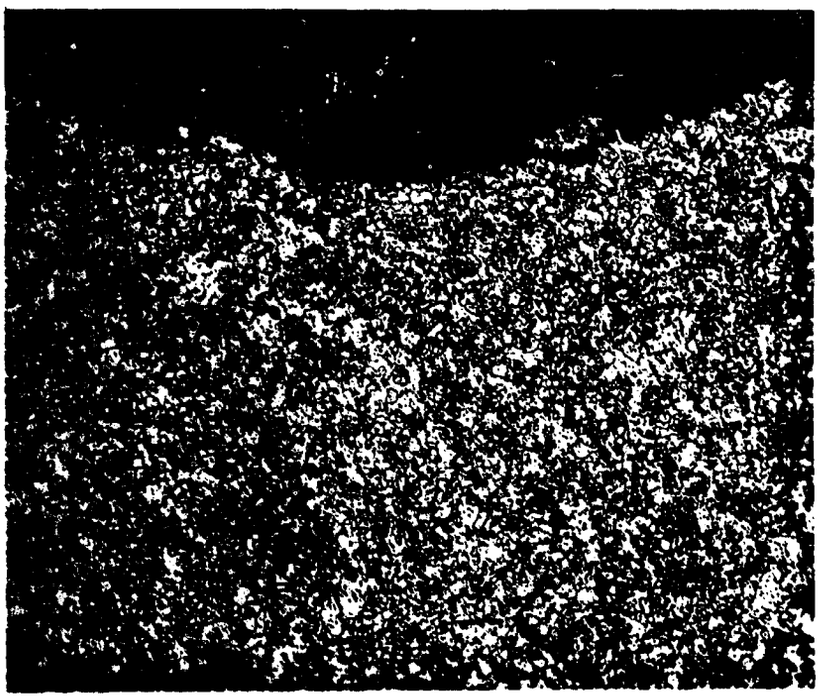

Figure 34. (U) Microstructure Around Eroded Area

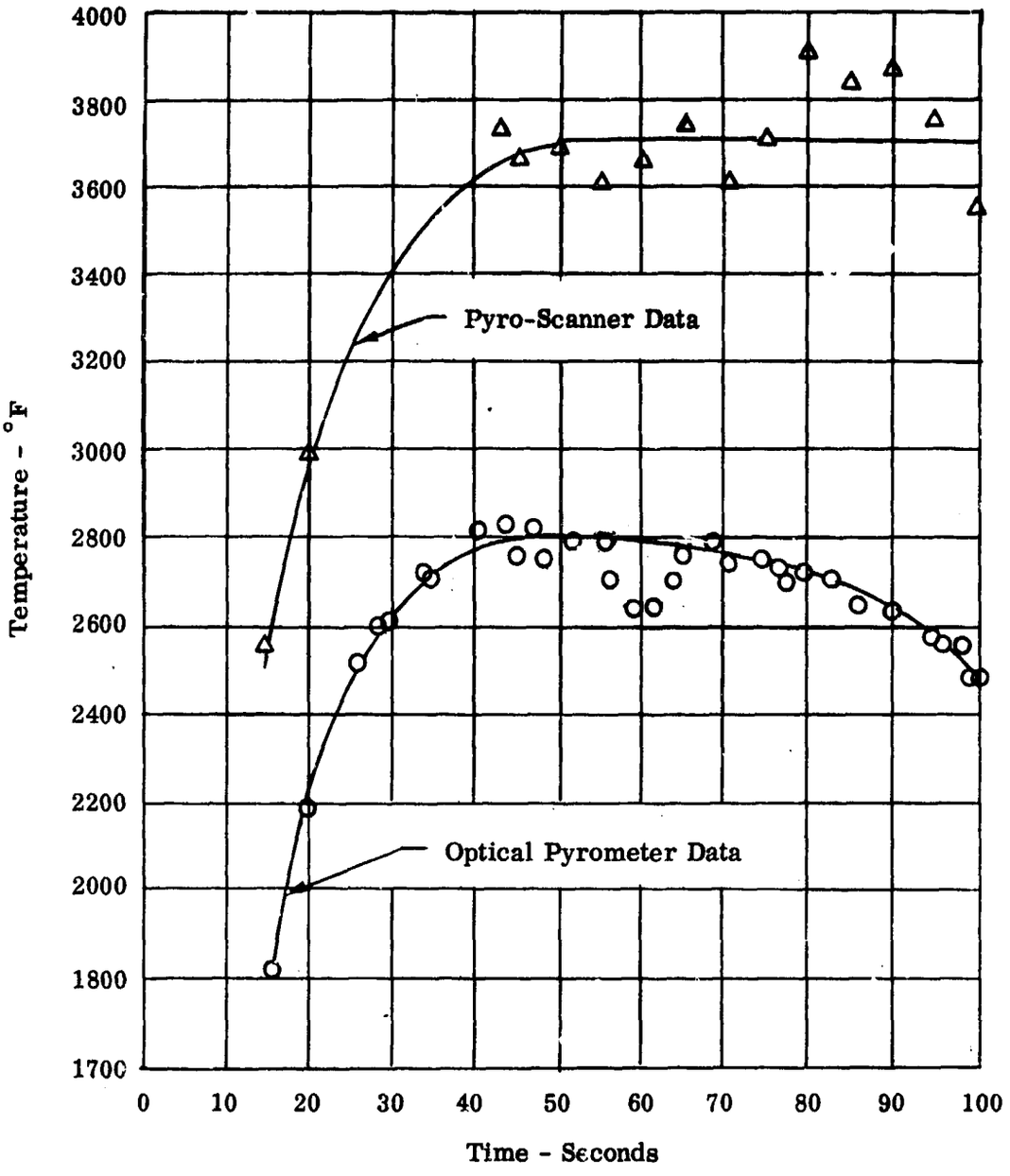


Figure 35. (U) Tungsten Chamber Time History (1AW - 623)

Figure 36. (U) Tungsten Chamber After Test — Chamber End Up

Figure 37. (U) Tungsten Chamber After Test — Nozzle End Up

(2) (U) Test Results of the Tungsten Retainer With the Graphite Sleeve

(U) The tungsten retainer was received from GT&E with an overflow of a silicide coating in the serrations at one end and, consequently, was sent to Super-Temp Corporation for remachining the serrations to remove the excess coating.

(U) The first test (1AW-621) was conducted for 100.8 seconds at a mixture ratio of 1.50 and a chamber pressure of 101 psia with the resultant combustion efficiency of 92.3%. The maximum external skin temperature was approximately 2800°F. Data from the optical pyrometer is shown as a time history in Figure 38. No detrimental effects were encountered on either the tungsten retainer or the graphite sleeve.

(U) Another test (1AW-622) was therefore conducted on the same hardware using a velbestos gasket at the nozzle end. This test was conducted at a mixture ratio of 1.96 and a chamber pressure of 100 psia with a resultant combustion efficiency of 90%. The maximum skin temperature obtained on this test was 2950°F, as shown in the time history in Figure 39. A heat transfer analysis was conducted to determine what the maximum internal graphite temperature was during this test. The results of this analysis indicated that the maximum internal graphite temperature was 3410°F predicated upon the 2950°F external measured temperature. Post-test inspection indicated no change in the tungsten retainer as shown in Figures 40 and 41, although some burning of the velbestos gasket was noted. Figures 42 through 44 showed that no significant change was noted on the graphite sleeve. However, some very minor erosion occurred on the graphite sleeve, which was so minor it is not apparent in the photographs of Figures 42 through 44.

(U) It can be concluded that graphite has the capability of operation at 3400°F in an environment composed of the products of combustion of $F_2$/BA-1014 over a mixture ratio range of 1.5 to 2.0. Therefore, graphite is a candidate material for use in the adiabatic wall thrust chamber design as a liner material. In addition, this test proved that tungsten can be utilized when adequately protected from thermal shock as was demonstrated by no detrimental results occurring on the two tests of 100 seconds duration each.

(3) (U) Results of Tantalum Alloy Tests

(U) Predicated upon the results of tests conducted at the Marquardt Corporation with chlorine trifluoride and hydrazine blend, a tantalum (10% tungsten) alloy chamber was designed and fabricated from material available in stock with a minimum amount of machining in order to determine the compatibility of the tantalum alloy with the products of combustion of fluorine/BA-1014. The wall thickness, therefore, was 0.275 inch compared to the tungsten chamber which was 0.22 inch thick. No external machining was done to bring the part to the same thickness as the tungsten chamber. The chamber was then coated with the GT&E R508C

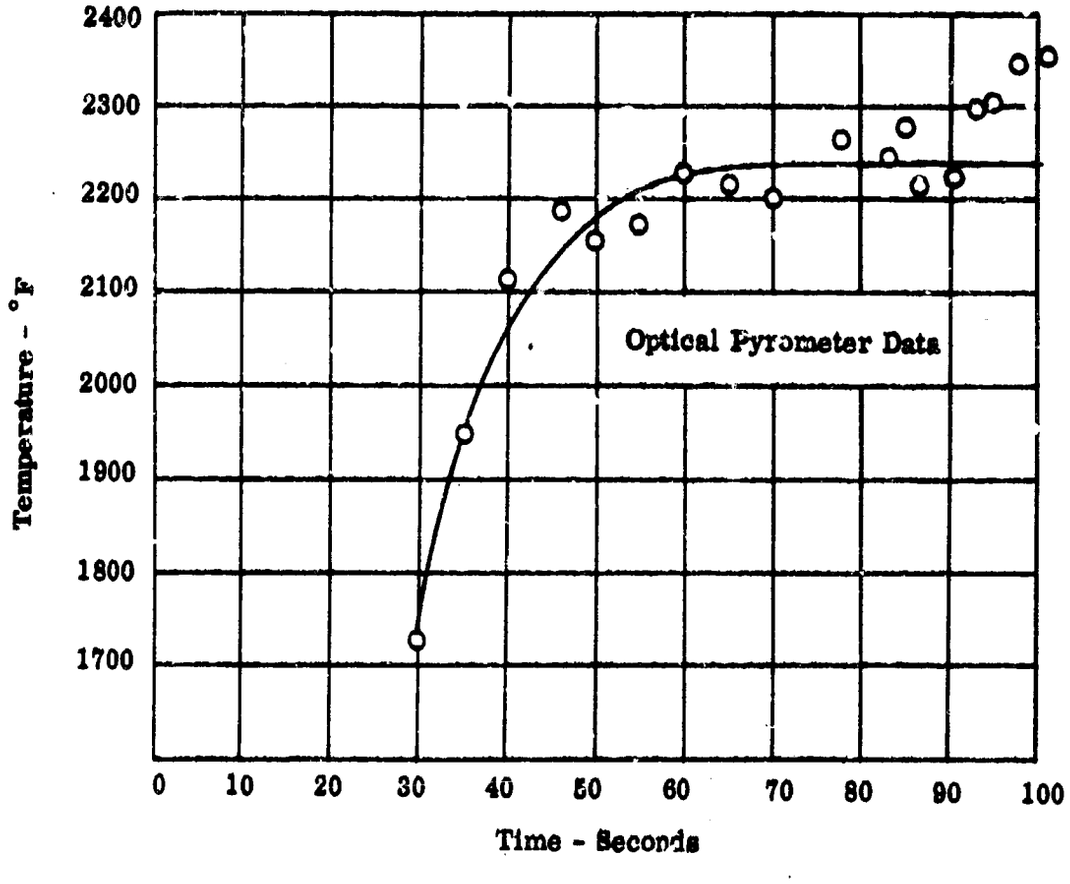


Figure 38. (U) Temperature History (1AW - 621)

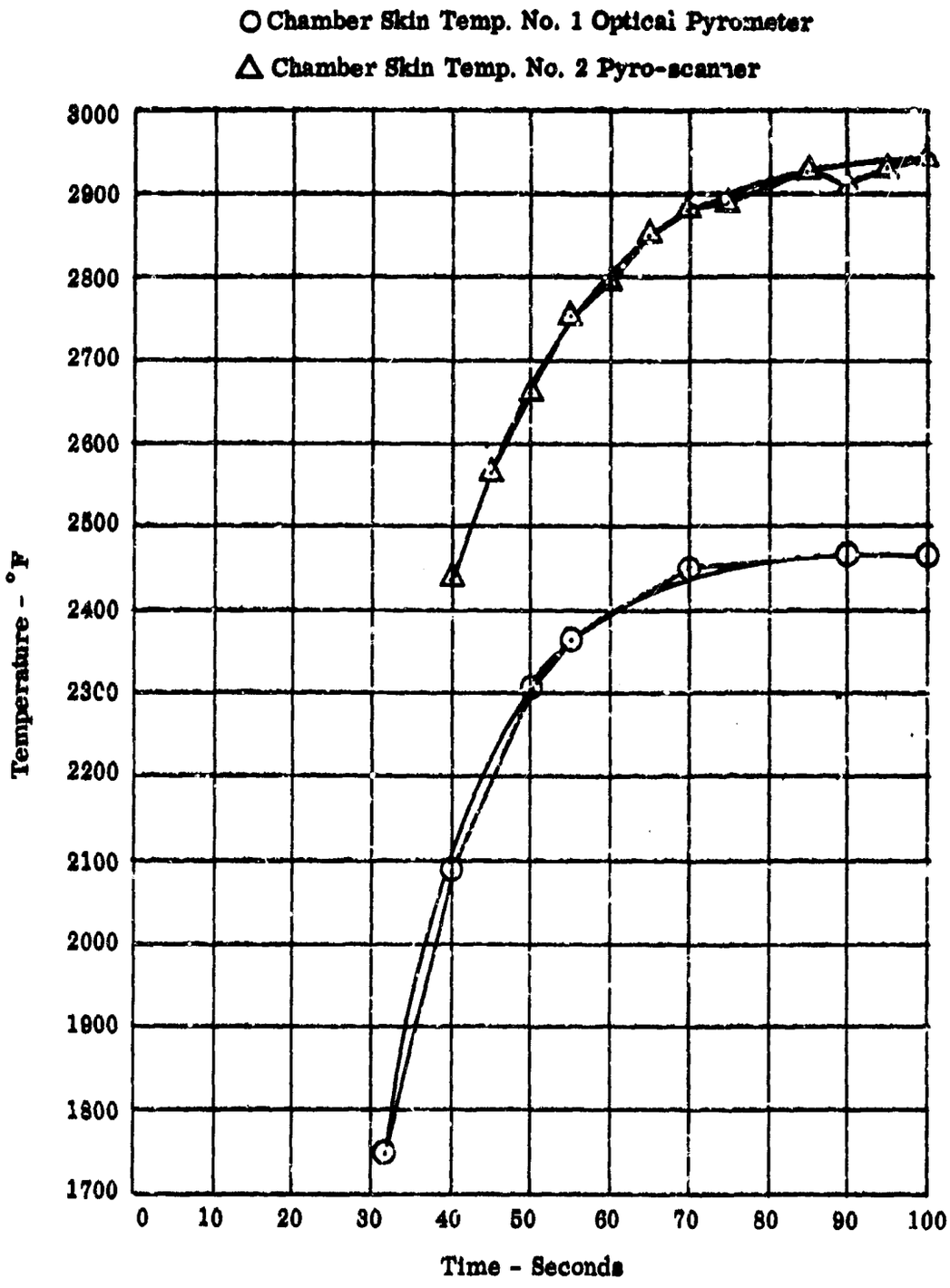


Figure 39. (U) Temperature History (1AW - 622)

Figure 40. (U) Tungsten Retainer After Test — Chamber End Up

Figure 41. (U) Tungsten Retainer After Test — Nozzle End Up

Figure 42. (U) Graphite Sleeve After Test — Chamber End Up

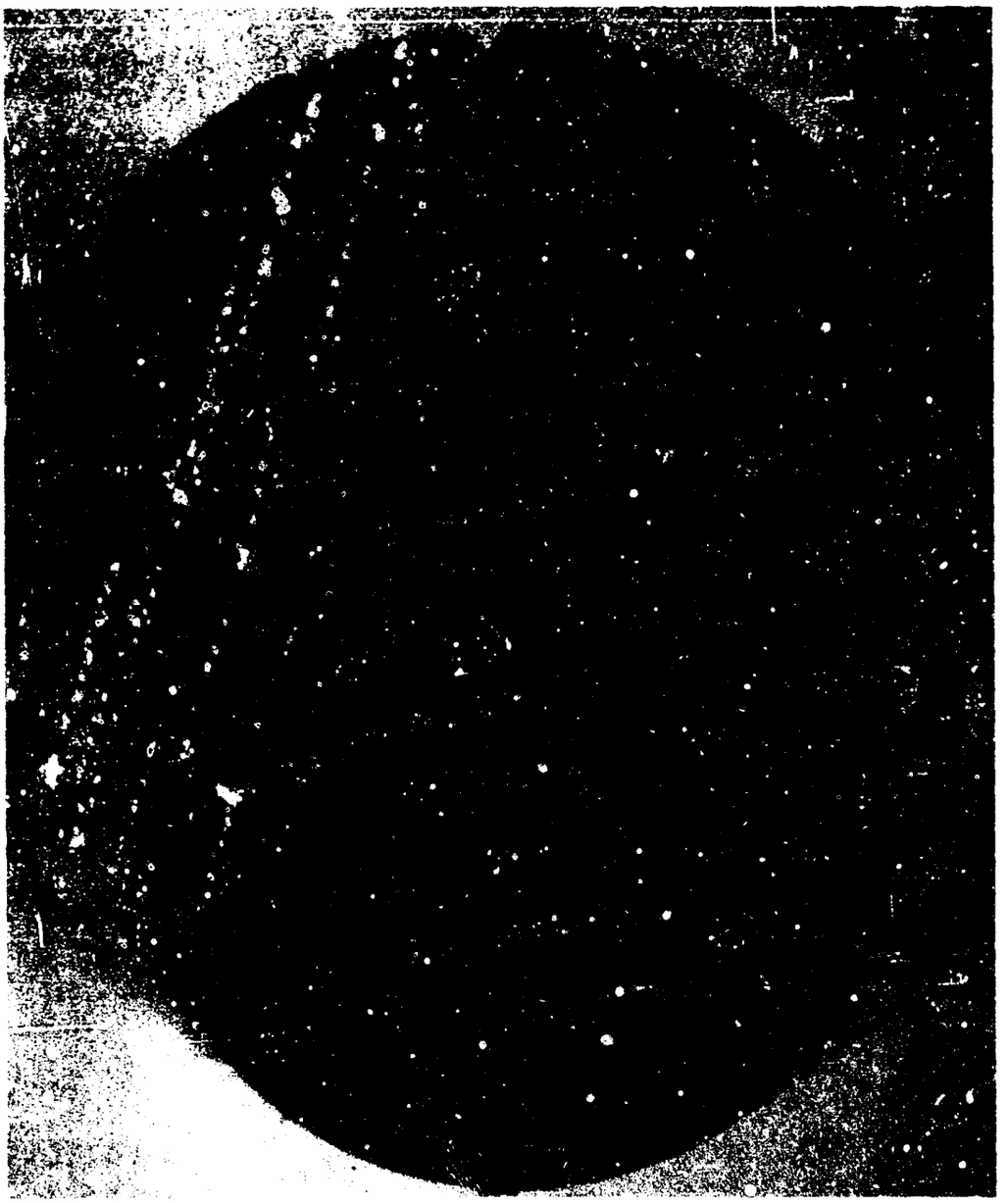

Figure 43. (U) Graphite Sleeve After Test — Nozzle End Up

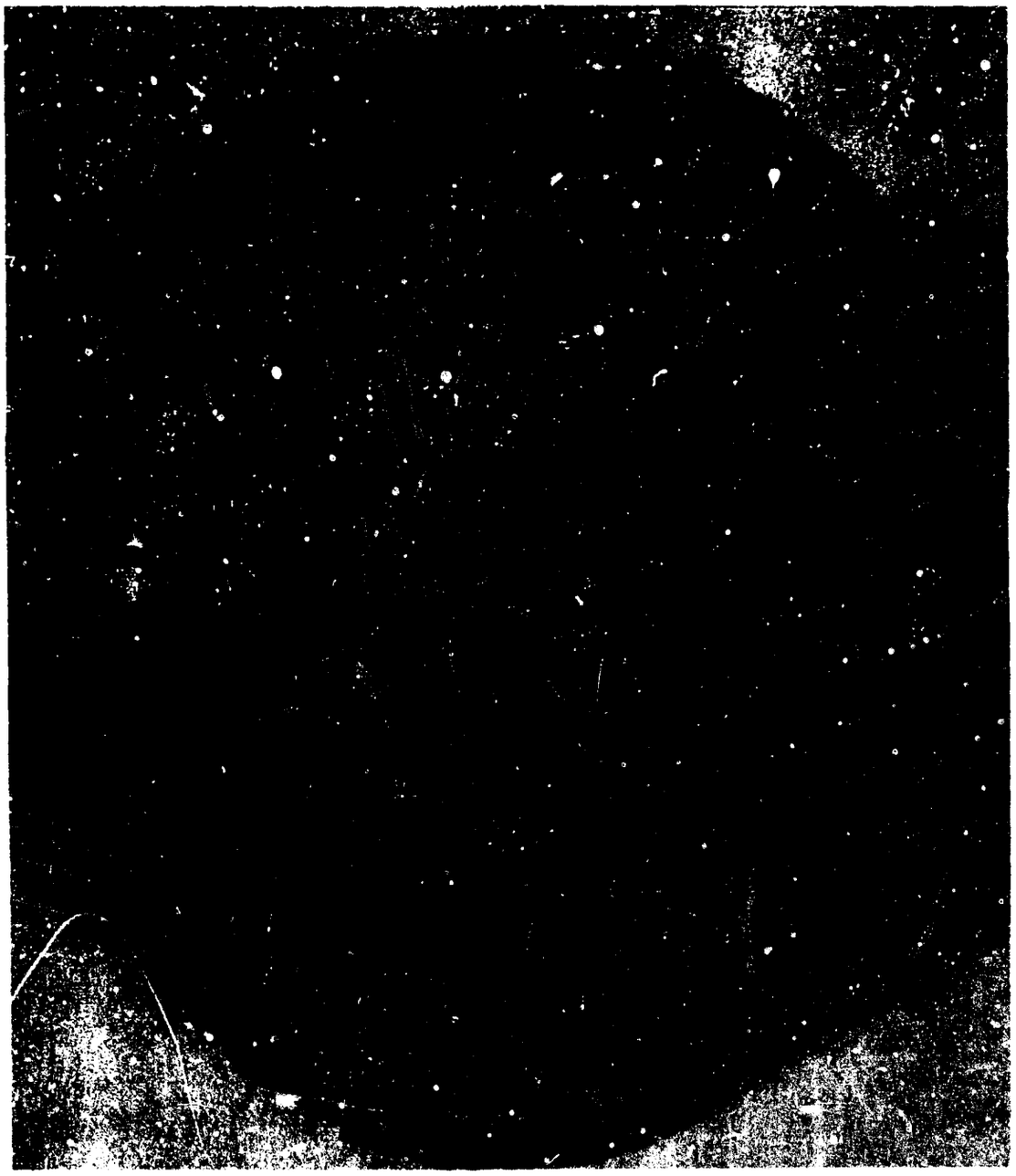

Figure 44. (U) Graphite Sleeve After Test — Nozzle End Up

(U) silicide coating externally to protect against oxidation due to the surrounding air environment and to allow for high emittance ( $\epsilon = 0.65$) to dissipate the heat by radiation. No coating was applied internally to determine the compatibility with the products of combustion.

(U) A 100.2-second test (1AW-627) was conducted at a mixture ratio of 2.06 and a chamber pressure of 96 psia with a resultant combustion efficiency of 86.2%. The temperature history indicated a maximum external temperature of 2900°F as shown in Figure 45, and a maximum internal temperature of 3240°F (heat transfer analysis). Post-test observation indicated a black and silvery discoloration on the internal wall of the thrust chamber. Therefore, a metallurgical investigation was conducted with the following results:

(a) (U) Theoretical thermochemistry indicated that the products of combustion would result in an environment of basically 59.5% HF, 15.4% $N_2$, 9.4% F, 2.3% $H_2$, and 10% H (mole %).

(b) (U) X-ray diffraction indicated the internal surface of the chamber in the silver discolored area was tantalum coated with a relatively thin transparent film of tantalum-oxyfluoride ($TaO_2F$).

(c) (U) X-ray diffraction of the black internal surface indicated that black residue to be primarily tantalum nitride (TaN).

(d) (U) Microexamination of the metallurgical sections taken from the two areas discussed above revealed identical microstructures which consisted of large grains indicating grain growth during the firing. Figure 46 shows the large grains which occurred as a result of test firing.

(e) (U) Contamination of the grain boundary was also observed as indicated in Figure 47. This contamination was indicated on both the internal and external surfaces of the chamber. The external surface contamination was probably due to oxidation during welding or from the received material from the supplier. The contamination detected extended to the base material approximately 25% from the internal surface and 25% from the external surface. The 25% contamination on the internal surface was probably due to HF attack.

(f) (U) Two longitudinal and one circumferential bend specimens were bent to determine the residual ductility of the material. One of the longitudinal specimens was loaded in the direction which placed the external surface coating in tension while the other longitudinal specimen was bent in the opposite direction which placed the external coating in compression. The circumferential specimen was bent placing the external surface in tension. The results of the bend tests indicated the material to be embrittled after firing; however, the degree of embrittlement was undefined.

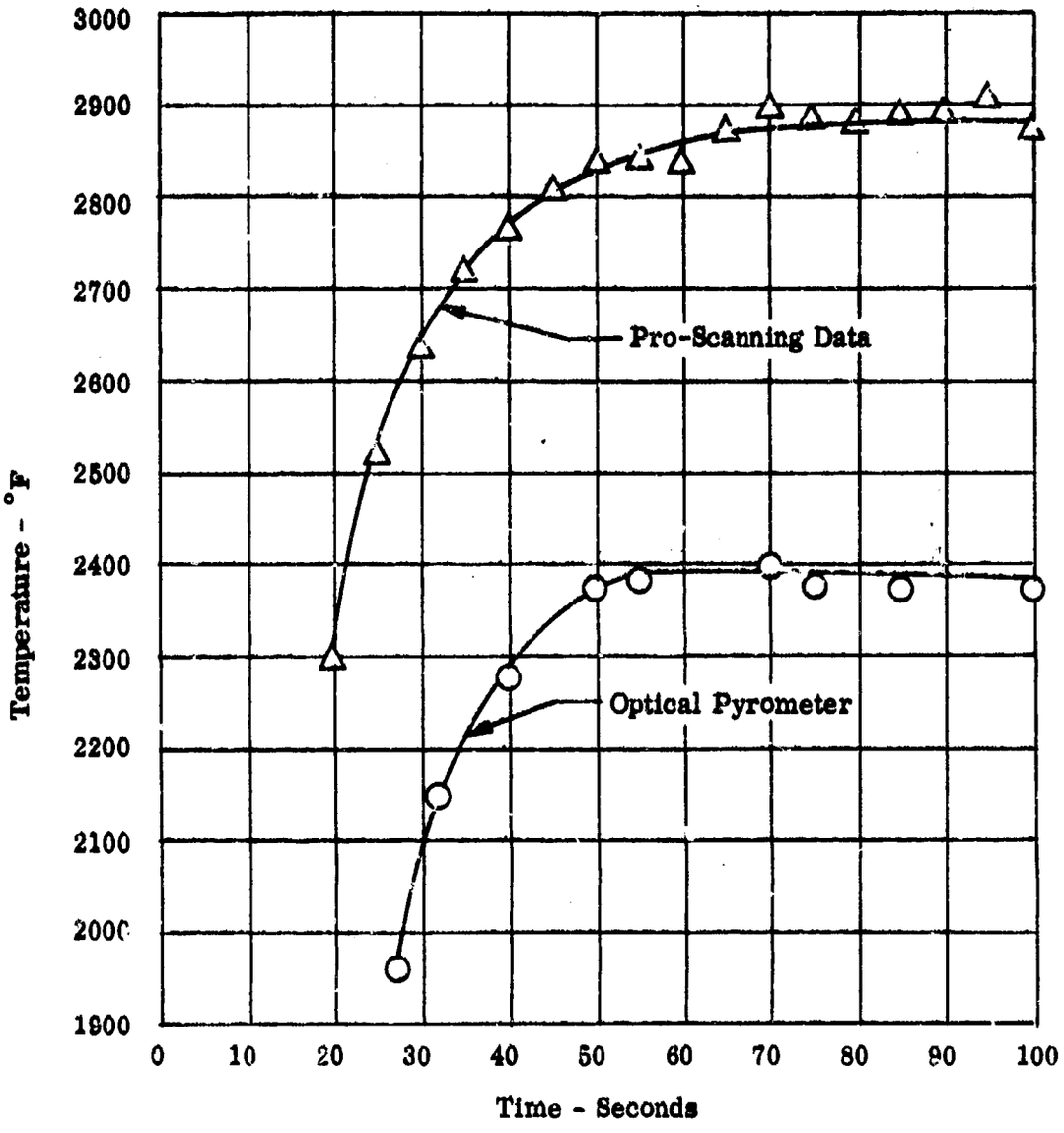


Figure 45. (U) Temperature History (1AW - 627)

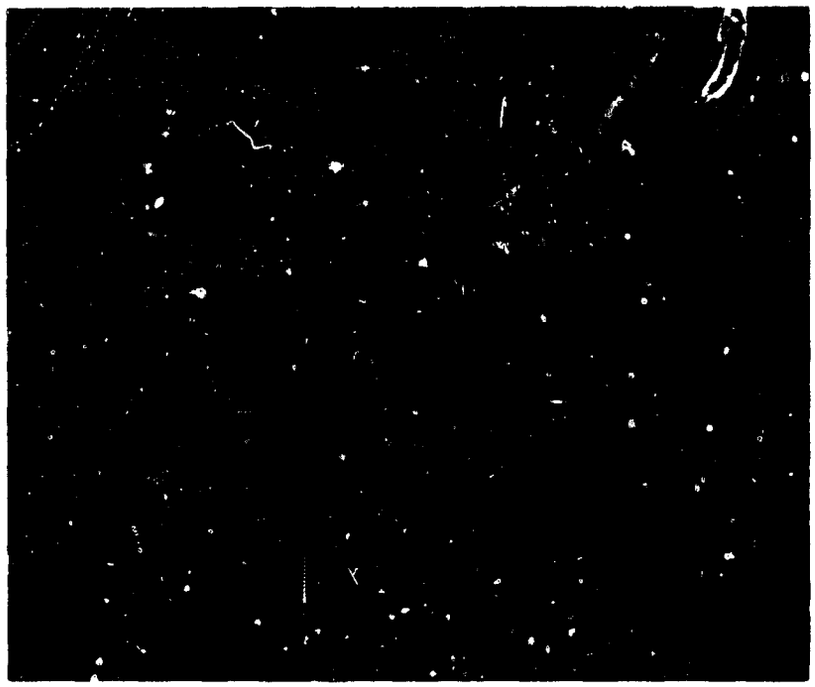

Figure 46. (U) Photograph Showing the Structure of the Ta-W Chamber

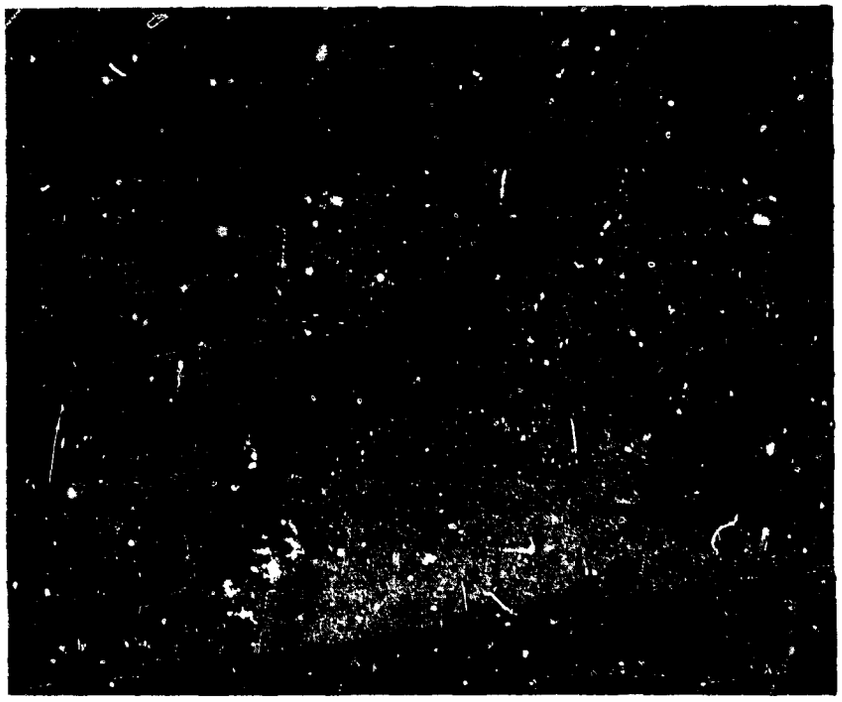

Figure 47. (U) Micrograph Showing Contamination in Grain Boundaries

(U) It can be concluded that tantalum (10% tungsten) alloy has the capability of operation at approximately 3250°F with the products of combustion of fluorine/BA-1014 operating at a mixture ratio of 2.1 and a chamber pressure of 100 psia. However, grain boundary contamination will occur which will limit the number of cycles of operation since this contamination is time limited. The extrapolation of these results to the adiabatic wall liner indicates that a tantalum (10% tungsten) alloy liner could survive for a maximum total duration of testing in excess of 100 seconds without any coating. If this liner was utilized for a greater time, the anticipated mode of failure of such a liner would be by cracks occurring through the grain boundary. Predicated upon experience from other programs, such a mode of failure could be of such an extent that it could cause detrimental damage to the hardware if a chunk of the liner would blow out. Therefore, the tungsten coating could be utilized on the tantalum alloy liner to protect against grain boundary contamination, since tungsten does have the capability of operation in this environment at temperatures in excess of 3900°F.

(4) (U) Test Results with a Columbium Alloy Chamber

(U) The columbium alloy (Cb-291) chamber was coated internally with a modified aluminide and externally with the GT&E silicide coating to protect against oxidation from the surrounding air environment and allow for high emittance ($\epsilon$ = 0.65) to dissipate the heat by radiation. The aluminide coating was utilized to protect the chamber from the products of combustion resulting from fluorine/BA-1014 combustion process.

(U) The first test firing on this chamber (1AW-624) was an intended 100-second duration test which was terminated after 25.5 seconds due to excessive skin temperatures noted on the test section. The maximum temperature recorded was 3000°F by the pyro-scanner and 2870°F with the optical pyrometer. A time history of these temperatures is shown in Figure 48. The red line temperature of this test was 2800°F predicated upon the mixture ratio of the test (0.83) and a chamber pressure of 94.1 psia. The resulting combustion efficiency was 94.9% and post-test observation indicated that the impingement of the injector was not ideal; therefore, the injector was backflushed, flowed and the impingement was improved prior to mounting on the stand for the next test.

(U) The second test firing (1AW-625) was an intended 100-second duration test firing which was terminated after 13.1 seconds due to visual observation of a leak in the test section. Post-test pressure check of the assembly verified a leak in the water cooled nozzle end. This test was conducted at a mixture ratio of 1.02 and the chamber pressure of 98.7 psia with a resulting combustion efficiency of 95.5%. The maximum temperature recorded during the test was 2895°F (see Figure 49).

(U) The third test of the series (1AW-626) was a successful 100.9-second test. This test was conducted at a mixture ratio of 1.06 and a chamber pressure of 101 psia with a resulting combustion efficiency of 95.0%. The maximum temperature recorded on this test was 3449°F as recorded at a localized streak using the pyro-scanner and a 3080° temperature recorded on the optical pyrometer. The results of this temperature history are shown in Figure 50.

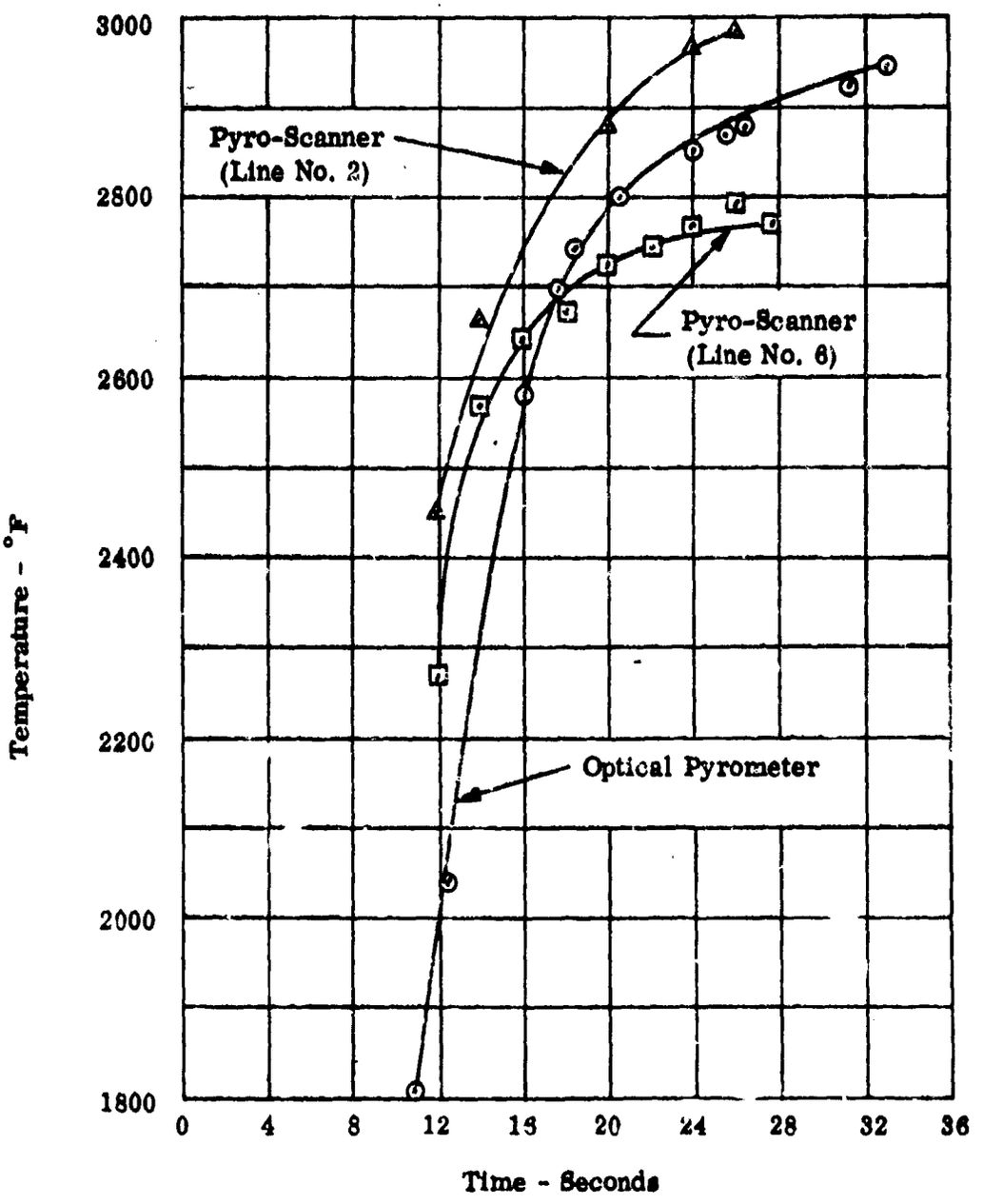


Figure 48. (U) Temperature History (1AW - 624)

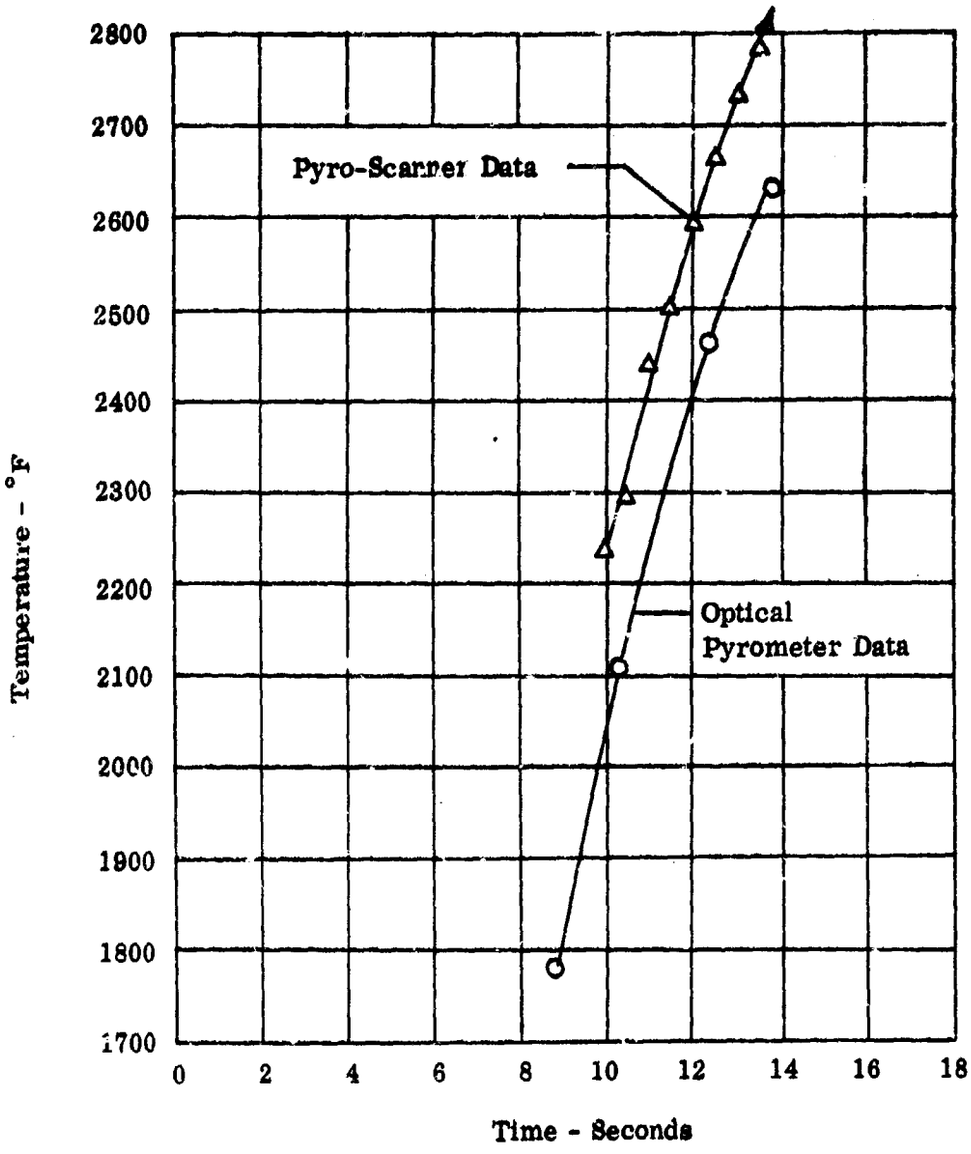


Figure 49. (U) Temperature History (1AW - 625)

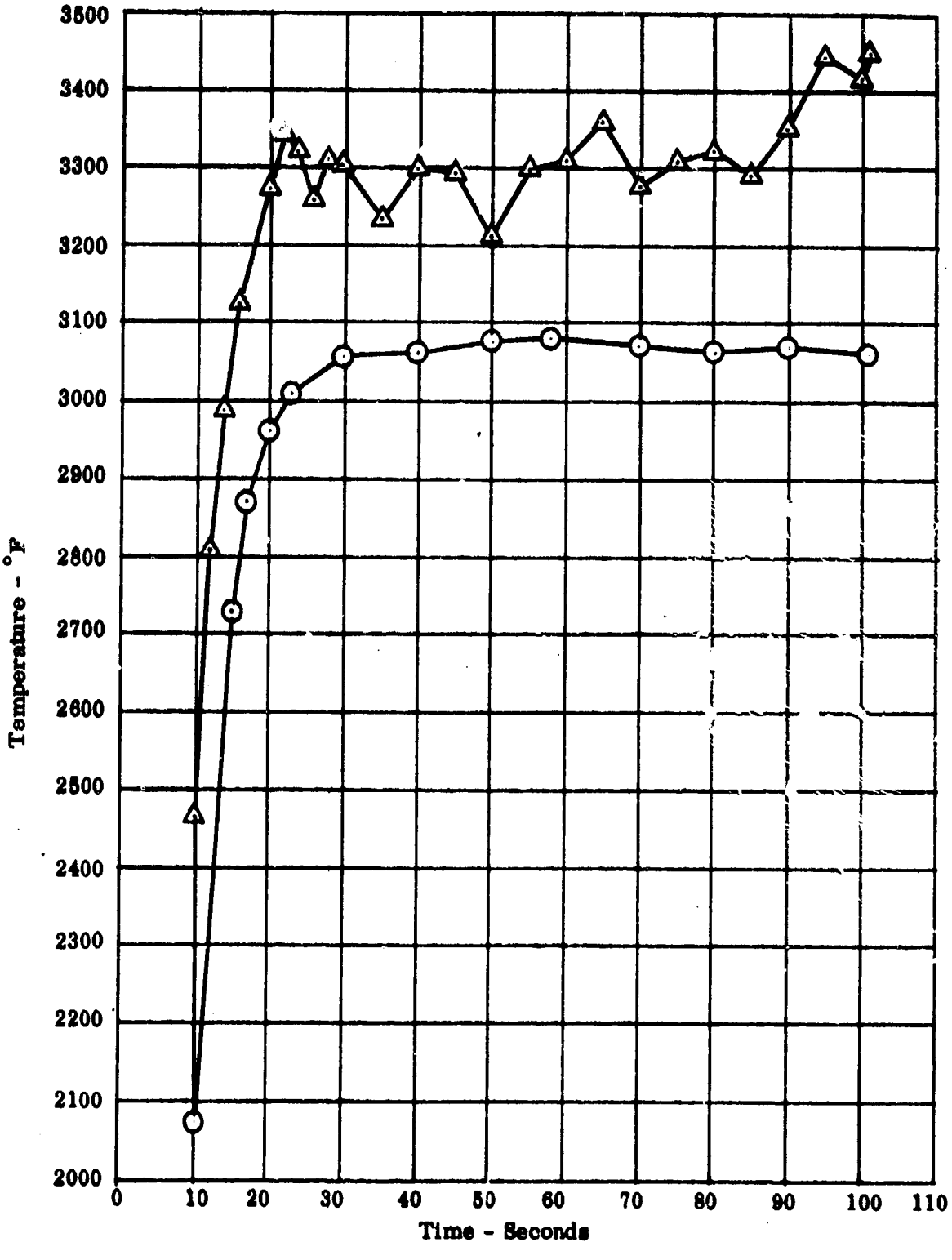


Figure 50. (U) Temperature History (1AW - 626)

(U) Figures 51 through 55 show the visual observation of the columbium test section after the completion of the fire test (1AW-624). These results indicate the start of a streak as shown in Figures 53 and 54. Figures 56 through 59 show the results of a chamber at the completion of the tests conducted in this series. No further testing was conducted on this chamber. It can be shown that the area where the 3449°F temperature was recorded was the cause of the streak as shown in Figures 54 (after test 1AW-624) and 57 (after test 1AW-626). Adjacent to this streaked area a bubble occurred in the coating. This bubble indicated oxidation from the HF products of combustion underneath the coating. A complete metallurgical investigation was conducted on this part to determine how protective the coating was from the products of combustion. The results of the metallurgical investigation revealed the following:

(a) (U) The aluminide coating was generally protective to the columbium with the products of combustion resulting from fluorine/BA-1014.

(b) (U) The following results were revealed in the localized streaked area which reached 3449°F.

(1) (U) The R512 silicide coating melted locally. Some minor oxidation of the base metal appeared.

(2) (U) Recrystallization occurred characterized by grain growth. Figure 60 shows the large grains in this area compared to other areas shown in Figure 61. Figure 62 shows the material prior to firing.

(c) (U) A bend test of the coated chamber after firing indicated the material was embrittled but not detrimental. The conclusion can be reached that the aluminide coating was protective to the SCb-291 alloy with the products of combustion resulting from fluorine/BA-1014. Therefore, this material and coating can be utilized for the large columbium alloy chamber to be tested on the adiabatic wall thrust chamber phase of the program.

d. (U) Summary of Test Program

(U) The results of the test program as summarized in Table XIV indicate that tantalum (10% tungsten) alloy, pure tungsten and graphite are candidate materials for use in the adiabatic wall thrust chamber as a liner material. In addition, SCb-291 columbium alloy coated with the aluminide coating can be used as the radiation cooled thrust chamber for use in the adiabatic wall thrust chamber design with the liners discussed above.

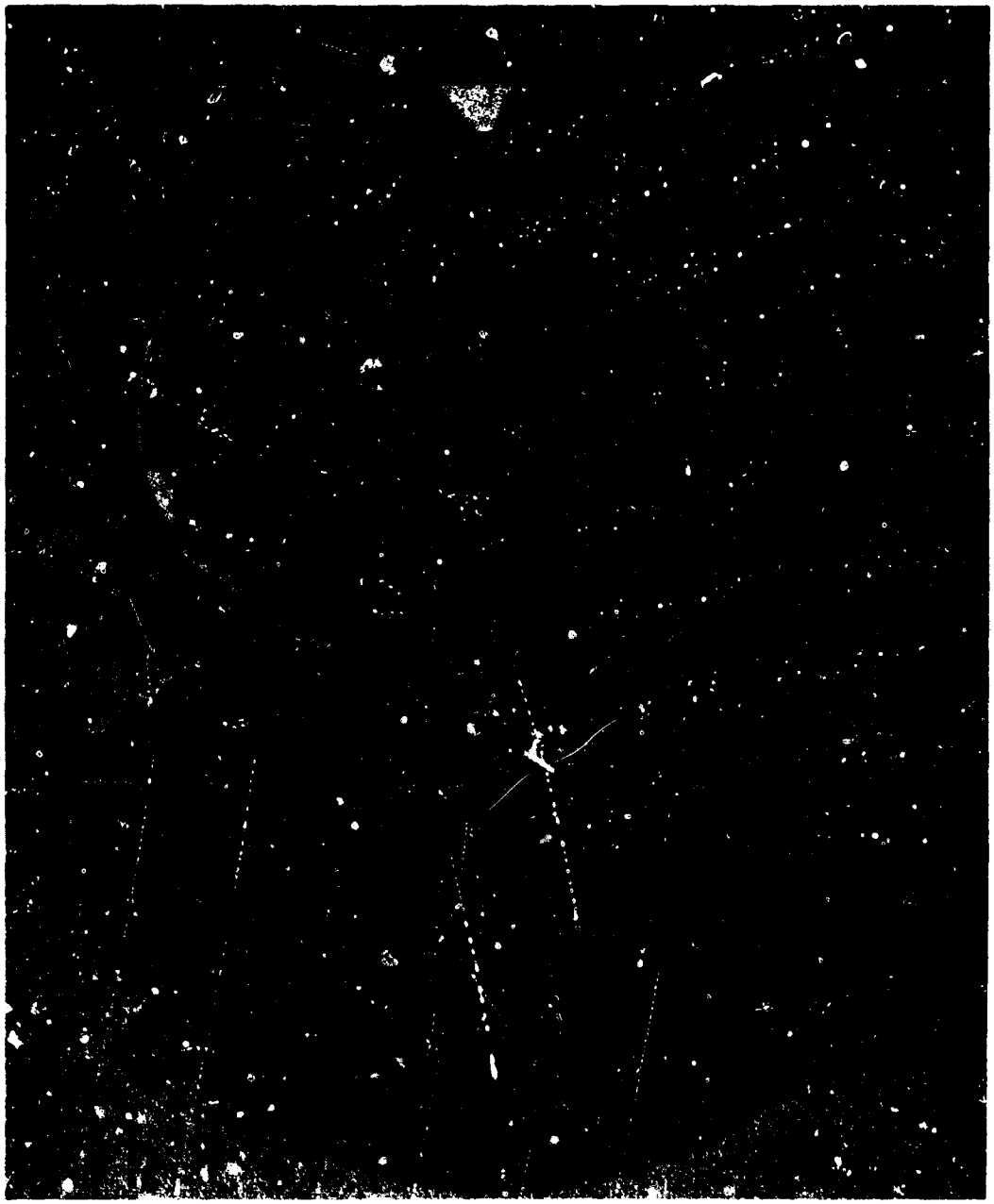

Figure 51. (U) Columbium Chamber After Test (1AW-624) — Chamber End Up

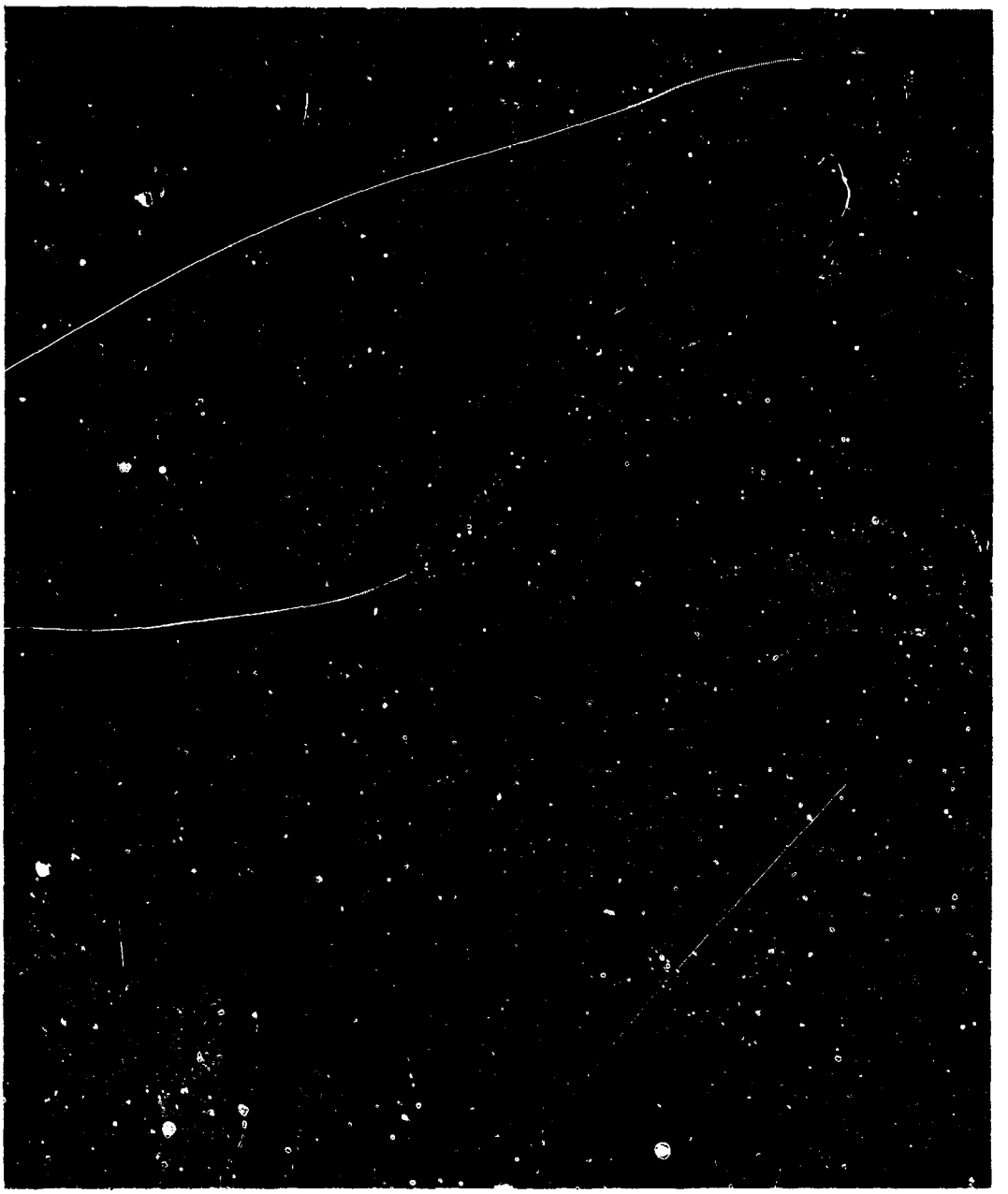

Figure 52. (U) Columbium Chamber After Test (1AW-624) — Chamber End Up

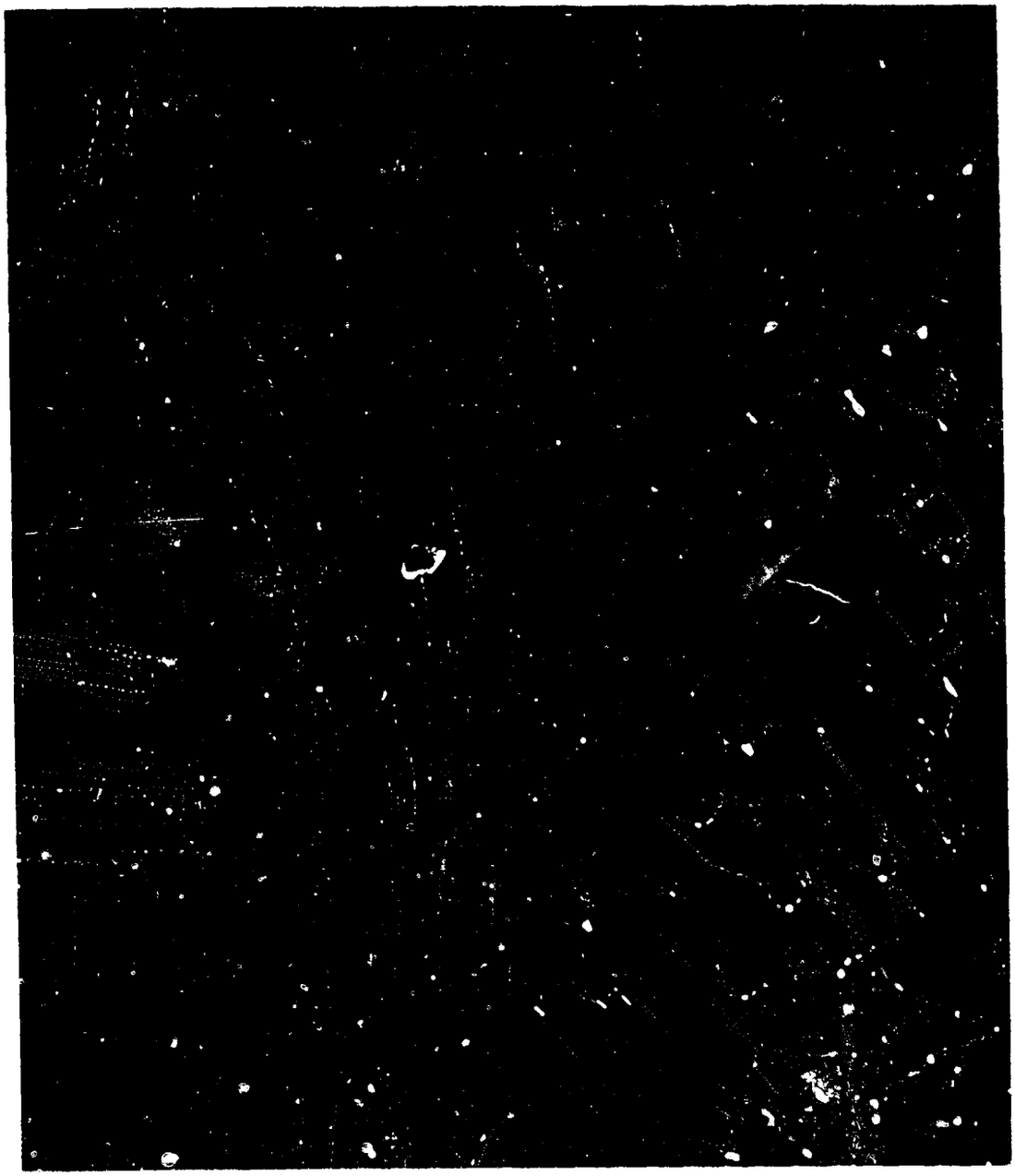

Figure 53. (U) Columbium Chamber After Test (1AW-624) — Chamber End Up

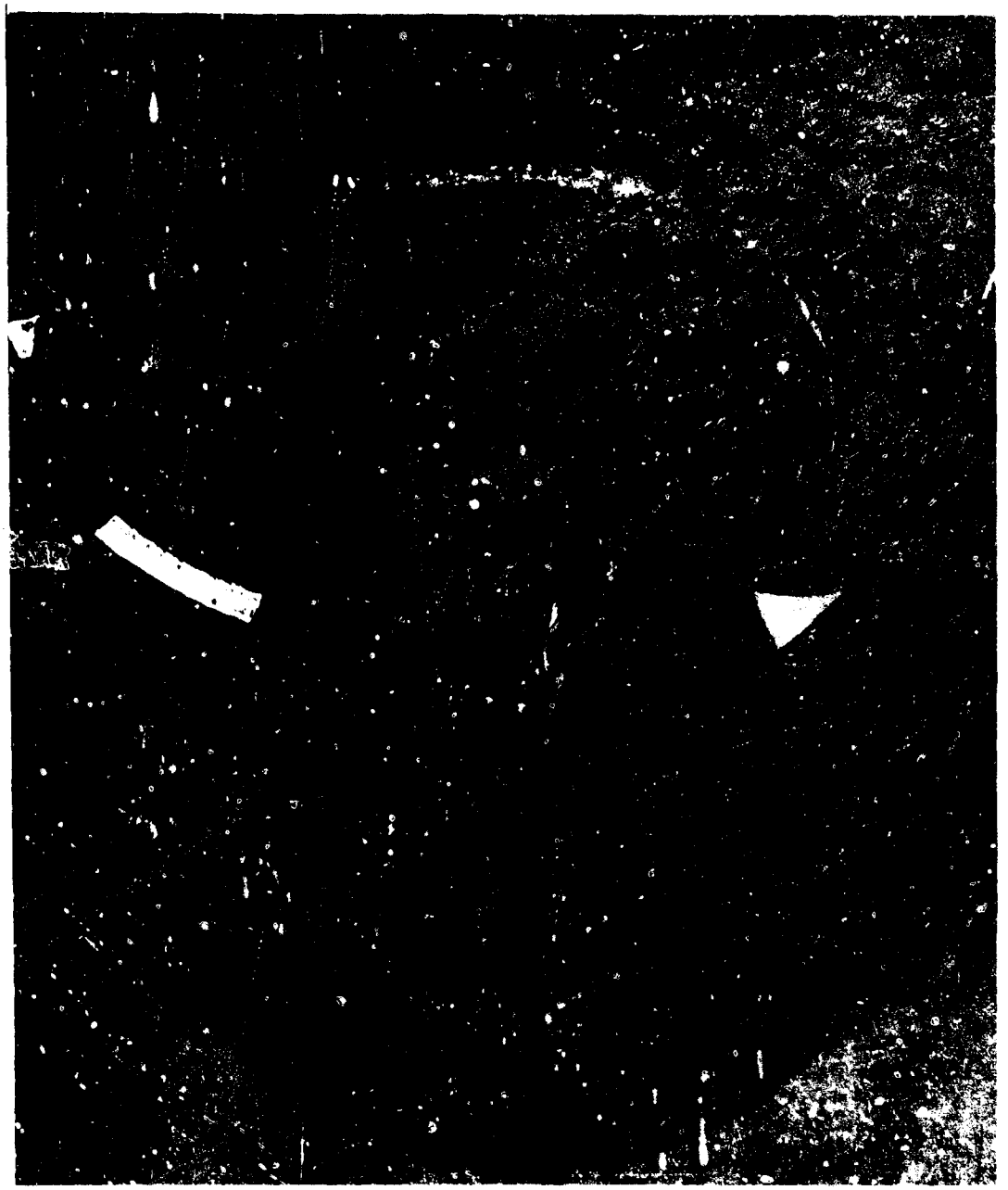

Figure 54. (U) Columbium Chamber After Test (1AW-624) — Nozzle End Up

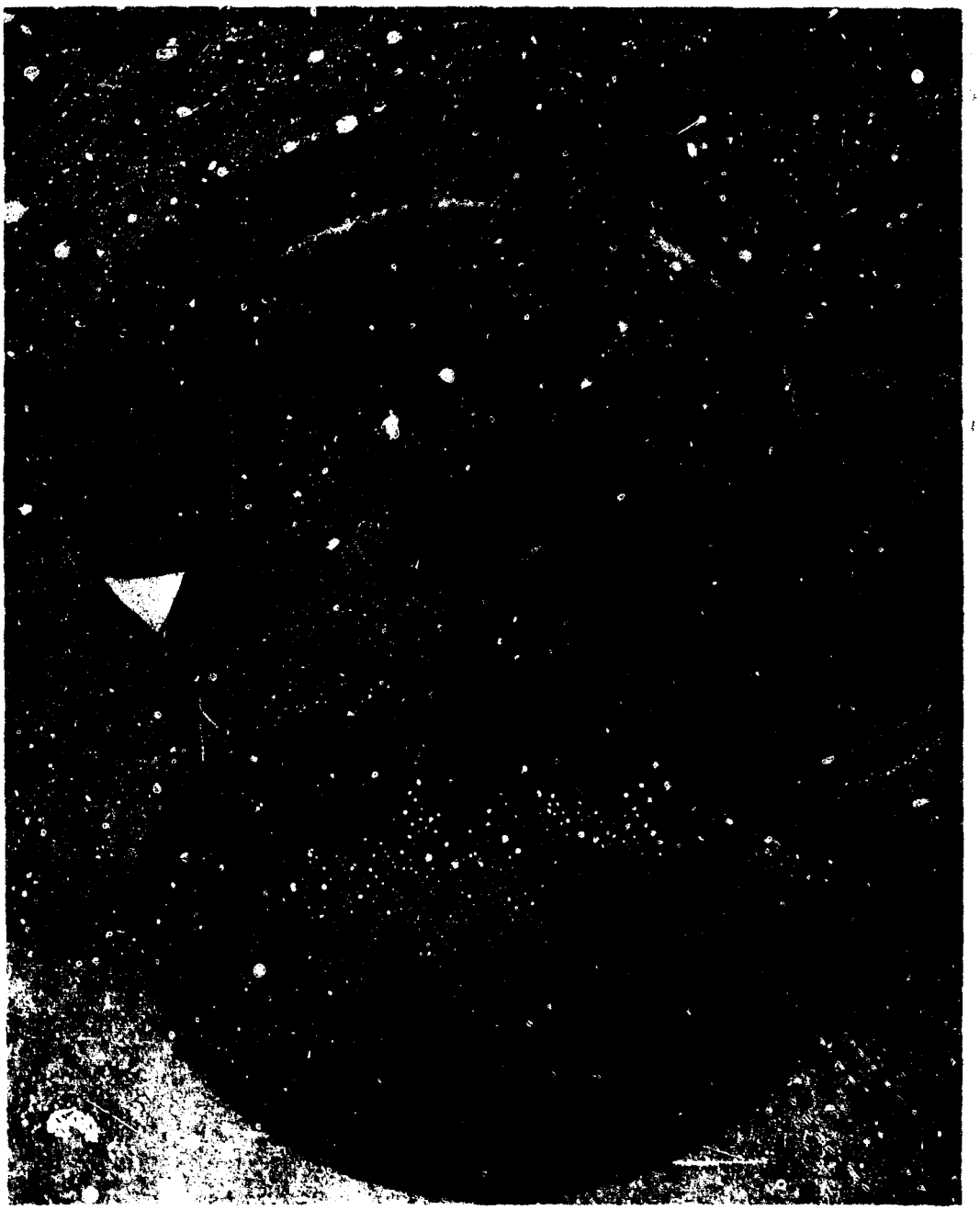

Figure 55. (U) Columbium Chamber After Test (1AW-624) — Nozzle End Up

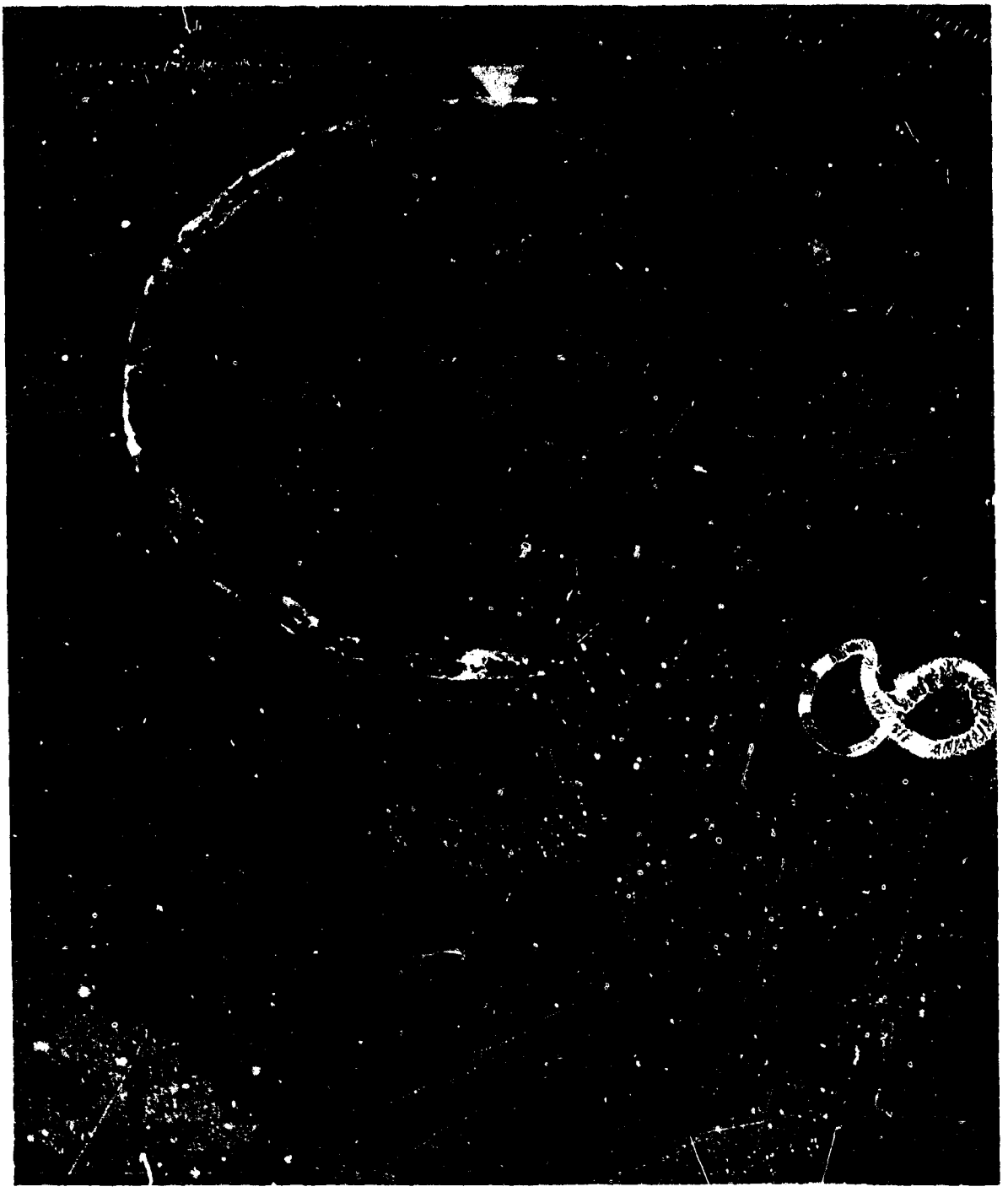

Figure 56. (U) Columbium Chamber After Test (LAW-626) — Chamber End Up

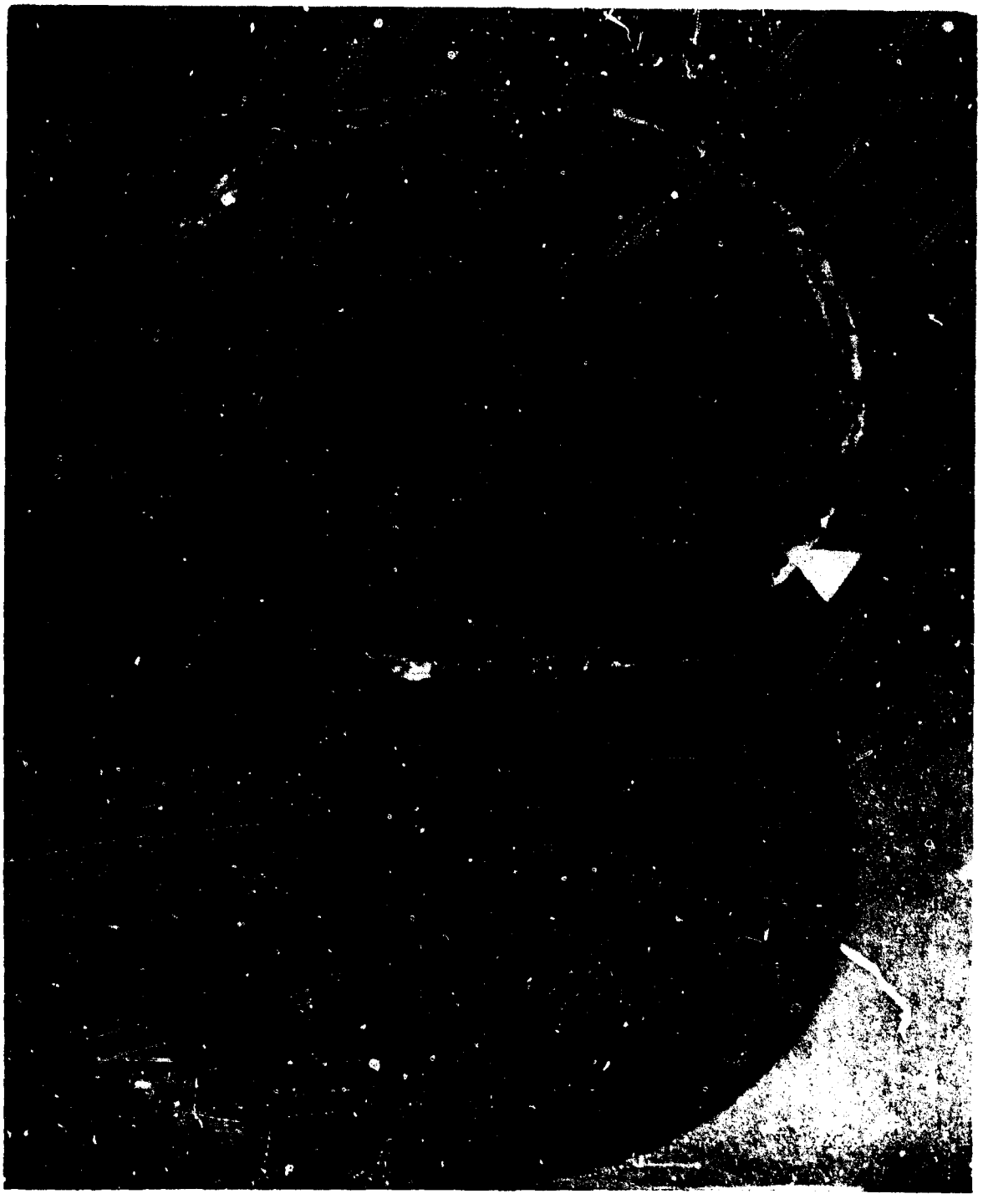

Figure 57. (U) Columbium Chamber After Test (1AW-626) — Chamber End Up

Figure 58. (U) Columbium Chamber After Test (1AW-626) — Nozzle End Up

Figure 59. (U) Columbium Chamber After Test (1AW-626) — Nozzle End Up

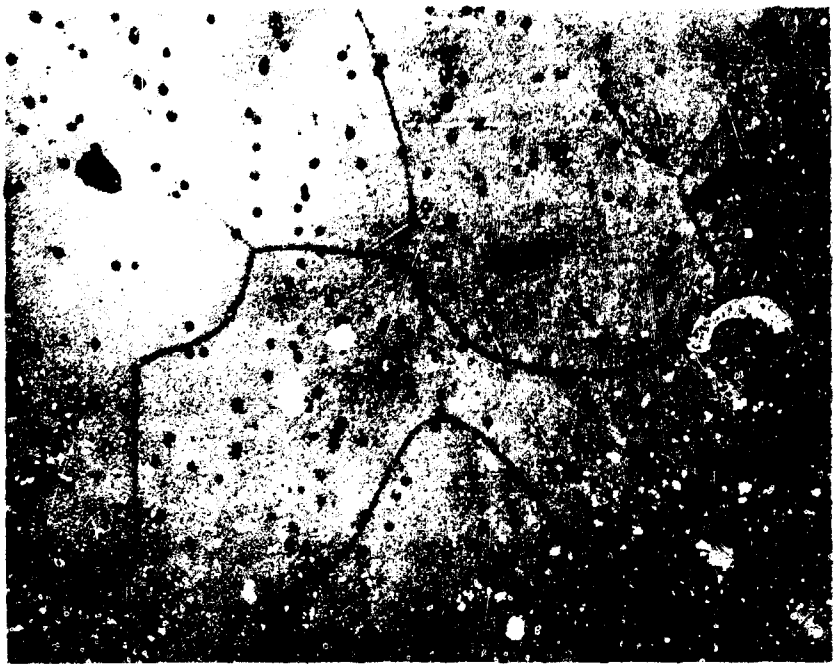

Figure 60. (U) Grain Size in Streaked Area

Figure 61. (U) Grain Size in Areas Other Than Streaked Area

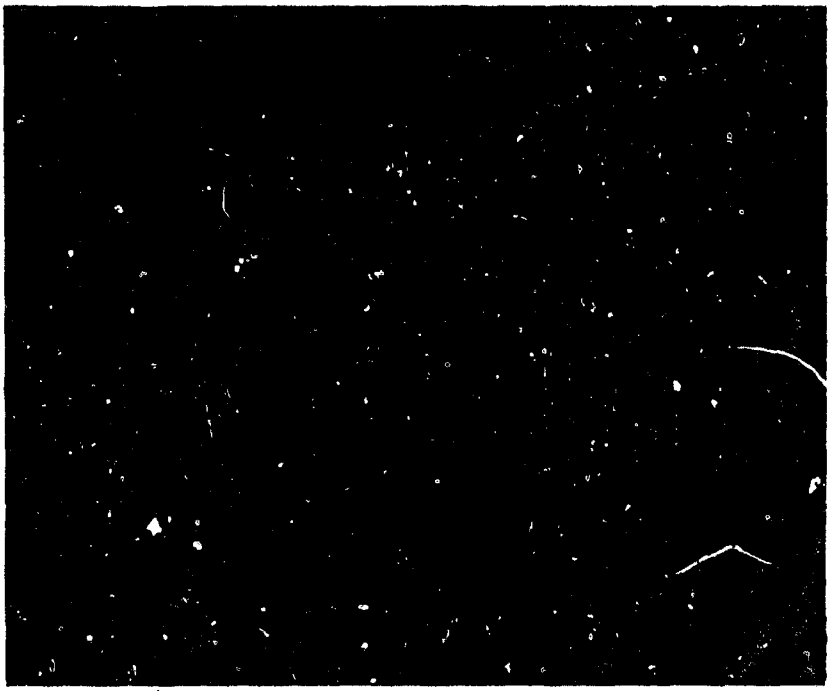

Figure 62. (U) Grain Size Prior to Firing

## TABLE XIV

## (U) MATERIALS EVALUATION TEST RESULTS

| Test No. | Length of Test (sec.) | r | $P_c$ psia | $\eta_c$ % | Max. Skin Temp. (Outside Wall) | Remarks |
|---|---|---|---|---|---|---|
| 1AW-618<br>11/10/64<br>(Tungsten) | 5.9 | 0.227 | 97.0 | 95.7 | 304 (chamber)°F<br>953 (Post Test)°F | Tungsten cylinder S/N 1. Velbestos gaskets used to seal. Crack at chamber end flange after tests. |
| 1AW-619<br>11/18/64<br>(Tungsten) | 100.9 | $\theta$ = 50 0.986<br>$\theta$ = 98.9 0.994 | 98.1<br>99.2 | 95.2<br>95.4 | 2758°F | Tungsten cylinder S/N 2. Copper gaskets used to seal. Part OK after test. |
| 1AW-620<br>11/19/64<br>(Tungsten) | 21.7 | $\theta$ = 9.2 1.529<br>$\theta$ = 17.0 1.529 | 95.7<br>96.6 | 90.4<br>91.5 | 3130+°F | Tungsten cylinder S/N 2.<br>Velbestos gasket used to seal at chamber end. Cracking occurred (post test inspection) in 3 areas and a hole (1/8" x 1/4") resulted. Slight erosion in one area. |
| 1AW-621<br>12/4/64<br>(Graphite) | 100.8 | $\theta$ = 50.0 1.512<br>$\theta$ = 98.8 1.488 | 100.4<br>101.2 | 92.6<br>92.8 | 2800°F | Tungsten retainer & graphite cylinder.<br>Copper gaskets used for sealing.<br>Part OK after test. |
| 1AW-622<br>12/14/64<br>(Graphite) | 98.8 | $\theta$ = 50 1.962<br>$\theta$ = 98.8 1.967 | 96.2<br>100.5 | 89.3<br>90.5 | ~ 3000°F | Tungsten retainer & graphite cylinder.<br>Velbestos gasket used at nozzle end, very slight erosion locally on graphite. |
| 1AW-623<br>12/15/64<br>(Tungsten) | 100 | 2.2 | 91 | 83.3 | 3320°F | Repaired tungsten cylinder S/N 1. Velbestos gasket used at nozzle end. Cracking of flange at nozzle end. Performance probably low due to leaks caused by cracks and high temperature at velbestos gasket. |
| 1AW-624<br>12/16/64<br>(Columbium) | 25.5 | 0.83 | 94.1 | 94.9 | 3000°F | Test terminated due to higher than anticipated temperatures caused by injector streaking. |
| 1AW-625<br>12/18/64<br>(Columbium) | 13.1 | 1.03 | 96.7 | 96.5 | 2895°F | Test terminated due to visual observations of a leak. |
| 1AW-626<br>12/21/64<br>(Columbium) | 100.3 | 1.86 | 101 | 96.0 | 3449°F | Injector streaking caused maximum temperature and a very local coating blistering. The temperature varied from 3000-3200°F over the rest of the chamber with no detrimental effects. |
| 1AW-627<br>12/21/64 | 100.2 | 2.06 | 96 | 86.2 | 2960°F | Silvery and black discoloration internally indicated grain growth. |

$\theta$ - Indicates time

## SECTION 6

## (C) ADIABATIC WALL THRUST CHAMBER

### A. (C) GENERAL

(C) An advanced thrust chamber rated at approximately 3500 pounds vacuum thrust (utilizing a 45:1 area ratio nozzle) at a chamber pressure of 65 psia with the propellant combination of fluorine and a hydrazine blend (BA-1014) was utilized to demonstrate the adiabatic wall cooling concept. This cooling concept can be utilized over a 12.5:1 throttling range or more although demonstration was limited to approximately a 2:1 range due to test stand limitations. Initially, this thrust chamber concept was to be demonstrated using a two-stage combustion injector similar to the injector tested with the $N_2O_4$/50% $N_2H_4$ + 50% UDMH propellant combination on the Maneuvering Satellite program. However, since development beyond the scope of the program was required to resolve oxidizer rich gas generator problems, the decision was made to utilize a fixed orifice injector to demonstrate the adiabatic wall thrust chamber concept with the high energy propellants.

### B. (C) TECHNICAL DISCUSSION

#### 1. (C) General Discussion

(C) The concept described as the adiabatic wall thrust chamber provided cooling of the thrust chamber wall by utilizing fuel rich combustion gases for cooling by providing a thermal barrier (boundary layer) between the main core combustion gases and the thrust chamber wall. The feasibility of operation of this cooling concept was demonstrated using a fixed orifice injector, an auxiliary fuel rich gas generator to generate the cooling gases, and an adiabatic wall thrust chamber. The objective of this phase of the program was to demonstrate:

(a) (C) A durability goal of 120 seconds continuous operation at a vacuum thrust level of 3500 pounds (45:1 area ratio nozzle) and a chamber pressure of 65 psia.

(b) (C) A goal of 95% combustion efficiency (characteristic velocity, c*).

(c) (C) Throttling over a 2:1 range (sea level limitations).

#### 2. (C) Injector Design and Fabrication

(C) A fixed orifice liquid conventional injector incorporating an impinging showerhead doublet design was designed as shown in Figure 63. This injector incorporated a 60 doublet configuration with 60 fuel holes located at the outer periphery for film cooling. This injector was designed for a mixture ratio of 1.8 with the propellant combination of $F_2$/BA-1014 at a chamber pressure of 65 psia. The velocities and momentum relationships were predicated upon the results of similar injectors built

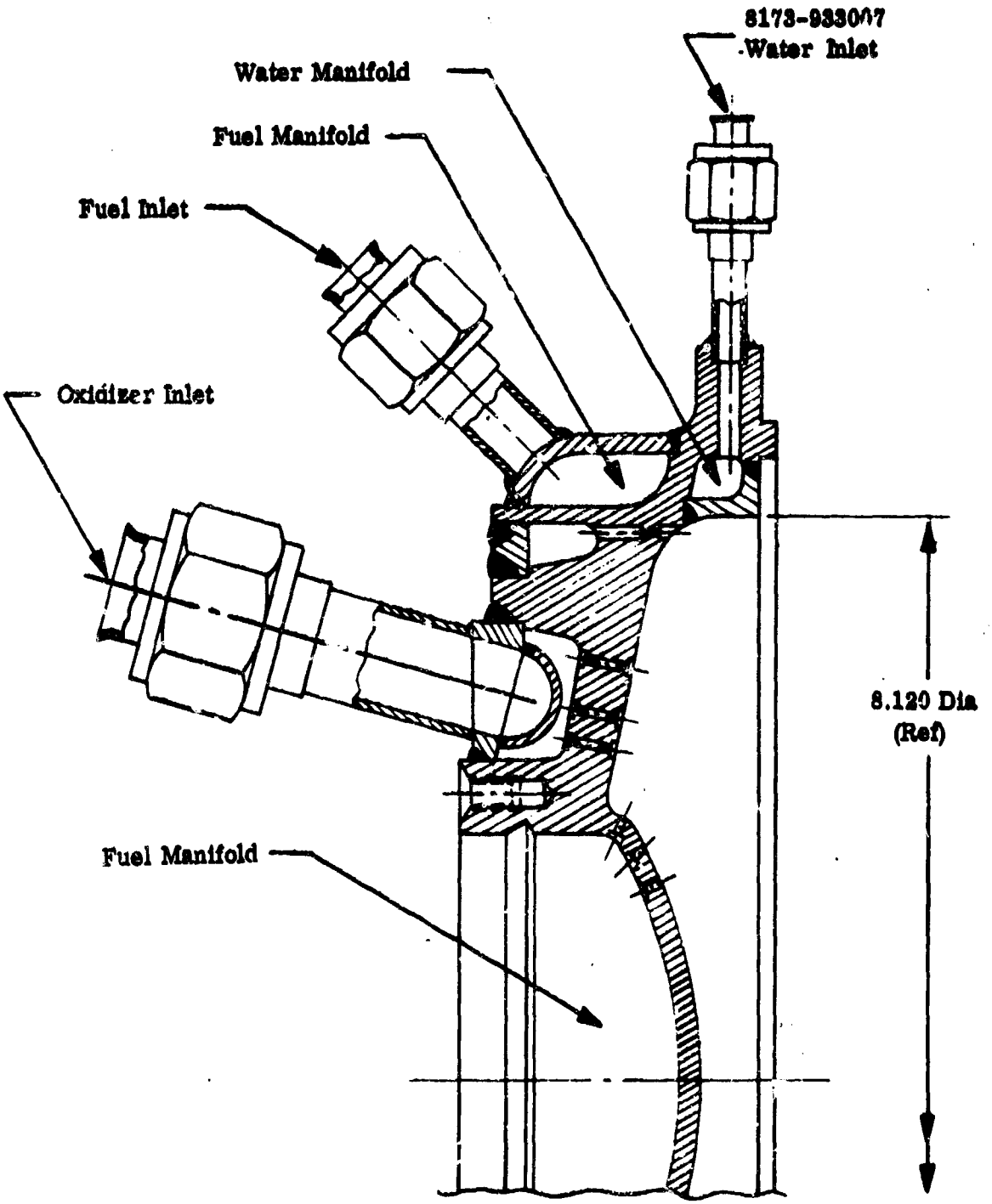


Figure 63. (C) 3.5K Injector (With Coolant)

(C) and tested by Bell Aerosystems Company on other programs with the same propellant combination.

(C) This injector was designed of 6061 aluminum for use in a 27 L* (characteristic length) chamber. The design incorporated a water cooled flange for utilization with the adiabatic wall thrust chamber to minimize the problems associated with a high temperature joint. In addition, this injector incorporates fuel cooling of the face of the injector and a zirconium oxide coating on the dome of the injector to act as a thermal and erosion barrier due to any recirculation caused by the combustion processes.

(C) An analysis was conducted on the fixed orifice injector to determine the heat transfer effects of the injector using film cooling compared to the injector with no film cooling. The information utilized was predicated upon the results of the tests on other programs using the propellant combination of fluorine/BA-1014. The results of the tests conducted on previous programs indicated a 24% reduction in chamber heat flux for a seven-inch long chamber and no reduction in nozzle heat flux. This indicated that the film cooling had been completely dissipated by the time it reached the convergent nozzle. Based on this input, an analysis was conducted to determine the justification for the liner of the adiabatic wall thrust chamber and the results indicated:

(a) (C) The barrel section of the thrust chamber would reach 3850°F without utilizing film cooling in the injector.

(b) (C) The barrel section of the thrust chamber would operate at a temperature of 3530°F with the film cooled injector.

(c) (C) Since these temperatures were substantially above the allowable temperatures for the columbium thrust chamber, a liner was required in order to operate the adiabatic wall thrust chamber.

(d) (C) The effect of utilizing an injector with film cooling versus one without film cooling would result in a change in the liner temperature of approximately 600°F. This indicated that the average downstream liner temperature would reach 3600°F with the injector utilizing no film cooling and 3000°F with the injector utilizing film cooling. It was anticipated that localized hot spots would possibly increase this temperature an additional 400°F in either case. These temperatures were predicated upon the test results obtained on other programs with the seven-inch chamber section. The Model 8173 chamber was approximately 12 inches long so these results indicated a larger reduction in temperature with the film cooling than would most likely occur due to the longer chamber section on Model 8173.

(e) (C) Since the above results indicated that the adiabatic wall thrust chamber and liner could be operated satisfactorily without injector film cooling, the injector design was modified to eliminate film cooling from the injector. This design is shown in Figure 64.

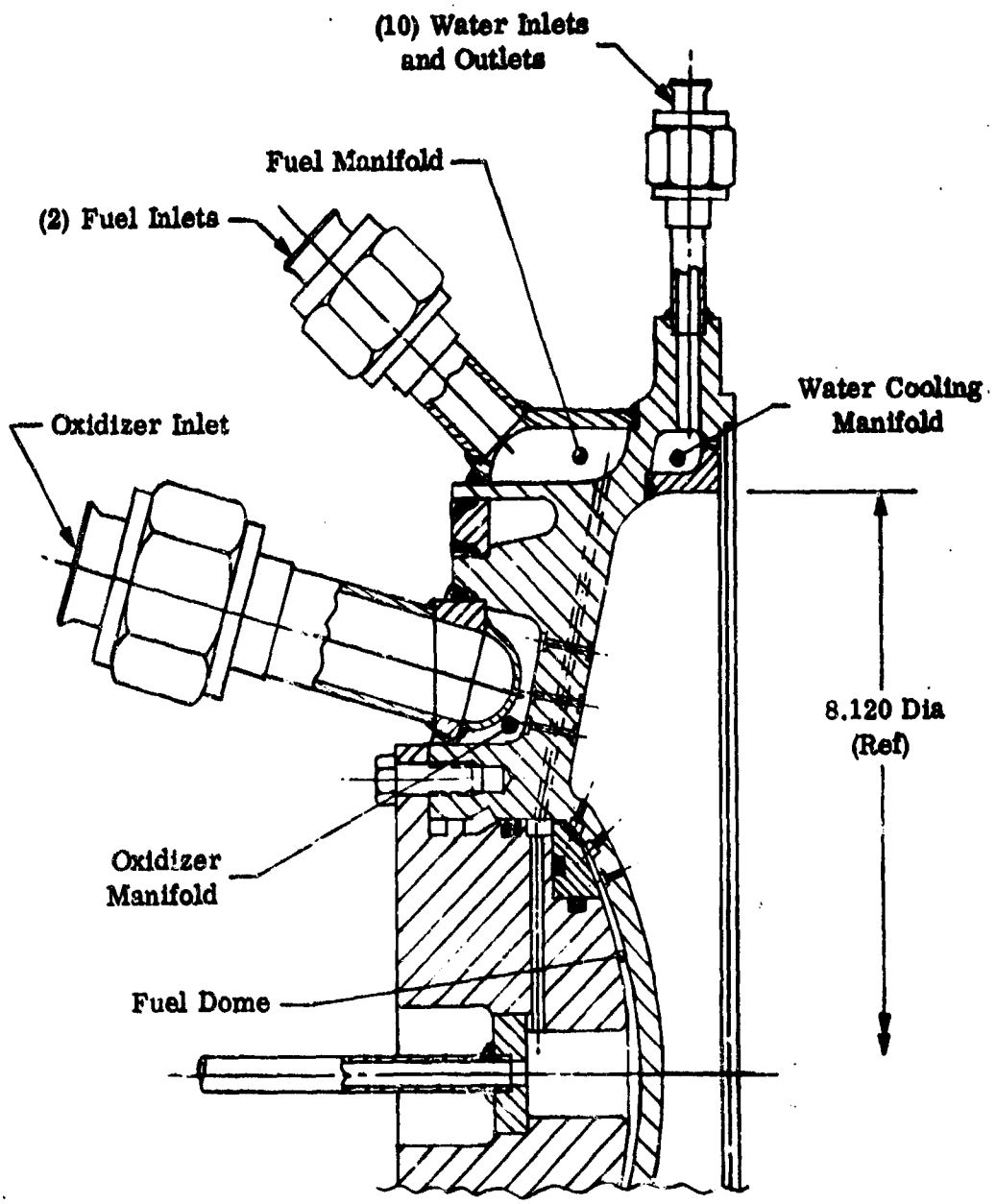


Figure 34. (C) 3.5K Injector (Without Coolant)

(U) Another heat transfer analysis was conducted to determine the actual heat flux values to be expected on this injector over the chamber pressure range of 35 to 70 psia which was the range to be tested. Two methods were employed to determine the heat fluxes of the various sections of the assembly (see Figure 65) to be tested to define the performance, heat rejection and durability of the injector. One method of analysis utilized was the Bartz method[1] which was based on frozen equilibrium transport properties, and the other method utilized was to employ a more conservative approach which was based on shifting equilibrium transport properties (Prandtl number of 0.5) and a variable correlating coefficient ($\bar{K}g$) which was a function of area ratio. The results of this analysis are shown in Figure 66.

3. (C) Auxiliary Fuel Rich Gas Generator-Manifold Assembly

(C) Various design configurations were conducted on the fuel rich gas generator-manifold assembly utilized with the adiabatic wall thrust chamber assembly to generate coolant gases to provide the thermal barrier between the main core combustion gases and the thrust chamber wall. This auxiliary generator was utilized to define the amount of fuel rich gases required to cool the nozzle and to define the effect of coolant flow rate on nozzle heat flux and overall thrust chamber performance. The auxiliary fuel rich gas generator-manifold assembly was fabricated of Haynes 25 and utilized an injector available from a previous Bell program (Figure 67) for demonstration of the feasibility of the adiabatic wall thrust chamber concept with the high energy propellant combination of fluorine/BA-1014.

(C) Figure 68 shows the design configuration of the gas generator-manifold assembly utilized in the program. The generator chamber section was nine inches long so that the volume per mass flow ratio was approximately 20% greater than that used on a previous Bell program with this injector. The reason for increasing the volume was to allow for adequate volume for recombination of the dissociated ammonia resulting from the BA-1014 blend. In addition, a baffle was utilized in the gas generator section to deflect any dissociated ammonia into the combustion process so that further reaction of the fuel rich gases did not occur in the manifold assembly. If further reaction did occur in the manifold assembly, high temperature regions would result which could be detrimental to the durability of the manifold assembly.

4. (C) Adiabatic Thrust Chamber Design

(C) The thrust chamber design contemplated for demonstration of the feasibility of the adiabatic wall cooling concept utilized a columbium alloy (SCb-291) radiation cooled thrust chamber and a refractory metal liner to insure the injection of the fuel rich coolant gases into the convergent nozzle. The interaction of the

---

[1] "A Simple Equation for Rapid Estimation of Rocket Nozzle Convective Heat Transfer Coefficients," by D.R. Bartz, Jet Propulsion, Vol. 27, January 1957

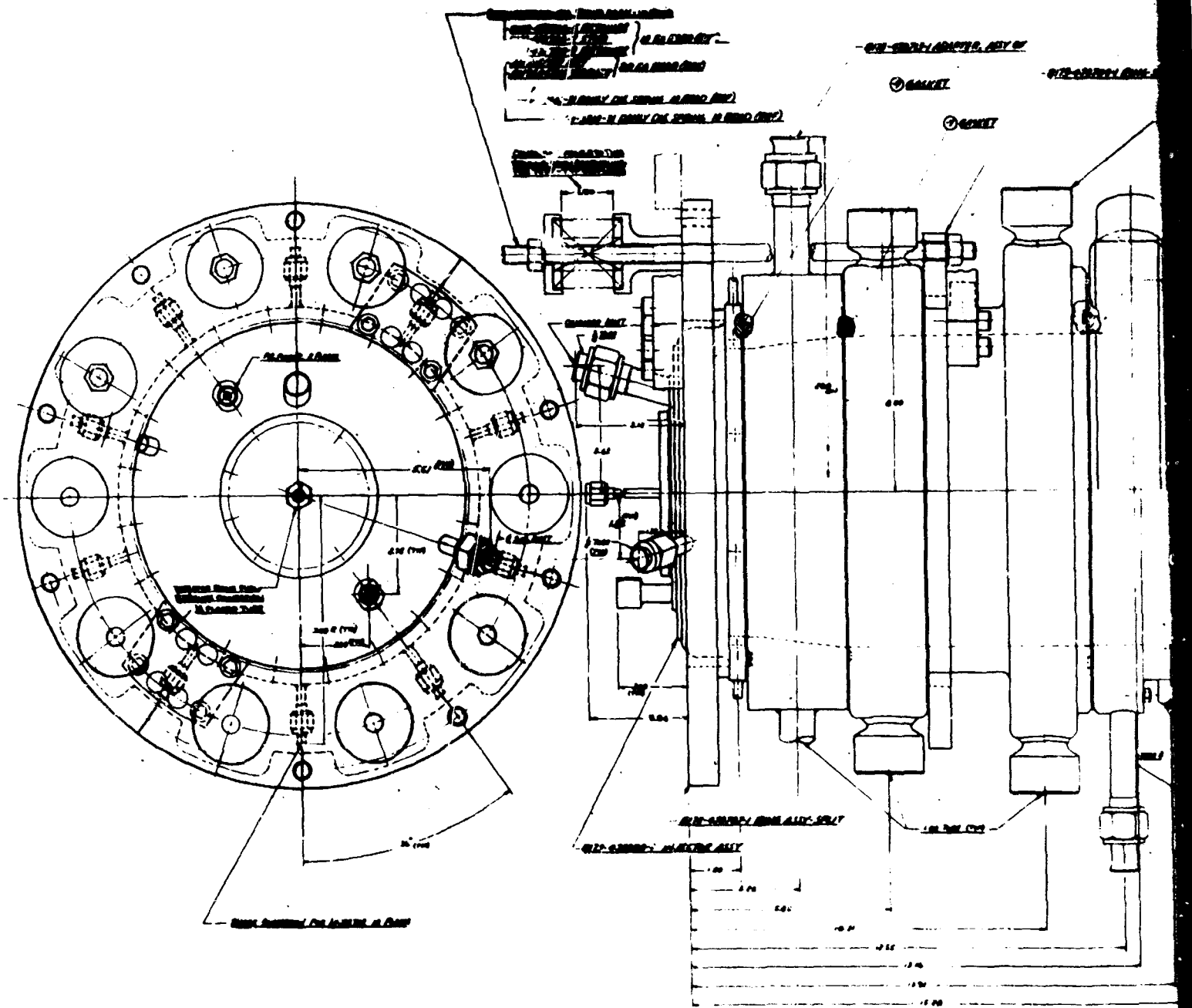

Figure 65. (U) Thrust Chamber Assembly, Water Cooled Start Hardware - Injector Test

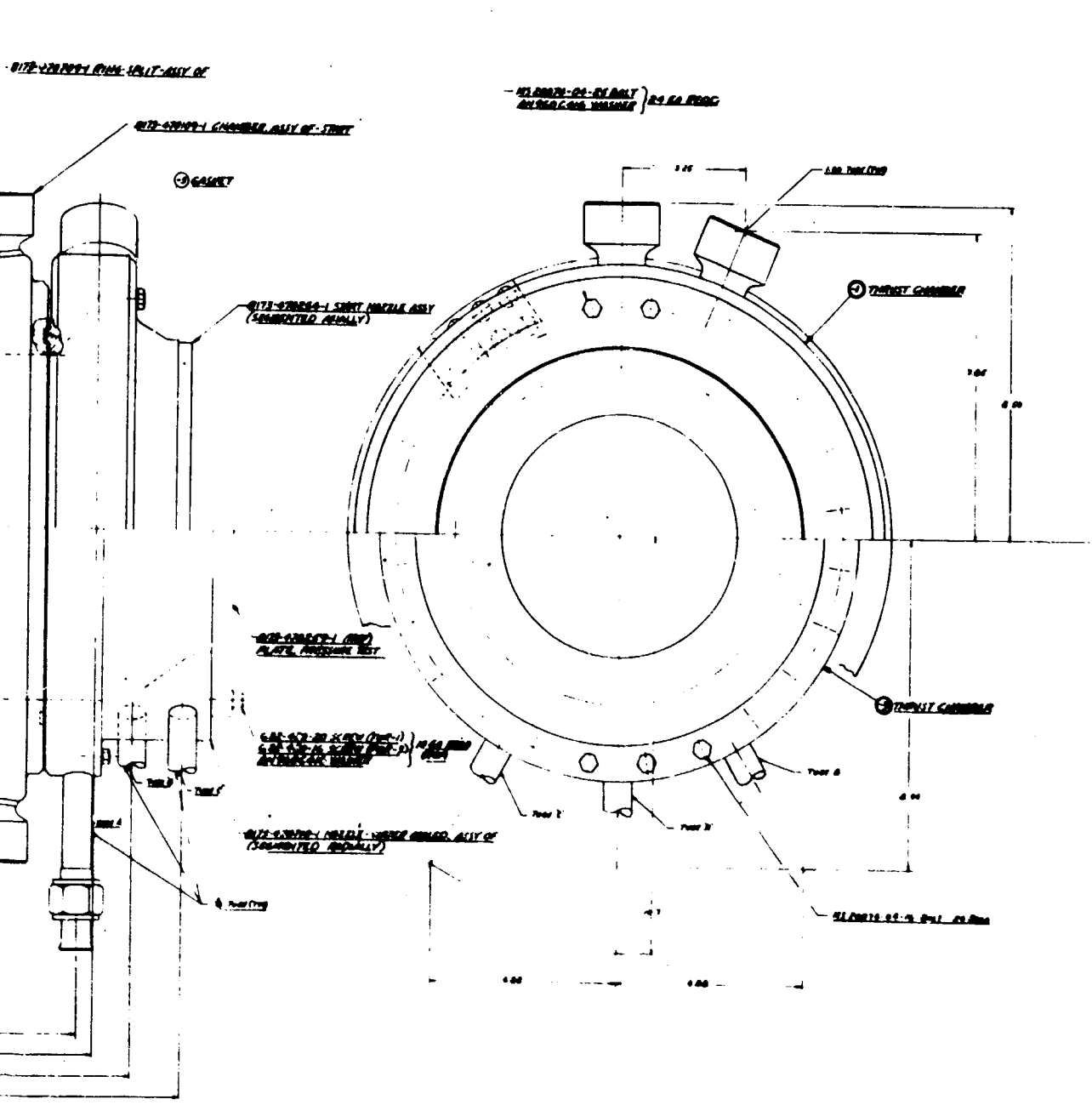


2

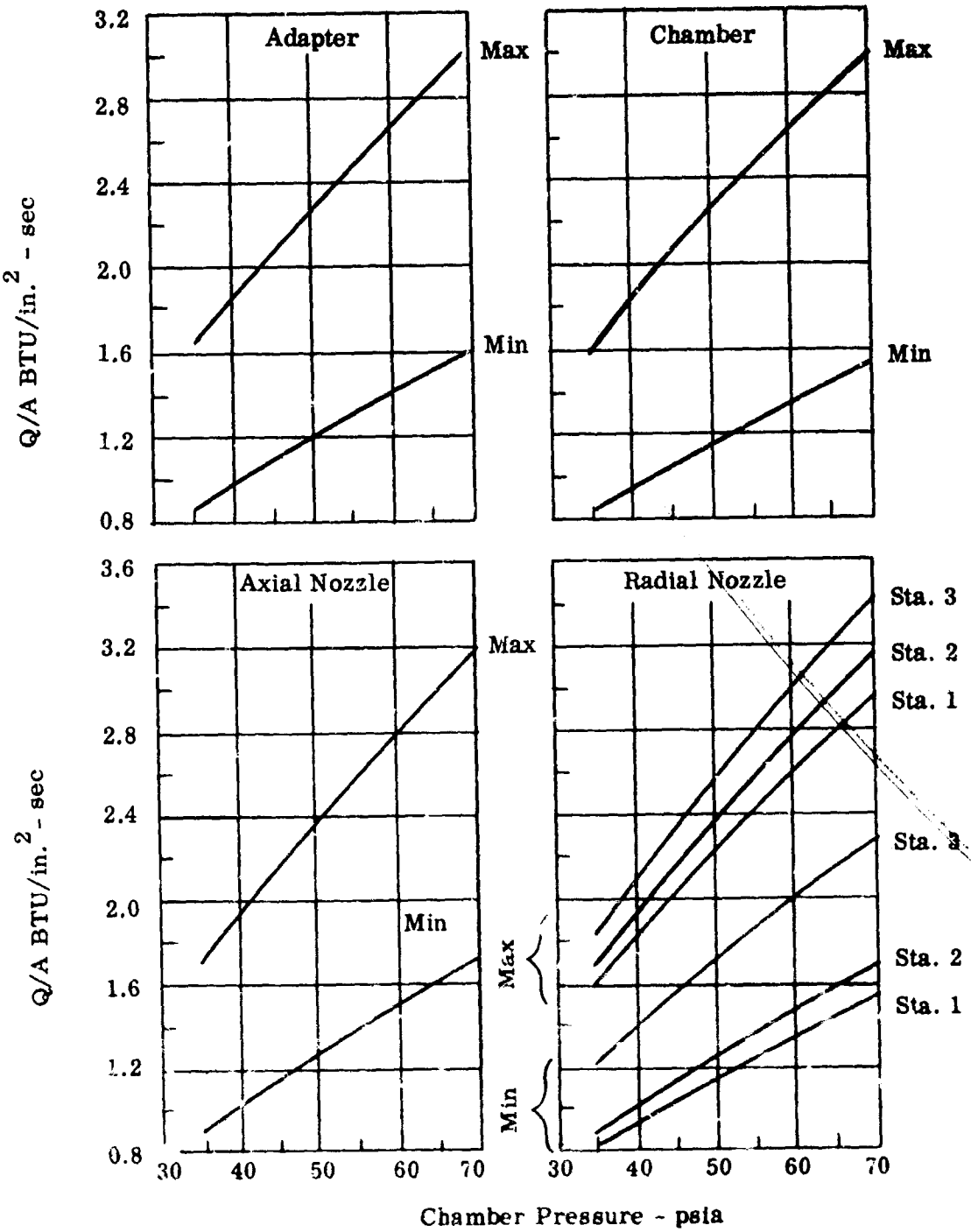


Figure 66. (U) Average Heat Flux With Varying Chamber Pressure

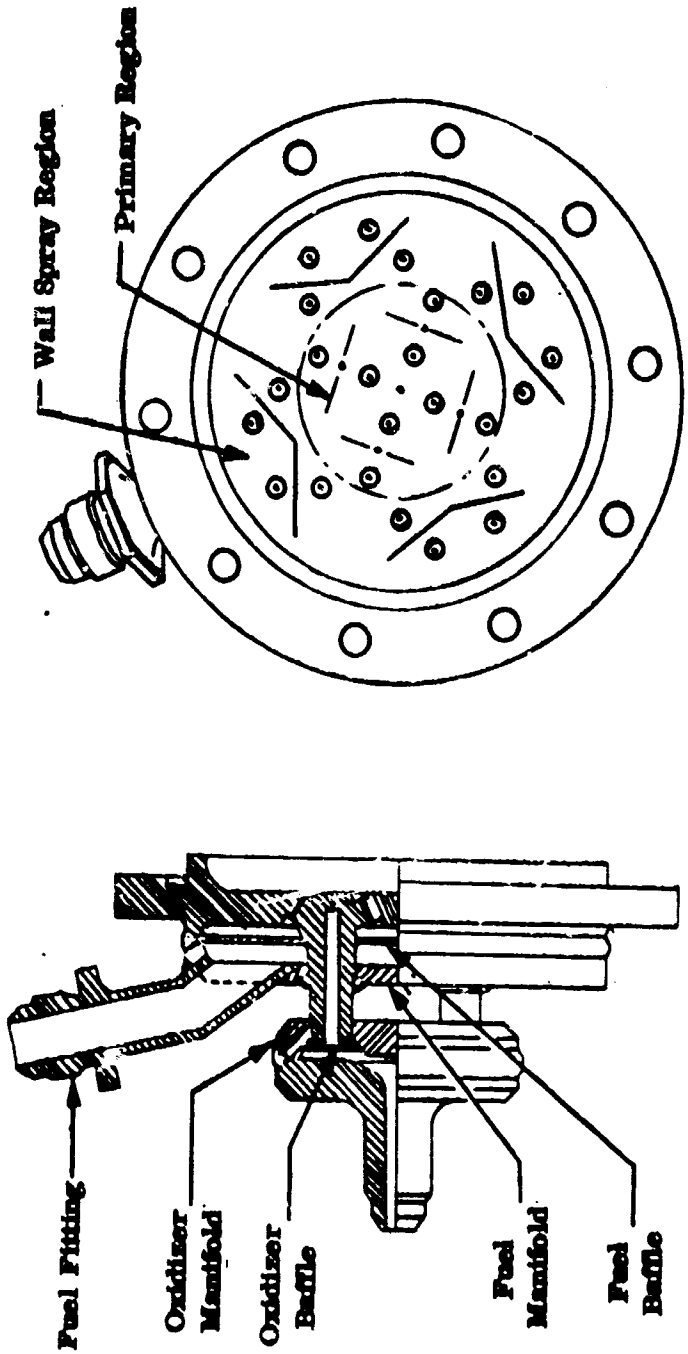


Figure 67. (U) Fuel Rich Gas Generator Injector

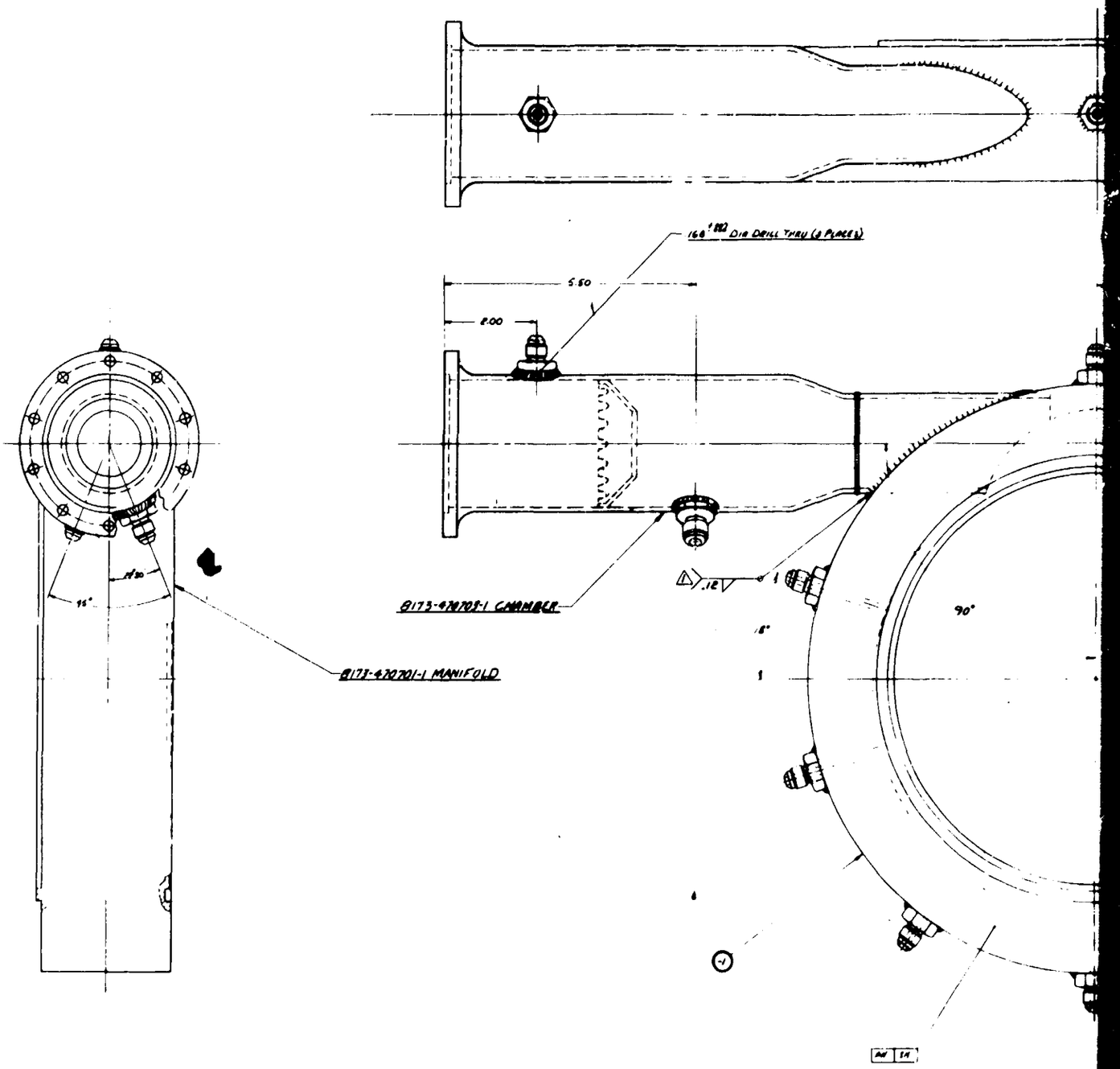
.160 +.002 DIA DRILL THRU (8 PLACES)
5.50
8.00
8173-470703-1 CHAMBER
8173-470701-1 MANIFOLD
.12
90°
45°
15°

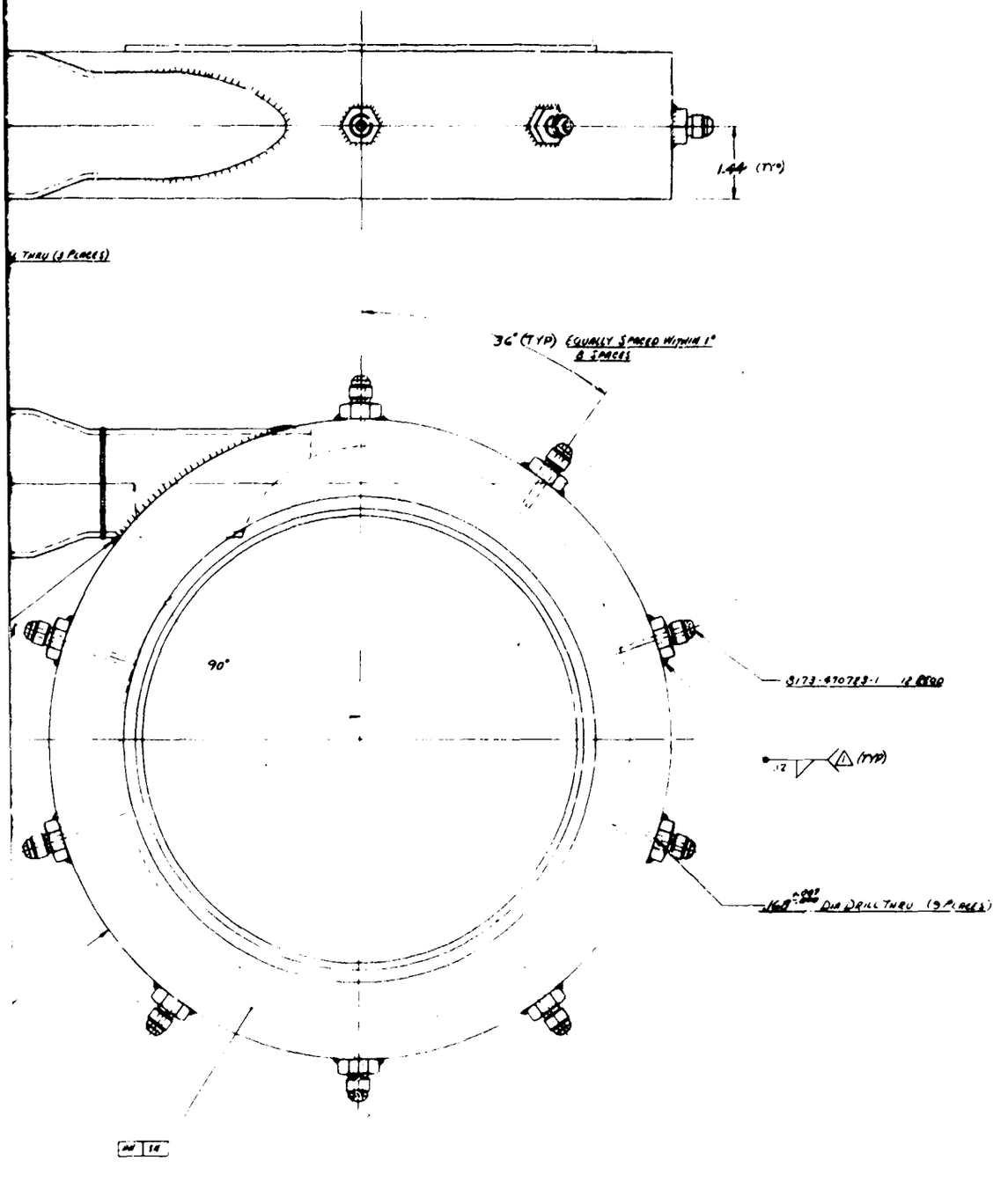


Figure 68. (U) Fuel Rich Gas Generator - Auxiliary Manifold Assembly




(This page is Unclassified)

(C) injector, auxiliary fuel rich gas generator assembly, columbium thrust chamber and liner required careful design to maintain alignment, minimize stresses, incorporate adequate protection from a heat transfer standpoint so that individual parts do not become overheated, and to allow for growth due to thermal expansion. Therefore, investigations were conducted in these areas in order to obtain sufficient information to incorporate into the design.

(C) The proper film cooling design criteria required that the coolant gas velocity as it flowed from the annulus be equal to or slightly less than the velocity of the main stream gases at this point. In order to properly design the liner to give the required velocity, a knowledge of the thermal effects on the annular gap was required. Therefore, a heat transfer analysis was conducted to determine the effect of annular gap on chamber and throat wall temperatures of the columbium thrust chamber and liner temperatures at the upstream end of the liner. The following analysis was predicated on a steady-state energy balance with fully developed flow of both the fuel rich gases and the main core combustion gases.

(C) Heat flux across the liner is given by:

$$q_1 + q_2 - q_3 = 0$$

Heat flux across the chamber section is given by:

$$q_3 + q_4 - q_5 = 0$$

where

$q_1$ - heat flux due to forced convection between the core gas and liner wall

$q_2$ - heat flux due to forced convection between the liner wall and coolant gas

$q_3$ - heat flux due to radiation between the liner wall and chamber wall

$q_4$ - heat flux due to forced convection between the coolant gas and chamber wall

$q_5$ - heat flux due to radiation from the chamber wall to space

These relationships can further be defined as follows:

$$h_g (T_g - T_{wg}) + h_c (T_c - T_{wg}) - \epsilon^1 \sigma (T_{wg}^4 - T_a^4) = 0$$

$$\epsilon^1 \sigma (T_{wg}^4 - T_a^4) + h_c (T_c - T_a) - \epsilon \sigma T_a^4 = 0$$

(C) where

$T$ = temperature, $^{\circ}R$

$h$ = heat transfer coefficient of film, BTU/in.$^2$-sec-$^{\circ}F$

$\epsilon$ = emissivity

$\epsilon^1$ = emissivity corrected for view factor

$\partial$ = Stefan-Boltzmann constant

subscripts

$g$ = core gas

$wg$ = liner wall, gas side

$c$ = coolant gas

$a$ = chamber wall

(C) The temperature rise of the coolant was found by considering that the heat to the coolant was equal to the heat rejected from the liner less the heat rejected to space or:

$$T_c = \frac{(q_1 - q_5)\, D_{wg}\, \Delta^1}{W_c C_{p_c}}$$

where

$\Delta T_c$ = temperature rise of the coolant gas

$D_{wg}$ = local diameter

$\Delta^1$ = element of length of the liner considered

$W_c$ = coolant mass flow rate

$C_{p_c}$ = coolant specific heat

The resistances (t/k) across the wall of the thrust chamber and liner were neglected since they are low compared to the coolant gas film resistants ($1/h_c$). The following inputs were utilized for this analysis:

| (C) Condition | Main Core Gas | Coolant Gas |
|---|---|---|
| Propellant Combination | $F_2$/BA-1014 | $F_2$/BA-1014 |
| Mixture Ratio | 1.8 | 0.045 |
| Pressure | 70 psia | 70 psia at liner exit |
| Combustion Efficiency | 97% | 93.4% |
| Total Weight Flow | 9.85% | 0.985 |

(C) Figure 69 shows the results of this analysis which was predicated upon equilibrium conditions for both the main core gas and the coolant. The design point was predicated upon 45% dissociation of ammonia for the coolant gas which was correlated from test data obtained with this injector on a previous program. Based on these results, it was predicted that the throat wall temperature will reach 2300°F. However, incorporating the differences between the calculated values and the data obtained from tests on the $N_2O_4$/50% UDMH-50% $N_2H_4$ phase of the program, it was estimated that the throat wall temperature would reach 2740°F as an average value and hot spots may reach a maximum of 3000°F.

(C) A series of analyses was conducted to determine the effect of coolant flow rate on heat rejection, throat temperature of the columbium thrust chamber, liner temperature and the effect of coolant flow rate on performance and overall mixture ratio. Since the initial testing of the liner concept was conducted in a water cooled chamber and either an axially segmented water cooled nozzle (to determine variations in heat flux around the periphery) or a radially segmented water cooled nozzle (to determine variations in heat flux at three stations in the convergent nozzle), a heat transfer analysis was conducted to determine the effect of coolant flow rate on heat flux for varying chamber pressure; the results are shown in Figure 70. In conjunction with this analysis, Figure 71 shows the effect of barrier flow on throat temperature and Figure 72 shows the effect of barrier flow on liner temperature. These results indicated that, theoretically, 7% barrier flow should be utilized to maintain a maximum throat temperature of 3050°F (2720°F average) and a maximum liner temperature of 4100°F (3700°F average). If 7% barrier flow was utilized, the overall engine mixture ratio would operate at 1.5 (based on r = 1.8 without barrier), as shown in Figure 73, with a resultant vacuum specific impulse of 364 lb-sec/lb ( $\epsilon$ = 45) as shown in Figure 74, which is approximately a 4% reduction in vacuum specific impulse over an engine using no barrier. These results were correlated with actual test data in the test program.

In addition, an analysis was conducted on the adiabatic wall thrust chamber to determine the effect of varying heat flux upon wall temperature for a 10% barrier/total flow ratio and these results are shown in Figure 75.

a. (U) Thrust Chamber

(U) An evaluation of vendors for manufacturing the SCb-291 columbium alloy thrust chamber resulted in the selection of Fansteel Metallurgical Corporation. The thrust chamber design (Figure 76) was released for fabrication by machining the thrust chamber from rough forgings (two) and welding the two forgings together. After

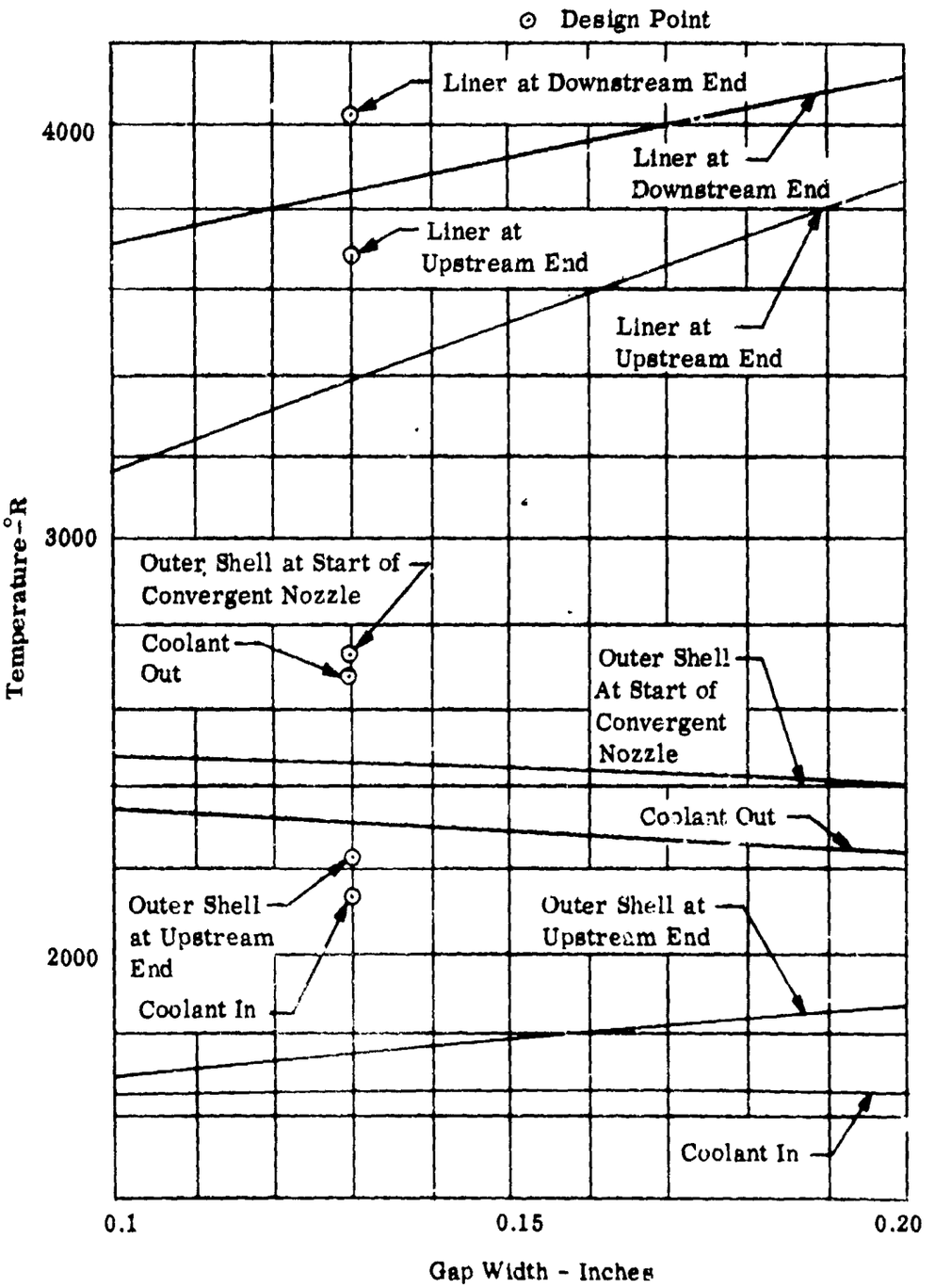


Figure 69. (C) Effect of Gap Width on Temperature

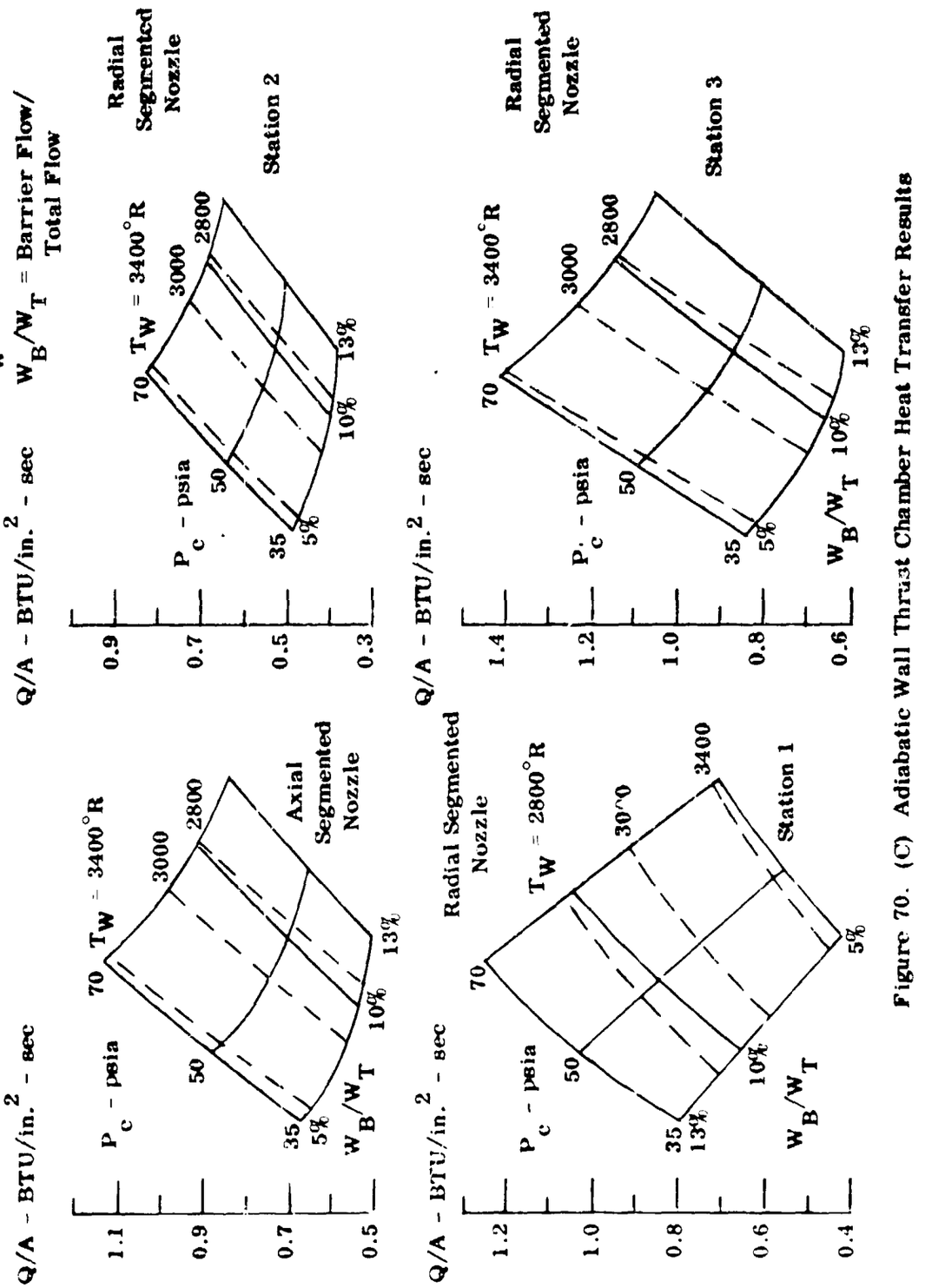


Figure 70. (C) Adiabatic Wall Thrust Chamber Heat Transfer Results

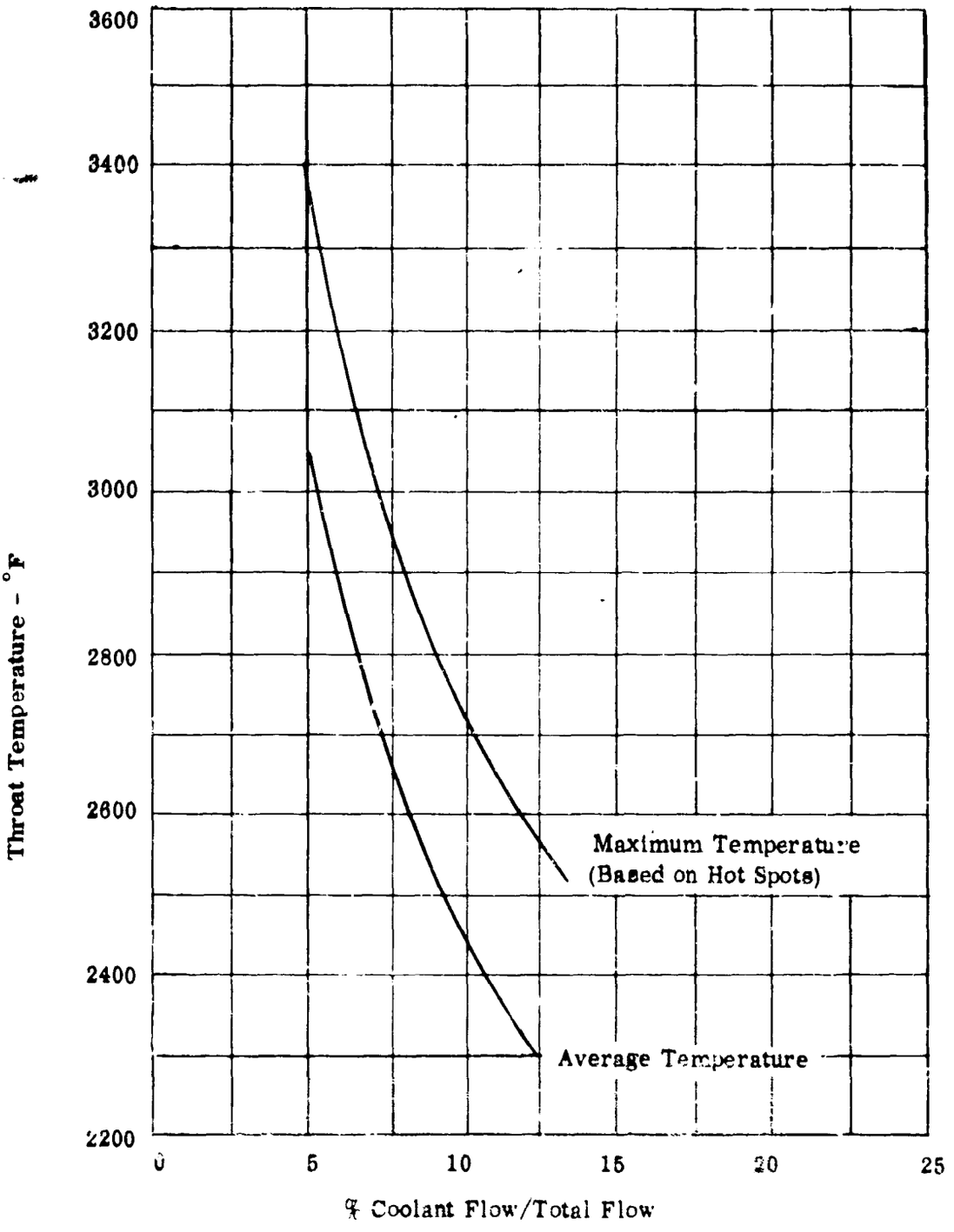


Figure 71. (C) Effect of Coolant Flow on Throat Temperature (Open Tube Cooling)

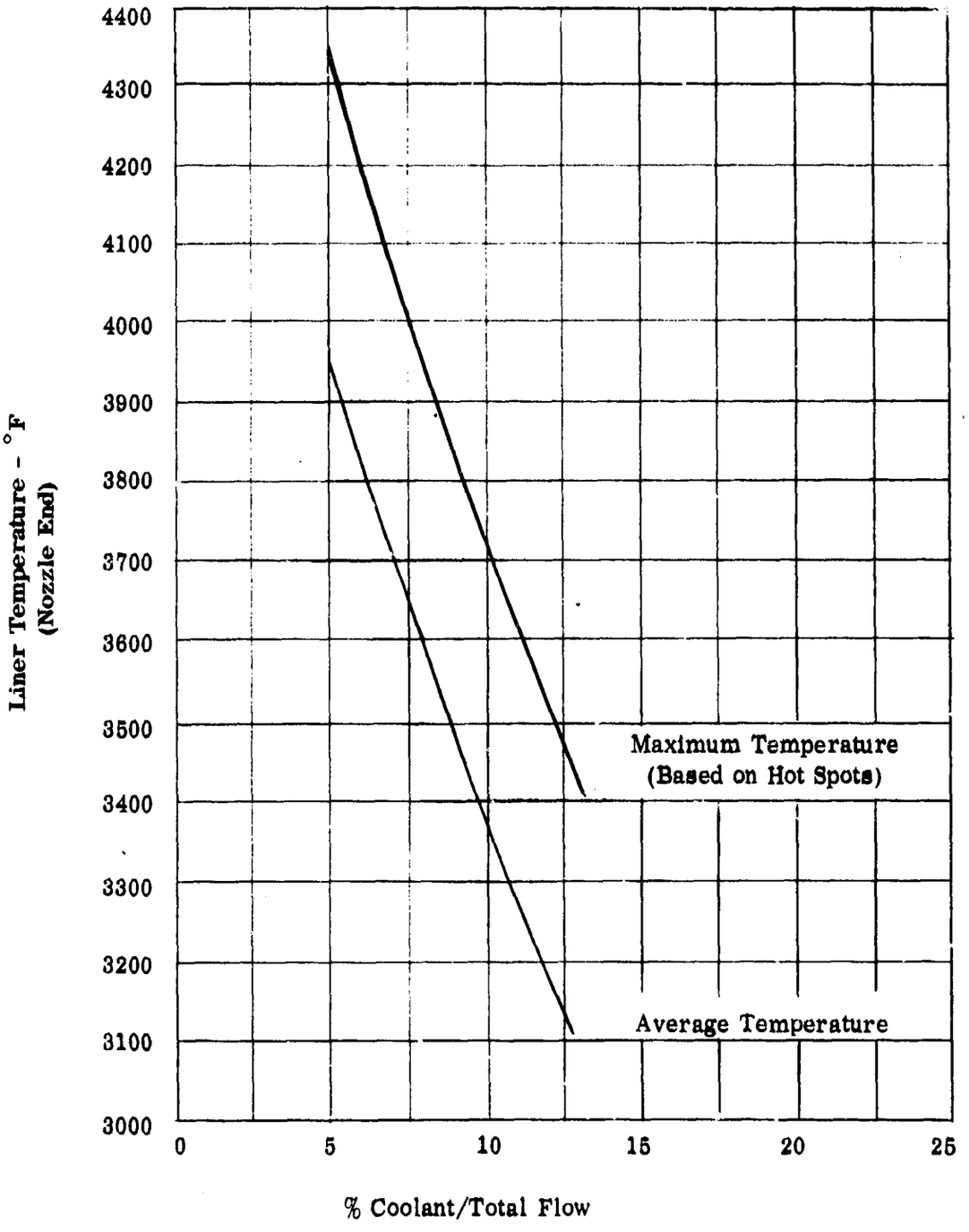


Figure 72. (C) Effect of Coolant Flow on Liner Temperature (Open Tube Cooling)

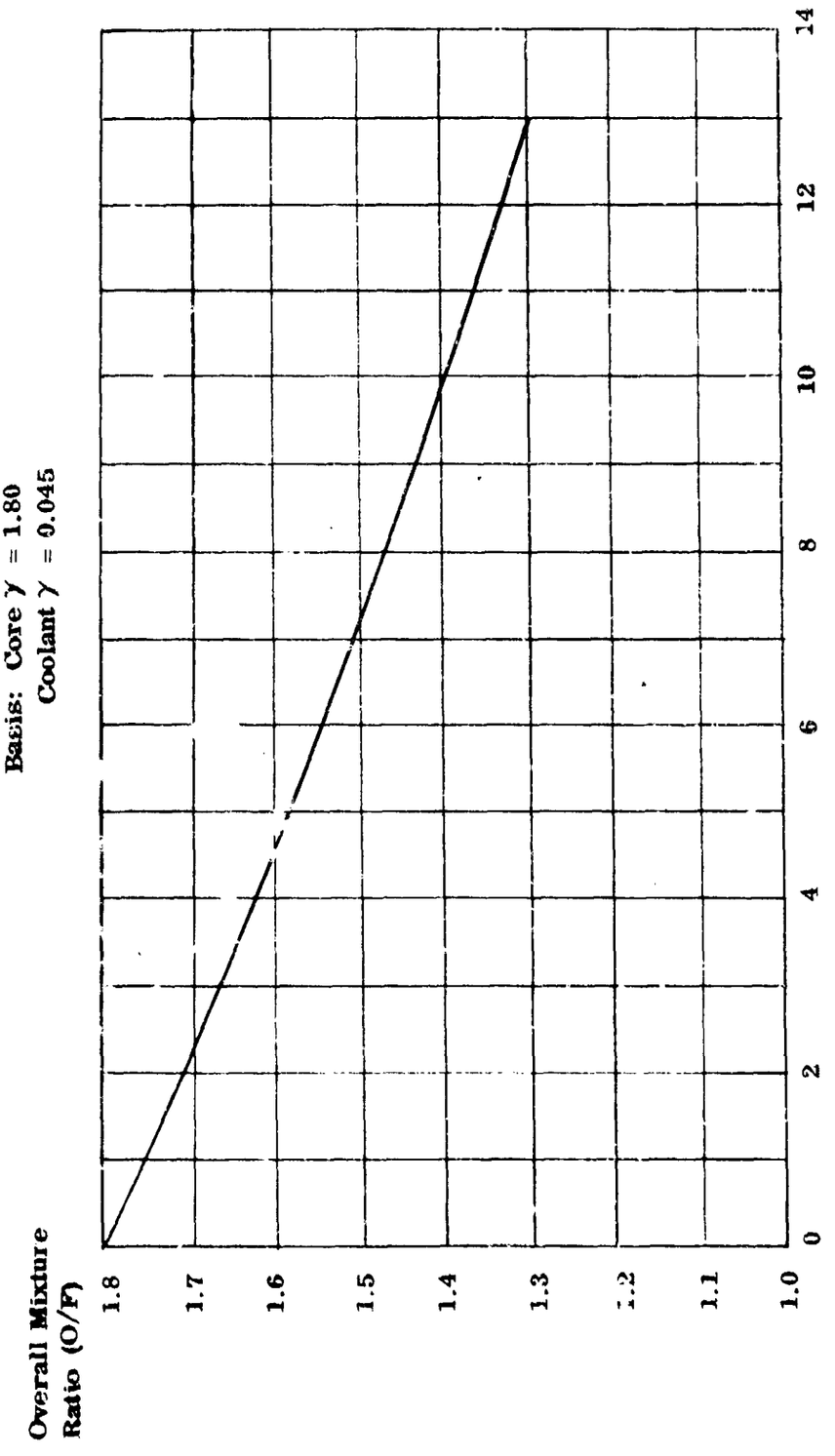


Figure 73. (C) Effect of Coolant Flow on Overall Mixture Ratio

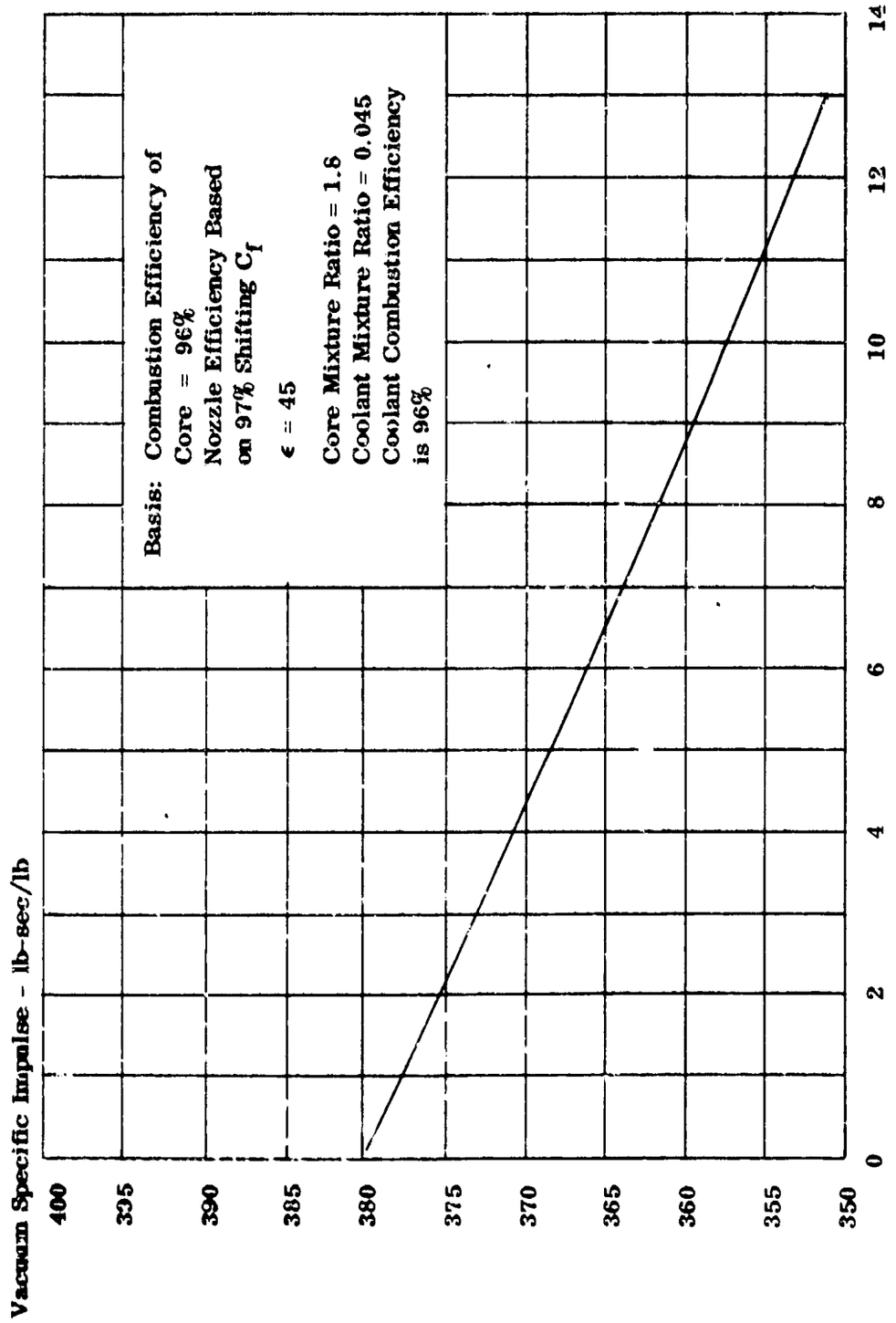


Figure 74. (C) Effect of Coolant Flow on Performance

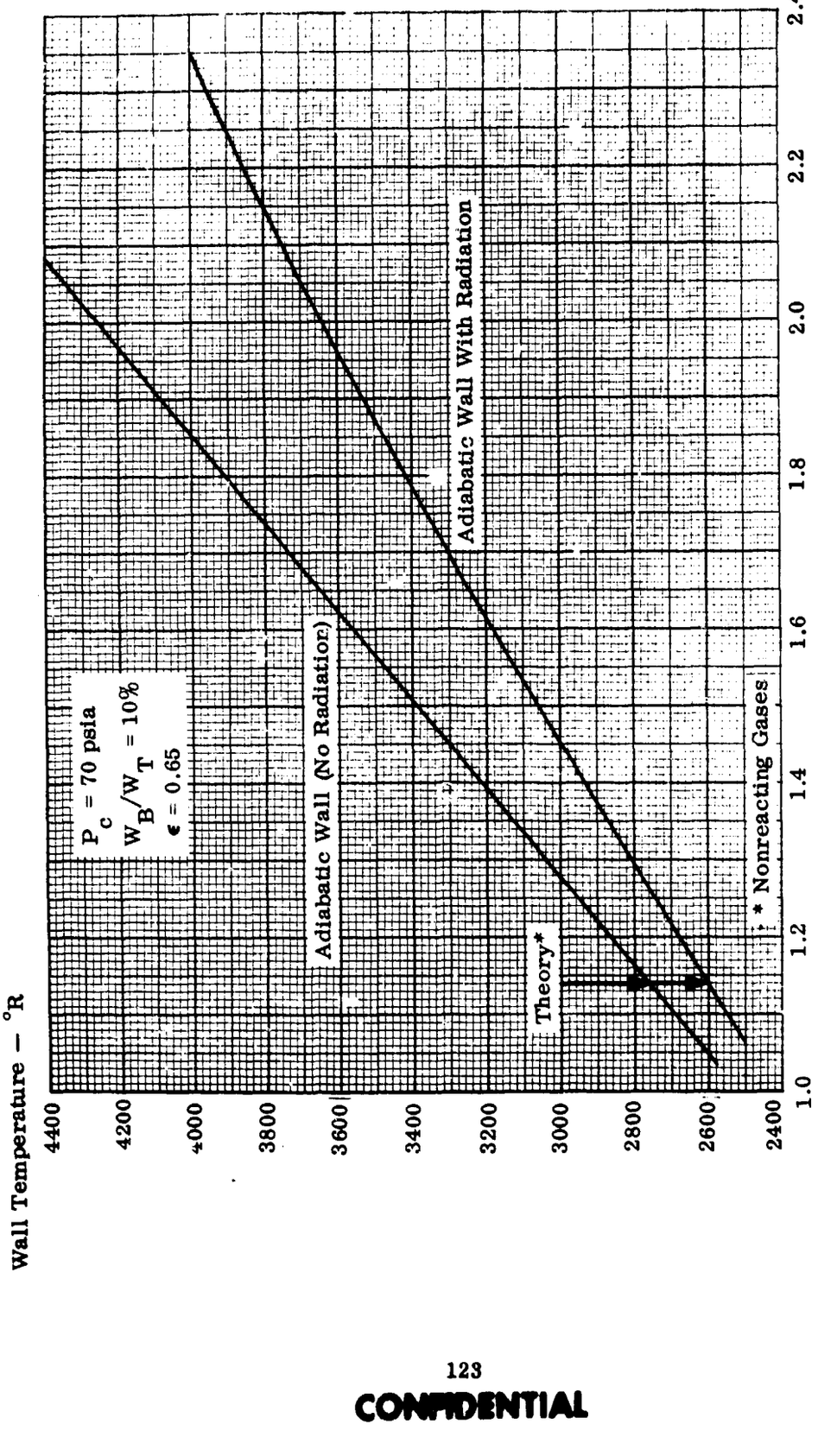


Figure 75. (C) Effect of Nozzle Heat Flux on Wall Temperature

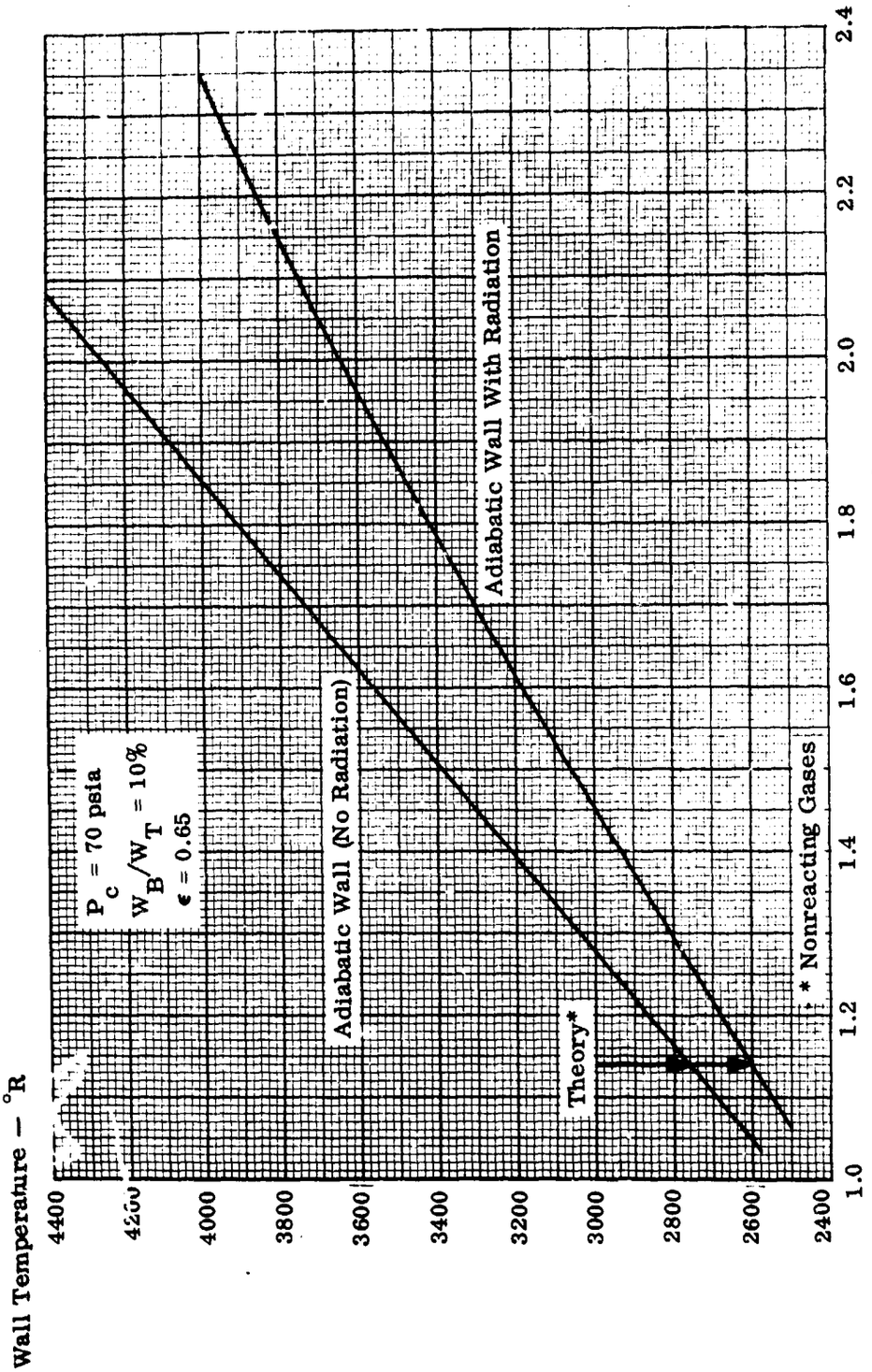


Figure 75. (C) Effect of Nozzle Heat Flux on Wall Temperature

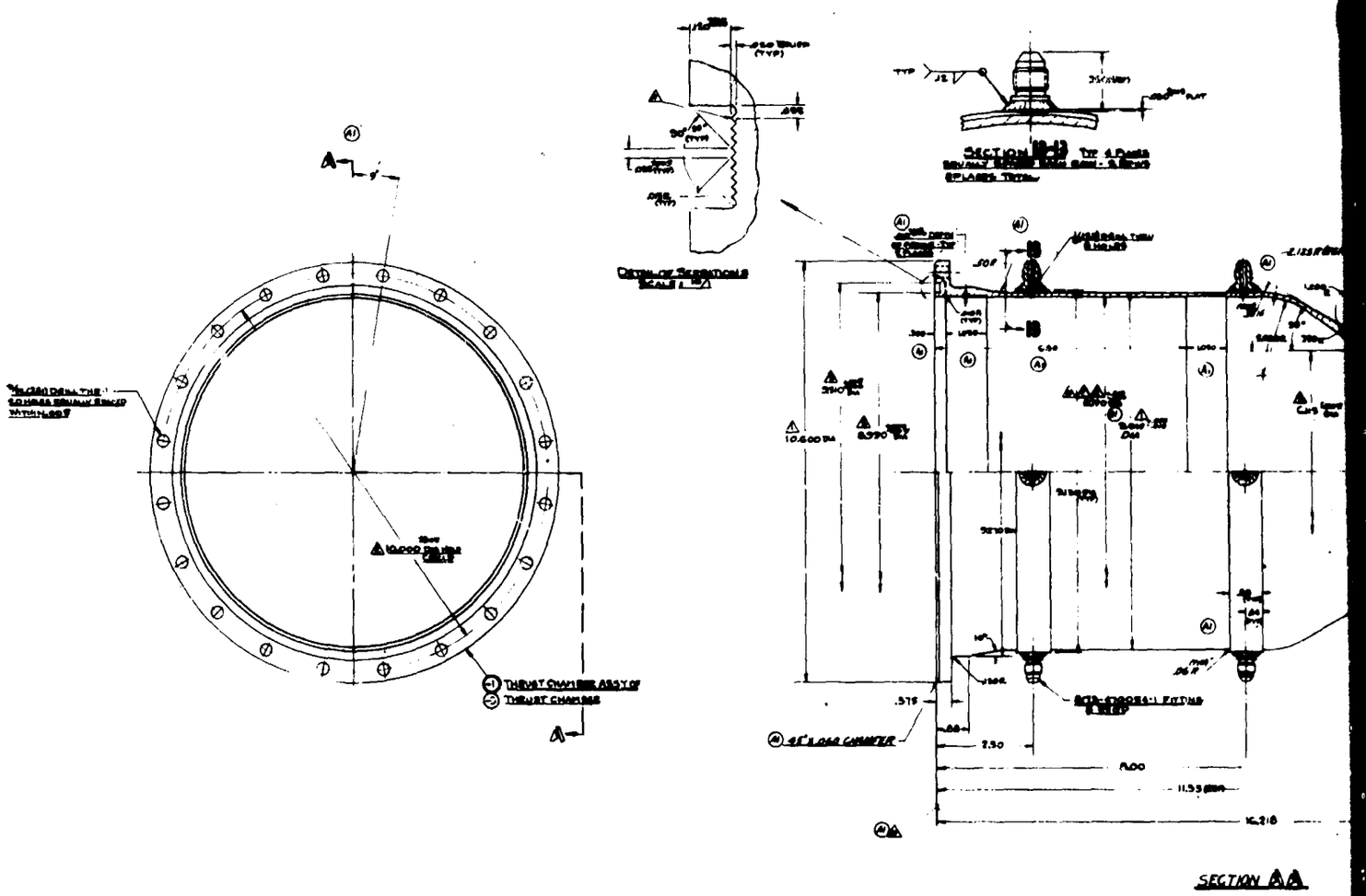

Figure 76. (U) Radiation Cooled Thrust Chamber

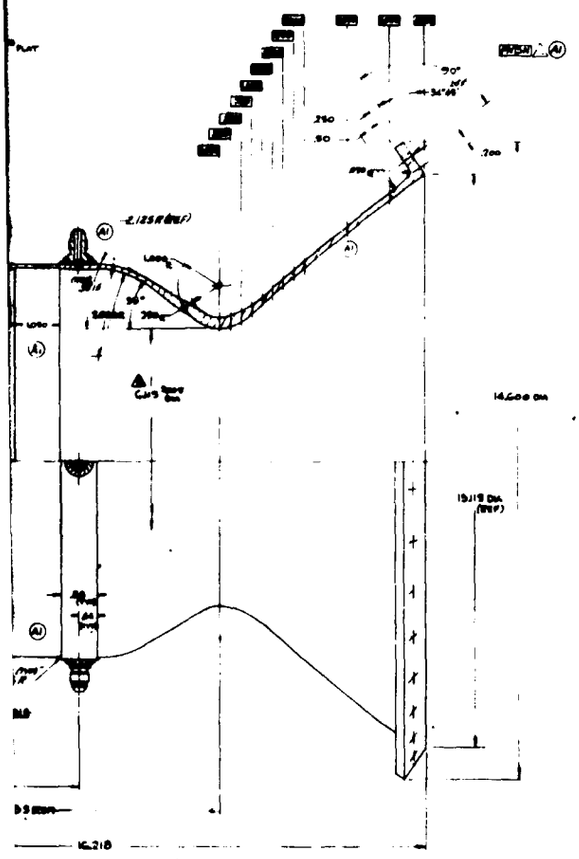

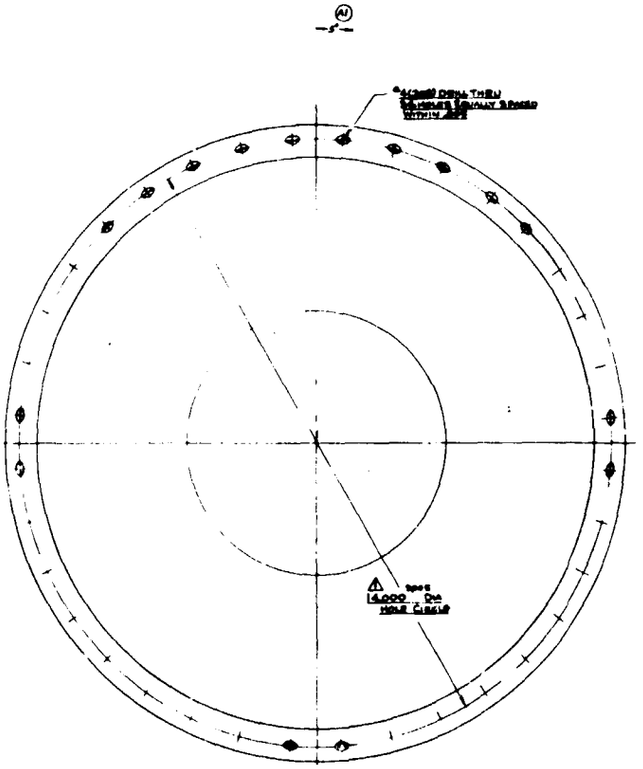

SECTION AA

(U) fabrication was complete, the thrust chamber was sent to Sylcor Division of GT&E for application of a modified aluminide coating internally to protect the base metal from the products of combustion of fluorine/BA-1014 and a silicide coating externally to protect the base metal from oxidation by the surrounding air environment and to provide a high emissivity (0.65). Figure 77 shows the coated columbium alloy thrust chamber as received.

b. (U) Liners

(U) Three liner materials were evaluated as a result of their compatibility with the products of combustion resulting from the materials evaluation tests: tungsten, tantalum (10% tungsten) alloy, and graphite. Discussions were conducted with various vendors on the fabrication techniques of tungsten and graphite liners.

(1) (U) Tungsten Liners

(U) Three different types of tungsten material (pressed and sintered, cast, and wrought) were evaluated based on inputs of various vendors. Inputs from vendors on fabrication techniques were evaluated and a design of the tungsten liner was initiated.

(U) Based on the potential problem associated with thermal shock characteristics of the tungsten as discussed in Section 5 of this report, a thermal stress analysis was conducted to determine whether or not the thermal stresses during the rocket firing were detrimental. Preliminary stress studies indicated that the critical thermally stressed region was at the flanged support and consequently, a detailed thermal stress analysis was performed on only the flanged end of the liner.

(U) Thermal stresses were computed using a Bell general matrix program for the analysis of complex structures. For analysis purposes, the liner was idealized at the flange support into 83 discrete triangular cross-sectioned ring elements. Thermal stresses were then computed for two temperature conditions which corresponded to times of 0.5 and 10.0 seconds in the temperature-time history of the tungsten liner. Since the elasticity and strength provided by the support were not precisely known, thermal stresses were computed for various ideal restraint or boundary conditions. Boundary conditions selected for analysis purposes ranged from complete fixity to completely free. Although not strictly correct in themselves, they gave results which bounded the correct thermal stress situation.

(U) The results of the analysis obtained were predicated upon two extreme boundary conditions; the flange end of the liner was completely fixed against rotation and radial and axial deflections. As such, this case simulated to some extent the situation in which the support structure, which was very stiff compared to the liner, remained at ambient temperature. This boundary condition resulted in the prediction of rather large thermal stresses at the support as shown in Figures 78

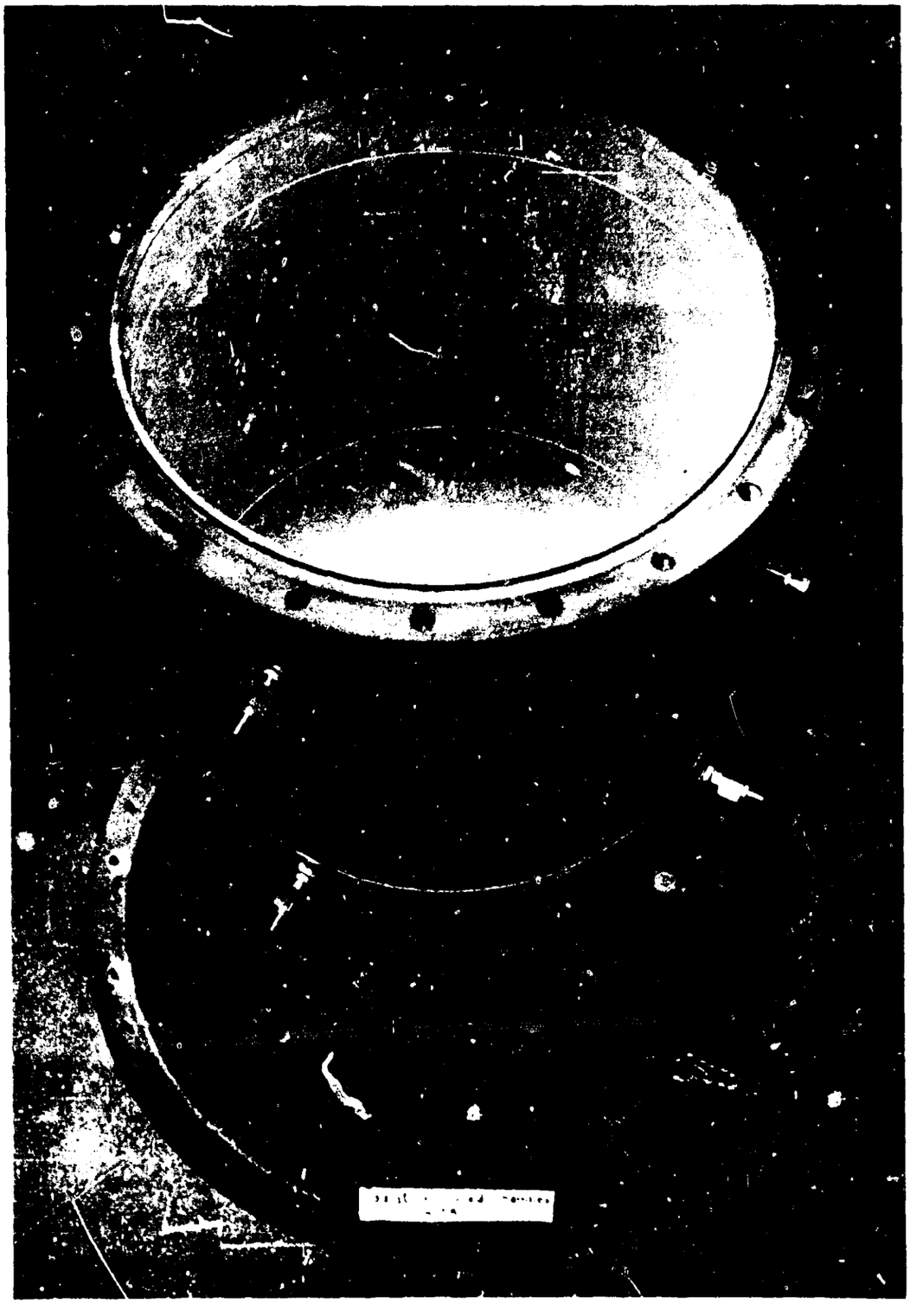

Figure 77. (U) Radiation Cooled Thrust Chamber

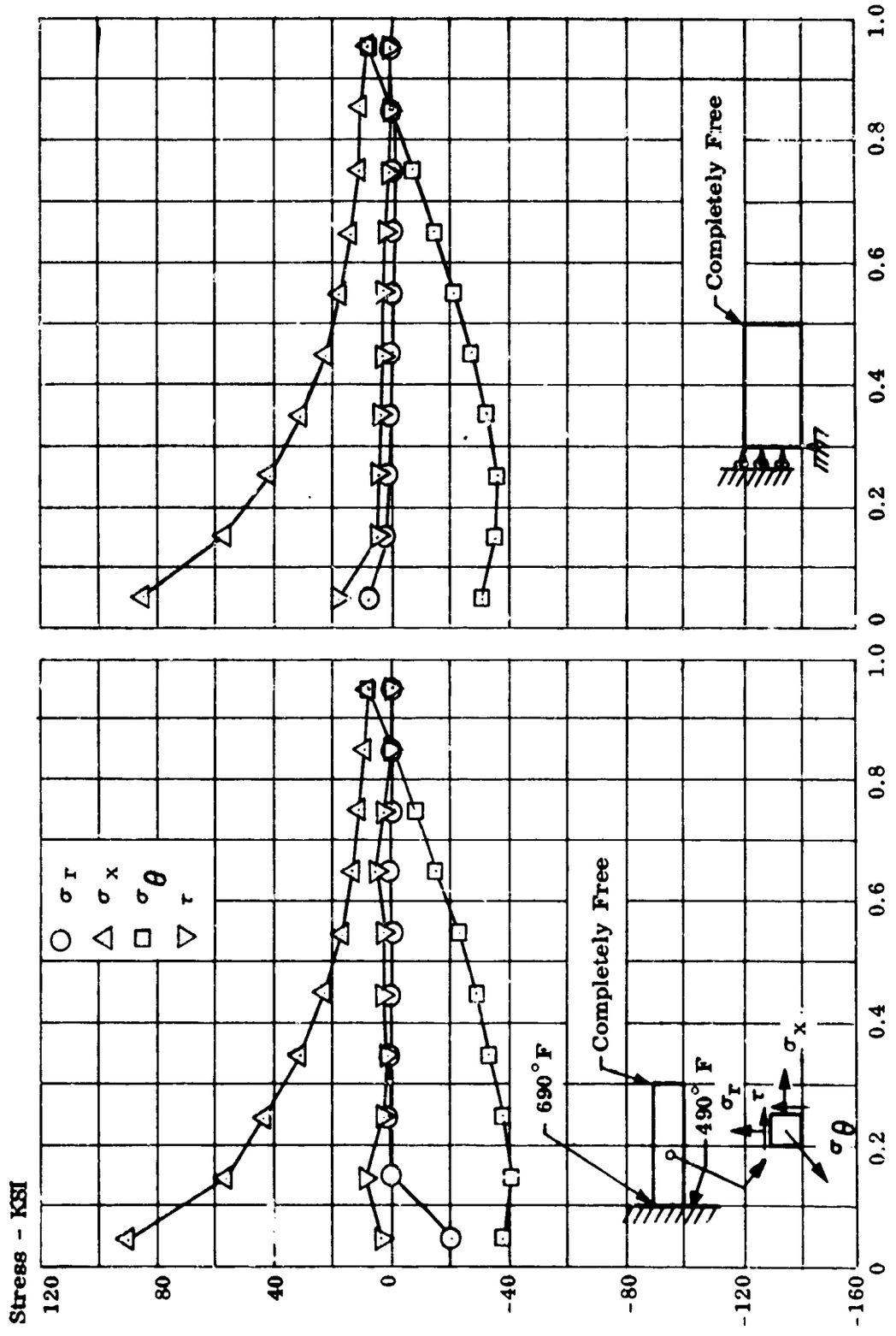


Figure 78. (U) Stress of Inner Fiber Along Length of Liner at Time of 0.5 Second

(U) and 79. These stresses were, in general, above the yield stress of the tungsten material used for the liner. In addition, in the next case, it was assumed that the flange edge was completely constrained against rotation and axial displacement, but was free to deflect radially. This case simulated the condition when the support structure experienced the same average radial thermal deflection as the liner. As indicated by the results shown for this case in Figure 80 and 81, maximum thermal stresses were relatively small compared to the previous case and were in the order of 15,000 psi. The thermal stresses arose primarily due to the presence of radial temperature gradients.

(U) In addition, the analysis conducted assumed that the liner was completely free at the downstream end of both bases. The results of the analysis indicated that the thermal stresses were relatively small when the support at the flange end of the liner was at the same average temperature as the liner. From a detailed study of the thermal strains induced on the support structure at the flange end of the liner, it was concluded that this case was more representative of the true situation than the initial case considered. Generally, the analysis indicated that the magnitude of the thermal stresses of the liner was very sensitive to the strength provided by the liner support structure.

(U) On the basis of the thermal stress analysis and the fabrication technique evaluation, final design modifications were made on the liner.

(U) The fabrication contract for the tungsten liner was awarded to the Super-Metals Corporation. The liner was fabricated by rolling and welding wrought tungsten; however, the porosity and distortion resulting during fabrication rendered the process unacceptable. Therefore, a decision was made to spin the tungsten liner from one piece of wrought material. This was successfully accomplished and the liner, in the as-received condition, is shown in Figure 82.

(2) (U) Graphite Sleeves

(U) Structural analyses performed on free standing graphite liners indicated some problems in the areas of bending moment and thermal shock. A cursory design analysis uncovered no unique configurations to solve these problems with any reasonable degree of success. Some research was performed on the fabrication of a graphite filament liner such as Carbitex, but was found to be impractical for this program due to the length of time required to develop such a liner.

(U) Based on the materials program where graphite was successfully used in conjunction with a refractory retainer, it was concluded that a liner fabricated with a refractory retainer and a graphite sleeve could be used with a high degree of success.

(U) A graphite sleeve was designed in conjunction with a retainer fabricated from a tantalum (10% tungsten) alloy. High density graphite sleeves were procured from Basic Carbon Division of the Carborundum Company.

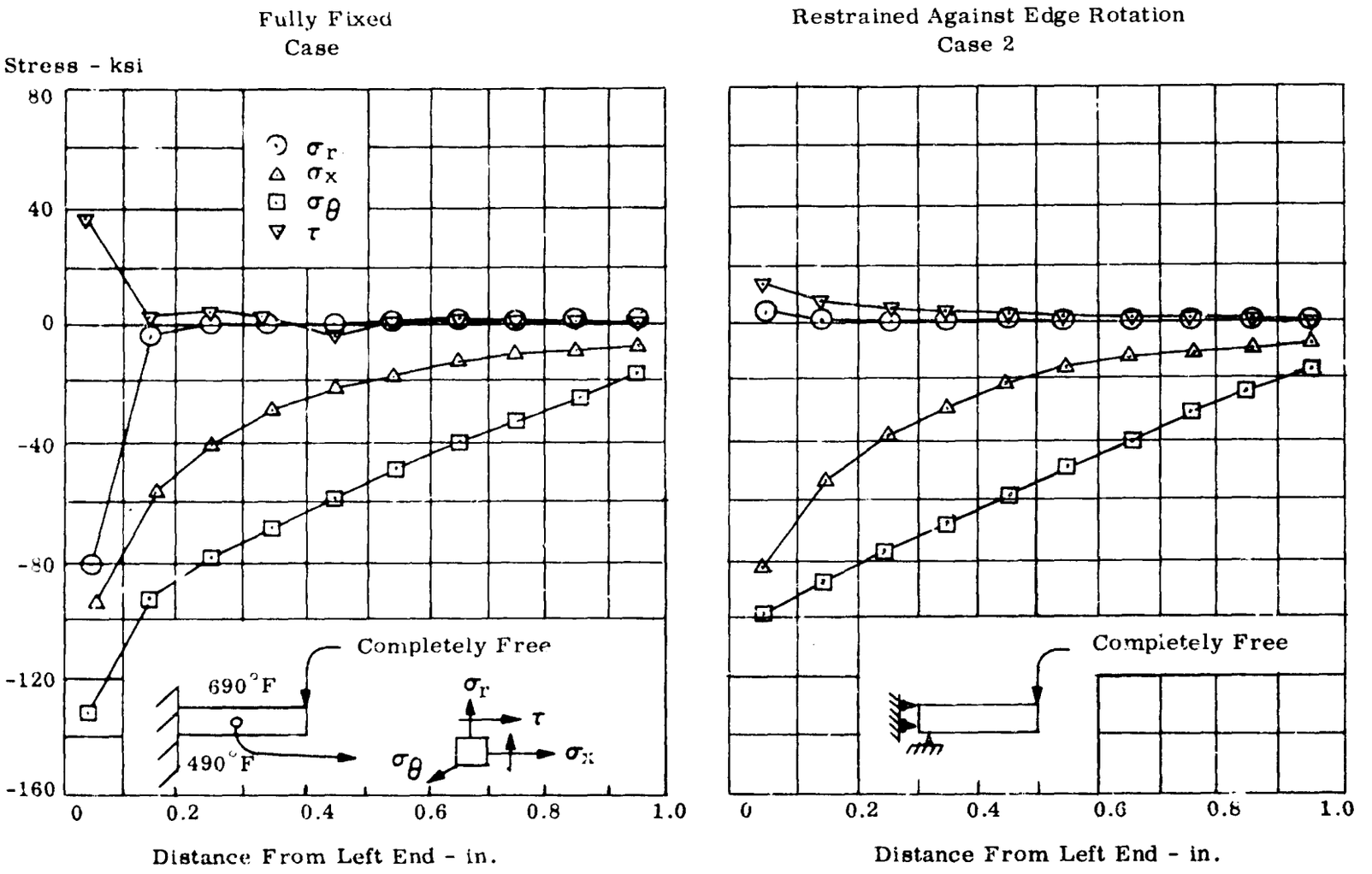


Figure 79 . (U) Stress at Outer Fiber Along Length of Liner at Time of 0.5 Second

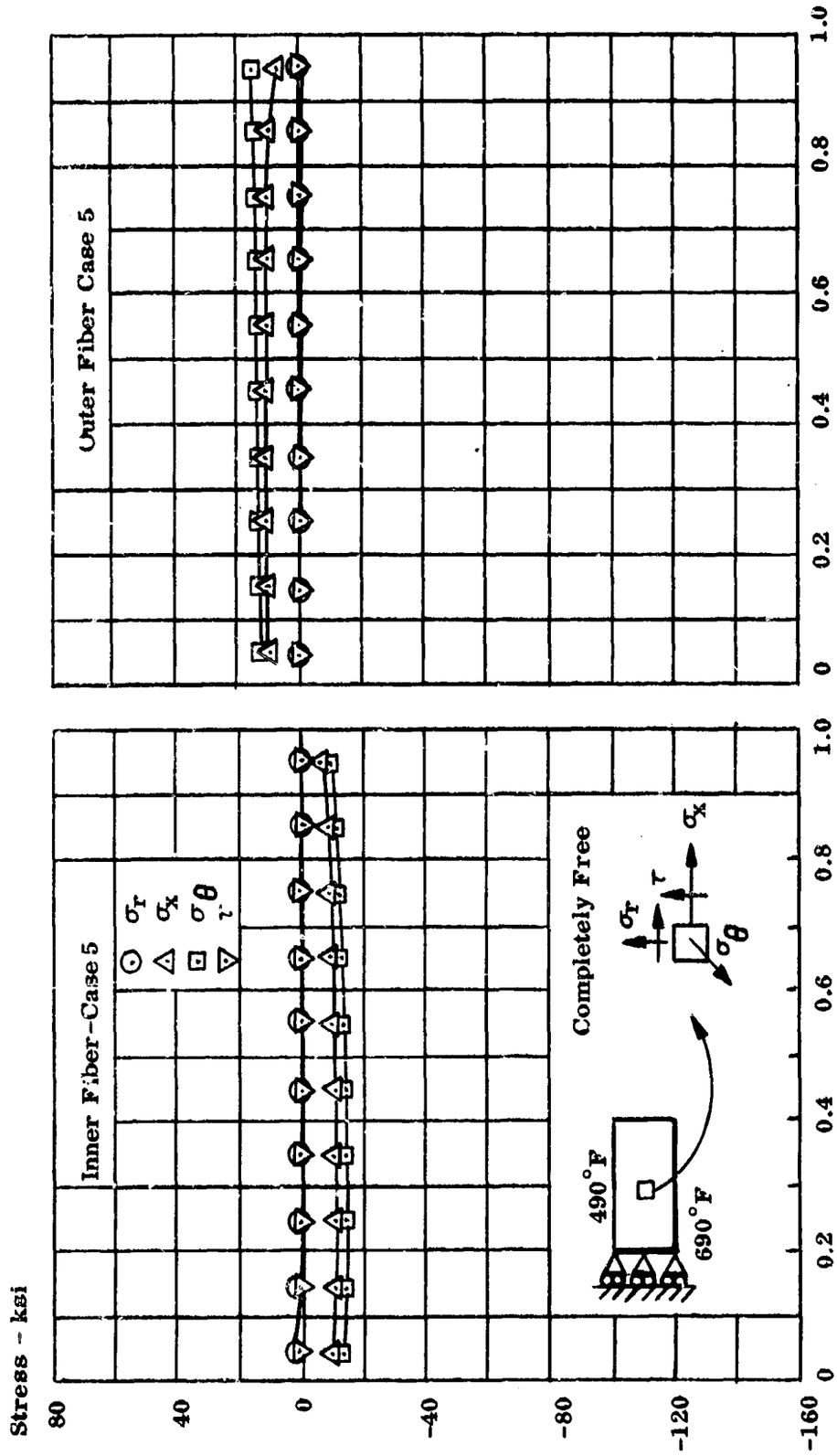


Figure 80. (U) Stresses at Inner and Outer Fibers Along Inner Length at Time of 0.5 Second

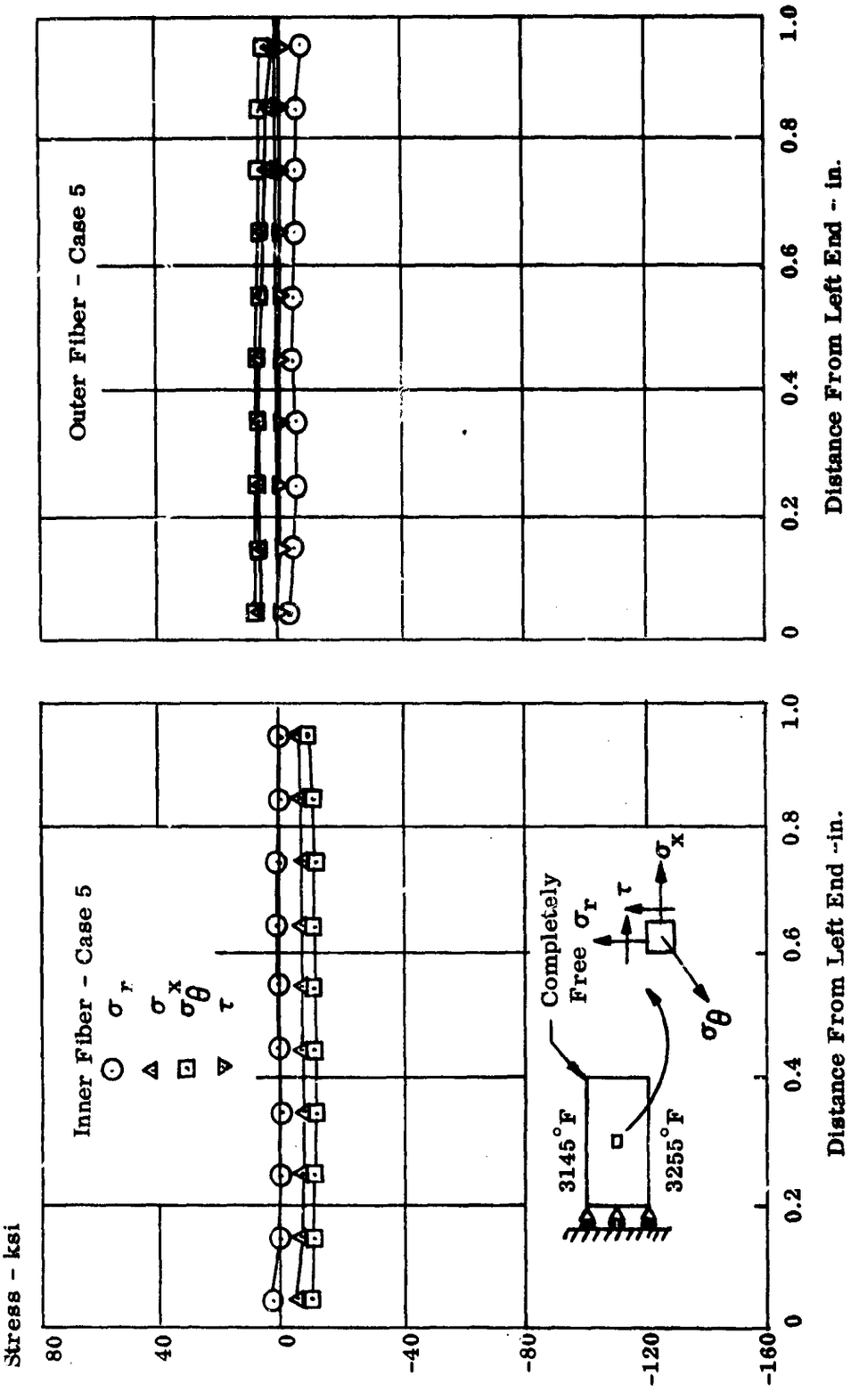


Figure 81. (U) Stresses at Inner and Outer Fibers Along Liner Length at Time of 10.0 Seconds

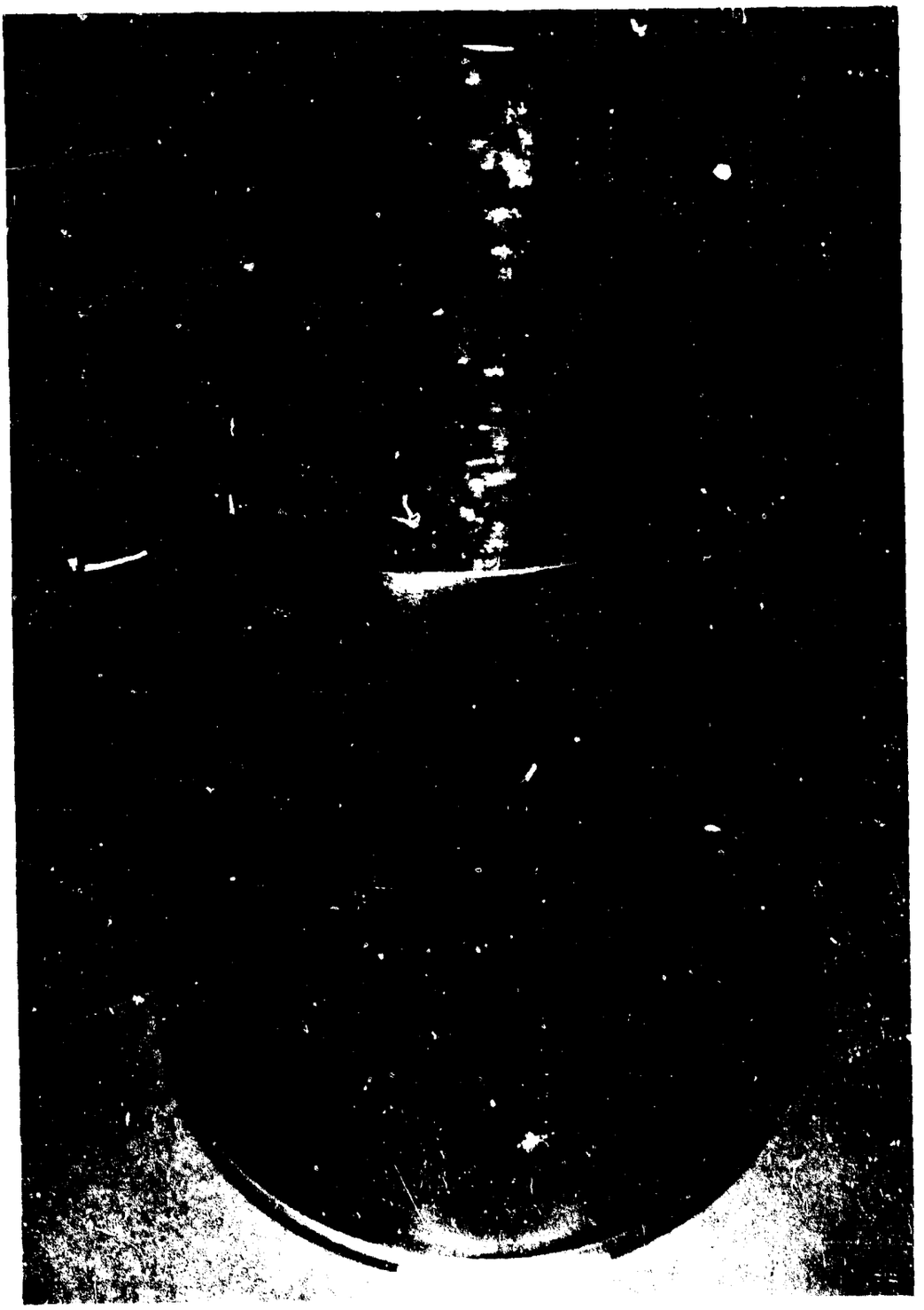

Figure 82. (U) Tungsten Liner

(3) (U) Tantalum Alloy Liners

(U) Two tantalum (10% tungsten) alloy liners were designed and fabricated. One liner was fabricated as a retainer for the above mentioned graphite sleeves and was not coated. The second liner was fabricated as a liner and was completely coated by National Research Corporation with pure tungsten by evaporating the tungsten by electron beam directly on the part. Vapor deposition of the tungsten was the preferred method but this could not be accomplished within the time available. The coated liner had the fabrication and structural qualities of tantalum (10% tungsten) alloy and the compatibility qualities of tungsten for use in the products of combustion resulting from the high energy propellant combination of fluorine/BA-1014.

5. (U) Test Program Philosophy

(U) The test program for the adiabatic wall thrust chamber was based upon the following philosophy:

(a) (C) The fixed orifice injector was fire tested in a water cooled chamber and nozzle with a water cooled adapter section to simulate the volume of the auxiliary fuel rich gas generator-manifold assembly in the chamber section. These tests defined the performance and heat rejection of the injector (main core only) over a 2:1 throttling range and demonstrated the durability of the injector.

(b) (C) The auxiliary fuel rich gas generator-manifold assembly was fire tested in simulated adiabatic wall thrust chamber hardware to determine the temperature and pressure distribution of the gases and the durability of the assembly.

(c) (C) The tantalum alloy retainer with the graphite sleeve was fire tested with the main injector, auxiliary fuel rich gas generator-manifold assembly and water cooled hardware (chamber and nozzles, axially and radial) to determine the effect of variation of coolant weight flow on performance and heat rejection.

(d) (C) The tantalum (10% tungsten) alloy liner coated with tungsten was checked out in water cooled hardware prior to use in the adiabatic wall thrust chamber assembly using the columbium alloy thrust chamber.

(e) (C) Both the tungsten-coated tantalum (10% tungsten) alloy liner and the pure tungsten liner were fired in the adiabatic wall thrust chamber assembly to demonstrate the feasibility of utilizing this cooling concept over a 2:1 thrust range.

C. (C) Fixed Orifice Injector Test Results

(C) Fabrication of the first fixed orifice injector (S/N 1) was completed during February 1965 and subjected to water flow tests to determine the flow patterns and pressure drops over the anticipated test range. The water flow test indicated the injector was within the allowable specifications. The injector was then installed on the test stand (1AW), as shown in Figures 83 and 84, for hot firing with the water cooled adapter section to simulate the auxiliary fuel rich gas generator-manifold volume, a water cooled chamber, and a water cooled longitudinally segmented nozzle. The test objectives during this series were the determination of injector performance, durability, stability and heat rejection. The test results are discussed as follows:

(a) (C) The first test (1AW-634) was a successful 10.5-second duration test (checkout) conducted at a mixture ratio of 1.87 and a chamber pressure of 67.1 psia. This test resulted in a combustion efficiency of 96.1%. Post-fire inspection indicated the test hardware was in excellent condition.

(b) (C) The next test (1AW-635), an attempted 100-second duration test at a chamber pressure of 35 psia, was aborted due to a test stand malfunction (a three-way solenoid did not operate and therefore did not open the fuel valve).

(c) (C) An attempted 100-second duration test (1AW-636) was successfully conducted for 100.9 seconds at a mixture ratio of 1.84 and a chamber pressure of 35 psia. The resulting combustion efficiency was 94.2%. Post-test inspection indicated that the hardware was in satisfactory condition.

(d) (C) An intended 40-second duration test (1AW-637) was successfully conducted for 40.2 seconds at a mixture ratio of 1.85 and a chamber pressure of 50.4 psia. The resultant combustion efficiency of this test was 95.7%. Post-test inspection showed the test hardware to be in satisfactory condition.

(e) (C) An attempted 80-second test (1AW-638) at a chamber pressure of 65 psia was terminated at approximately 1.3 seconds due to a fire surrounding the injector area. Inspection of the injector (S/N 1) revealed a bulge over 45° of the circumference, and cracking of the outer weld of the oxidizer manifold cover over approximately 210° of the circumference. In addition, one chamber pressure pick-up on the injector was sheared off as shown in Figures 85 and 86. A detailed analysis was conducted to determine the cause of the incident and methods of preventing and alleviating future occurrences. The discussions and conclusions are summarized as follows:

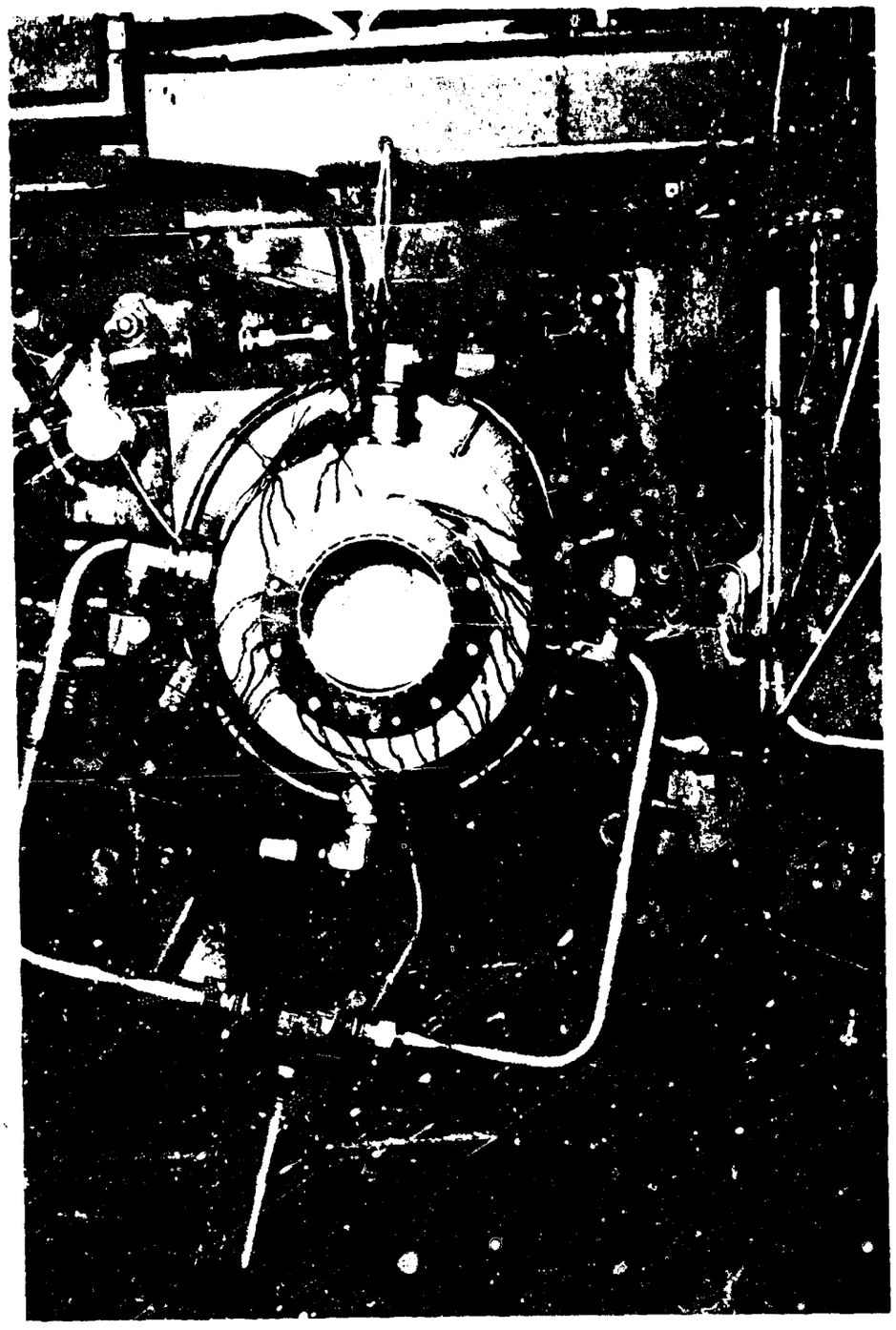

Figure 83. (C) Injector Test Setup

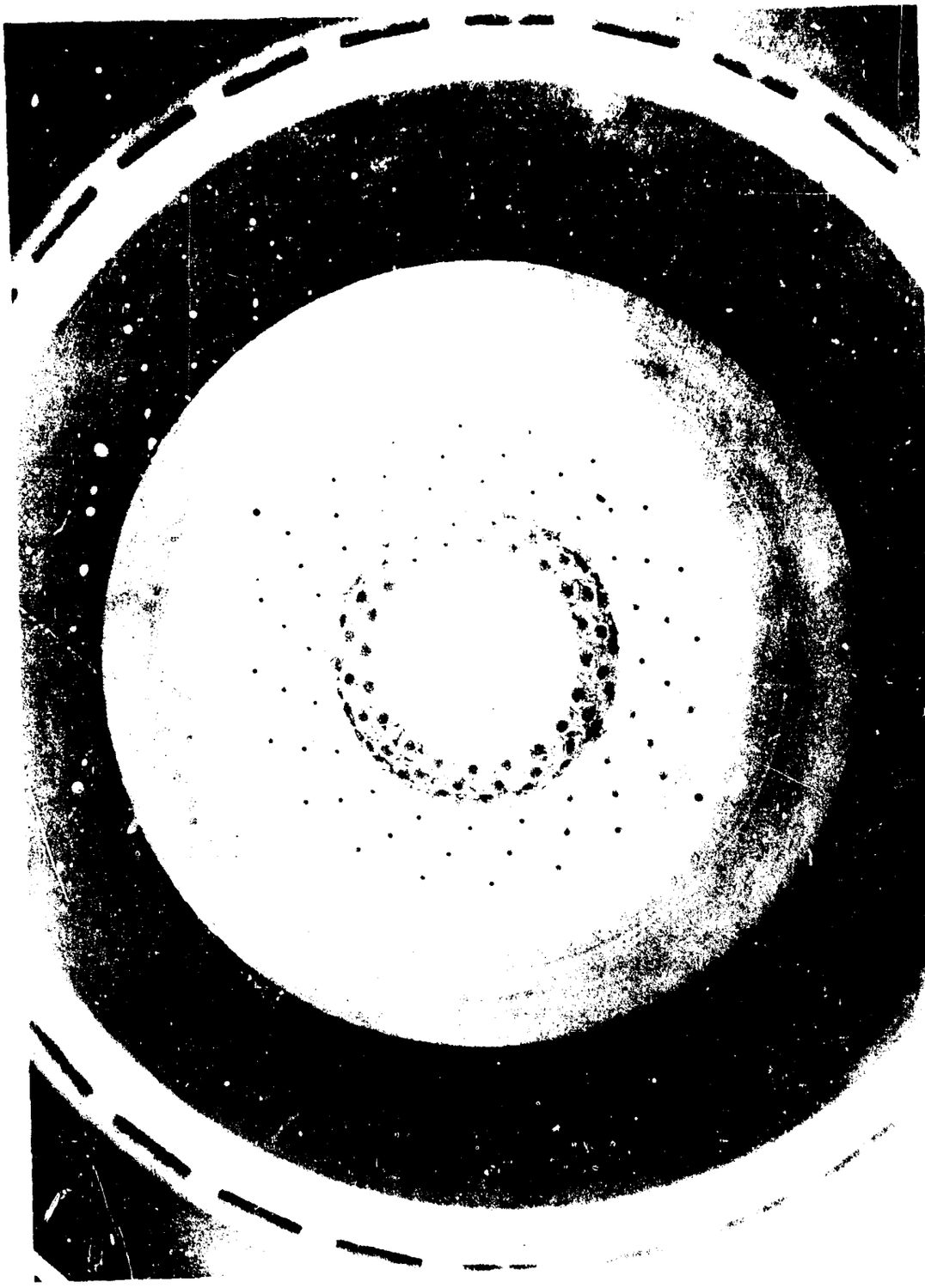

Figure 84. (C) Test Injector


Figure 85. (U) Injector (Back Plate)


Figure 86. (U) Injector (Back Plate)

(1) (C) The outer weld of the oxidizer (fluorine) cover of the injector was cracked over 216° of the circumference, and the cover was bowed (raised) 1/8 inch at the high point. There were no indications of cracking on the inner weld of the oxidizer cover. In addition, one pressure pickup boss was sheared off, and the fluroine inlet tube was deformed. This deformation was apparently due to a reaction occurring in the oxidizer manifold.

(2) (C) The oxidizer cover was removed and the fractured joint was examined as shown in Figure 87. This was typical of the entire circumference of the outer manifold weld except that the uncracked portion had a slightly larger weld penetration in the area where no cracking occurred and 0.12 inch for area in which cracking did occur). There was a deep narrow crevice which was produced by the combination of incomplete joint fusion plus a step at the root. This was capable of entrapping solvents and other foreign material or contaminants. Since the drawing called for a 0.17 inch weld + 0.04 inch of penetration below the groove, better inspection methods were required. In addition, the recommendation was made that the weld procedures be revised and the design improved for allowing better weld penetration. Both of these recommendations were incorporated into the repair of this injector.

(3) (C) After the cover was removed, five blackened areas were noted in the outer weld joint. The largest blackened area, about five inches long, plus two smaller ones were located in the half which fractured. Figure 88 is a photograph taken in the large area. Drops of aluminum, melted by the reaction, were visible in the lower end of the joint. The entire weld was blackened but there was no melting of the sharp upper edge of the weld fracture. This implies that the reaction was extinguished shortly after the joint opened. Two more significant burned areas were those which existed on the opposite half of the cover where it did not fracture. Figure 89 shows one of these areas. The fire blackened area was in the crevice of the joint; the weld metal (intentionally broken for examination) was clean and sound unlike that in Figure 88 which was black. In the lower or crevice region of the joint, drops of metal were seen as well as the burn-eroded surface often seen in fluorine reaction. The evidence indicated that a reaction occurred in five places before the cover blew open and that the cover failure resulted from a sudden pressure buildup accompanying the fluorine reaction. A simple structural failure of the weld could not account for the multiple reaction locations.

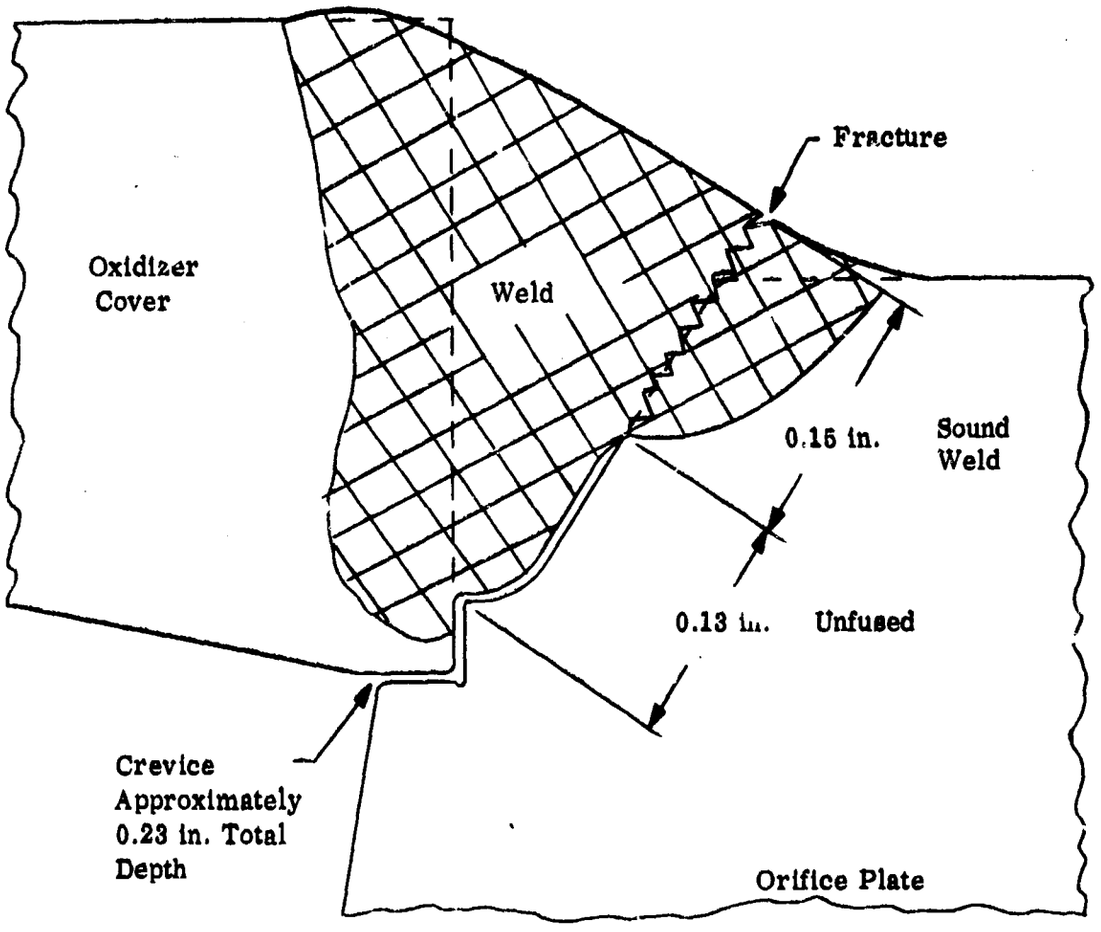


Figure 87. (U) Section Through Outer Weld of Oxidizer Manifold Cover

6X

Typical Area Blackened by Reaction in Fractured Half of Weld Circumference. Local Melting at Root of Joint. Blackening Over Weld Fracture. No Melting at Top Rim of Weld.

Figure 88 (U) Injector Weld Area

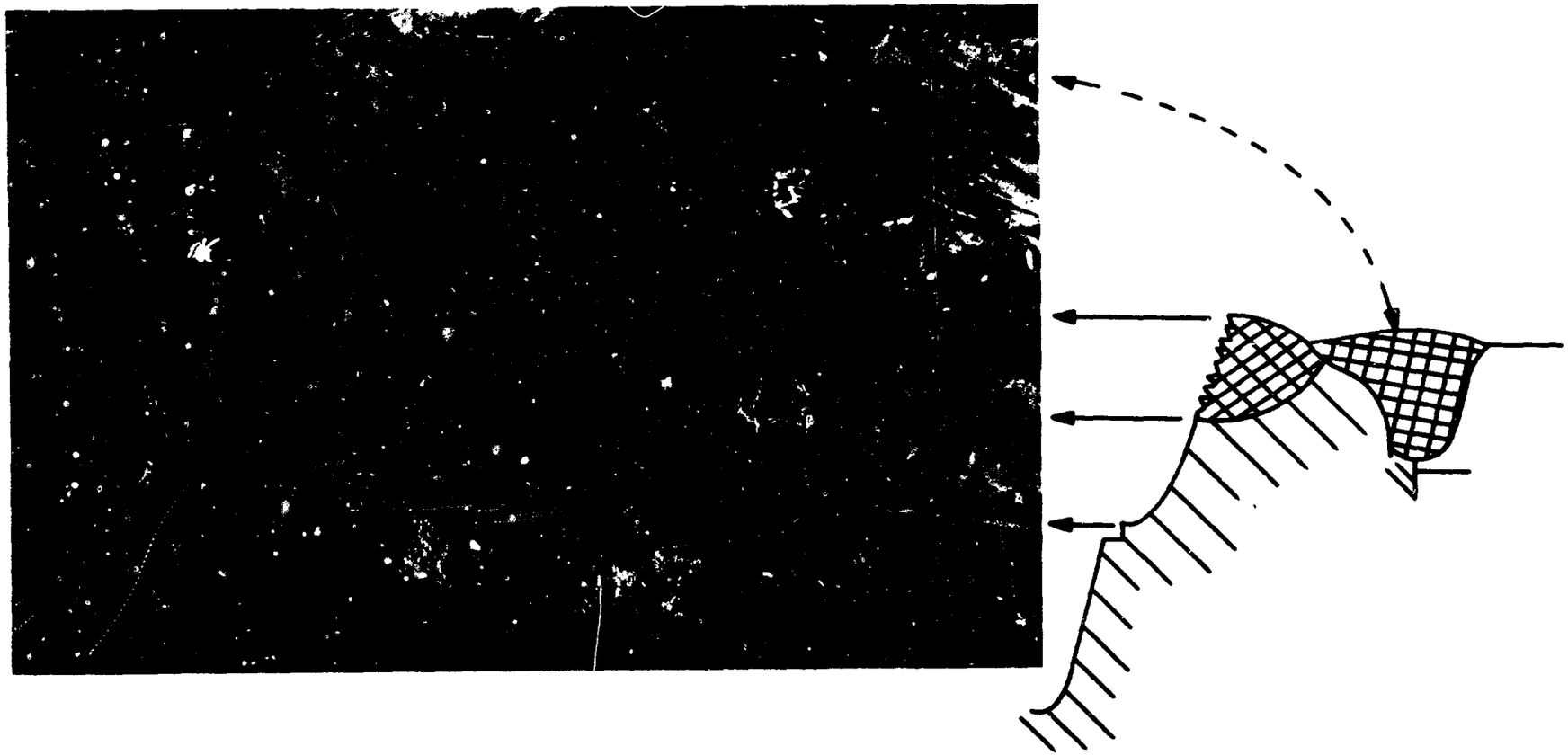

6X

Blackened Reaction Area Under the Part of Cover Which Did Not Crack Open. Weld is Clean, Having Been Broken Later in Lab. Note Burned – Eroded Places in Step (Bottom) of Joint.

Figure 89. (U) Injector Weld Area

(4) (C) A semi-toroidal shaped baffle about 1.5 inches long which was welded to the oxidizer cover directly beneath the oxidizer inlet and was semi-circular in cross-section was sharply deformed in one area as shown in Figure 90. A deformation started at the edge of the weld where high strain had produced a shallow (1/8 inch long) crack. The deformation had the original smooth surface which indicated that mishandling was not the cause. The only explanation that can be offered for the deformation is that it was a manifestation of a pressure surge.

(5) (C) A review of the oscillograph record indicated that the start was normal for 1.30 seconds but a spike occurred at 1.34 seconds from fire command on the oxidizer and fuel injector inlet pressures and chamber pressure. The magnitude of these sudden rises indicated that the oxidizer inlet pressure was 103 psi higher than normal, the fuel injector inlet pressure was 55 psi higher than normal and chamber pressure was 51 psi higher than normal. Predicated upon this finding, in conjunction with the cracked oxidizer cover and deformed oxidizer inlet tube as well as reactions indicated in the oxidizer manifold, it was concluded that a reaction in the oxidizer manifold occurred, thus causing failure of the injector.

(6) (C) Based upon the above findings, the weld procedures were revised and the design of the oxidizer cover was modified to allow for improved weld penetration. The injector (S/N 1) was then repaired incorporating these improvements. The face of the injector was not damaged during the fire test and is shown in Figure 91.

(f) (C) An intended 40-second duration test (1AW-648) was conducted successfully at a chamber pressure of 34.8 psia at mixture ratio of 1.95 using the circumferentially segmented nozzle to determine station-by-station nozzle heat rejection. The results of this test indicated a combustion efficiency of 93.7%. Post-test observation indicated the hardware was in satisfactory condition.

(g) (C) An intended 35-second test (1AW-649) was successfully conducted using the circumferentially segmented nozzle at a chamber pressure of 67.6 psia and a mixture ratio of 1.52. The results of this test indicated a combustion efficiency of 96% and post-test-inspection revealed that the hardware was in satisfactory condition.

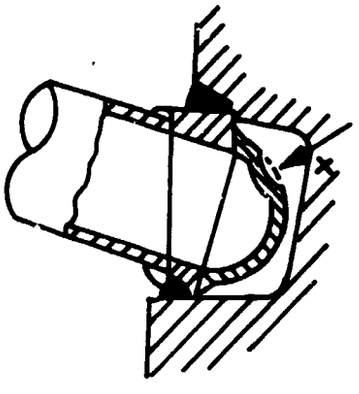


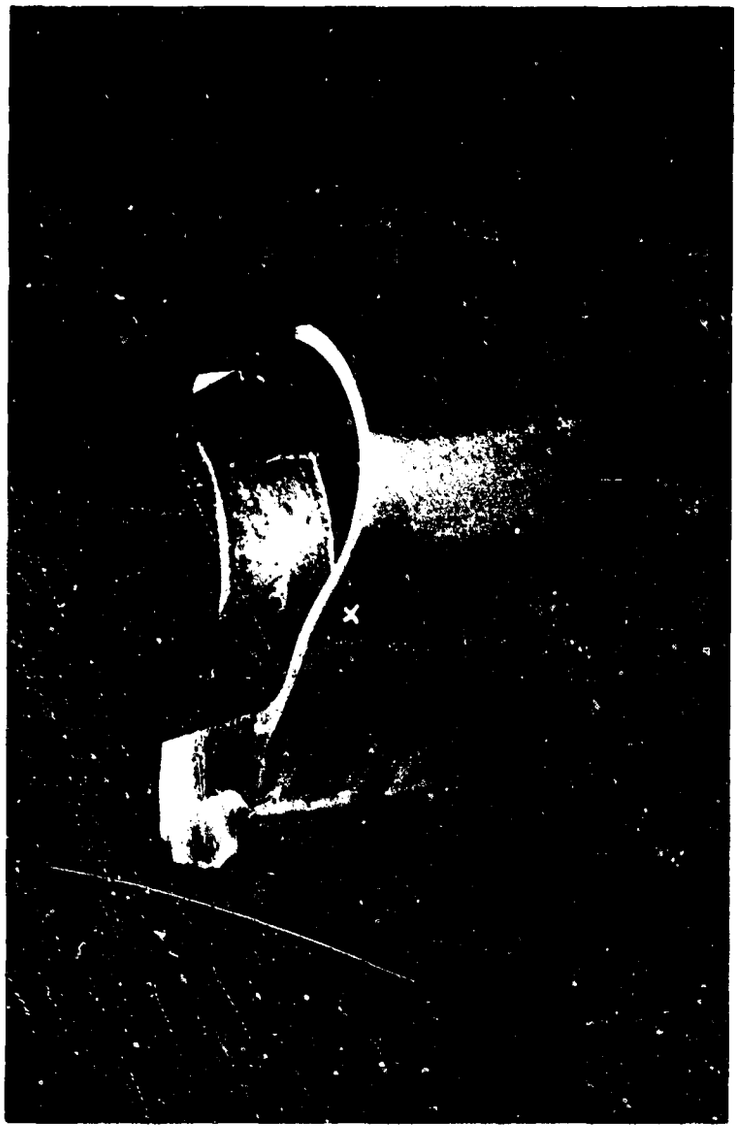


3X

Baffle Under End of Oxidizer Inlet Tube. Sectioned Directly Beneath Inlet Opening. This Baffle was Made as a Half Cylinder (See Section Sketch). Note The Deformation at X, Presumably Caused by a Manifold Pressure Surge.

Figure 90. (U) Injector Baffle


Figure 91. (C) Injector Face After Test (1AW-638)

(h) (C) An intended 65-second test (1AW-650) was successfully conducted at a chamber pressure of 67.7 psia and a mixture ratio of 1.82. This test was conducted with the longitudinally segmented nozzle in order to determine the injector durability as well as to define the injector heat rejection at high chamber pressure. The results of this test indicated that the injector had the capability of operation for full duration. The hardware was in satisfactory condition after the test. Combustion efficiency was 95.9%.

(C) A correlation of the heat transfer data with the heat transfer analysis indicated that the actual test data more readily approached the shifting equilibrium transport property heat transfer analysis (maximum values of heat flux) than the Bartz method. This was true for the adapter section, the chamber section, and the radially segmented nozzle. However, the axial nozzle more closely approximated the heat transfer analysis obtained using the Bartz method. This was primarily due to the fact that the data obtained with the longitudinal nozzle was questionable since the temperature increase of the water through the nozzle was quite low (6 to 10°F). The data obtained using the adapter and the radial nozzle utilized large temperature increases (approximately 30 to 50°F) of the water during the test. A summary of the heat flux data is shown in Figure 92. The heat transfer values obtained with this injector would allow the adiabatic wall thrust chamber to operate successfully, since the heat transfer values used to design the thrust chamber were predicated upon shifting equilibrium transport properties. Heat transfer analysis indicated the adiabatic wall thrust chamber would operate successfully ($T_{max}$ = 3200°F) if the nozzle heat flux did not exceed 2.03 BTU/in.$^2$-sec. Therefore, the next test series was conducted using the adiabatic wall thrust chamber.

(C) Figure 93 shows the performance obtained with this injector over a chamber pressure range varying from approximately 70 to 35 psia chamber pressure. The results indicated a 2.5% decrease in combustion efficiency at a mixture ratio of 1.8 in this chamber pressure range. During the injector checkout series portion of the program, 7 tests were conducted for a total accumulated time of 293.4 seconds and a maximum single run duration of 100.9 seconds. A summary of the injector test data is shown in Table XV.

7. (C) Fuel Rich Gas Generator-Manifold Assembly Test Results

(C) The fuel rich gas generator-manifold assembly as shown in Figure 68 was completed and prepared for test. Five tests were intended for this program at a mixture ratio of 0.045. This test series consisted of a 10-second checkout test with a total flow of 1.0 lb/sec (the nominal generator flow rate required for the adiabatic wall thrust chamber operating at a chamber pressure of 70 psia), a 120-second test at a total weight flow of 1.0 lb/sec, a 120-second test at a total weight flow rate of 1.3 lb/sec (the maximum intended flow rate required for operation at a chamber pressure of 70 psia), a 120-second test at a total weight flow of 0.6 lb/sec (the maximum intended flow rate required for operation at a chamber pressure of 40 psia), and a 120-second test at a flow rate of 0.45 lb/sec (the nominal flow rate required for operation of the adiabatic wall thrust chamber at a chamber pressure of 40 psia). The results of this test series are summarized as follows.

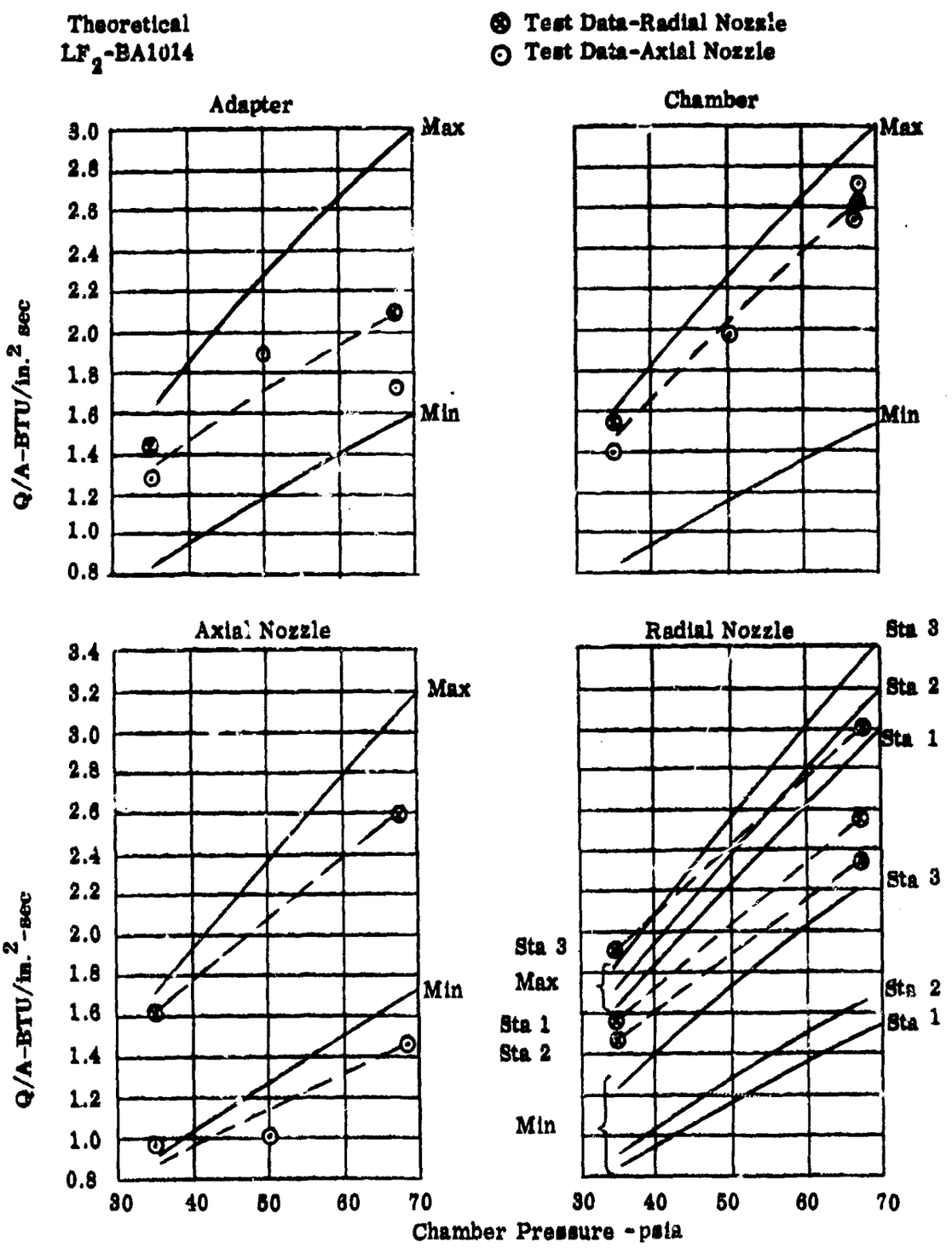


Figure 92. (C) Average Heat Flux With Varying Chamber Pressure

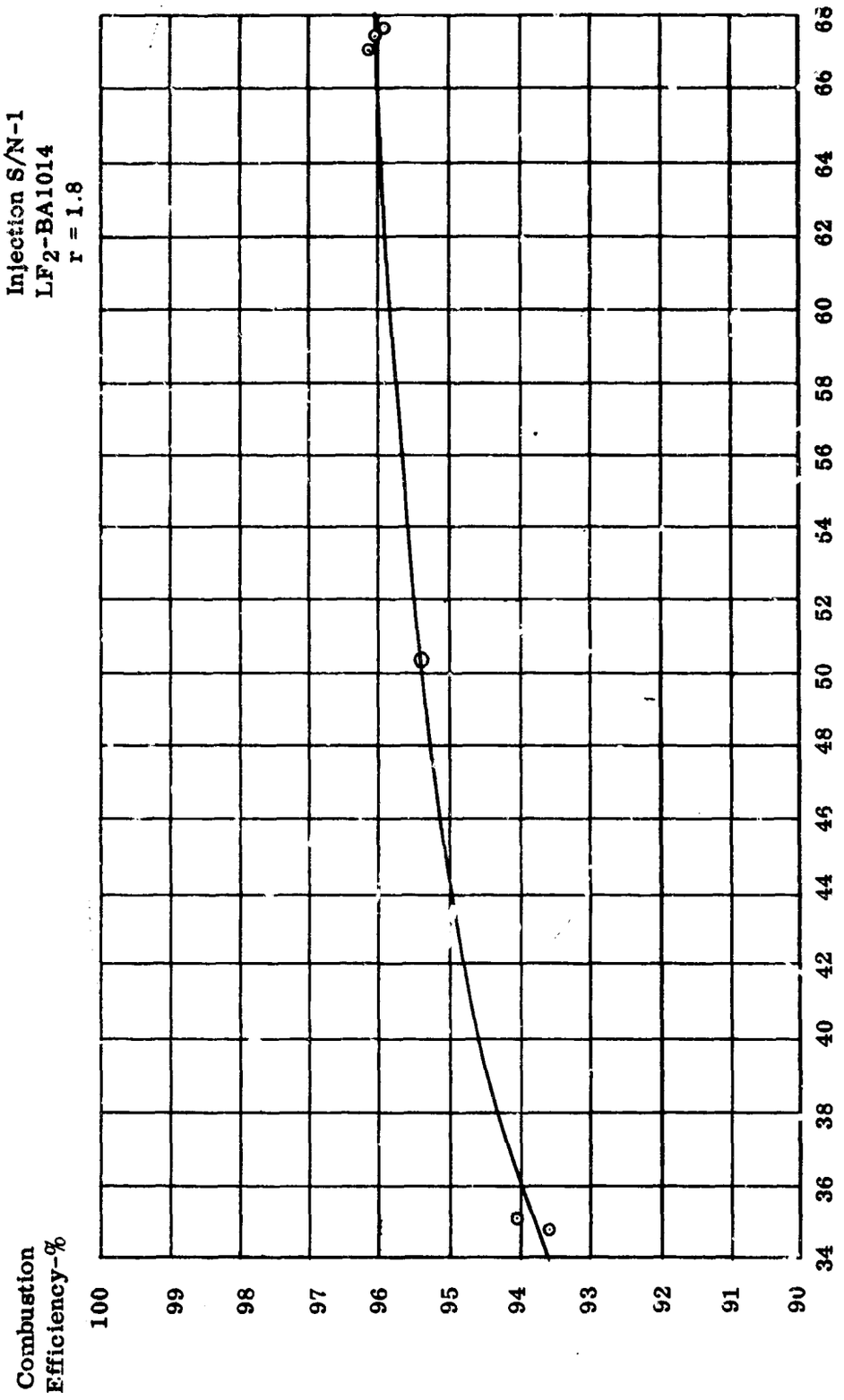


Figure 93. (C) Combustion Efficiency versus Chamber Pressure

## TABLE XV

## (C) SUMMARY OF INJECTOR FIRE TEST DATA

| Test No. | $\theta$ | r | $P_c$ psia | $\eta_c$ % | Q/A Adapter BTU/in.$^2$-sec | Q/A Chamber BTU/in.$^2$-sec | Q/A Nozzle BTU/in.$^2$-sec Max. | Q/A Nozzle BTU/in.$^2$-sec Avg. | |
|---|---|---|---|---|---|---|---|---|---|
| 1AW-634 LOR=10.5 | 10 | 1.868 | 67.07 | 96.1 | 1.741 | 2.567 | 1.994 | 1.723 | |
| 1AW-636 | 9.5 | 1.681 | 33.32 | * | 0.911 | 1.326 | 1.185 | 0.964 | |
| LOR=100.9 | 30 | 1.841 | 35.06 | 94.24 | 1.236 | 1.405 | 1.53 | 1.134 | |
| | 50 | 1.337 | 35.12 | 94.24 | 1.251 | 1.388 | 1.626 | 1.155 | |
| | 100.4 | 1.855 | 35.17 | 94.05 | 1.512 | 1.394 | 1.667 | 1.145 | |
| 1AW-637 | 9.5 | 1.801 | 50.08 | * | 1.342 | 1.942 | 1.323 | 1.039 | |
| | 30 | 1.845 | 50.38 | 95.8 | 1.857 | 1.977 | 1.764 | 1.187 | |
| | 39.4 | 1.855 | 50.48 | 95.64 | 1.887 | 1.978 | 1.571 | 1.177 | |
| 1AW-648 | 10 | 1.822 | 34.35 | * | – | 1.466 | — | | radial |
| LOR=40.3 | 30 | 1.940 | 34.70 | 93.89 | 1.564 | 1.620 | — | | |
| | 39.8 | 1.955 | 34.78 | 93.44 | 1.426 | 1.542 | | 1.61 | |
| 1AW-649 | 9.5 | 1.805 | 67.36 | * | 2.176 | 2.727 | — | | nozzle |
| LOR=35.5 | 30 | 1.819 | 67.16 | 95.57 | 2.703 | 2.624 | — | | |
| | 35 | 1.826 | 67.64 | 96.34 | 2.111 | 2.63 | | 2.59 | |
| 1AW-650 | 9.5 | 1.784 | 67.50 | * | Lost | 2.679 | — | | |
| LOR=63.0 | 30 | 1.816 | 67.64 | 95.97 | Lost | 2.698 | 1.784 | 1.48 | |
| | 65.5 | 1.818 | 67.70 | 95.81 | Lost | 2.685 | 1.764 | 1.458 | |

* Oxidizer flow not stabilized

a. (C) A 9.2-second test (1AW-639) was conducted at a total flow rate of 0.93 lb/sec but the chamber pressure exceeded the intended chamber pressure value of 75 psia. A review of the oscillograph indicated a value of approximately 140 psia.

b. (C) An intended 20-second test (1AW-640) was conducted at a total weight flow of 0.58 lb/sec but stabilization was not reached.

c. (C) A 26.8-second test (1AW-641) was conducted at a total weight flow of 0.58 lb/sec and a generator chamber pressure of 58.5 psia. A review of the data indicated that the chamber pressure was substantially higher than anticipated (14 psi higher), indicating a combustion efficiency 20% higher than theoretically predicted. This indicated that the geometrical throat was not the controlling restriction. An analysis was conducted to determine if there was a critical area causing the choked flow condition. The result of this analysis indicated there was no choked flow condition predicated upon the areas shown in Figure 94.

d. (C) A gasket twice the thickness of the previously used gasket was installed in the manifold assembly in an effort to provide increased flow area to reduce the pressure in the generator manifold assembly. An intended 120-second test was successfully conducted with a total weight flow of 0.58 lb/sec and a chamber pressure of 68.3 psia for a total duration of 121.0 seconds (1AW-642). The chamber pressure was still higher than anticipated.

e. (C) An intended 120-second test (1AW-643) was conducted at a total weight flow rate of 0.70 lb/sec and a chamber pressure of 88 psia. The double-thick gasket was utilized. Higher chamber pressure than anticipated was experienced.

f. (C) A one-inch long adapter section was installed in the manifold section and an intended 120-second test (1AW-644) was terminated after 37.0 seconds due to an apparent plugging on the oxidizer side. The situation was rectified by cleaning the oxidizer flow controlling venturi.

g. (C) An intended 120-second test (1AW-645) was terminated due to high chamber pressure after 6.0 seconds at a total weight flow of 1.01 lb/sec. A review of the data indicated a chamber pressure in excess of 106 psia. To obtain durability of the generator manifold section at the rated flow condition of 1.0 lb/sec, high pressure instrumentation was utilized.

h. (C) An intended 120-second test (1AW-646) was terminated after 15.1 seconds due to an inadvertent shutdown.

i. (C) An intended 120-second test (1AW-647) was successfully conducted at a total weight flow of 1.01 lb/sec and a chamber pressure of 158 psia. Post-test observation indicated some erosion of the lip of the injector and at the inlet flange of the generator. This was rectified prior to initiating the next series of tests.

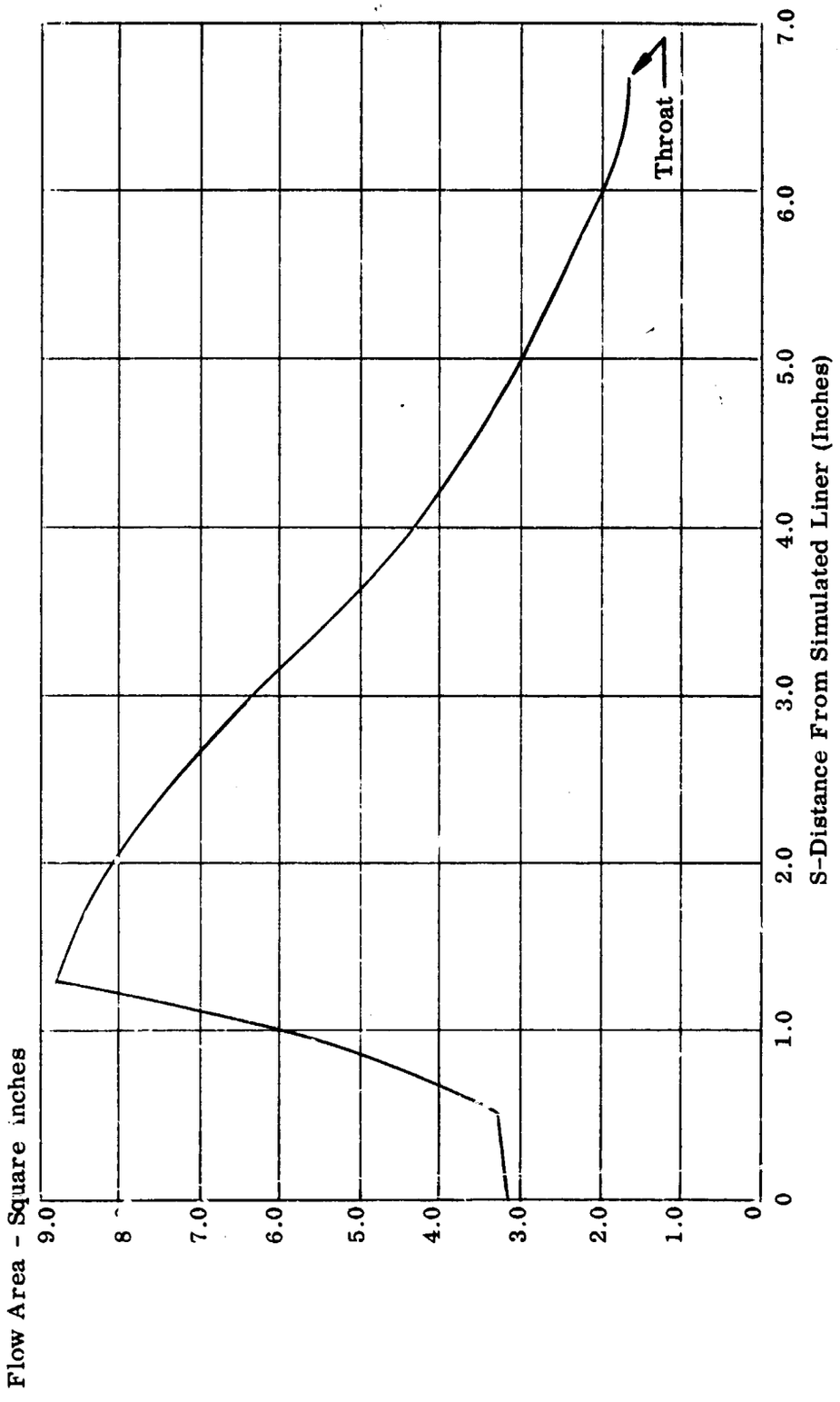


Figure 94. (U) Flow Area of Gases

(C) The results of the test series indicated that the injector generator-manifold assembly had durability for operation to 1 lb/sec total flow. However, operation at a chamber pressure of 158 psia could cause some erosion of the injector lip-flange area of the generator. In addition, vortexing action occurred on the test setup. However, with a normal thrust chamber firing setup, this condition would not occur. The pressure and temperature distribution of the gases were found to be fairly consistent. The temperature distribution of the gases around the periphery of the manifold ranged from approximately 1200 to 1600°F with an average of 1500°F. There were no radical variations of pressure to indicate a poor distribution of flow rate in the manifold assembly. Therefore, it was concluded that the generator manifold assembly could be successfully utilized with the adiabatic wall thrust chamber assembly. A total of 478 seconds was accumulated on the gas generator-manifold assembly.

8. (C) Adiabatic Wall Thrust Chamber Test Results

(C) The adiabatic wall thrust chamber utilizing a tantalum (10% tungsten) alloy retainer with a graphite sleeve as the liner was assembled using water cooled hardware (chamber and nozzle) as shown in Figure 95. The assembly was then set up on the test stand as shown in Figure 96 so that tests could be conducted to determine the effect of coolant flow (gases from the fuel rich gas generator-manifold assembly) on performance and heat rejection. The results of these tests are summarized in Table XVI and the following paragraphs.

a. (C) An attempted 15-second checkout test was terminated on start due to the oxidizer venturi plugging the inlet to the fuel rich gas generator-manifold assembly. To eliminate the plugging, a stainless steel filter (0.015 inch holes drilled in stainless steel plates) was installed in the system.

b. (C) A 15-second test (AW-652) of 25.8 seconds duration was conducted at a main core stabilized chamber pressure of 70.0 psia and a barrier/total flow ratio of 9.1% giving an overall thrust chamber mixture ratio of 1.42 (core mixture ratio = 1.78) with the resultant overall combustion efficiency, when related to a mixture ratio of 1.8, of 92.0%. Post-fire inspection of the injector revealed that the outer fuel manifold cover was cracked in the heat effective zone adjacent to the weld. This crack was rectified by cutting out the cover weld and rewelding this area. Although no metallurgical investigations were conducted, visual observation indicated that this crack was caused by a combination of bending and fatigue imposed on the injector by the complete thrust chamber assembly. Upon pressure testing of the injector after welding the fuel manifold cover, a leak was found in the water manifold due to erosion occuring in this area of the fuel barrier orifices (this injector had only primary core without barrier flow). This area was machined and rewelded to correct the situation prior to utilizing the injector for further testing. A review of the heat transfer information obtained from the test revealed that the chamber and nozzle heat flux were reduced substantially from that obtained from the injector itself.

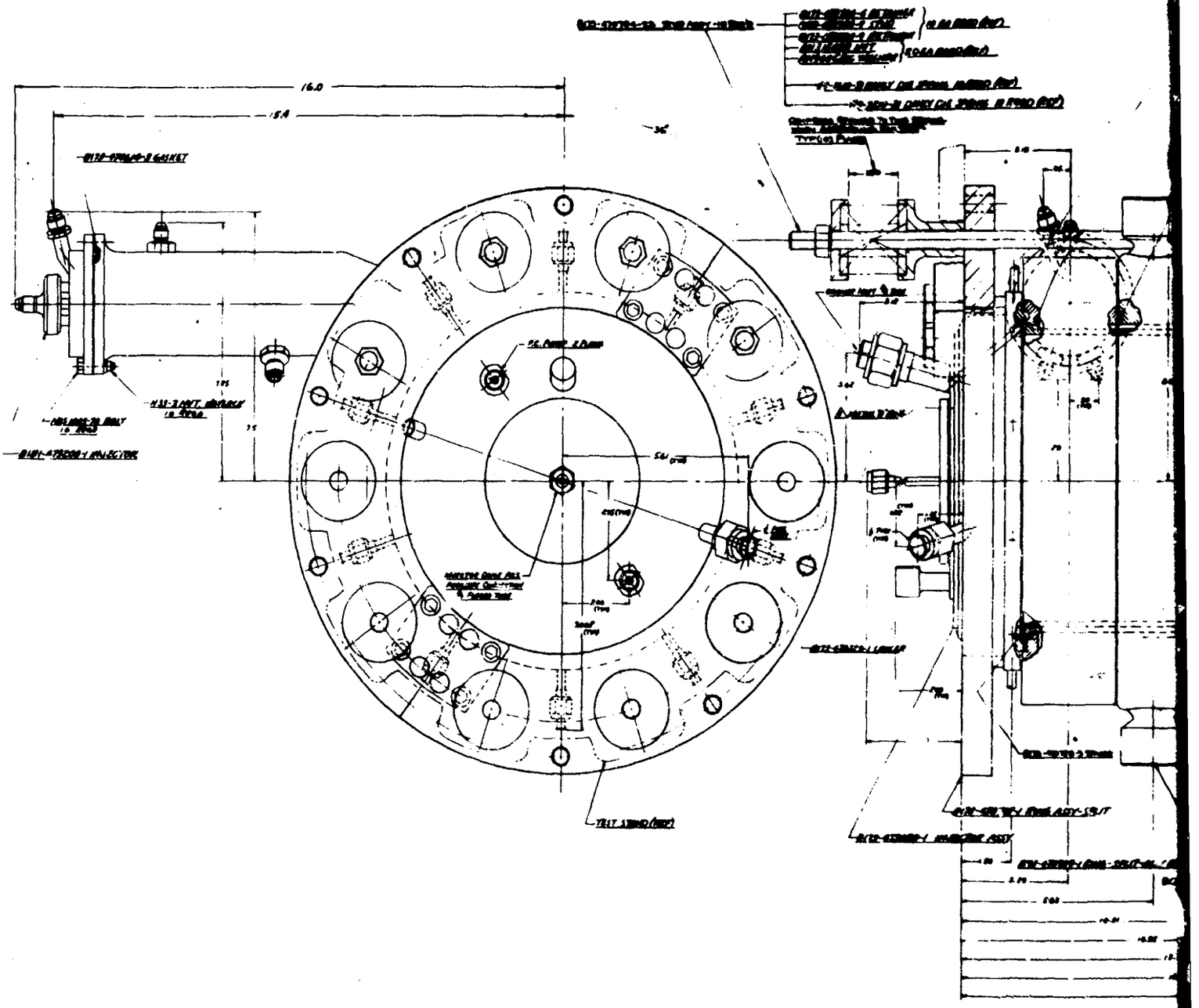
16.0
15.4
36°

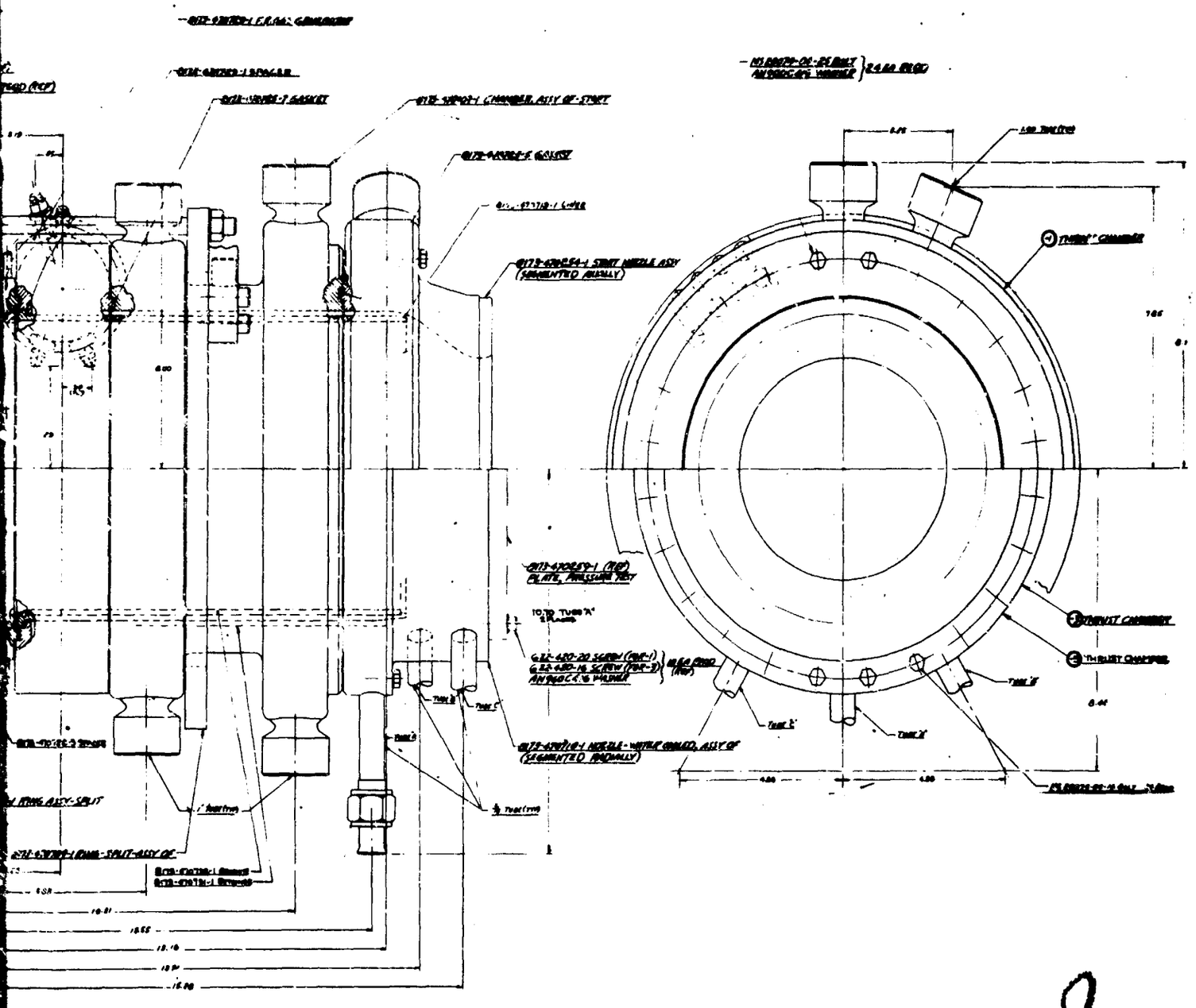

Figure 95. (C) Thrust Chamber Assembly, Water Cooled Start Hardware - Liner Test

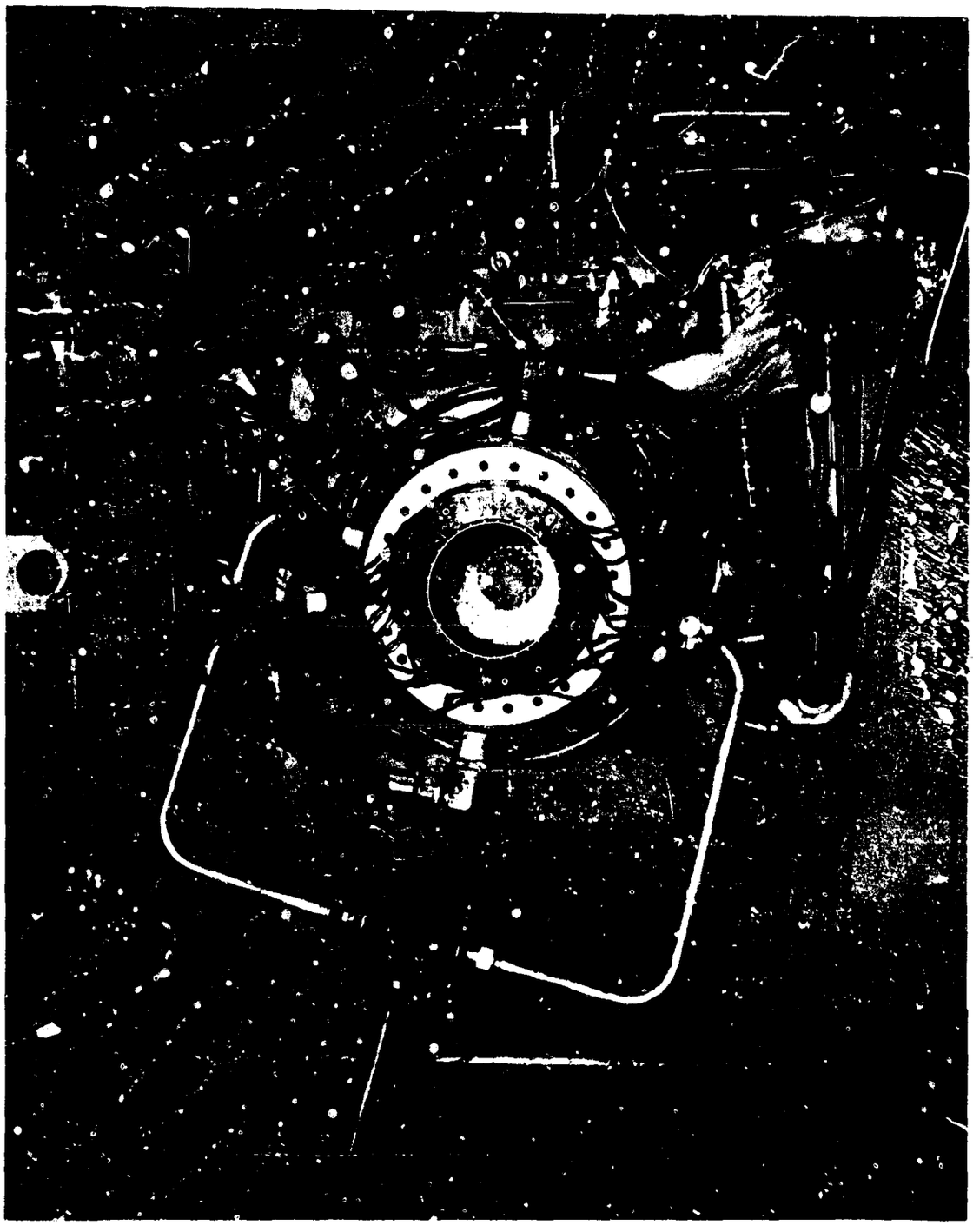

Figure 9d. (C) Adiabatic Wall Thrust Chamber Test Setup

TABLE XVI

(C) SUMMARY OF ADIABATIC WALL T

| Test No. 1AW- | $P_c$ (psia) | $W_B/W_T$ (%) | Mixture Ratio (r) Core | Mixture Ratio (r) T.C. | Combustion Efficiency ($\eta_c$) At $r_{T.C.}$ | Combustion Efficiency ($\eta_c$) At r = 1.8 | Test Q/A (BTU/in.$^2$-sec) Chamber Section | Nozzle Test Data N-1 | N-2 | N-3 | Nozzle Avg. |
|---|---|---|---|---|---|---|---|---|---|---|---|
| 652 | 70.02 | 9.1 | 1.78 | 1.42 | 93.5 | 92.0 | 0.90[illegible] | Longitudinal Nozzle | | | 0.834 |
| | | | | | | | | | | | 1.081 max |
| 653 | Malfunction - Flow Directors Cocked | | | | | | | | | | |
| 654(1) | 72.22 | 9.06 | 1.81 | 1.44 | 95.6 | 94.2 | 1.676 | 1.398 | 1.360 | 2.242 | 1.61 |
| | 72.22 | 9.0 | 1.83 | 1.46 | 95.2 | 93.9 | 1.783 | 1.498 | 1.476 | 2.372 | 1.73 |
| 655 | Malfunction - Flow Directors Cocked | | | | | | | | | | |
| 656(1) | 72.23 | 9.03 | 1.818 | 1.44 | 95.3 | 94.2 | 1.679 | 1.389 | 1.548 | 2.257 | 1.69 |
| | 71.74 | 8.93 | 1.85 | 1.47 | 94.7 | 93.6 | 1.803 | 1.544 | 1.686 | 2.413 | 1.83 |
| 657 | 36.80 | 8.88 | 1.86 | 1.52 | 92.3 | 91.7 | 0.937 | 0.770 | 0.790 | 1.318 | 0.926 |
| 658(1) | 71.54 | 11.15 | 1.799 | 1.358 | 93.3 | 91.8 | 2.157 | 1.697 | 1.470 | 2.027 | 1.71 |
| | 70.98 | 11.15 | 1.806 | 1.364 | 92.7 | 90.6 | 2.114 | 1.713 | 1.490 | 2.080 | 1.73 |
| 659 | 32.76 | 9.88 | 1.93 | 1.491 | (2) | (2) | 0.692 | 0.629 | 0.769 | 0.839 | 0.73 |
| 660(1) | 65.48 | 9.09 | 1.801 | 1.430 | (2) | (2) | 1.519 | 1.287 | 1.425 | 1.899<br>2.07 est | 1.51 |
| 661 RCTC | 39.63 | 9.9 | 1.825 | 1.418 | 96.0 | 94.5 | | | | | |
| 662 RCTC | 36.99 | 9.3 | 2.016 | 1.572 | 93 | 92.5 | | | | | |
| 663 RCTC | 74.34 | 11.15 | 1.762 | 1.333 | 96 | 9[illegible] | | | | | |
| 664 RCTC | 73.15 | 11.0 | 1.813 | 1.372 | 94 | 92.3 | | | | | |
| 665 RCTC | 74.25 | 11.2 | 1.784 | 1.346 | 95.6 | 93.9 | | | | | |

(1) Data at $\theta \cong$

(2) Roughness

(3) Checkout -

(4) 137 seconds

(5) 42 seconds

(6) 38 seconds
Post-test in

(7) Maximum t
temperatur

TABLE XVI

TIC WALL THRUST CHAMBER TESTS

| sec) Data | | Test Q/A with Liner / Test Q/A Without Liner | | | | | Test Q/A With Liner / Theoretical Q/A With Liner | | | Estimated Throat Temperature (°F) (RCTC; $\epsilon$ = 0.65) | |
|---|---|---|---|---|---|---|---|---|---|---|---|
| -3 | Nozzle Avg. | Chamber Section | N-1 | N-2 | N-3 | Nozzle Avg. | N-1 | N-2 | N-3 | Avg. | Max. |
| zle | 0.834<br>1.081 max | 0.333 | | | | 0.54 | | | | | |
| 242<br>372 | 1.61<br>1.73 | 0.66 | 0.58 | 0.62 | 0.78 | 0.65 | 1.50 | 2.08 | 1.97 | 3540 | 4290 |
| 257<br>413 | 1.69<br>1.83 | 0.67 | 0.60 | 0.70 | 0.79 | 0.69 | 1.54 | 2.37 | 2.00 | 3550 | 4340 |
| 318 | 0.926 | 0.63 | 0.48 | 0.52 | 0.67 | 0.52 | 1.22 | 1.93 | 2.00 | 3100 | 3720 |
| 027<br>080 | 1.71<br>1.73 | 0.79 | 0.66 | 0.62 | 0.68 | 0.65 | 1.59 | 2.19 | 1.89 | 3260 | 3900 |
| 839 | 0.73 | 0.50 | 0.43 | 0.55 | 0.47 | 0.49 | 0.97 | 1.92 | 1.29 | 2300 | 2680 |
| 899<br>07 est | 1.51 | 0.59 | 0.51 | 0.62 | 0.65 | 0.60 | 1.31 | 2.07 | 1.68 | 3060<br>3260 | 3650<br>3900 |
| | | | | | | | | | | | <2000[3] |

) Data at $\theta \cong 14$ Seconds of Stabilized $P_c$ . — ~2900[4] Stabilized

) Roughness and two-phase Fluorine Caused Large Decrease in $\eta_c$ — ~3100[5] Stabilized

) Checkout - 33 seconds

) 137 seconds duration — ~3000[6] Stabilized

) 42 seconds duration

) 38 seconds duration wall temperature; Stabilized at 30 seconds then rose. Post-test inspection revealed a hole in the throat section of the chamber. — 3150[7]

) Maximum temperature prior to burnthrough. During 115.1 second operation, temperatures stabilized and then streak occurred causing burnthrough.



2

(C) However, the nozzle heat rejection with the longitudinally segmented nozzle resulted in lower values than obtained with the circumferentially segmented nozzle, due primarily to the inaccuracy obtained by the small rise in the water outlet temperature and the inability to properly define thermocouple locations in the exact center of each passage. The heat transfer information indicated that the maximum nozzle heat flux was 30% higher than the average, meaning that the maximum throat temperature would be 6.8% higher than the average. Since the longitudinal nozzle gave low heat rejection information, further testing was conducted using the circumferentially segmented nozzle.

c. (C) The injector was then assembled to the water cooled adiabatic wall thrust chamber assembly using the circumferentially segmented nozzle. An attempted 35-second test with stabilized chamber pressure was terminated after 7.3 seconds (1AW-653) due to an apparent restriction of the coolant gases through the liner assembly. Post-test inspection revealed that the flow directors had cracked and lodged in a position restricting the coolant flow. A metallurgical investigation of the flow directors indicated that contamination had occurred primarily in the area where the corrugation of the flow director touched the tantalum retainer, therefore creating a brittle structure. The nozzle was removed and both the upstream and downstream flow directors were removed and replaced with one new flow director in the downstream position only. This was done since replacing the upstream director would have required disassembly of the entire adiabatic wall thrust chamber assembly. In addition, new flow directors were fabricated and were sent to General Telephone and Electronics Corporation for application of the aluminide coating for further use to prevent embrittlement in the corrugated regions of the flow directors.

d. (C) A 46.1-second test (1AW-654) was conducted at a chamber pressure of 72.2 psia and a barrier/total flow ratio of 9.1% giving an overall thrust chamber mixture ratio of 1.46 (core mixture ratio = 1.83) with an overall resultant combustion efficiency of 95.2%. The overall combustion efficiency would be 93.9% when related to a mixture ratio of 1.8. The heat transfer information of this test indicated a chamber heat rejection of 1.97 times that obtained on test 1AW-652. In addition, the heat rejection was significantly greater than theoretically predicted by as much as 100% variation.

e. (C) Test 1AW-655 was an attempted repeat of the previous test in order to confirm the heat rejection data, but this test was terminated after 12.3 seconds due to a malfunction occurring on the restriction in the fuel (upon start) of the fuel rich gas generator assembly. Post-test inspection revealed "cocking" of the flow director which was lodged in a position restricting the coolant gas flow.

f. (C) Two new flow directors were installed in the assembly by incorporating tabs in the flow directors to be held in place by the chamber (gap between chamber and manifold to hold the upstream flow director and between chamber and nozzle to hold the downstream flow director). Test 1AW-656 (46.7 seconds duration) was conducted at a chamber pressure of 71.7 psia and a barrier/total flow ratio of

(C) 8.93%, resulting in an overall thrust chamber mixture ratio of 1.47 (core mixture ratio of 1.85) with a resultant combustion efficiency of 94.7%. When relating this combustion efficiency to a mixture ratio of 1.8, the resultant combustion efficiency was 93.6%. The results of this test indicated that the heat rejection of the chamber and nozzle was similar to that obtained on test 1AW-654. Heat transfer analyses indicated that chamber heat rejection should be approximately 1.8 BTU/in.$^2$-sec which was primarily caused by the small gap between the retainer and the chamber wall since the retainer was hot and the chamber was cold. However, the retainer was tapered at the exit end so that a velocity imbalance was not created. The nozzle heat rejection was significantly higher than the theoretical value shown in Figure 70. A review of the actual test data indicated by analysis that using a barrier/total flow ratio of 9% would result in an average throat temperature of the columbium thrust chamber of approximately 3500°F, this was beyond the capability of the columbium thrust chamber. Therefore, testing was continued by increasing the barrier flow rate by approximately 35% in an effort to define whether this increased flow rate was adequate for cooling the columbium thrust chamber.

g. (C) Test 1AW-657, a 56.5-second duration test, was conducted at a chamber pressure of 36.8 psia and a barrier/total flow ratio of 8.88% resulting in an overall thrust chamber mixture ratio of 1.52 (core mixture ratio of 1.86). The resultant overall combustion efficiency was 92.3%. Post-test inspection revealed that the flow directors were damaged. The next test was conducted with tantalum flow directors coated with aluminide. Heat transfer test data indicated that the heat flux obtained at 37 psia chamber pressure was still high by essentially the same degree as that obtained at 70 psia. In addition, a decrease in combustion efficiency of 2% had resulted by reducing the chamber pressure from 70 to 37 psia. Post-test inspection of the tantalum retainer and graphite sleeve indicated some erosion of the graphite sleeve at the injector end and a 3/16 inch diameter hole at the injector end of the retainer. The graphite sleeve was removed but a new graphite sleeve could not be inserted due to the distortion from fire tests. At this point, it was decided to replace the retainer-graphite sleeve with the tungsten coated tantalum (10% tungsten) alloy liner and check the liner out in water cooled hardware prior to testing it in the columbium thrust chamber. A total of 195 seconds (140 seconds at stabilized main core $P_c$) was accumulated on the retainer-graphite sleeve. Figures 97 through 99 show the retainer and sleeve.

h. (C) Since testing with the barrier flow rate of 9% indicated heat rejection significantly higher than theoretically predicted, a 34-second test (1AW-658) was conducted using a barrier/total flow of 11.15% with the tungsten-coated tantalum (10% tungsten) alloy liner. This test was conducted at a chamber pressure of 71 psia at an overall mixture ratio of 1.36 (core mixture ratio of 1.81) with a resultant combustion efficiency of 82.7%. The results of this test indicated a heat rejection significantly greater than theoretically predicted. Projecting the test results to the radiation cooled thrust chamber would indicate an expected average temperature of 3260°F and a maximum temperature of 3900°F, predicated upon the variations obtained by using the longitudinally segmented nozzle.

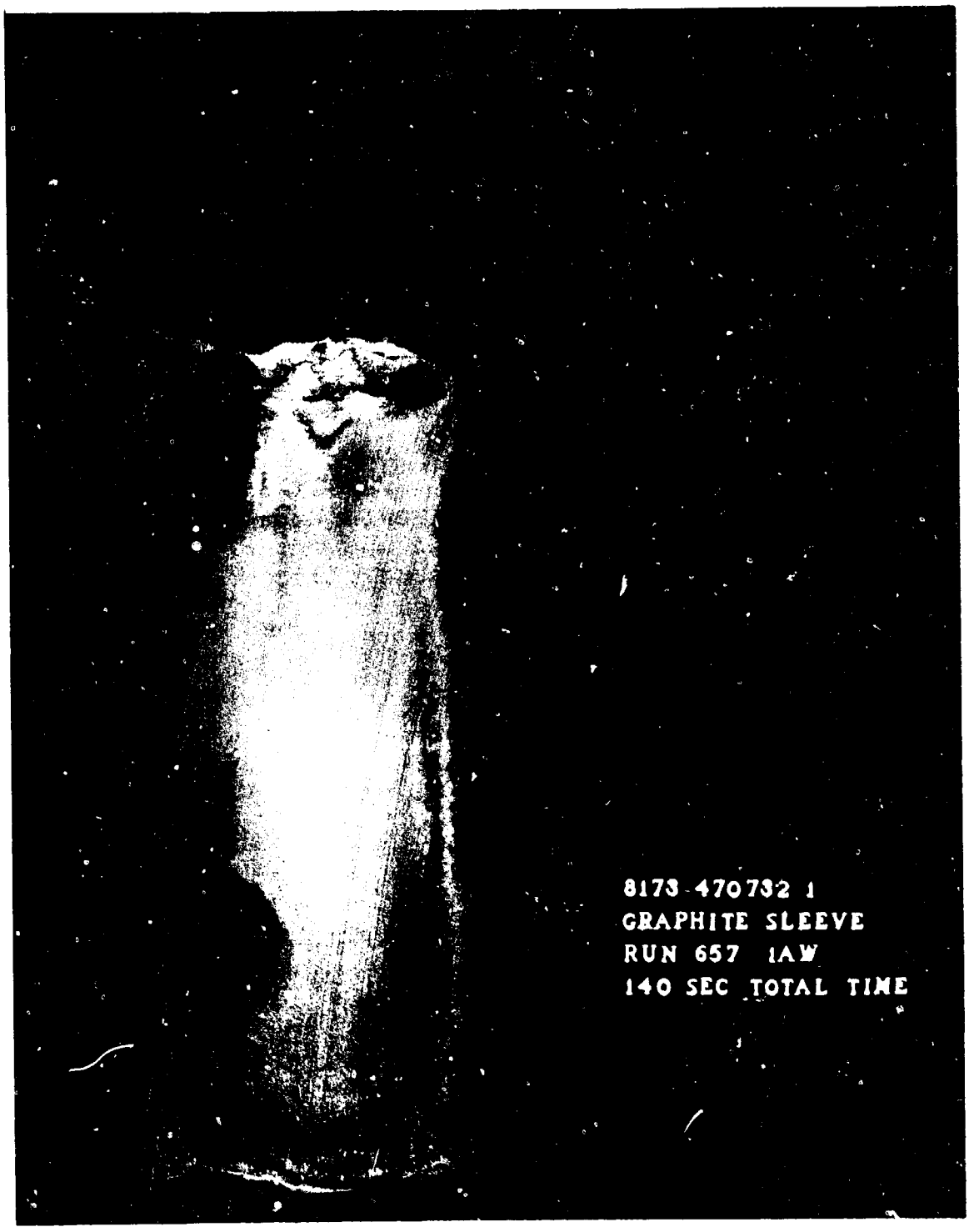


Figure 97. (U) Graphite Sleeve


Figure 98. (U) Tantalum Retainer

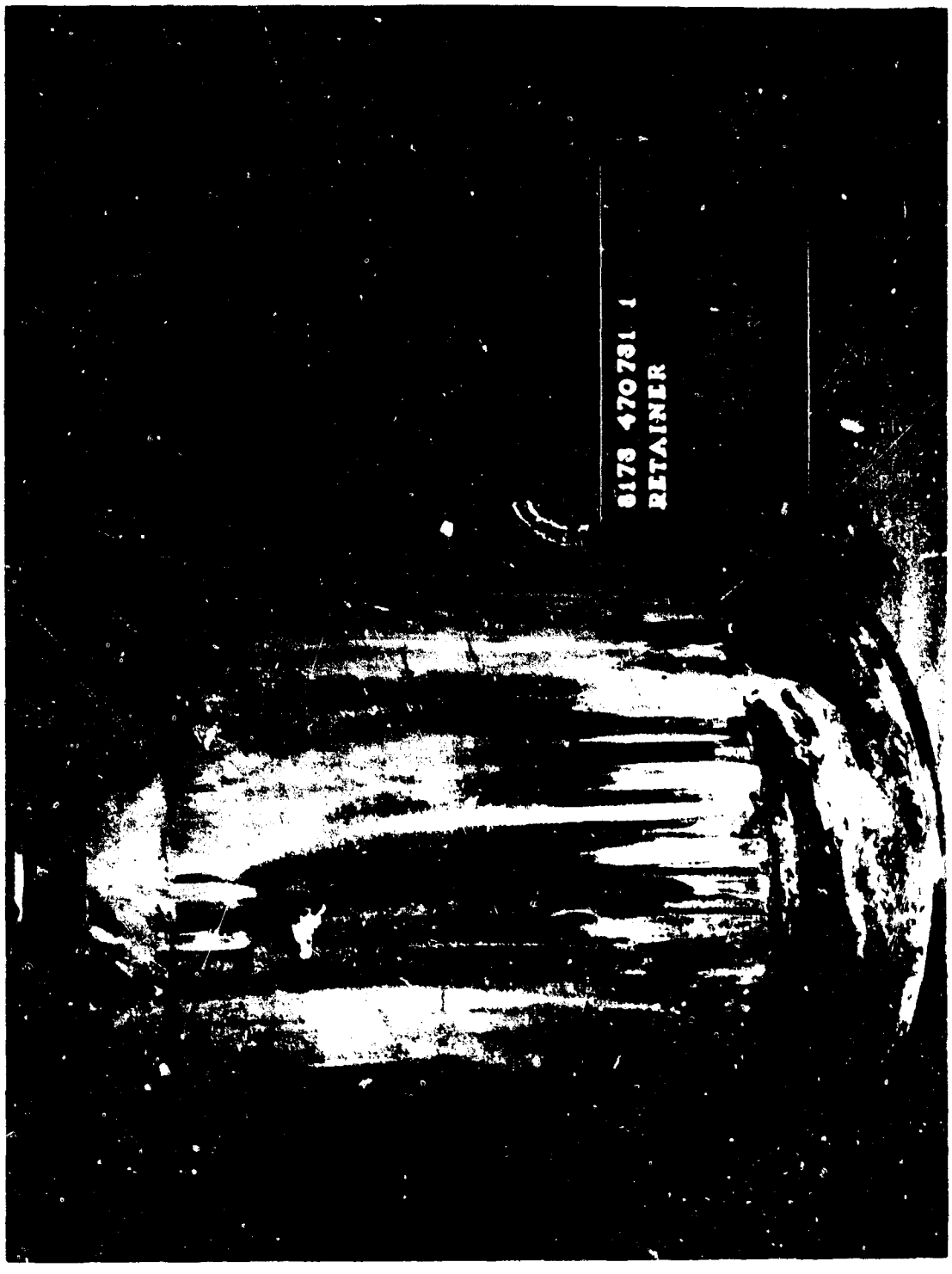


Figure 99. (U) Tantalum Retainer

i. (C) Test 1AW-659 was conducted for a duration of 59 seconds using the same liner but at a chamber pressure of 32.8 psia and a barrier/total flow rate of 9.9%. A certain degree of roughness occurred during this test. Analysis of the test data indicated that the roughness was due to propellant vaporization in the fluorine inlet line. Chamber pressure and heat rejection data were lower than expected, but considered unreliable due to the fluorine gassing in the feed line.

j. (C) A repeat of test 1AW-656 (1AW-660) was conducted with this liner to determine if there was a significant change between the combination retainer-graphite sleeve and the liner. The expected change would result in hotter coolant gas exiting from the liner than would be obtained on similar tests using the retainer-graphite sleeve combination. This 59-second test also indicated roughness and projected radiation cooled thrust chamber temperatures similar to that expected based on test 1AW-658. Post-test observation indicated a leak in the chamber pressure port on the injector which was rectified by welding this area. In addition, a revision to the cooling procedures was incorporated as a result of the gassing that occurred on tests 1AW-659 and 660. The fuel rich gas generator injector lip indicated erosion from all the tests accomplished on this hardware and was therefore repaired by building up this area with weld and remachining prior to initiating the next test. Post-test observation of the tungsten coated tantalum liner indicated cracking of the weld area near the flange end (Figure 100) and removal of the tungsten coating. Localized burning at the exit end of the liner at the 6:30 o'clock position (looking from the nozzle as shown in Figure 101) was also noted. Indications are that the cracking experienced in the weld was caused by a combination of roughness as well as inadequate weld. The localized burning of the liner was caused by a plugged fuel hole in the main core injector which allowed a stray oxidizer stream to impinge on the liner in this area. Figure 102 shows distortion of the liner after the fire test. As a result, the injector was back-flushed and flowed prior to initiation of the next test. Since the tungsten-coated tantalum liner was not acceptable for testing at this point, it was planned that all further testing would be conducted with the tungsten liner. However, a program was initiated in an effort to reweld the cracked areas of the liner (tantalum liner) which was successfully accomplished and therefore this liner was used as a backup.

k. (C) Since the results of the water cooled hardware test (as summarized in Table XVI) indicated that the columbium thrust chamber would operate successfully if streaking did not cause excessive temperatures (3300°F maximum), the decision was made to test the radiation cooled thrust chamber and monitor skin temperatures so that shutdown could be initiated prior to thrust chamber overheating. The test assembly is shown in Figures 103 and 104. A checkout test (1AW-661) of 33 seconds duration (15 seconds of stabilized main core pressure) was conducted at a chamber pressure of 40 psia with an indicated performance of 96.0% combustion efficiency based on an overall mixture ratio of 1.42. The results of this test indicated temperatures below 2000°F which would allow operation of the adiabatic wall thrust chamber to steady-state conditions. This test was conducted using the spun pure tungsten liner. Figure 82 shows this liner as received and


Figure 100. (U) Tantalum Liner Crack

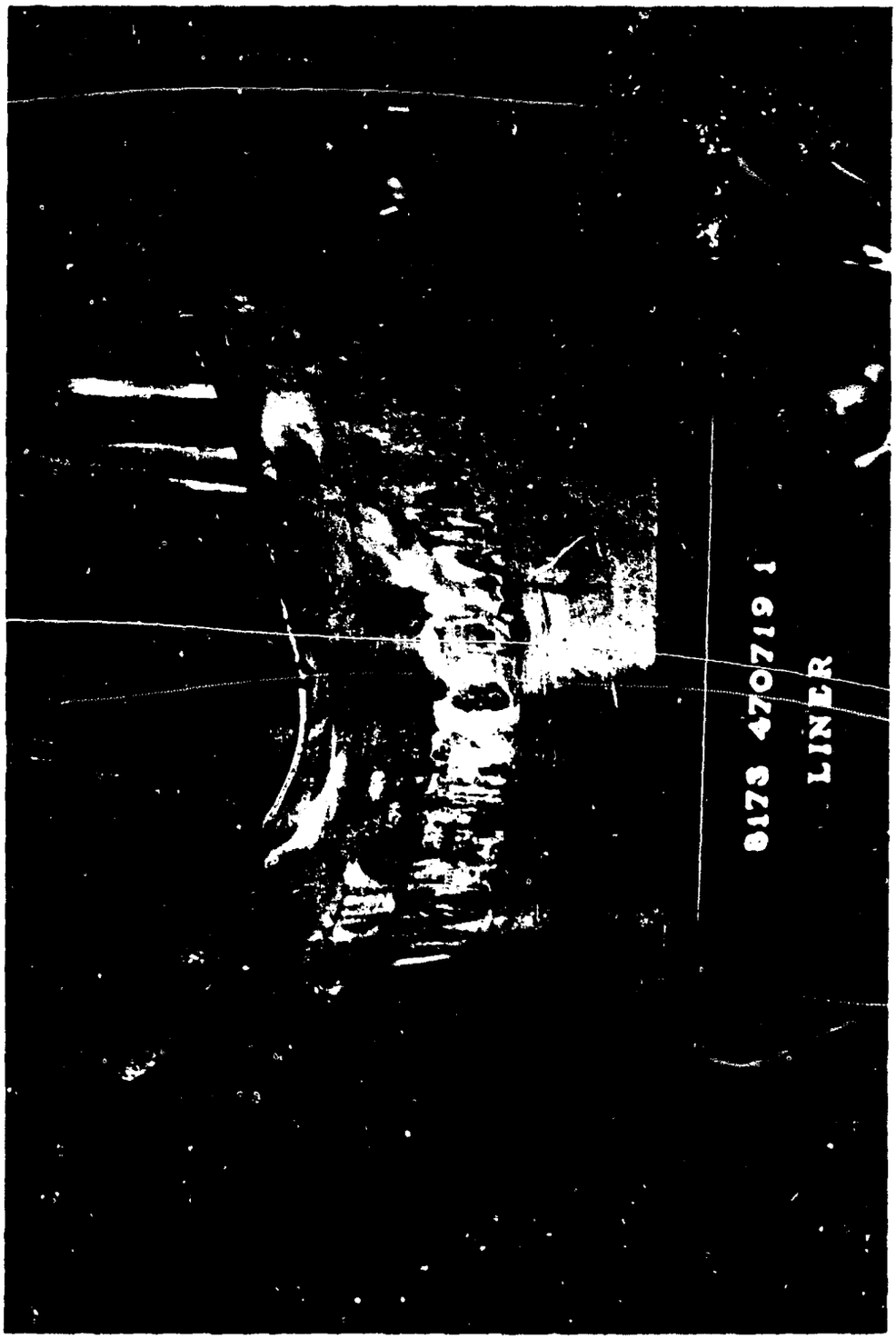


Figure 101. (U) Tantalum Liner Burned Area

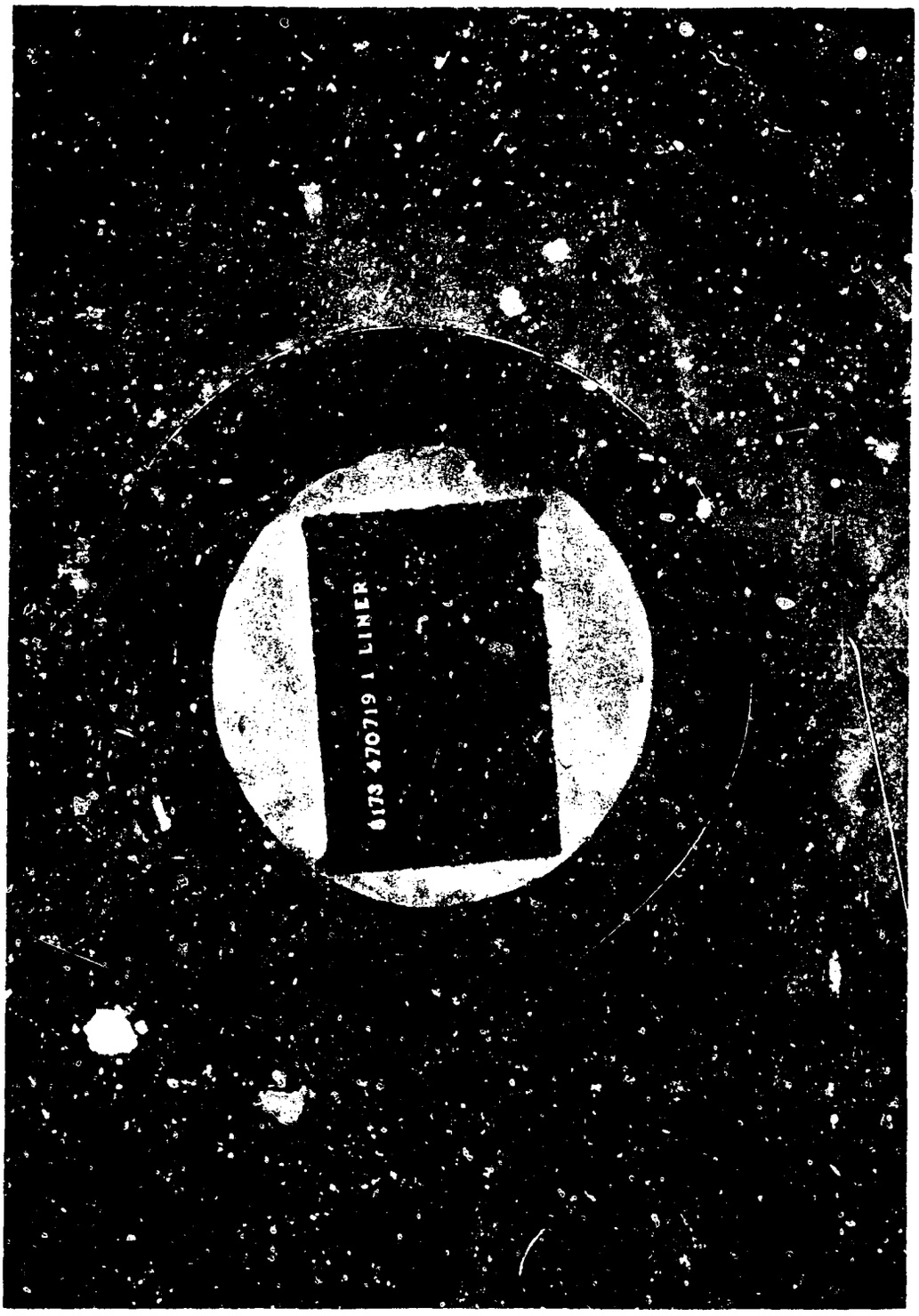


Figure 102. (U) Tantalum Liner

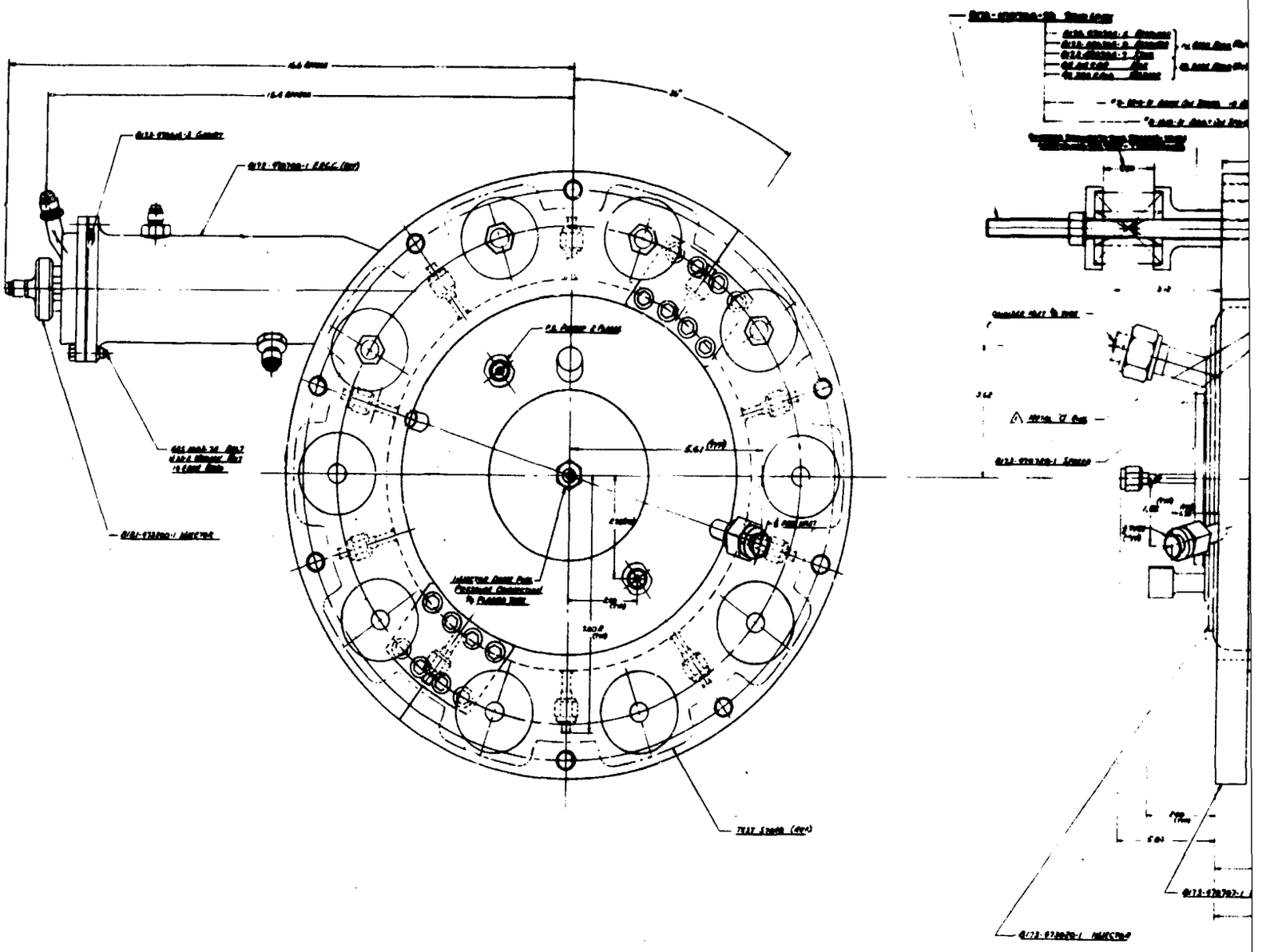

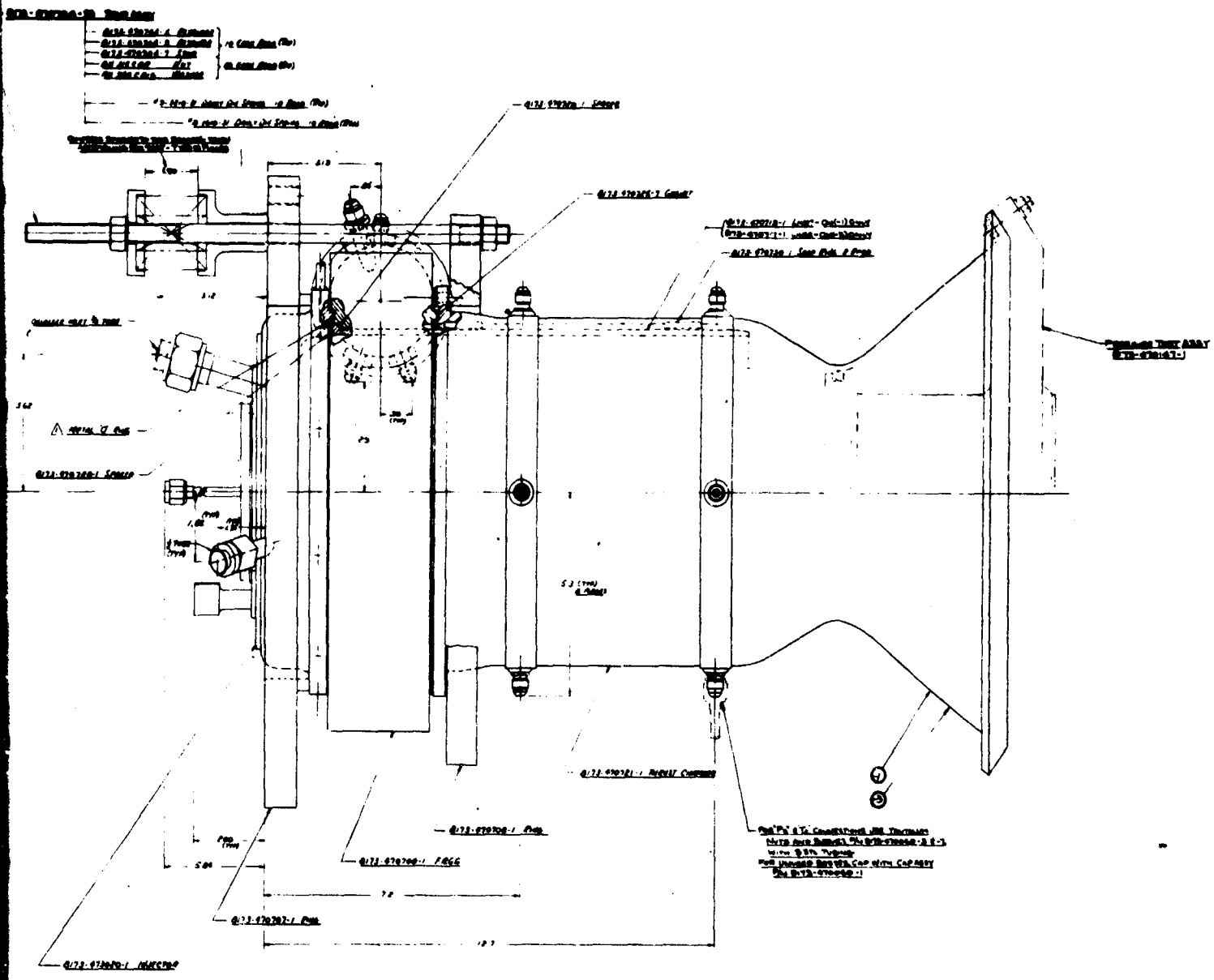

Figure 103. (C) Thrust Chamber Assembly,
Radiation Cooled Chamber - Adiabatic Wall Test

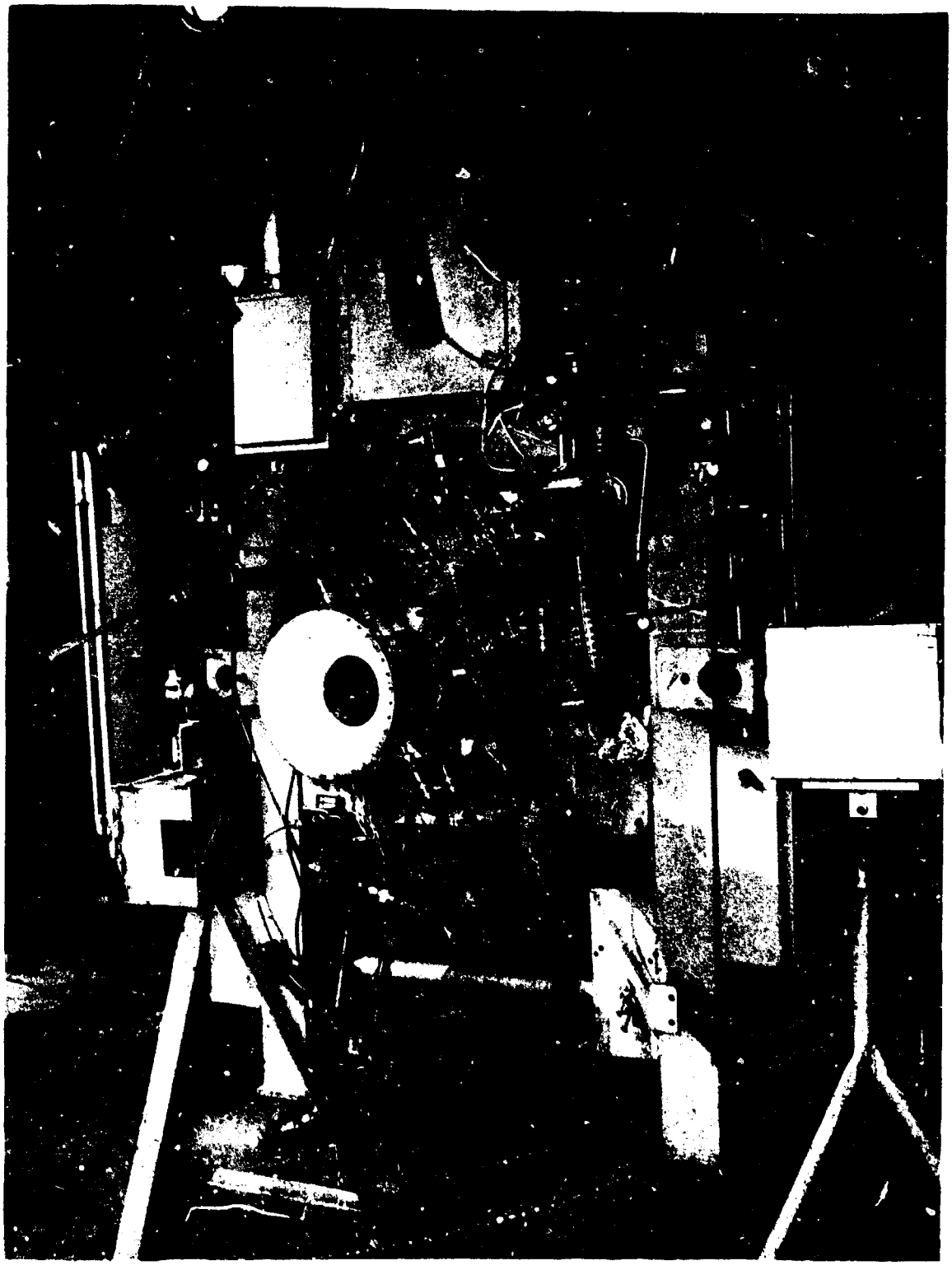

Figure 104. (U) Radiation Cooled Thrust Chamber Test Setup

(C) Figures 105 and 106 show this liner after fire test. Post-test observation indicated cracking through the wall of the liner at the flange area located near the injector end. A metallurgical investigation of this area revealed that the crack was induced by thermal shock occurring on start due to uneven heating. Figure 107 shows the I.D. side of the crack and Figure 108 shows the O.D. side of the crack. Figure 109 shows how the crack propagated through the wall. The cracking by thermal shock was of such a nature that the liner could not be utilized for further testing without propagating the cracks and jeopardizing the columbium thrust chamber. Therefore, the liner was removed after this test (1AW-661). For the next test series, the tantalum (10% tungsten) retainer was reworked (the lip which held in the graphite sleeve) and installed in the columbium thrust chamber for feasibility and durability demonstrations.

l. (C) A 120-second test (1AW-662) was successfully conducted for 122 seconds of stabilized main core chamber pressure of 37 psia (137 seconds total) with a maximum indicated temperature of 2900°F. The data indicated a barrier/total flow ratio of 9.3% at overall mixture ratio of 1.57 (core mixture ratio of 2.02). Post-test observation indicated three pinholes in the liner and a visual indication of contamination occurring in the liner which was not detrimental. The columbium thrust chamber was in excellent condition. A time history of the temperature is shown in Figure 110.

m. (C) Test 1AW-663 was scheduled for 120 seconds and was conducted at a chamber pressure of 74.3 psia, however, the test was terminated after 42 seconds due to overheating of the fuel rich gas generator injector end. The results of this test indicated a combustion efficiency of 96% at an overall mixture ratio of 1.33 with a barrier/total flow ratio of 11.15%. The maximum stabilized temperature recorded on the columbium thrust chamber was 3000°F as shown in Figure 111. Thrust chamber skin temperatures stabilized after approximately 30 seconds of operation. Post-test observation indicated distortion of the liner (localized area at the 3:00 o'clock position) and contamination of the liner with some flaking of the liner (Figures 112 and 113) due to the contamination. A metallurgical investigation of the liner indicated contamination throughout. Figures 114 and 115 show the microporosity of the liner. However, the material did have the ductility and strength at elevated temperature to withstand 332 seconds of operation. The next series of tests on the program was conducted with the repaired tungsten-coated tantalum alloy liner and columbium thrust chamber (Figure 116).

n. (C) Test 1AW-664 was an intended 120-second durability test which was terminated after 38 seconds of operation at a chamber pressure of 73.2 psia due to excessive temperatures in the nozzle section of the columbium thrust chamber. This test was conducted with the repaired tungsten coated tantalum alloy liner. Temperatures had stabilized at approximately 2800°F after 30 seconds of operation. A temperature rise in the nozzle observed at 38 seconds necessitated termination of the test. Post-test inspection revealed a small hole in the thrust chamber approximately 1 inch wide and 2 inches long (Figure 117). Two other significant items were noted during the post-test inspection: (1) the flow director standoffs were broken which could have blocked off gas flow, causing the burned out area; and (2) a streak was noted on the tantalum liner in line with the burned out area.

Figure 105. (U) Tungsten Liner

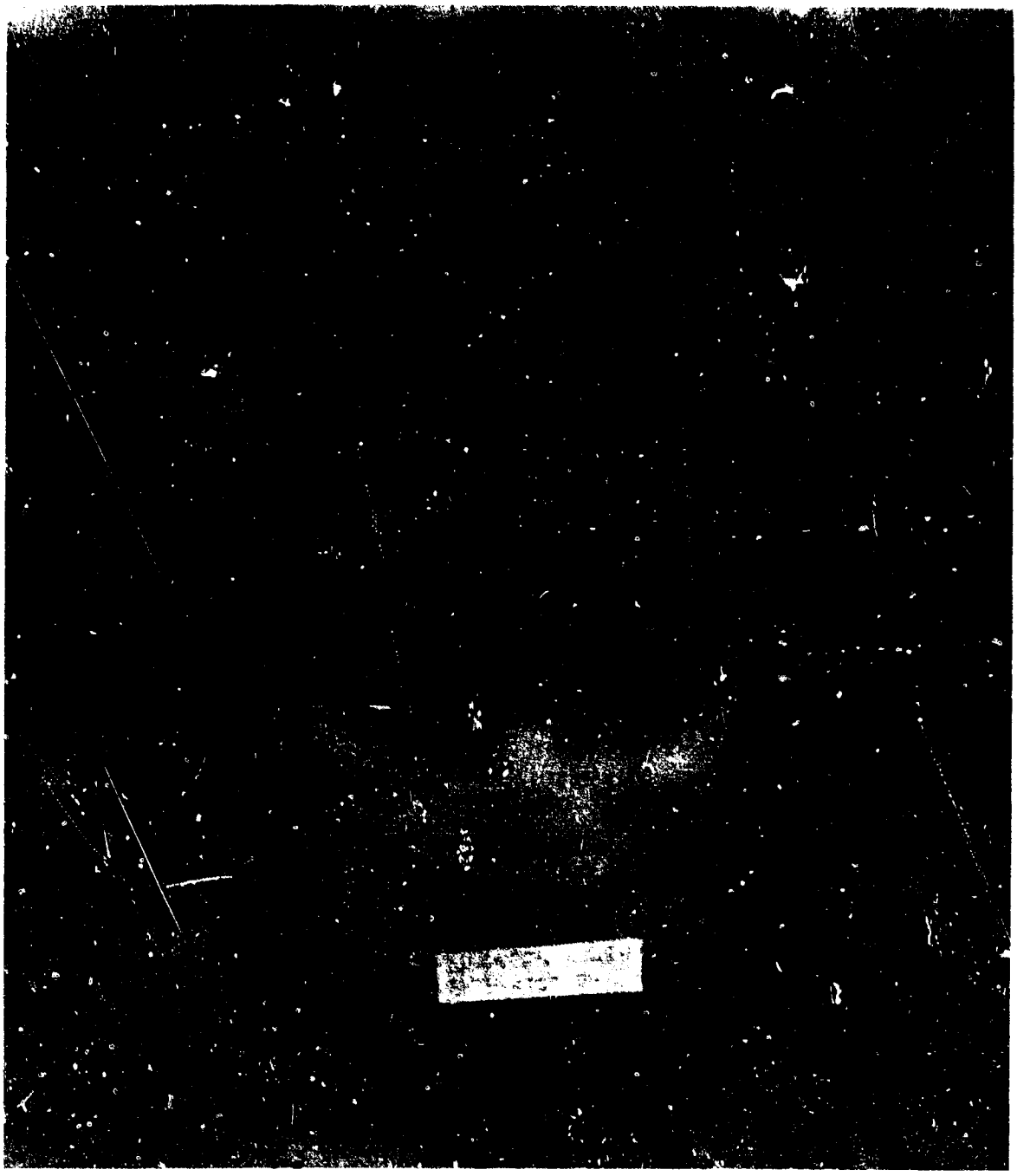

Figure 106. (U) Tungsten Liner

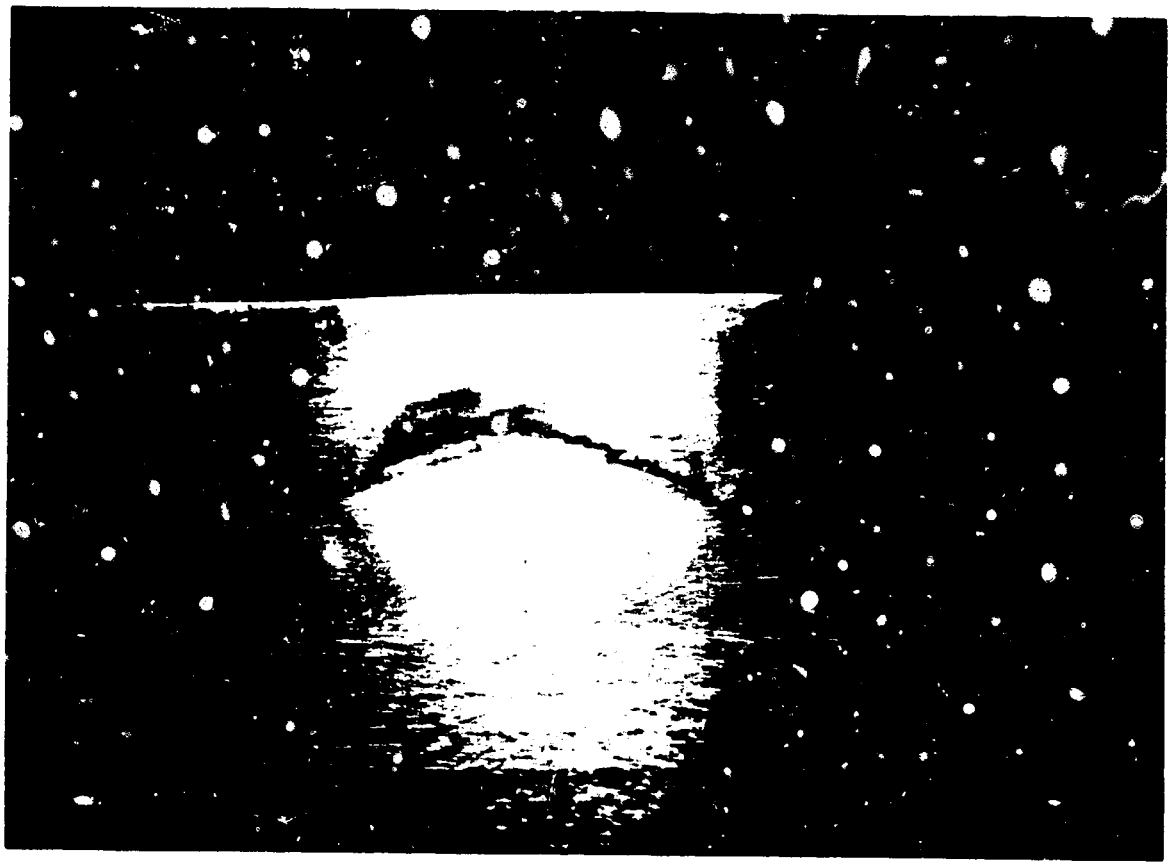

Figure 107. (U) Tungsten Liner Crack (I.D.)

Figure 108. (U) Tungsten Liner Crack (O.D.)

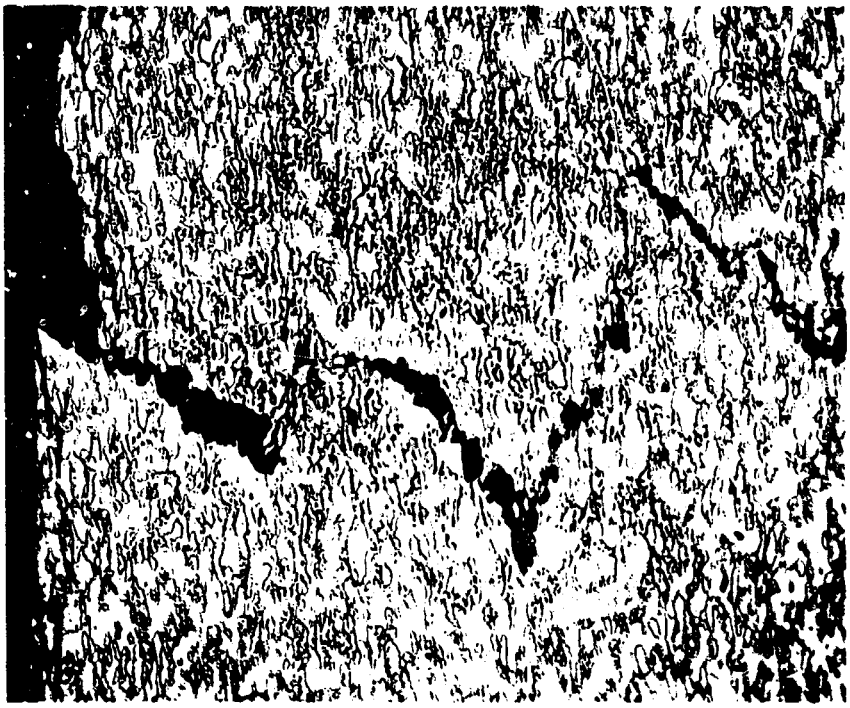

Figure 109. (U) Micrograph of Crack in Tungsten Liner

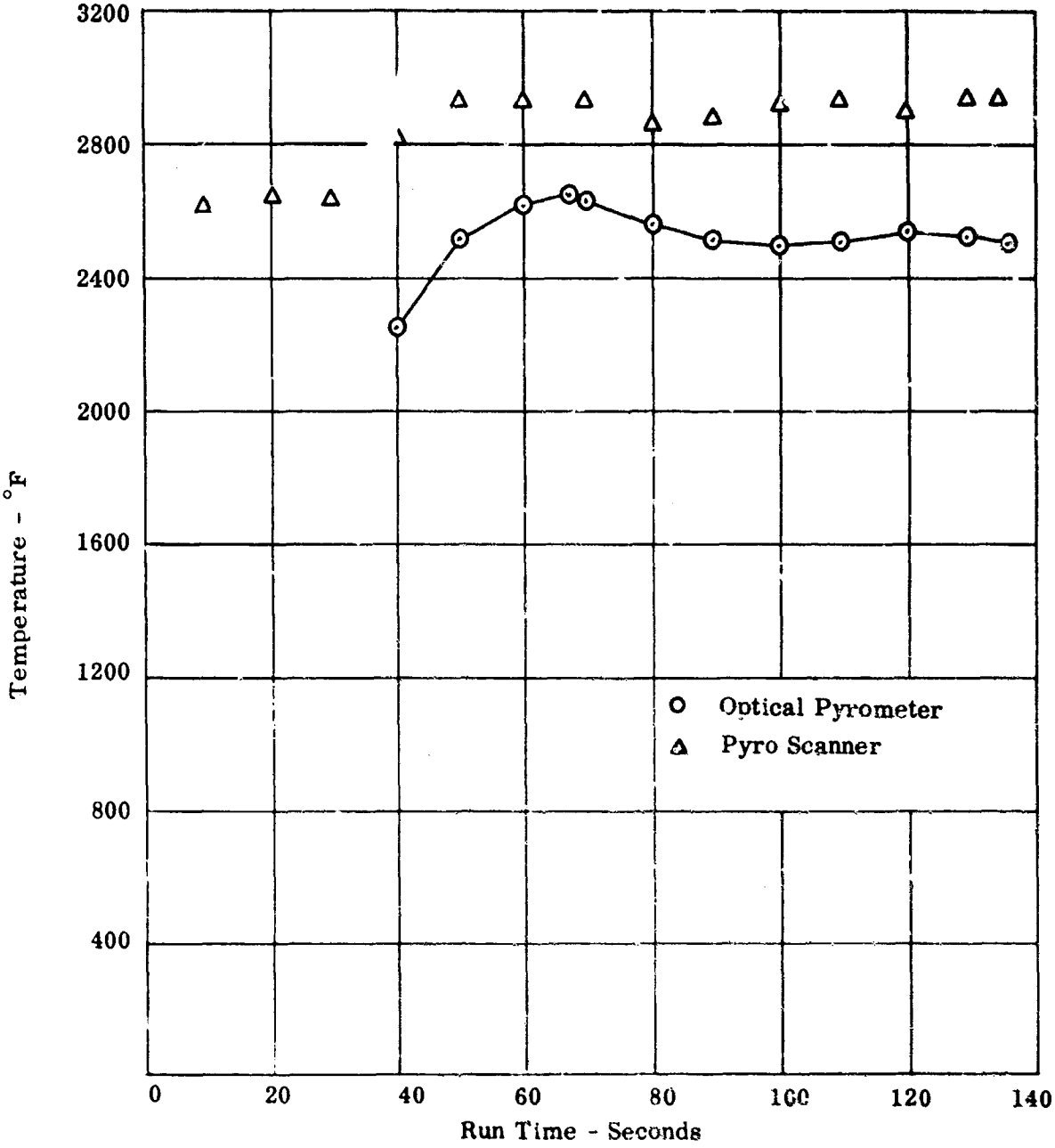


Figure 110. (U) Time History (1AW 562)

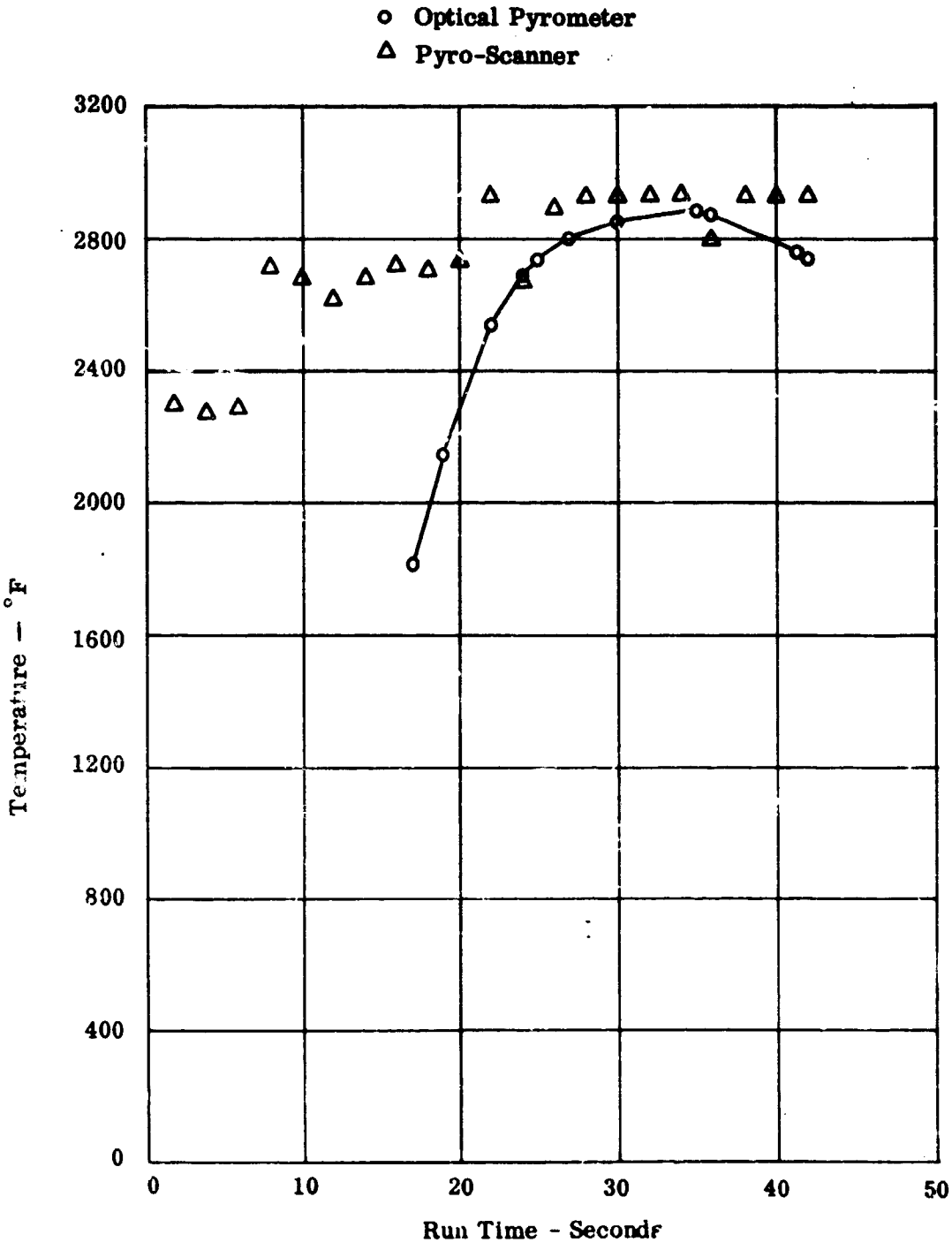


Figure 111. (U) Time History (1AW 663)


Figure 112. (U) Ta-10W Coated Liner (Cell 1AW)

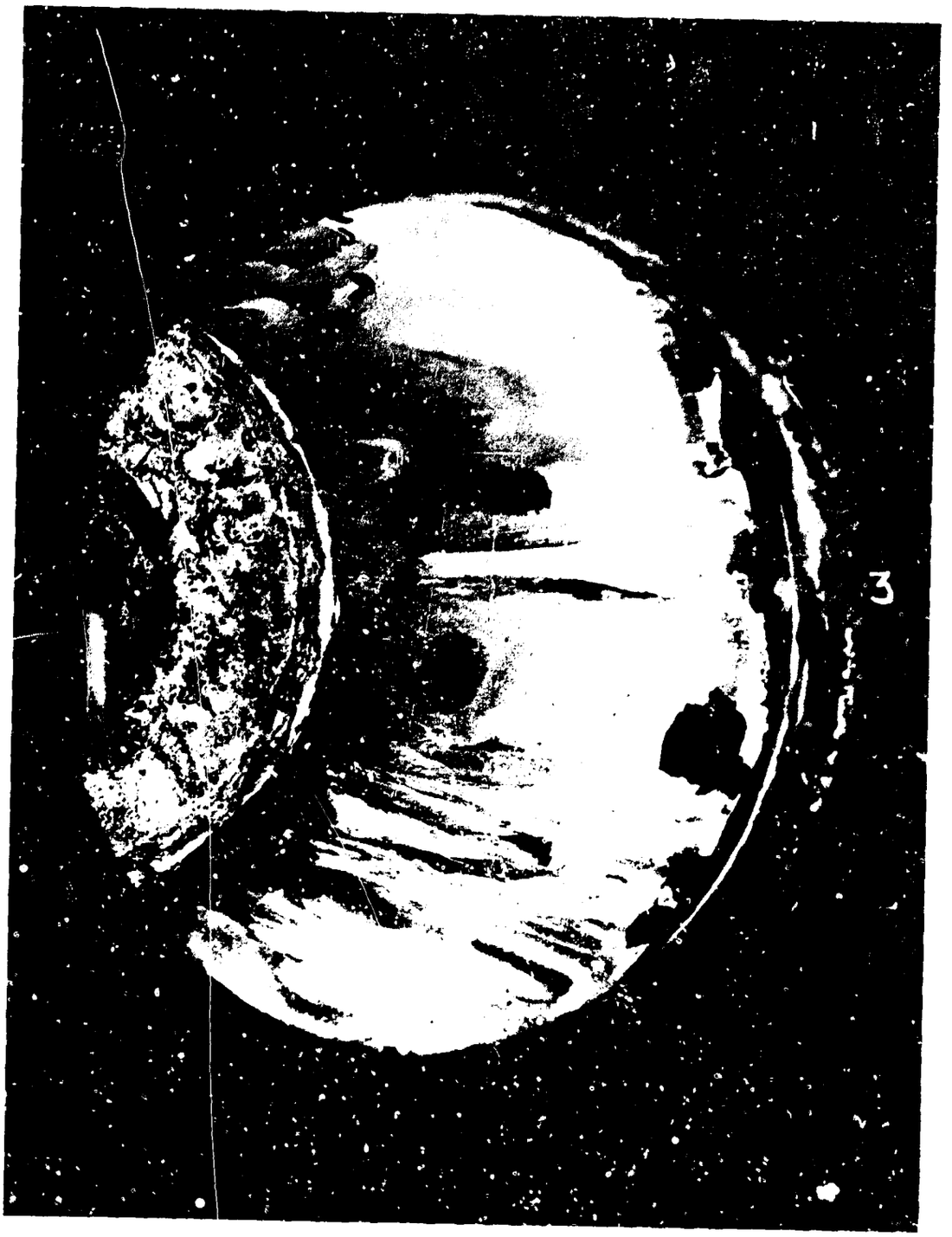


Figure 113. (U) Post-Run View of Core Injector, Liner, and Thrust Chamber on Stand (1AW-663)

Figure 114. (U) Tantalum Liner Contamination (75X Size)

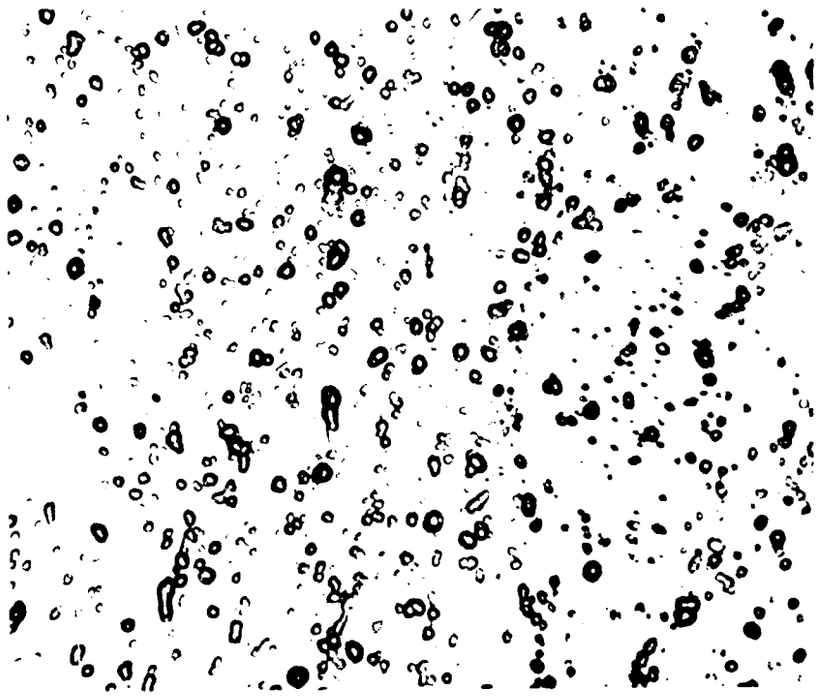

Figure 115. (U) Tantalum Liner Contamination (500X Size)

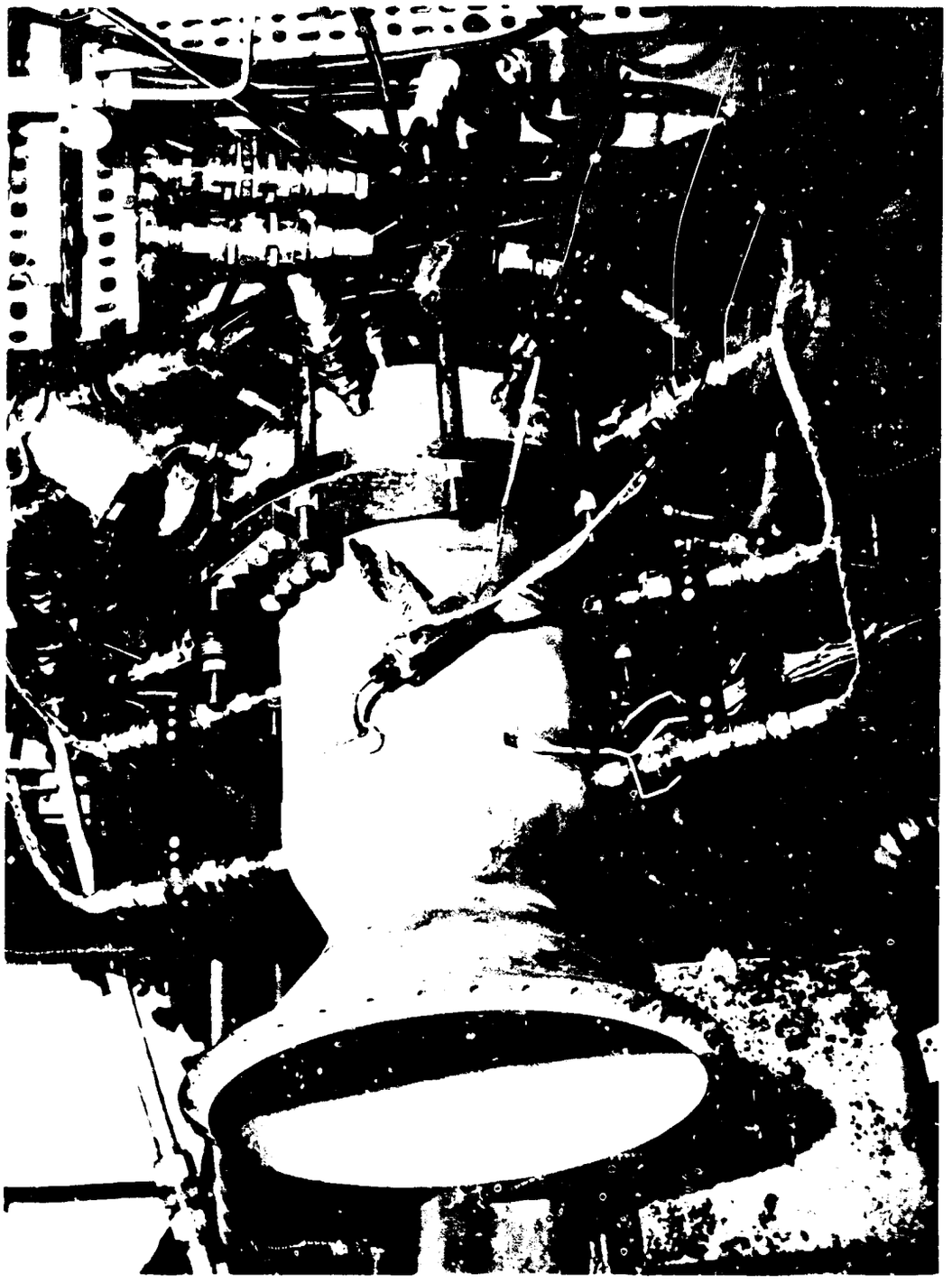

Figure 116. (U) Post-Run View of Thrust Chamber Assembly on Stand (1AW-663)

Figure 117. (U) Post-Run View of Thrust Chamber (1AW-664)

(C) Either of these items or a combination of both could have caused the localized excessive temperature. Test data indicated a combustion efficiency of 94% at an overall mixture ratio of 1.37 with a barrier/total flow ratio of 11%.

o. (C) The second columbium thrust chamber was utilized to demonstrate the durability of the adiabatic wall thrust chamber at the rated thrust chamber condition. New flow director standoffs and the repaired tungsten-coated tantalum alloy liner were used during the test. An intended 120 second test (1AW-665) was terminated after 115 seconds due to an indicated hot streak visually detected during the last few seconds of the test resulting in a burnthrough of the chamber. Post-test observation and analysis indicated the following:

(1) (C) The burnthrough of the columbium thrust chamber occurred at approximately 105 seconds (stabilized chamber pressure) of the test. The burnthrough of the thrust chamber was approximately three inches long and one inch wide as shown in Figure 118.

(2) (C) The liner had several burned through holes and a large section of the liner folded back into the hot core side as shown in Figure 119. A streak on the liner was noted in line with the chamber burnthrough.

(3) (C) The time-temperature history (Figure 120) of the hottest area indicated 3150° F prior to burnthrough and indicated that the temperature had stabilized prior to the hot streak.

(4) (C) Flow test of the injector after post-test flushing indicated no plugging; however, a review of the hardware and temperature history indicated the injector streaked (probably due to some contamination) causing the burnthrough.

(5) (C) Performance during the test indicated 95.6% combustion efficiency using a barrier/total flow ratio of 11.2% at a chamber pressure of 74.25 psia and a mixture ratio of 1.35. This performance was 93.9% when related to an overall mixture ratio of 1.8.

9 (C) Conclusions of the Adiabatic Wall Thrust Chamber Program

(C) The results of the adiabatic wall thrust chamber test program utilizing the columbium alloy thrust chamber are shown in Table XVI. Feasibility and durability were demonstrated using the propellant combination of $LF_2$-BA1014 between 35 and 75 psia chamber pressure on the basis of a 137-second duration test at a chamber pressure of 37 psia and a 115-second duration test at a chamber pressure of 74.3 psia. High performance (96% combustion efficiency) at an overall mixture ratio of 1.35 (11% coolant at high thrust and 9.9% at low thrust) was obtained over this 2:1 throttling range with no degradation in performance. The performance was still high (94% combustion efficiency) when related to an overall mixture ratio of 1.8.

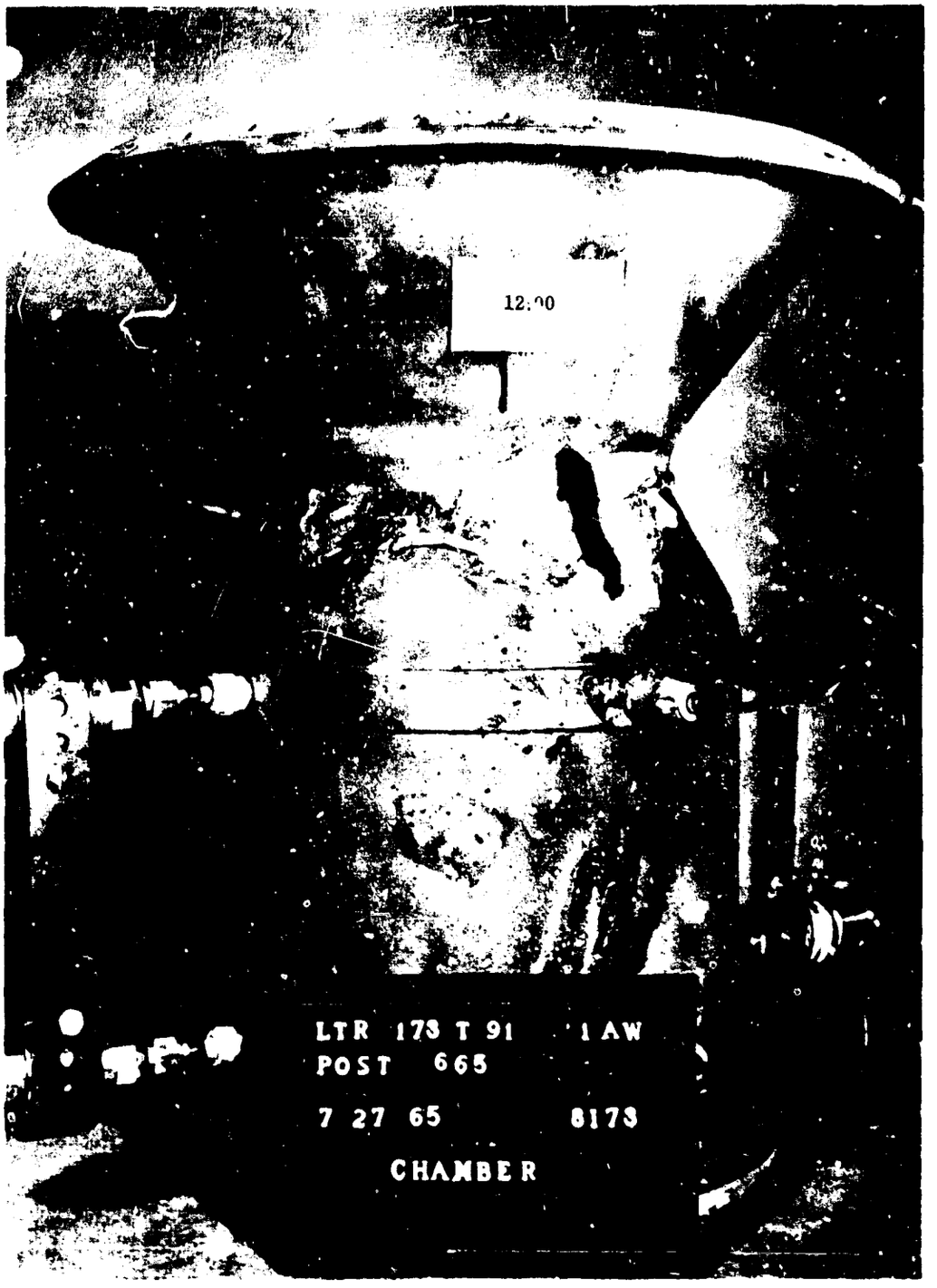


Figure 118. (C) Columbium Thrust Chamber After Test 1AW-665

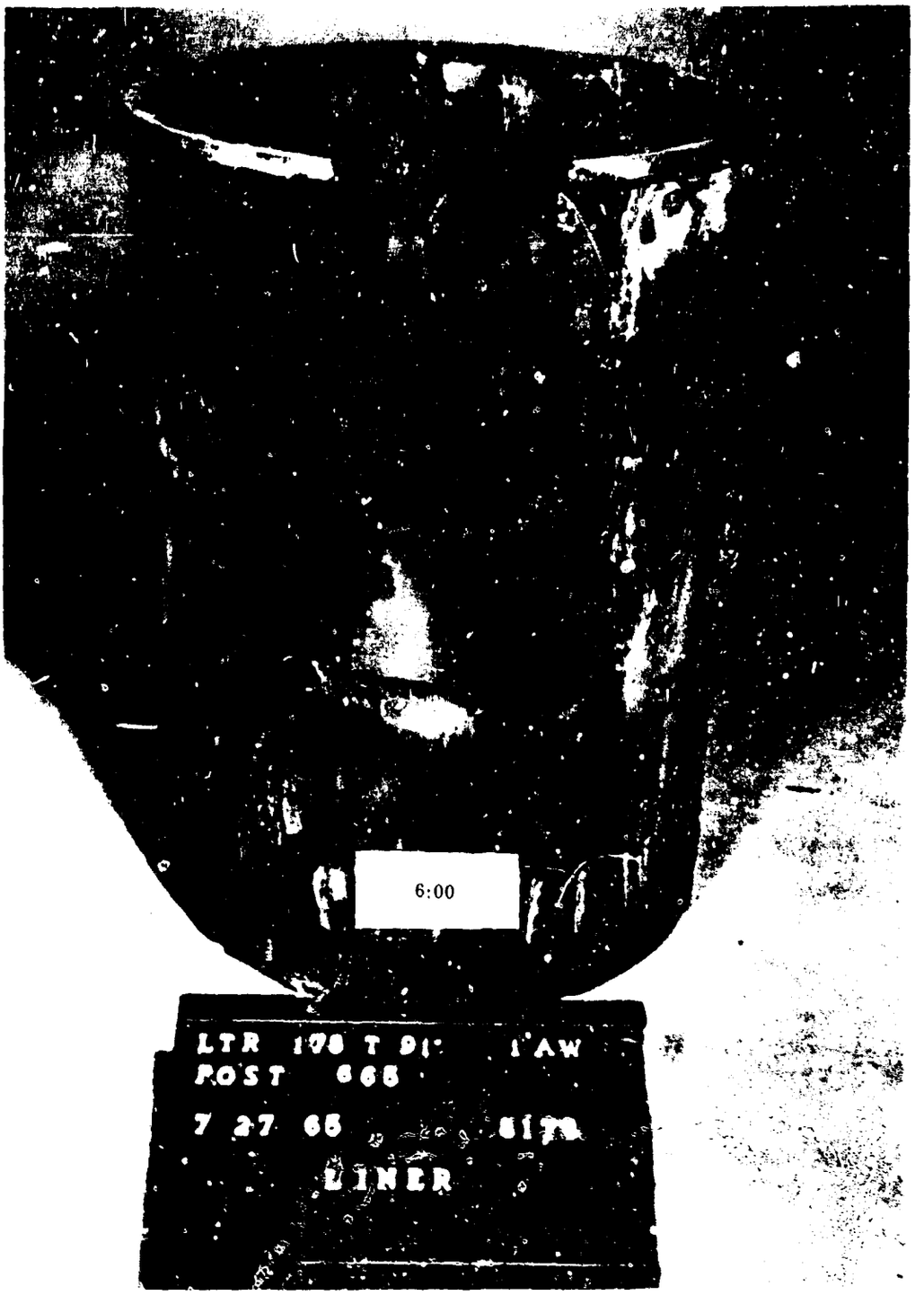


Figure 119. (C) Tantalum-Tungsten Liner After Test IA2-665

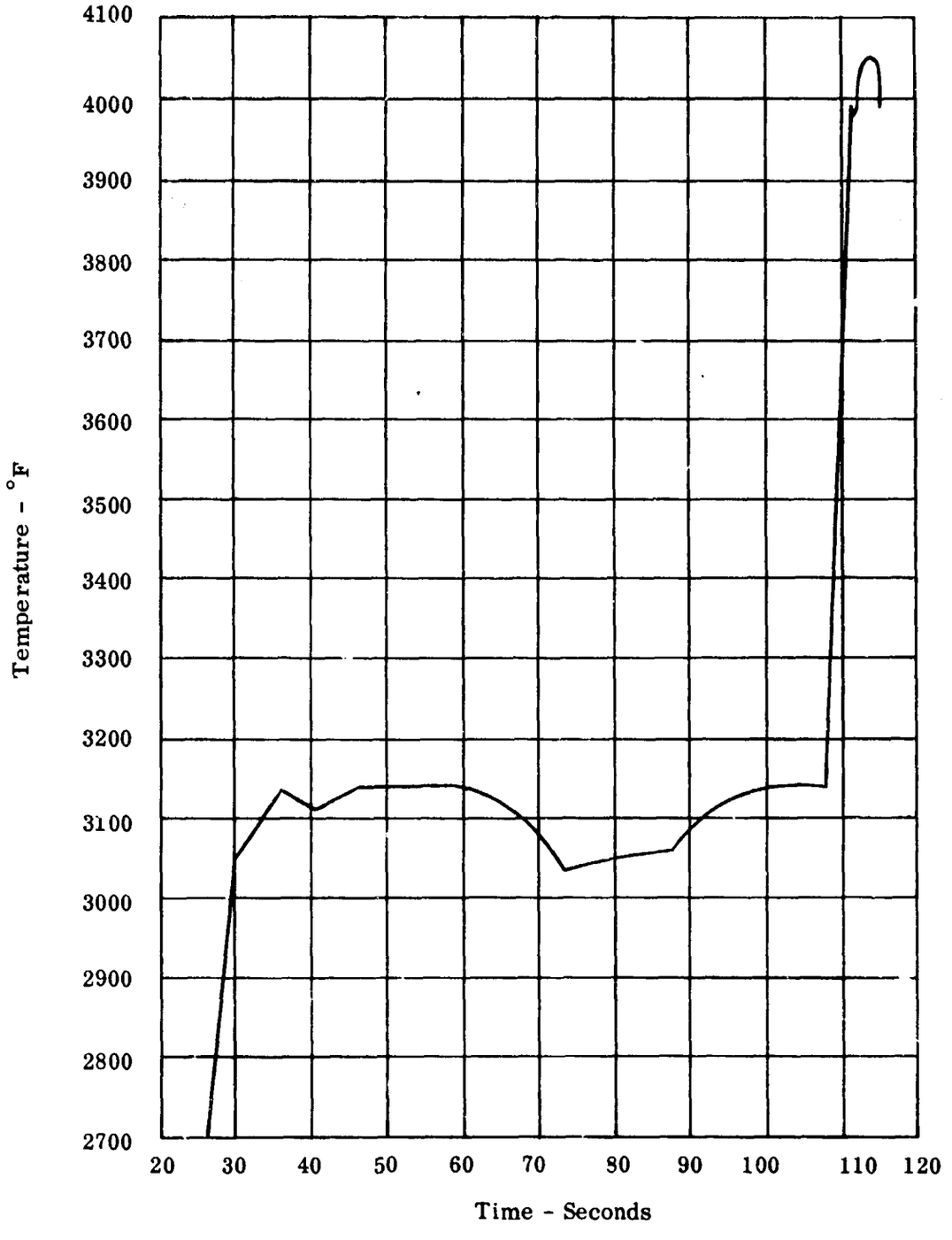


Figure 120. (C) Time History of Maximum Skin Temperatures 1AW-665

(C) The thrust chamber was in relatively good condition, as shown in Figure 121, with the exception of the area burned through. The main injector accumulated 884 seconds during the test program and the fuel rich gas generator accumulated 1189 seconds. The injector and generator are shown in Figure 122.

(C) The test program proved that columbium was an acceptable material for use with high energy propellants ($LF_2$-BA1014) as the adiabatic wall thrust chamber. Uncoated graphite and tungsten were demonstrated as acceptable for use as liners, but both have problems due to their poor thermal shock resistance. Tantalum (10% tungsten) coated with a pure tungsten coating was demonstrated as acceptable for use as a liner, but had a problem with adherence of the tungsten coating. The particular coating method (electron beam melting of tungsten on the part) was not the Bell accepted coating (vapor deposition), but was utilized as an alternate due to scheduling problems and a possible state-of-the-art advancement. In addition, the effect of predicted wall temperatures as compared to actual wall temperatures is shown in Figure 123 as a function of chamber pressure.

(C) The performance goals and the actual achievements on the adiabatic thrust chamber are as follows:

(a) A durability goal of 120 seconds was met at the low thrust range (37 psia chamber pressure) by demonstration of 137 seconds (127 seconds of main core chamber pressure) duration. At the high thrust range (74 psia chamber pressure tested compared to 65 psia specified) a test of 115 seconds (105 seconds of main core chamber pressure) duration was demonstrated.

(b) A goal of 95% combustion efficiency was met by demonstration of 96% combustion efficiency over the 2:1 throttling range at an overall engine mixture ratio of 1.35. When relating this performance to a mixture ratio of 1.8, high performance (94% combustion efficiency) was still achieved although slightly less than the goal. This would result in a vacuum specific impulse of 366 seconds based on a 45:1 area ratio nozzle (nozzle efficiency of 97% of shifting equilibrium).

(c) Throttling over a 2:1 range (sea level limitations) was demonstrated.

(U) As a result of the above achievements, the adiabatic wall thrust chamber cooling concept with the high energy propellant combination of $LF_2$-BA1014 (hydrazine blend) has demonstrated feasibility and is ready for final development into a usable engine for a particular mission.


Figure 121. (C) Columbium Thrust Chamber After Test 1AW-665

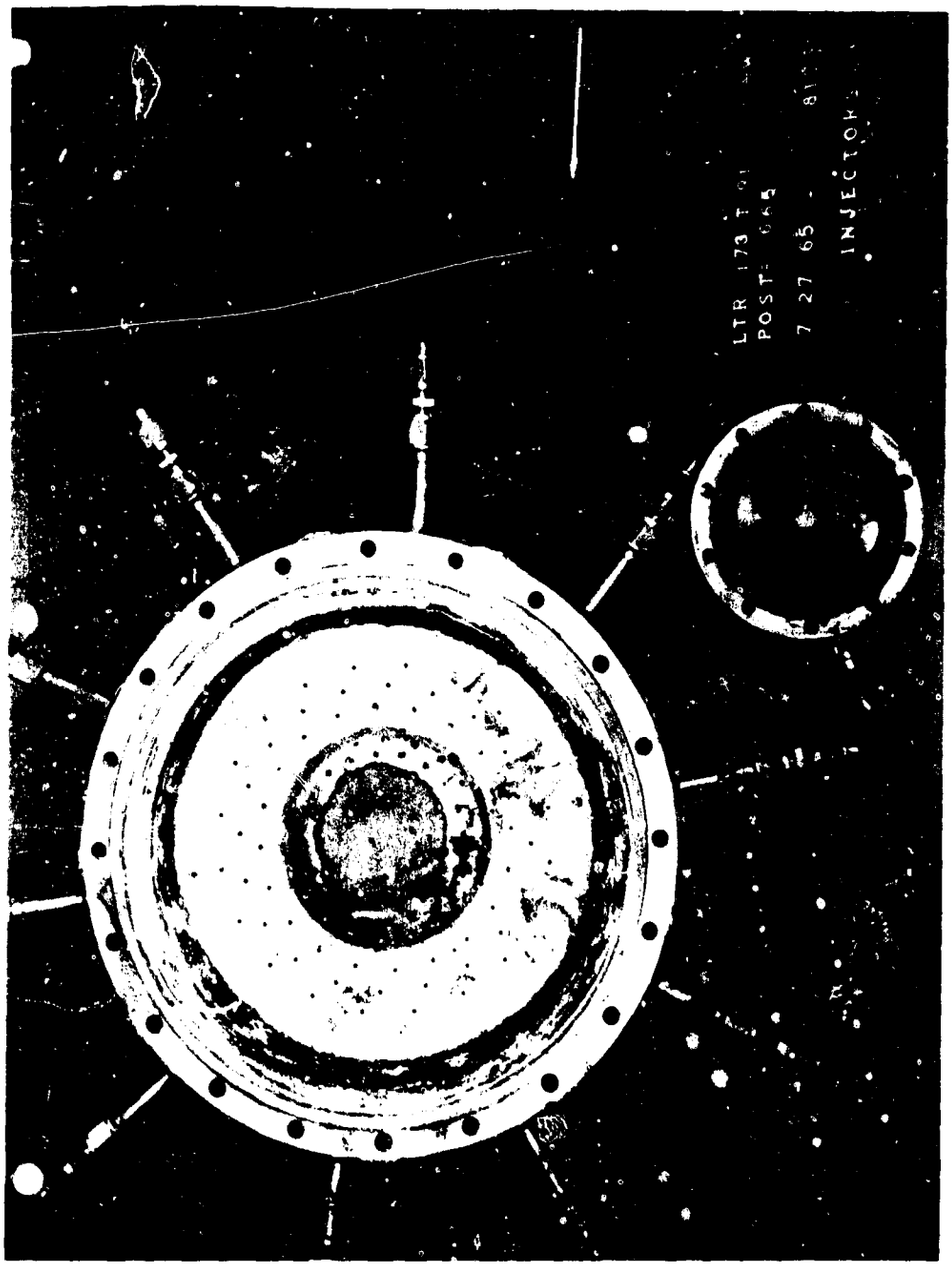


Figure 122. (C) Main Injector & Fuel Rich Gas Generator Inspection After Test 1AW-665

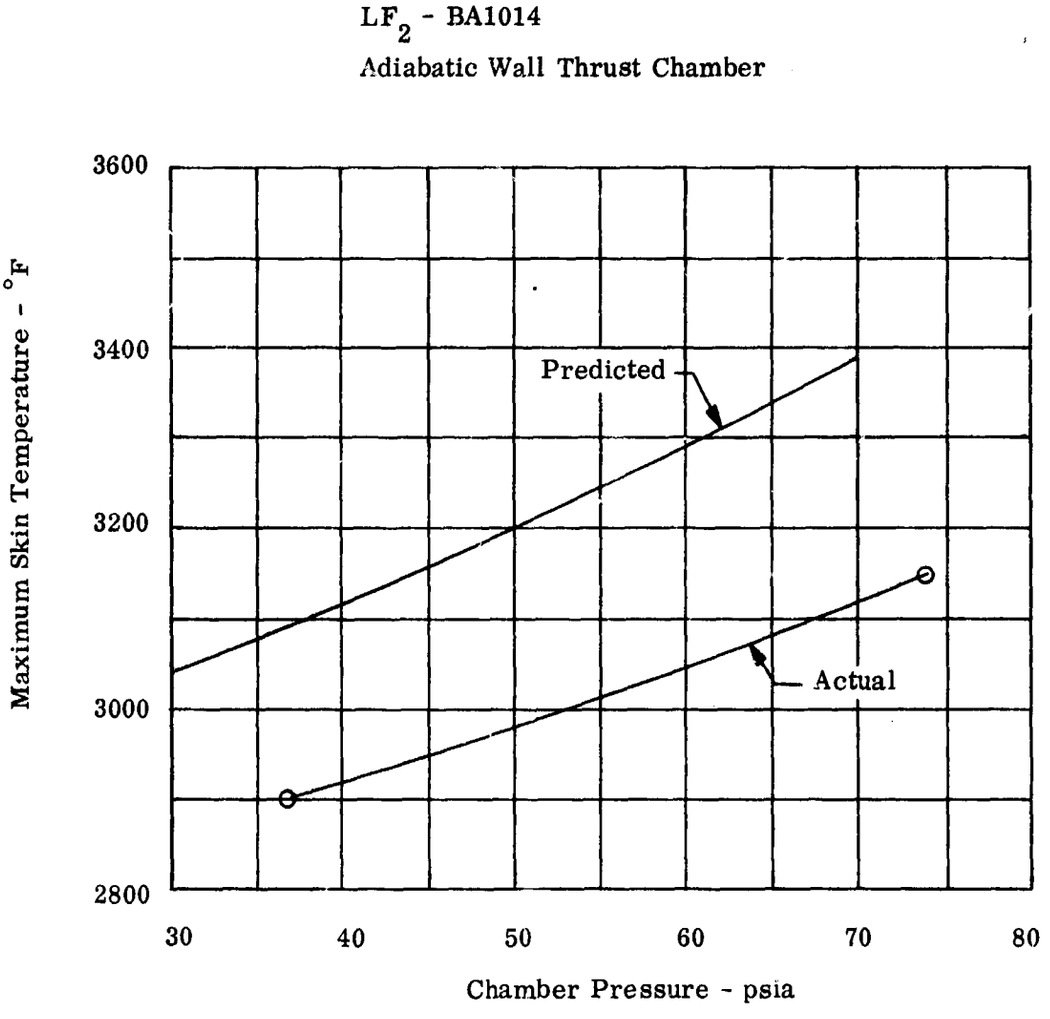


Figure 123. (C) Effect of Chamber Pressure on Skin Temperature

# SECTION 7

# (U) MIXED PHASE INJECTION

## A. (U) GENERAL

(U) Previous experiments using impinging injectors have indicated that to attain high combustion performance over a deep throttling range, it is desired that the velocity relation between the reacting streams be relatively constant over the throttling range. Furthermore, feed system stability warrants that injector pressure drop at low thrust levels be sufficient to preclude hydraulic instability. The affinity of cryogenic propellants to attain thermal equilibrium after heat addition and expansion in a relatively short time, suggested that the decreasing density and high velocity of the mixture could be effectively applied to provide a simple, nonmechanical, stable, high performance injection system which would require no higher then normal injector feed pressures at rated thrust.

(U) A program of fabrication, test and analysis was performed to demonstrate the feasibility of this concept in liquid fluorine propulsion systems. Included in the test program was a series of cold flow tests whereby fluorine alone was heated and expanded to sea level pressure. During these tests, a fluorine flow rate range of 8:1 was investigated while varying the propellant enthalpy at the inlet to the injector. In addition, six fire tests were performed with fluorine and BA-1014 fuel while operating over a chamber pressure range of 35 to 105 psia and a mixture ratio range of 0.91 to 1.55. During these cold flow and fire tests, injector feed system stability was demonstrated. However, combustion instability was experienced at low chamber operation. A review of instrumented data indicated that instability was combustion induced.

(U) Correlation of measured injector feed pressures taken during the test program with theoretical injector expansion models was made for extremes of possible injection inlet statepoint conditions. These statepoint extremes were calculated because the exact definition of quality and propellant temperature at the inlet to the injector was not possible. The two methods consisted of a thermal equilibrium condition at the heat exchanger outlet, and a stratified model whereby the liquid bulk temperature was below saturated vapor temperature. The latter represents a probable upper limit of quality, while the thermal equilibrium prediction of quality is a lower limit, at the heat exchanger outlet. The choked expansion models investigated while using these two initial statepoint predictions were: homogeneous metastable flow; homogeneous thermal equilibrium flow, homogeneous nonequilibrium flow; and separated phase flow with no change in quality (metastable). In general, all of these expansion models underpredicted the flow rate as compared to measured fluorine flow rate. However, good comparison was obtained from the separated phase, metastable flow expansion.

## B. (U) TECHNICAL DISCUSSION

### 1. (U) Design and Fabrication

#### a. (U) System Description

(U) In the throttling thrust chamber configuration, the mixed phase fluorine injection system consists of a thrust chamber injector with fixed orifice area and a heat exchanger. Thrust control is obtained by flow rate modulation at a throttling valve located upstream of the heat exchanger. As thrust is reduced, the ratio of heat transfer rate to propellant flow rate is increased. Over the upper part of the throttling range ($F/F_{max} > 0.33$) the fluorine is injected into the combustion chamber as a subcooled liquid. During the deep throttling portion of the thrust range ($F/F_{max} < 0.33$), the propellant is injected as a two-phase fluid. As thrust is further reduced, the quality of the liquid-vapor fluorine mixture is increased and the overall density of the fluid is reduced. A possible application of two-phase injection is the fluorine/BA-1014 pressure-fed, throttling thrust chamber studied in Reference 5. In this configuration, the oxidizer is heated from an initally subcooled liquid to a two-phase mixture in a nozzle extension heat exchanger. The fluorine mixture is then injected into the combustion chamber. The fuel velocity is maintained by use of a fuel rich gas generator. These combustion products are reacted in the chamber with the injected two-phase mixture. Injection with a relatively uniform velocity relation between reacting streams provides high combustion efficiency over the throttling range. Furthermore, for this configuration, part of the fuel rich reactants could be bled off to the periphery of the thrust chamber and used as the barrier for the adiabatic wall thrust chamber design.

#### b. (U) Test Hardware

(U) Throttling thrust chamber operation (fluorine side only) was simulated by a test setup shown in Figure 124. The fluorine feed system consisted of a venturi flow control, heat exchanger, and a one-inch Annin start valve. Flow rate was varied in steps during a run by sequencing of 0.5 inch Annin valves located in series with the venturis. For a set tank pressure, four discrete oxidizer flow rates were obtained during each cold flow test. The fluorine heat exchanger consisted of a stainless steel concentric tube design with 1.5 and 1.0 inch tubes. Liquid fluorine passing through the inner tube was heated and vaporized by gaseous nitrogen introduced into the annulus. Gaseous nitrogen control was obtained by pressure regulation upstream of a calibrated orifice. Oxidizer flow rate was determined from pressure and temperature measurements upstream of the venturi flow control loop. Pressure and temperature measurements were made across the heat exchanger on both the fluorine and gaseous nitrogen. The fuel feed system used during fire testing included two flowmeters, a cavitating venturi, and a 0.5 inch Turansky valve. Fuel flow rate was not varied during the fire tests; however, the fuel flow was adjusted to the desired value by presetting fuel tank pressure. The cavitating venturi served as both a flow control and as a flow rate measurement check against the flowmeters. During fire test, existing 200-lb water cooled hardware was fired at sea level. The

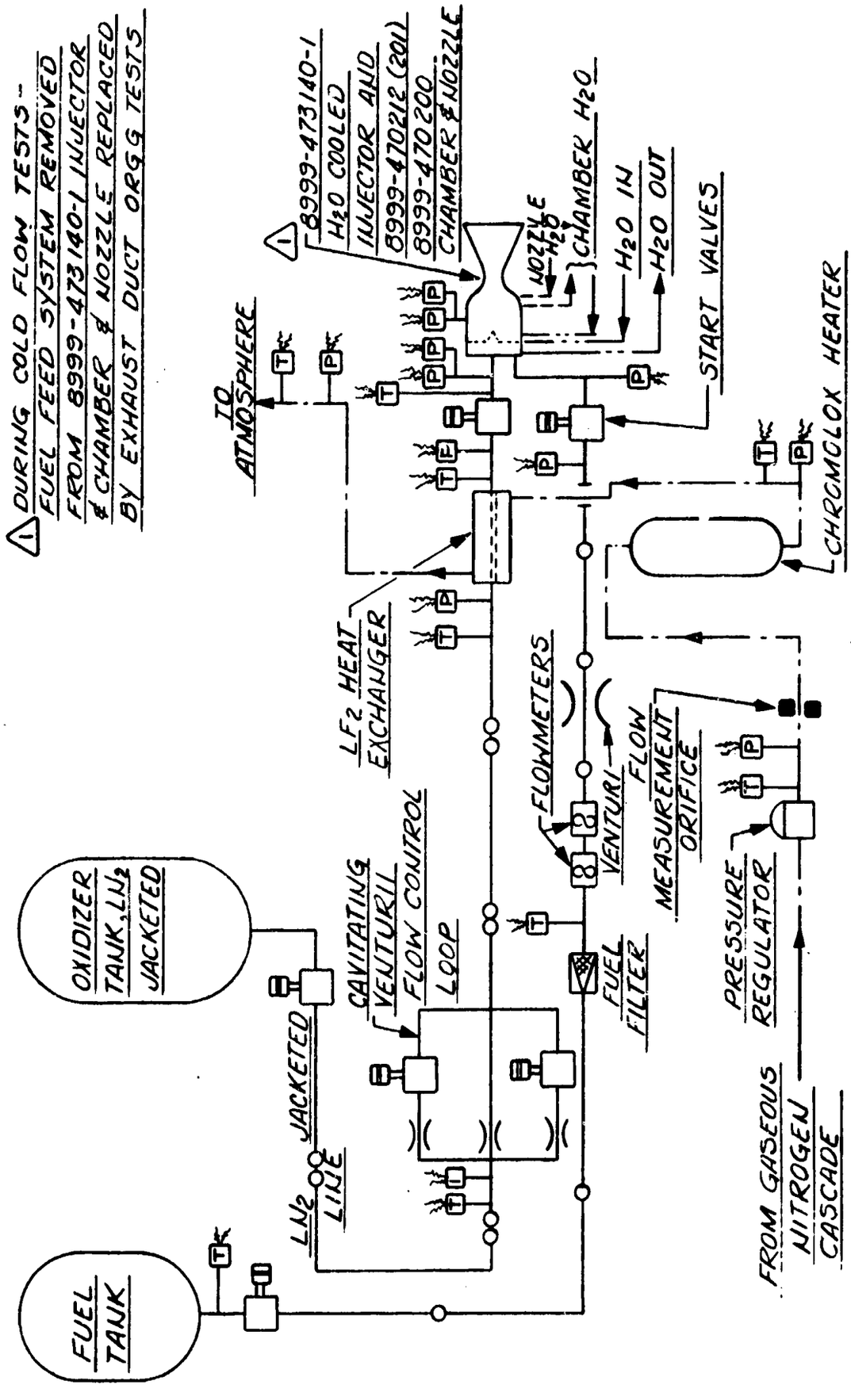


Figure 124. (U) Test Cell Schematic, Mixed Flow Injector Tests

(U) thrust chamber installed in the test cell is shown in Figure 125. The injector alone was used during the cold flow tests. During these runs, the fuel system was inactive and heated fluorine was expanded through the injector to the atmosphere.

2. (U) Test Results

a. (U) Cold Flow Test Series

(U) Six tests were performed while expanding fluorine through the injector, while the fuel system was inactive. The purpose of this test series was to demonstrate stable, two-phase flow at various flow rates and to obtain instrumented data for analysis of the two-phase flow regime. A plot of fluorine feed pressure versus gaseous nitrogen heating rate and fluorine flow rate are presented in Figures 126 and 127, respectively. A summary of this test series follows.

(U) During test 1AW-610, the fluorine flow rate was varied over a range of 0.12 to 0.44 lb/sec while the gaseous nitrogen heating rate was varied over a range of 5.7 to 7.4 BTU/sec. Total test duration was 167 seconds. After a 60-second cooldown period, stable two-phase flow resulted.

(U) Two liquid fluorine tests were made to check temperature and pressure instrumentation. Run 1AW-611 was a 122-second run at 0.19 lb/sec; fluorine flow run 1AW-612 was performed for 124 seconds at a maximum flow rate of 0.45 lb/sec.

(U) Run 1AW-163 consisted of a 347-second run at a fluorine flow rate of 0.12 to 0.43 lb/sec with the gaseous nitrogen heating rate varied over a range of 3 to 6 BTU/sec with each fluorine flow rate. Again, the pressure drop during two-phase operation remained high and was stable. No indication of unstable flow due to bubble agglomeration or a slug type flow was evident from the oxidizer pressure oscillograph traces.

(U) Run 1AW-614 was conducted for 354 seconds over a fluorine flow rate range of 0.055 to 0.2 lb/sec while the gaseous nitrogen heating rate was varied from 1.9 to 3.9 BTU/sec during the test. Stable flow with high injector pressure drops was experienced during the run.

(U) Run 1AW-615 was a 349-second run covering an oxidizer flow rate range of 0.12 to 0.44 lb/sec. Gaseous nitrogen heating rate was varied from 2.7 to 5.9 BTU/sec as the fluorine flow was controlled. During the low fluorine flow rates and high gaseous nitrogen heating rates, the heat exchanger nitrogen temperatures were questionable because of a recording sensitivity change. However, fluorine flow rate was steady during the run and injector pressure drop remained high.

Figure 125. (U) Test Setup

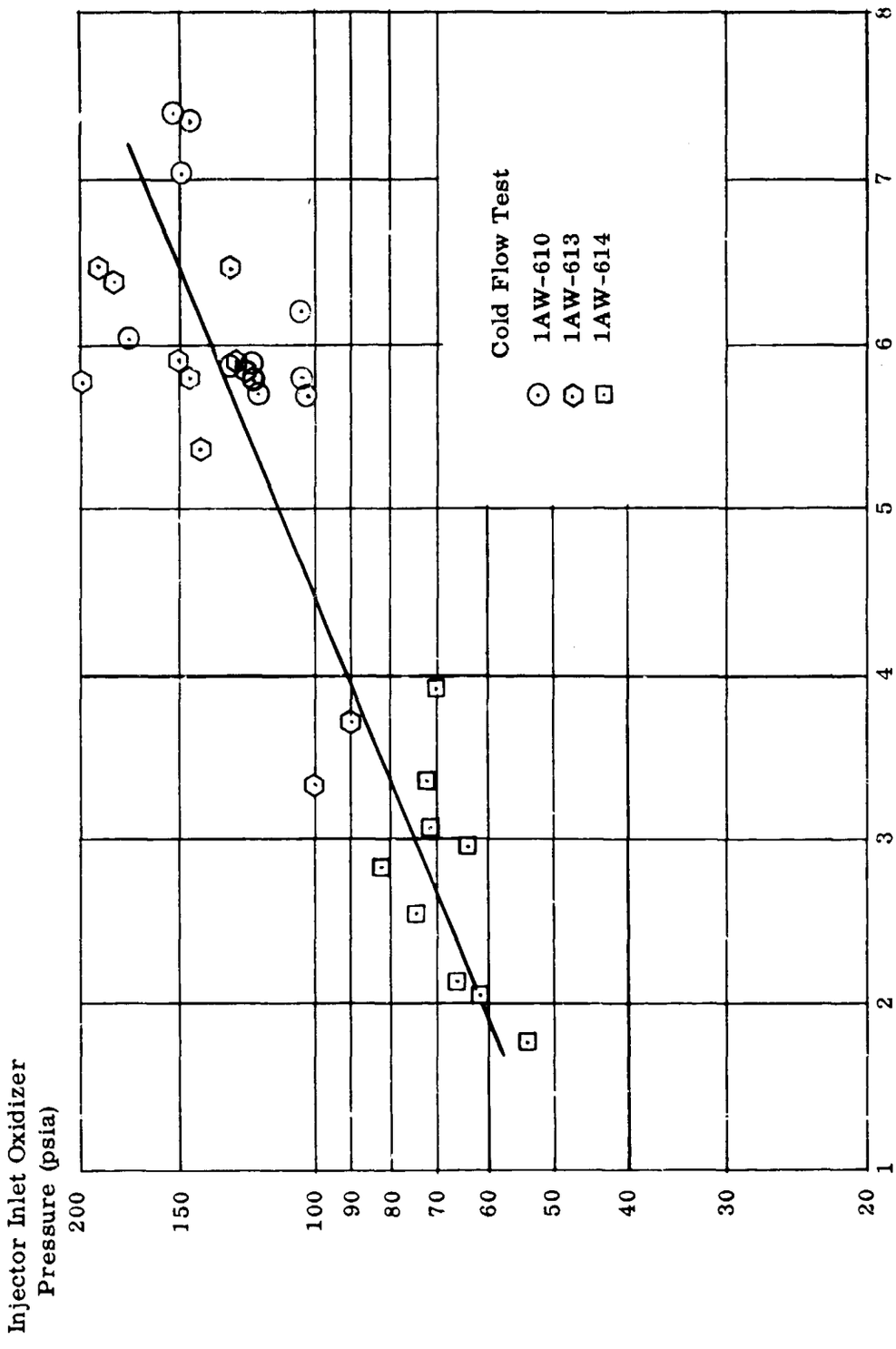


Figure 126. (U) Injector Feed Pressure versus Heat Input

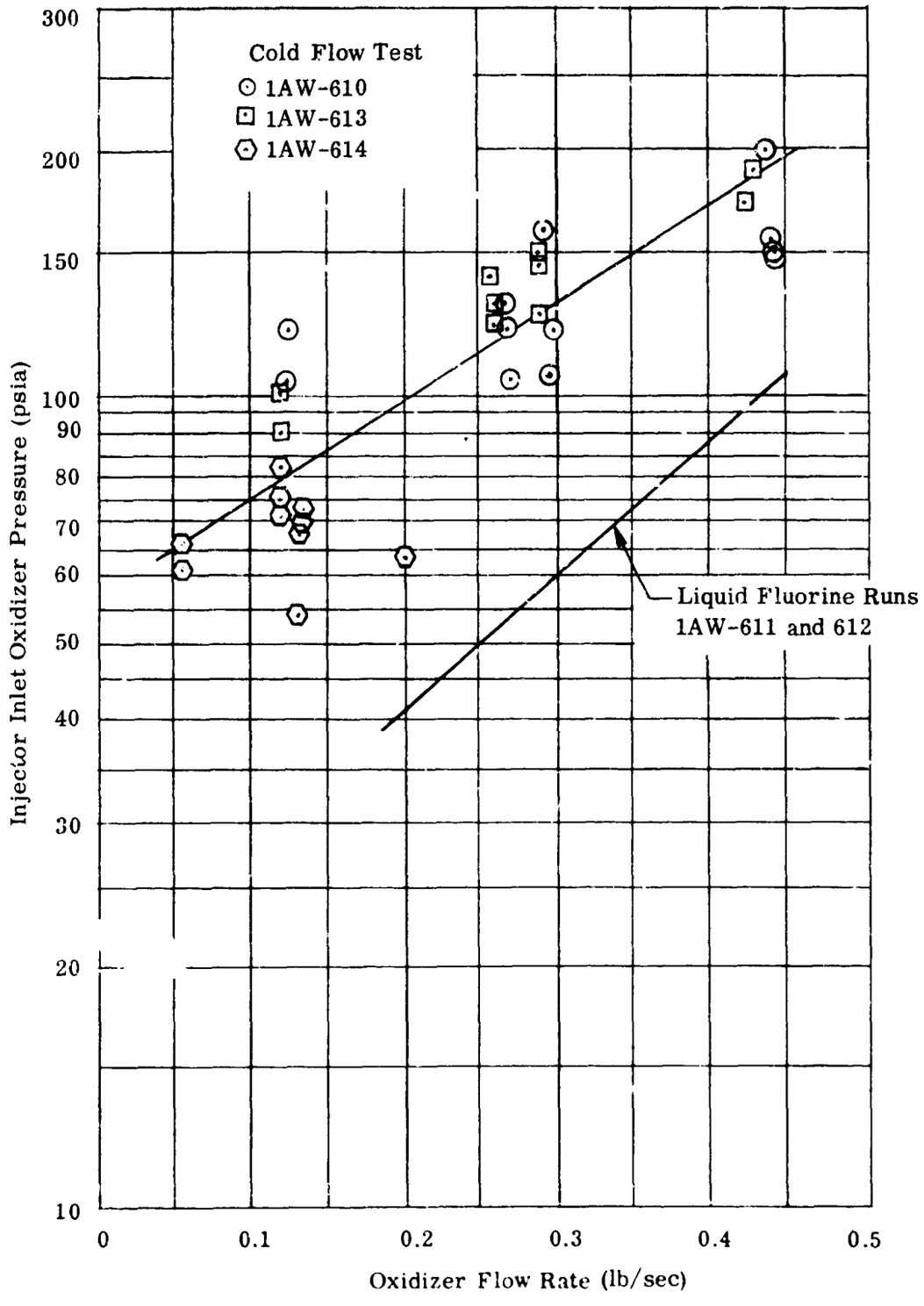


Figure 127. (U) Injector Feed Pressure versus Fluorine Flow Rate

b. (U) Fire Test Series

(U) Run 1AW-616 was a 10.4-second test at 105.5 psia chamber pressure to obtain baseline performance and stability data on the injector. As indicated in Table XVII, the combustion efficiency was 93.7% at a 1.50 oxidizer to fuel mixture ratio.

(U) Therefore, the first two-phase fluorine fire test was conducted but was terminated after 3.8 seconds due to the chamber pressure switch (ground safety). Analysis of the test data indicated possible plugging of the oxidizer flow venturi.

(U) A repeat of the test was set up; however, during the fluorine bleed-in procedure, a pressure surge was experienced resulting in damage to the feed system between the flow control loop and the main stand valve. Investigations conducted showed no evidence of contamination in the fluorine feed system. Inspection of feed system components revealed that the tip of the heat exchanger inlet temperature probe burned off indicating that the pressure surge was initiated at this point.

(U) After resumption of the fire test program, a 37.6-second test was performed with two-phase fluorine at the injector. Stable operation was experienced while operating at 97.3 psia chamber pressure.

(U) Test 1AW-630 consisted of 30 seconds of operation with liquid fluorine and 55 seconds of two-phase fluorine operation. Stable operation at a nominal 65 psia chamber pressure was experienced during both parts of the run.

(U) Test 1AW-631 was performed in the same manner as the previous run. However, chamber pressure was approximately 35 psia. During liquid fluorine injection, the chamber pressure oscillograph trace indicated a three cps oscillation with approximately 11% double amplitude superimposed on a 220 cps oscillation. During two-phase fluorine operation, the low frequency oscillation was 0.6 cps superimposed on a 220 cps oscillation with a double amplitude in excess of 60% of nominal chamber pressure. Unstable operation with subsonic flow at the thrust chamber throat was induced by the oscillation.

(U) Fluorine flow rate was stepped by sequencing of the venturi flow control Annin valve during run 1AW-632. Mixture ratio during this two-phase fire test was 1.45 at 93.7 psia chamber pressure and reduced to 1.0 at the lower 80.3 psia chamber pressure step. Stable operation was experienced during this test.

(U) The final fire test (1AW-633) was a 49-second two-phase run with oxidizer flow rate stepped at constant fuel flow rate. Chamber pressure was 53.2 psia at a mixture ratio of 2.15 and 38.3 psia at 0.907 mixture ratio. During the low chamber pressure step, stabilization of chamber pressure did not occur.

TABLE XVII

(U) SUMMARY OF MIXED PHASE INJECTION FIRE TESTS

| Test No. | Length of Test (sec) | $P_c$ psia | r | $N_c$ % | Remarks |
|---|---|---|---|---|---|
| 1AW-616 | 10.4 | 105.5 | 1.50 | 93.7 | Baseline test with liquid fluorine |
| 1AW-629 | 37.6 | 97.3 | 1.486 | 88.0 | Mixed Phase Test |
| 1AW-630 | 84.5 | | | | |
| | $\theta$ = 28 | 65.1 | 1.532 | 92.9 | Liquid fluorine part of test |
| | $\theta$ = 83.5 | 62.5 | 1.554 | 88.8 | Mixed phase part of test |
| 1AW-631 | 77.5 | | | | |
| | $\theta$ = 28 | 35.2 | 1.446 | 90.5 | Liquid fluorine part of test |
| | $\theta$ = 75.9 | 32.9 | 1.435 | 85.1 | Mixed phase part of test |
| 1AW-632 | 81 | | | | |
| | $\theta$ = 27.5 | 93.7 | 1.448 | 87.4 | Mixed phase test - Oxidizer flow stepped only |
| | $\theta$ = 80.0 | 80.3 | 1.004 | 93.1 | |
| 1AW-633 | 49 | | | | |
| | $\theta$ = 29.5 | 53.2 | 2.152 | 80.8 | Mixed phase test - Oxidizer flow stepped only |
| | $\theta$ = 47.9 | 38.3 | 0.907 | * | |

* ($P_c$ not stabilized at $\theta$ = 47.9 sec)

(U) Combustion efficiency versus chamber pressure for liquid and two-phase operation at a propellant weight mixture ratio of approximately 1.5 are compared in Figure 128. At 35 and 100 psia chamber pressures, a reduction of approximately 6% was experienced during two-phase operation as compared to corresponding data points with subcooled liquid fluorine injection. As chamber pressure was reduced, the combustion efficiency decreased approximately 3.5% for both two-phase and subcooled liquid runs. During these runs, the BA-1014 fuel velocity was not maintained and decreased with the square root of the fuel side injector pressure loss. The corresponding increase in oxidizer to fuel momentum ratio (as explained later in Section 7, B, 3, c) is the major contributing factor to the decrease in combustion efficiency.

(U) A stability study was conducted and the results indicate that the liquid fluorine tests were generally stable. One expection to this is the 35 psia chamber pressure level which had a 33% double amplitude in chamber pressure at 8 to 10 cps. The mixed phase data shows an increase in the degree of instability as chamber pressure is reduced. This can be seen in Figure 129. At 35 psia chamber pressure, the mixed phase injection was quite unstable, reaching approximately 95% double amplitude at one cps. This resulted in subsonic nozzle flow at the minimum chamber pressures. A detailed investigation of the oscillograph records indicated that the chamber pressure decreased and was then closely followed by the oxidizer injection inlet pressure and fuel injection inlet pressure. The reduced oscillograph data shown in Figure 130 indicates that the cause of the instability was due to the combustion process. On run 1AW-614 during the cold flow series, two-phase conditions at the same oxidizer flow rate and heat exchanger heating rates as on the 35 psia fire tests were experienced. Oscillograph recordings at this two-phase data point showed stable oxidizer injector inlet pressure traces. This can be seen from a portion of the oscillograph record shown in Figure 131. For the fire test, had the two-phase injection feed process been disrupted by the heat rejection into the injector by the combustion zone, there would have been a possibility of agglomeration of the vapor within the injector. With uniform flow distribution to each triplet, this would tend to result in periodic reduction in oxidizer flow (and chamber pressure) while increasing injector pressure drop. However, the oscillograph traces of the fire test indicated that injector pressure did follow the chamber pressure. Therefore, it is concluded that the instability was induced within the combustion zone.

3. (U) Analysis of the Test Data

a. (U) Summary

(U) An analysis was made to correlate the cold flow and fire test two-phase test data with theory. Several expansion models were applied to the calculated propellant conditions at the inlet to the injector. Each injector expansion model was based on choking of the mixture (homogeneous flow) or of the vapor (separated flow), and on the premise that injection could be described as one-dimensional inviscid flow as in an ideal nozzle. The cold flow test setup did not allow experimental verification of choked flow; i.e., by reduction in back pressure with no increase in

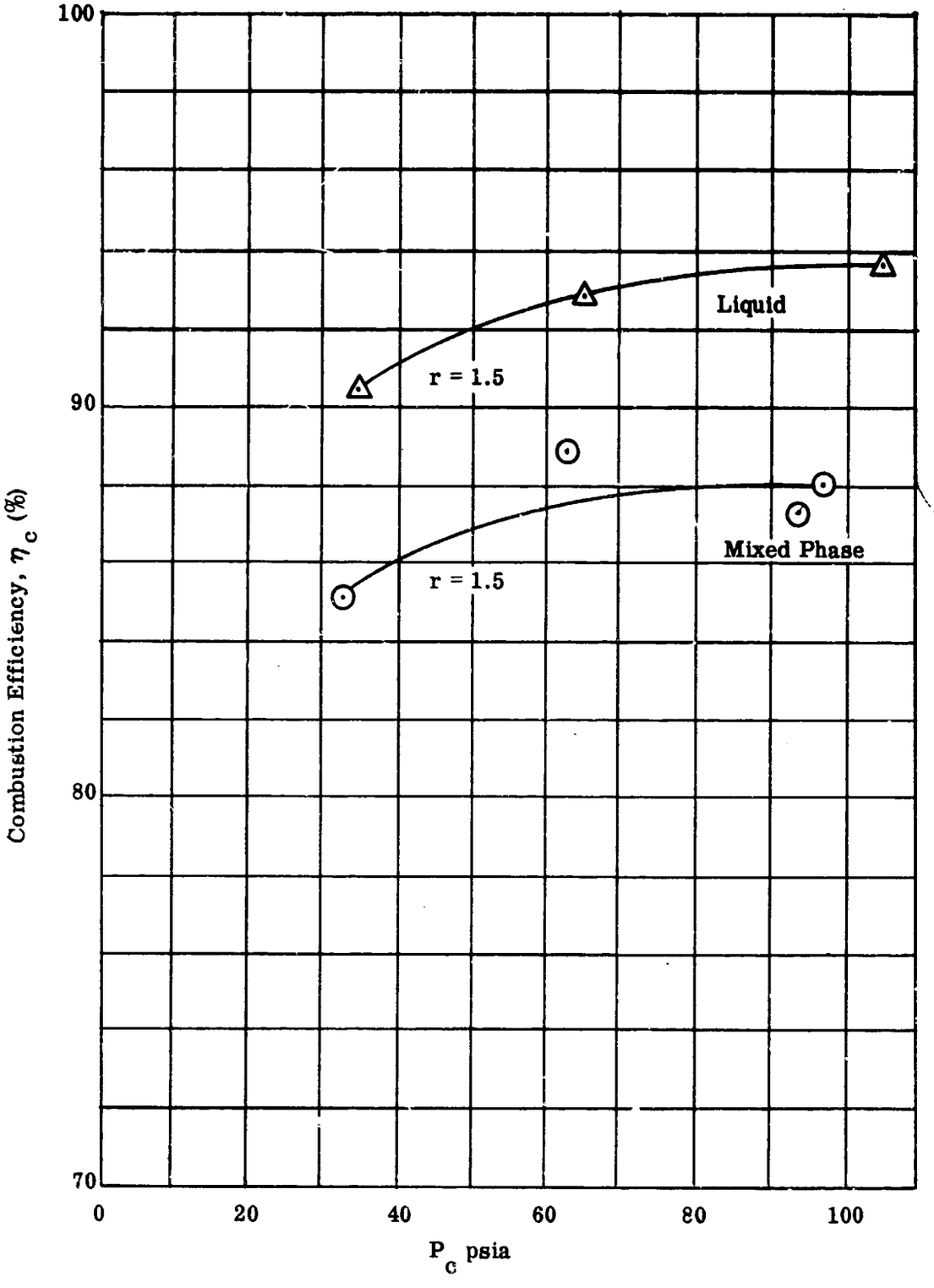


Figure 128. (U) Combustion Efficiency versus Chamber Pressure

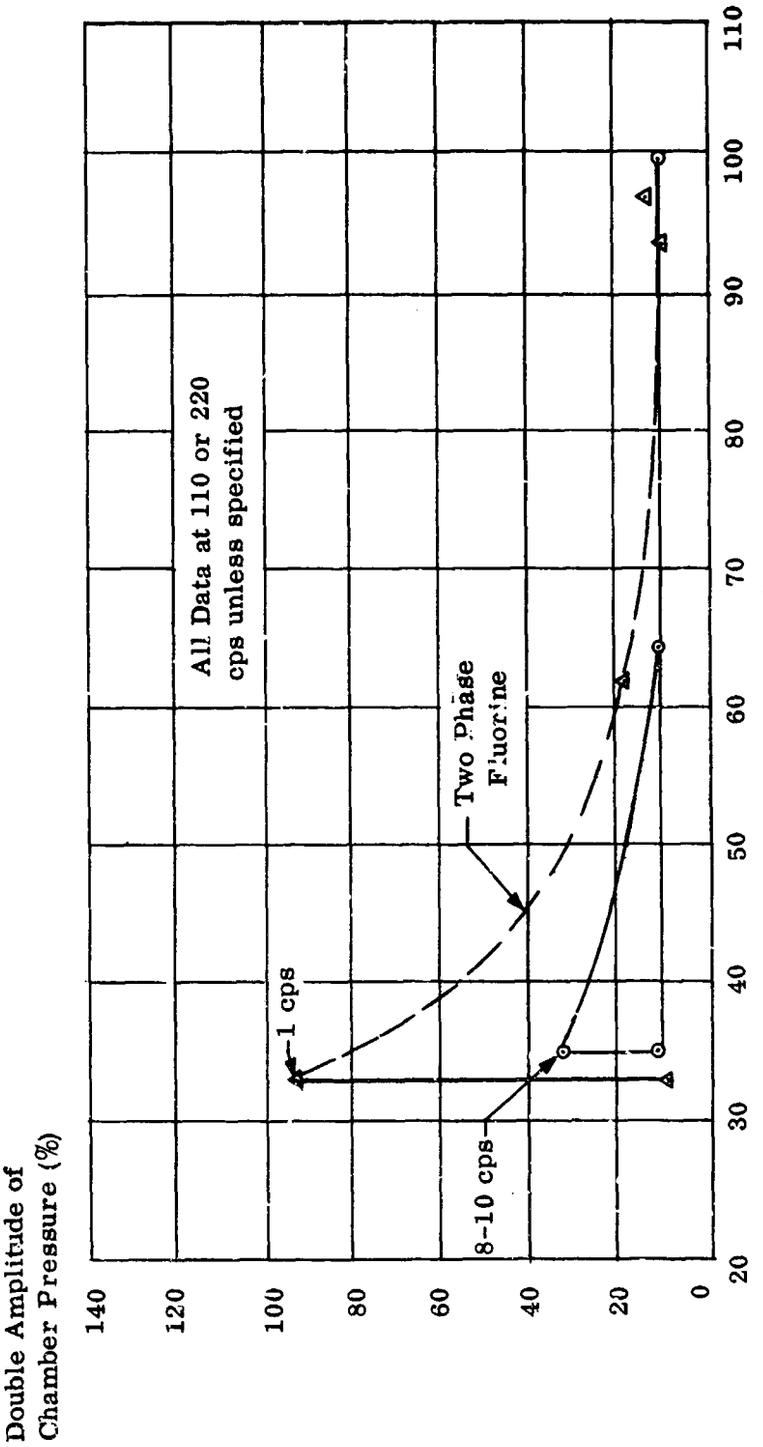


Figure 129. (U) Stability Representation of the Triplet Injector

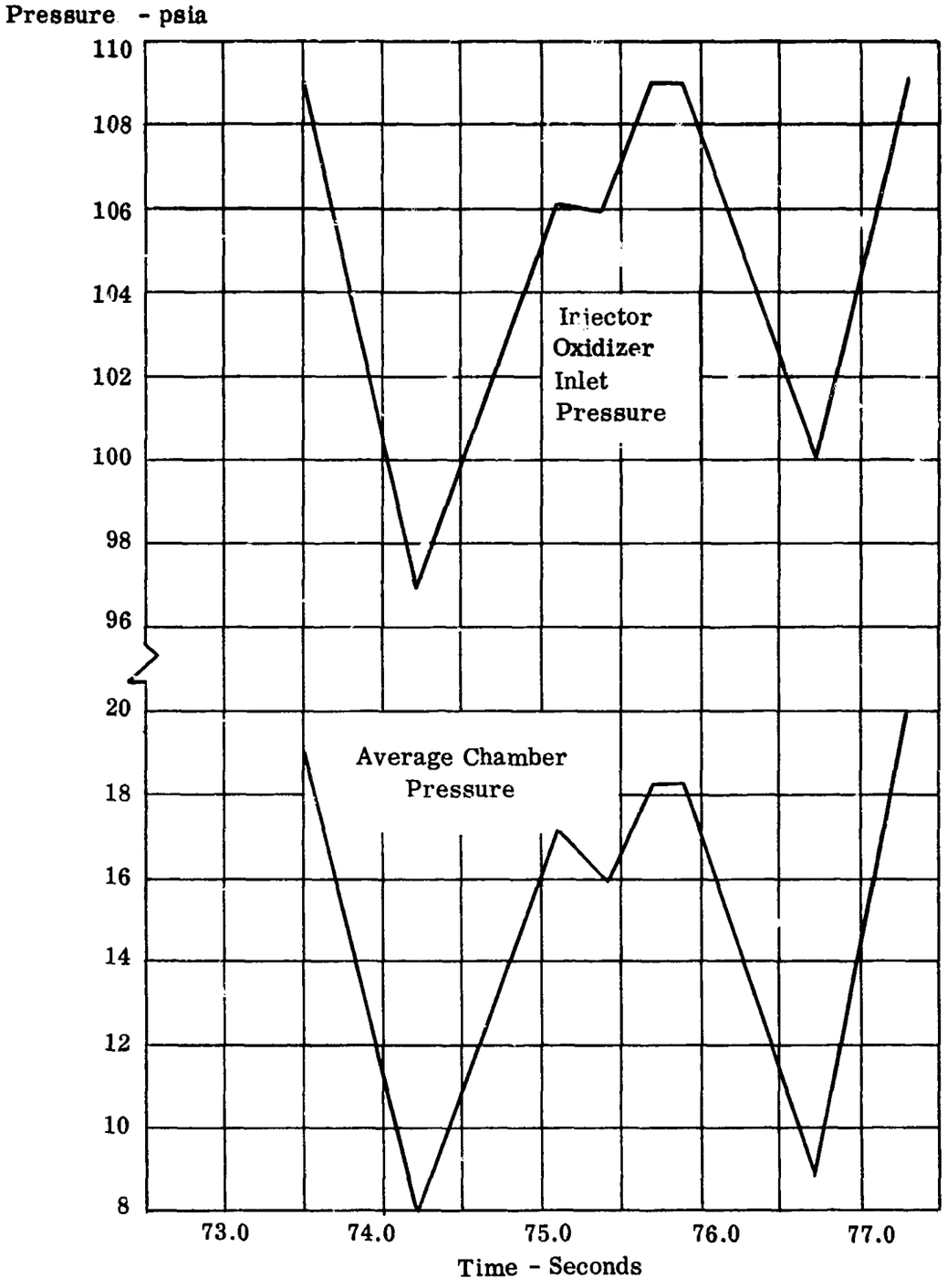


Figure 130. (U) Run 1AW-631, Oxidizer Injector Inlet Pressure and Chamber Pressure Oscillations

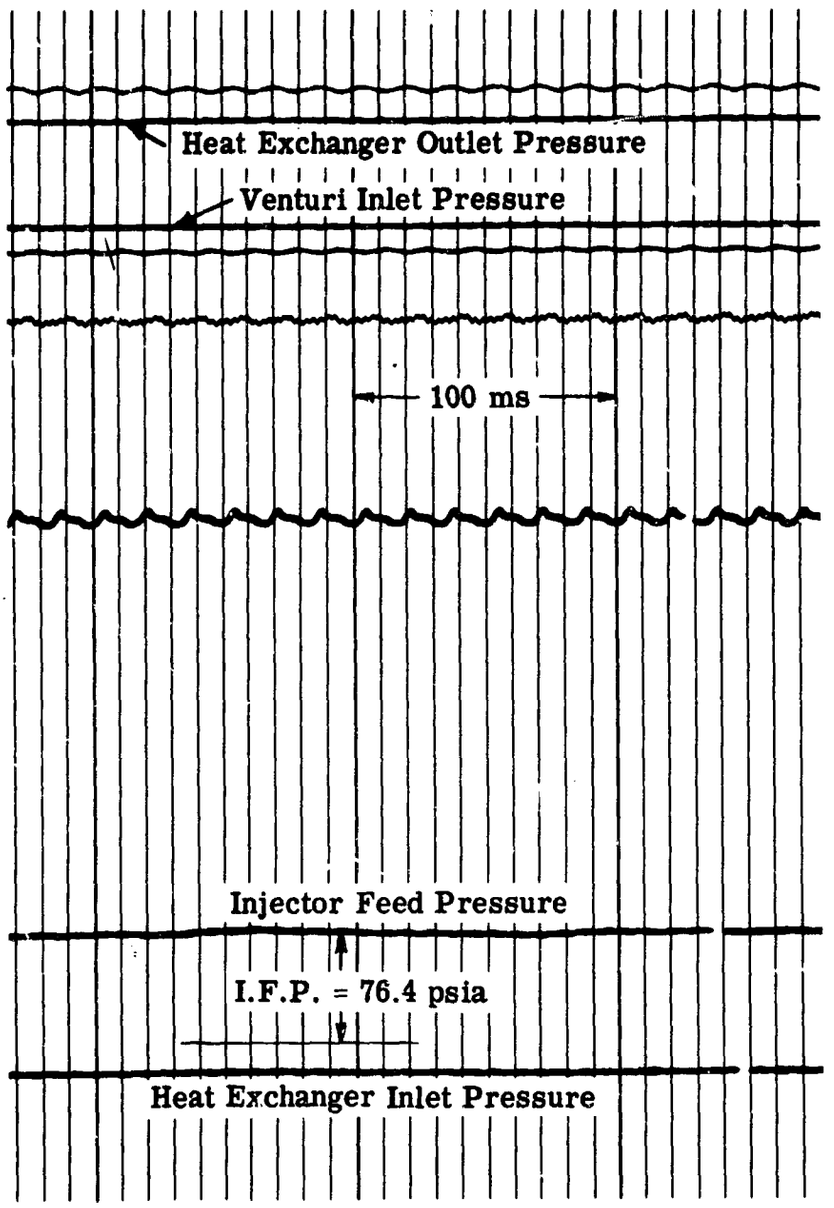


Figure 131. (U) Oscillograph Data; Run 1AW-614 at Time 210 Seconds

(U) fluorine flow rate. However, upstream conditions and back pressure or chamber pressure during cold flow and fire test did satisfy the conditions for predicted choked flow during the expansion. This condition is consistent with a homogeneous mixture; or vapor (separated flow) acoutic velocity at the point of choking. Aside from the practical consideration of two-dimensional effects in the actual flow, the premise of choked flow within the expansion during the injection is warranted. Description of each expansion was found by solution of the following differential equations, with boundary conditions equivalent to the initial state of the propellants and the measured injector pressure drop. For the separated flow cases, the vapor alone satisfied these equations and the liquid phase was treated as an incompressible fluid.

(1) Energy Equation

$$dq + dh + \frac{udu}{g_c J} = 0$$

where, dq = heat transfer during the expansion, BTU/lb

u = velocity, fps

dh = enthalpy change, BTU/lb

$g_c = 32.174$ fps$^2$

J = 778 ft-lb/BTU

(2) Equation of Motion

$$udu + 144\, g_c v dP = 0$$

where, v = specific volume, ft$^3$/lb

P = pressure, psia

(3) Physical Definition of Acoustic Velocity

$$a^2 = 144\, g_c \left(\frac{\partial P}{\partial \rho}\right)$$

where, a = sonic velocity, fps

$\frac{\partial P}{\partial \rho}$ = partial derivative of pressure with respect to density for the assumed process

(U) In equation (1), the path function dq could not be calculated from fire test data. Therefore, the approach was to accept the gross heating effect during fire test as an increase in quality of the mixture and as sensible heat gain of the liquid (based on measured temperature and pressure data) and therefore reduce the

(U) expansion to a simplified isentropic process. It is believed that propellant heating within the injector during the cold flow test series was very small. This method then reduced each problem to solution of the above three equations with $\frac{\partial P}{\partial \rho}$ evaluated for the isentropic expansion through an ideal nozzle with the condition that choking of the propellant flow rate occurred identically with the local pressure within the injector at the critical value which was consistent with the acoustical velocity, a.

(U) The pure theoretical models discussed herein generally underpredicted the fluorine flow rate for the measured oxidizer injector feed pressure, as compared to the measured test flow rates. This is equivalent to overprediction of injector pressure drop had the test flow rate value been used to calculate injector oxidizer pressure drop for each expansion model. The degree of underpredication of oxidizer flow rate varied for each model. However, the scatter of predicted results was much less for the compressible flow theories as compared to incompressible flow calculations for the two-phase propellants. Therefore, it is concluded that the two-phase mixture did behave as a compressible fluid as expected. However, the pure theoretical analysis must be modified by the use of empirical coefficients to allow correlation with the test data. This is true since in general, the density times velocity, $\rho$ u, of the fluid was low in the theoretical predictions, i.e., a constant multiplier of the theoretical $\rho$ u must be used for test correlation. A summary of the resultant solutions to the differential equations (1), (2), and (3), and the comparison of the theory to the test data are discussed in the following paragraphs.

b. (U) Propellant Conditions at the Inlet to the Injector

(U) Initial calculations of vapor mass fraction were based on thermal equilibrium of the liquid and vapor as the fluid was heated in the gaseous nitrogen heat exchanger, and while heat was rejected as the propellant flowed through the downstream lines which were liquid nitrogen jacketed. For many of the runs, these calculated injector inlet qualities were zero. This was not consistent with the relatively high pressure loss across the injector during the test series. Therefore, two methods were subsequently used to determine a vapor mass fraction and propellant statepoint at the inlet to the injector:

Method 1 - Thermal equilibrium at the heat exchanger outlet, with a nonequilibrium condition as the propellant is cooled in the lines downstream from the heat exchanger.

Method 2 - Nonequilibrium propellant conditions during heating in the gaseous nitrogen heat exchanger and during subsequent downstream cooling.

(U) In Method 1, the known heating rate to the initially subcooled fluorine as it passes through the gaseous nitrogen heat exchanger was assumed to produce a sensible heat gain in the liquid while subsequent liquid and vapor temperatures were identical to the saturation temperature at the measured local pressure.

(U) A cooling rate for the downstream lines leading to the heat exchanger was calculated. It was assumed that a fraction of the total heating load resulted in a partial vapor condensation. This amount of heat was taken as $x_{te}\, q_{F_2 \rightarrow LN_2}$ and resulted in determination of a final vapor mass fraction and phase temperature at the inlet of the injector. Here, $x_{te}$ is the thermal equilibrium quality at the heat exchanger outlet and $q_{F_2 \rightarrow LN_2}$ is the cooling rate through the liquid nitrogen jacketed lines. This approach resulted in vapor mass fraction predictions less than those obtained by the following method.

(U) A nonequilibrium condition at the heat exchanger outlet and injector inlet was suggested by the measured temperature. These values were below saturation values at the measured local pressure. This suggested that the liquid and vapor were not in thermal equilibrium, although it was realized that two-phase propellant temperature measurements are difficult to interpret. To determine the liquid and vapor energies at the heat exchanger outlet, the vapor was assumed to be at its saturation temperature while the liquid was at a temperature equal to the average of the measured heat exchanger inlet and outlet values. Referring to Figure 132, the total fluid is raised in temperature from the initial condition ($T_o$) to the liquid outlet condition ($T_a$). A fraction of the fluid, $x_1$, is further raised in temperature to the saturation value ($T_b$) at the measured local pressure. This fraction of the fluid is then vaporized and has resultant specific enthalpy ($h_d$). This vapor mass fraction $x_1$, can be solved from the following heat balance and used to determine the conditions at the injector inlet after heat rejection from the downstream lines.

$$(4)\quad \dot{q}_{GN_2} = \dot{\omega}_{N_2} C_{P_{N_2}} \Delta T_{N_2} = \dot{\omega}_{o} (1-x_1)(h_a - h_o) + \dot{\omega}_{o} (h_d - h_o)\, x_1$$

where, $\dot{\omega}_{N_2}$ = weight flow rate of gaseous nitrogen, lb/sec

$\dot{\omega}_{o}$ = fluorine weight flow rate, lb/sec

$C_{P_{N_2}}$ = specific heat of gaseous nitrogen at constant pressure, BTU/lb-°R

$\Delta T_{N_2}$ = temperature differential of the gaseous nitrogen between the heat exchanger inlet and outlet measurements

$x_1$ = mass fraction of fluorine vaporized to the final state-point with specific enthalpy, $h_d$

$h_a$ = final specific enthalpy of the liquid at the heat exchanger outlet (BTU/lb)

$x$ = Vapor Mass Fraction = $\dfrac{\dot{\omega}_v}{\dot{\omega}_v + \dot{\omega}_L}$

$T_o$ = Initial Temperature

$T_a$ = Liquid Temperature at Heat Exchanger Outlet

$T_{sat}$ = Fluorine Saturation Temperature at OIIP

OIIP = Oxidizer Pressure at Inlet To Injector ≈ Heat Exchanger Pressure

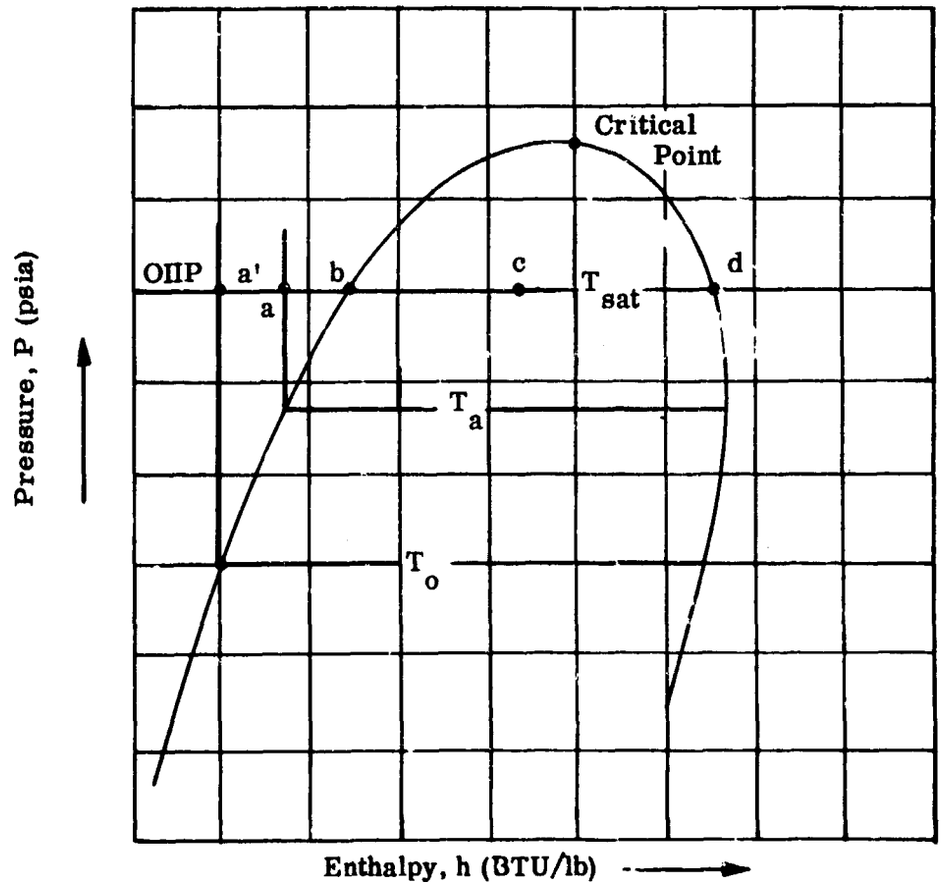


Figure 132. (U) Illustration of Nonequilibrium Thermodynamic Process Used to Obtain Vapor and Liquid Statepoints

(U) $h_o$ = initial fluorine specific enthalpy (BTU/lb)

$h_d$ = specific enthalpy of saturated vapor (BTU/lb)

(U) The final vapor mass fraction at the injector inlet was calculated using an appropriate fluorine side film coefficient while assuming that a fraction of the total heat rejected from the fluorine to the liquid nitrogen heat sink resulted in condensation. This amount of heat was taken as $x_1\, q_{F_2 \rightarrow LN_2}$ and resulted in a sensible heat gain of the liquid. This resulted in determination of a bulk temperature for the liquid phase and a quality.

c. (U) Compressible Flow Theories

(U) Three homogeneous flow and separated phase flow models were applied to the test data to correlate empirical results with theoretical predictions. The homogeneous flow models included a metastable expansion with heat transfer between phases and were applied to the initial propellant conditions calculated by the previously discussed methods. Also investigated were a thermal equilibrium expansion with heat and mass transfer between phases, and a nonequilibrium expansion with heat and mass transfer between phases. The metastable, separated flow cases included an expansion with no momentum interchange between phases and investigations with slip ratio as a function of phase specific volume ratio. These expansion calculations were applied to the point of choking consistent with sonic velocity during the pressure reduction.

(U) In general, each flow model underpredicted the actual fluorine flow rate when applied to the limits of propellant initial conditions derived from the calculated initial statepoint limits. Therefore, an empirical constant was derived for each expansion representation. This constant multiplied by the predicted fluorine flow rate brought the majority of test points within ±20% of the measured flow rate. Correlation of theory with test data was more successful for the separated phase models as compared to the homogeneous expansion representations which assume a fog type flow with vapor and liquid velocities being identical at any pressure during the expansion. The latter type of flow was anticipated to occur during the test program since the injector inlet passages represented a potentially good mixer as the two-phase mixture progressed from the inlet manifold to the face plate. No visual observations were possible to determine the two-phase fluorine flow distribution during the tests. However, if separated flow did ensue during the expansion, the injector flow rate remained stable. This was evident from pressures recorded during cold flow testing on oscillographs. The following paragraphs summarize the final developments of each expansion model, and include a discussion on the correlation with measured flow rate.

(1) (U) Metastable, Homogeneous Flow

(a) (U) Assumptions

(U) This model assumes steady, one-dimensional frictionless flow similar to that obtainable within an ideal nozzle. The expansion is assumed to occur adiabatically with no change in vapor mass fraction; i.e., time during the expansion is not sufficiently long for mass transfer. The initial temperature differential between the vapor and liquid which exists at the injector inlet (nonequilibrium case) is constant through the expansion, although the respective vapor and liquid temperatures reduce during the pressure reduction. The liquid density and specific heat are assumed to be constant, and the liquid and vapor are distributed to generate a fog type flow with no velocity slip between the phases. This assumption of fog flow was suggested by the natural mixing which was expected with the injector configuration tested.

(b) (U) Final Development

(U) For the case of variable vapor properties, the following equations were derived:

(U) From the acoustic velocity relation, equation (3):

$$(5)\quad a^2 = 144\, g_c \left(\frac{\mu}{1+\mu}\right)\left(1+\frac{1}{\delta^*}\right)^2 v_V^* \left[\frac{P^*\,(C_8 + C_9 P^*)\left(C_{11} + C_{12} P^* + \frac{C_L}{\mu}\right)}{C_5 P^* (C_8 + C_9 P^*) + C_8\left(C_{13} + C_{14} P^* + \frac{C_L}{\mu}\right)}\right]$$

where $\mu = \dfrac{x_2}{1 - x_2}$ = a constant

$$\delta^* = \mu \frac{v_V^*}{v_L}$$

$v_V^*$ = vapor specific volume at point of choking, $ft^3/lb$

$v_L^*$ = liquid specific volume, $ft^3/lb$

$P^*$ = critical pressure, psia

$C_L$ = liquid specific heat, BTU/lb-°R

$Z = C_8 + C_9 P$, compressibility factor

$C_{VV} = C_{13} + C_{14} P$, vapor specific heat at constant volume, $\dfrac{BTU}{lb\text{-}°R}$

$C_{PV} = C_{11} + C_{12} P$, vapor specific heat at constant pressure, $\dfrac{BTU}{lb\text{-}°R}$

(U) From the equation of motion (2):

$$(6)\quad a^2 = \frac{288 g_c v_L}{1+\mu}\left[P_o\left(1-\frac{P^*}{P_o}\right) - \int_{P^*}^{P_o} \delta_o \left(\frac{P_o}{P^*}\right)^{\Omega_1}\left(\frac{C_8+C_9P_o}{C_8+C_9P^*}\right)^{\Omega_2}\left(\frac{C_{11}+C_{12}P_o+\frac{C_L}{\mu}}{C_{11}+C_{12}P^*+\frac{C_L}{\mu}}\right)^{\Omega_3} dP\right]$$

where, $P_o$ = measured injector oxidizer inlet pressure, psia and $\Omega_1, \Omega_2, \Omega_3$ are constants, where

$$\Omega_1 = \frac{C_L + \mu C_{13}}{C_L + \mu C_{11}}, \qquad \Omega_2 = -1, \Omega_3 = \frac{C_{14}}{C_{12}} + 1 - \Omega_1$$

(The values of the constants for the thermodynamic properties and their accuracy are presented in Table XVIII.)

(U) Simultaneous solution of equations (5) and (6) results in the determination of the critical pressure, P*. However, equation (6) must be numerically integrated. For a simplification that the vapor specific heats and compressibility factors are constant during the expansion, the problem reduces identically to one previously studied for an ideal gas (Reference 1).

Equations (5) and (6) become:

$$(5a)\quad a^2 = 144\, g_c\left(\frac{\mu}{1+\mu}\right)\left(\frac{P_o}{P^*}\right)^{\Omega_1}\left(\frac{v_{Vo}P^*}{\Omega_1}\right)\left[1+\frac{1}{\delta_o}\left(\frac{P^*}{P_o}\right)^{\Omega_1}\right]^2$$

$$(6a)\quad a^2 = \frac{288\, g_c v_L}{1+\mu}\left(\frac{P_o}{1+\Omega_1}\right)\left\{\delta_o\left[1-\left(\frac{P^*}{P_o}\right)^{1-\Omega_1}\right]+\left(1-\frac{P^*}{P_o}\right)\right\}$$

where, $v_{Vo}$ = initial vapor specific volume, $ft^3/lb$

$$\delta_o = \mu\frac{v_{Vo}}{v_L}$$

(U) The critical pressure ratio, $P^*/P_o$, obtained from the simultaneous solution of equations (5a) and (6a) is shown in Figure 133. Over the range of initial vapor and liquid temperatures, the critical pressure ratio for the mixture is not too different than that of the vapor (x = 100%). Use of either equation (5a) or (6a) resulted in sonic mixture velocities of 140 to 360 fps as compared to a "dry" vapor sonic velocity of approximately 500 fps. The calculated oxidizer flow rate was obtained from evaluation of the continuity equation at the critical pressure, P*.

$$(7)\quad \dot{\omega}_o = \frac{K A_o a}{144\, v^*}$$

where, K is the flow nozzle flow coefficient obtained from calibration test and is a function of Reynolds number. However, in the high Reynolds number, two-phase region $0.95 < K < 1.0$. $A_o$ is the total

TABLE XVIII

(U) EQUATIONS FOR SOME THERMODYNAMIC PROPERTIES OF SATURATED FLUORINE

| Property | Equation | Values of Constants | Maximum Deviation From Data Tabulated* Over the 13.7 to 496.1 psia Vapor Pressure Range (%) |
|---|---|---|---|
| Liquid Specific Volume, $v_L$ ($ft^3/lb$) | $v_L = C_1 + C_2P + C_3P^2$ | $C_1 = 0.01044463$<br>$C_2 = 1.699246 \times 10^{-5}$<br>$C_3 = -2.840572 \times 10^{-8}$ | +0.93<br>-0.55 |
| Vapor Specific Volume, $v_V$ ($ft^3/lb$) | $v_V = C_4 P^{C_5}$ | $C_4 = 36.79774$<br>$C_5 = -0.9448157$ | +2.00<br>-1.14 |
| Liquid Specific Entropy, $S_L$ $\frac{BTU}{lb-^\circ R}$ | $S_L = C_{3a} + C_{3b}P$ | $C_{3a} = 0.766527$<br>$C_{3b} = 0.0491855 \times 10^{-2}$ | +1.58<br>-0.56 |
| Vapor Specific Entropy, $S_V$ $\frac{BTU}{lb-^\circ R}$ | $S_V = C_{4a} + C_{4b}P + C_{4c}P^2$ | $C_{4a} = 1.261748$<br>$C_{4b} = -0.1156977 \times 10^{-2}$<br>$C_{4c} = 0.297315 \times 10^{-5}$ | +0.69<br>-0.99 |
| Liquid Specific Enthalpy, $h_L$ (BTU/lb) | $h_L = C_{5a} + C_{5b}P + C_{5c}P^2$ | $C_{5a} = -149.5915$<br>$C_{5b} = 0.170245$<br>$C_{5c} = -3.115008 \times 10^{-4}$ | +0.63<br>-0.54 |
| Vapor Specific Enthalpy, $h_V$ (BTU/lb) | $h_V = C_{6a} + C_{6b}P + C_{6c}P^2$ | $C_{6a} = -72.98451$<br>$C_{6b} = 6.894509 \times 10^{-2}$<br>$C_{6c} = -2.084863 \times 10^{-4}$ | +0.98<br>-0.245 |
| Vapor Compressibility Factor, Z | $Z = C_8 + C_9P$ | $C_8 = 0.9840$<br>$C_9 = -0.00082$ | +1.00<br>-1.50 |
| Vapor Specific Heat at Constant Pressure $C_{pv}$ (BTU/lb-°R) | $C_{pv} = C_{11} + C_{12}P$ | $C_{11} = 0.1792$<br>$C_{12} = 0.000336$ | +0.10<br>-0.10 |
| Vapor Specific Heat at Constant Volume, $C_{vv}$ (BTU/lb-°R) | $C_{vv} = C_{13} + C_{14}P$ | $C_{13} = 0.1278$<br>$C_{14} = 0.000379$ | +0.30<br>-0.40 |

* "Fluorine Thermodynamic Tables", P.S. Morris, General Chemical Division, Allied Chemical Corporation, December 2, 1963

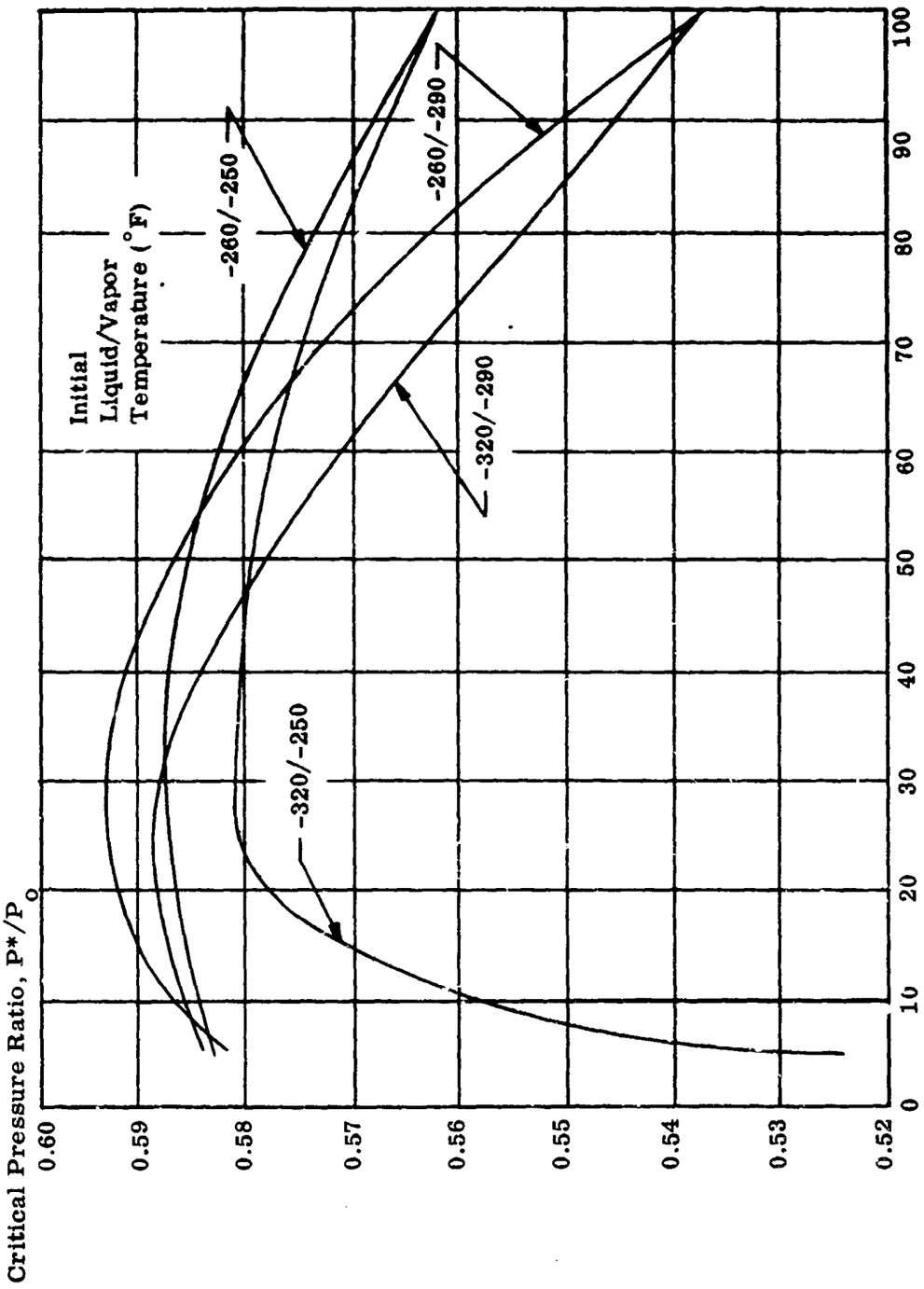


Figure 133. (U) Critical Pressure Ratio for Various Initial Conditions - Metastable Expansion

(U) area of the injector "orifices". (Actually a flow nozzle)

$$v^* = \frac{\mu}{1+\mu} v_V^* + \frac{v_L}{1+\mu},$$

the mixture specific volume at the point of choking, and $v_V^*$ was obtained from solution of the differential equations (1) and (2).

(c) Correlation with Test Results

(U) Figure 134 shows a plot of flow rate error versus quality for the nonequilibrium initial condition predicted by Method 2. The majority of data are within ±20% of an average line of deviation -60%. This indicates that the $\rho$ u calculated from this method must be multiplied by a constant 2.5 to yield flow rate correlation. The corresponding deviations for the injector initial statepoints calculated by Method 1 where thermal equilibrium was assumed at the heat exchanger outlet are shown in Figure 135. Here, the majority of points fall within ±20% of a deviation of -45%. Therefore, a correction multiple of $\rho$u of 1.8 must be used to get flow rate correlation. Note that the zero quality cases predicted at the injector inlet over predict flow rate (underpredict pressure drop). These are incompressible calculations obtained from equations (6a) and (7). From this, it is evident that the thermal equilibrium assumption at the heat exchanger outlet underpredicts the quality at the injector inlet.

(2) (U) Homogeneous, Thermal Equilibrium Flow

(a) (U) Assumptions

(U) This model assumes steady, one-dimensional frictionless flow as in the metastable expansion model. However, conditions during the expansion are assumed to be sufficient to allow a two-phase mixture initially at thermal equilibrium at the injector inlet to attain instantaneous thermal equilibrium throughout the expansion. Therefore, during the isentropic pressure reduction, the mixture quality and specific volume increase as the pressure is reduced to the critical choking value. The mixture is assumed to expand in a fog type vapor and liquid distribution with both phases moving at the same velocity (zero velocity slip between phases).

(b) (U) Final Development

(U) Using a polynominal expansion for the vapor and liquid entropy and specific volume, the equation of motion (2) at the critical pressure becomes:

$$(8)\quad -\frac{a^2}{2} = \int_{P_o}^{P^*} v_L(P_s)\, dP + \int_{P_o}^{P^*} x_{te} \left[ v_V(P) - v_L(P) \right] dP$$

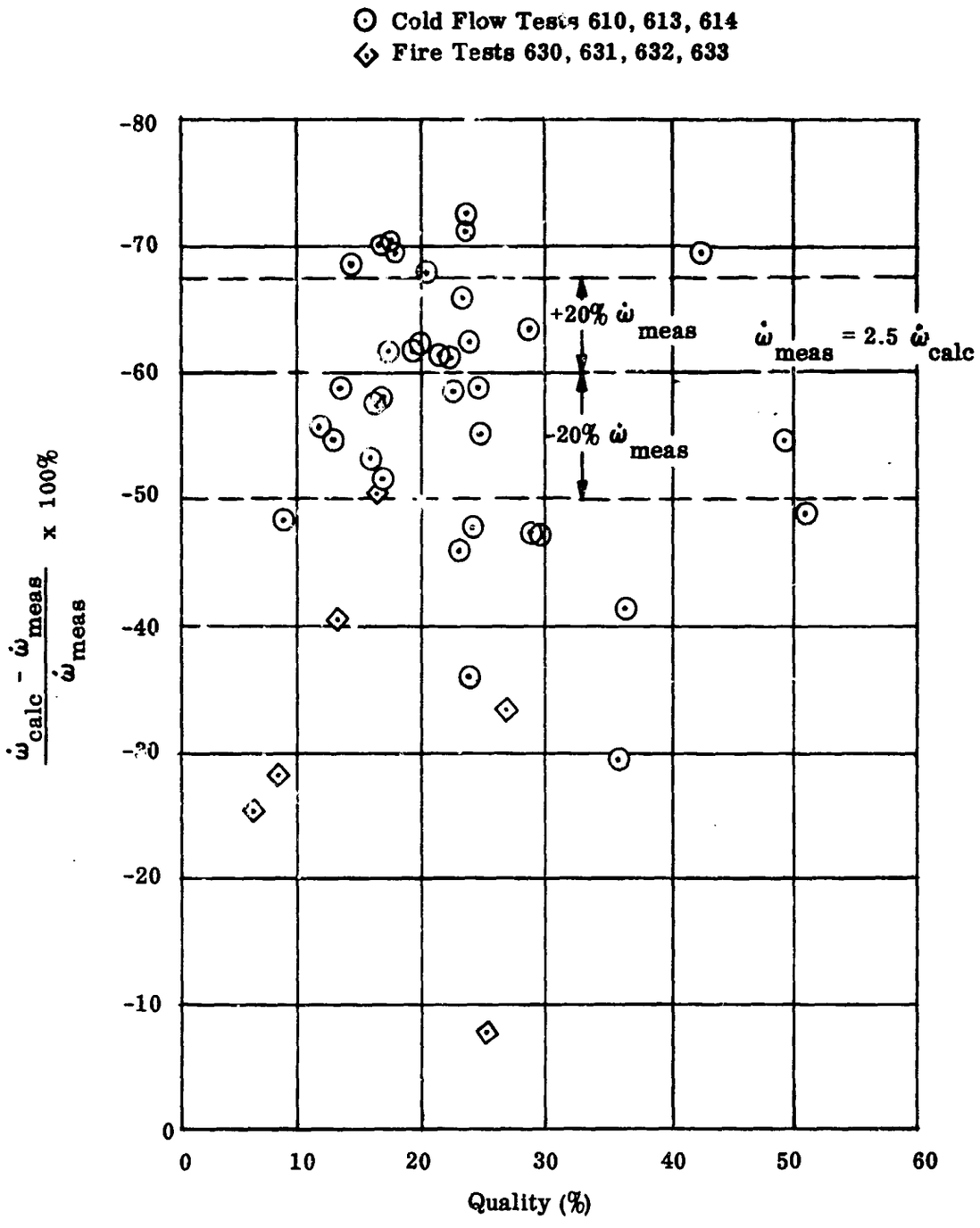


Figure 134. (U) Error in Flow Rate Prediction - Metastable Expansion From Initial Nonequilibrium Condition (Method 2)

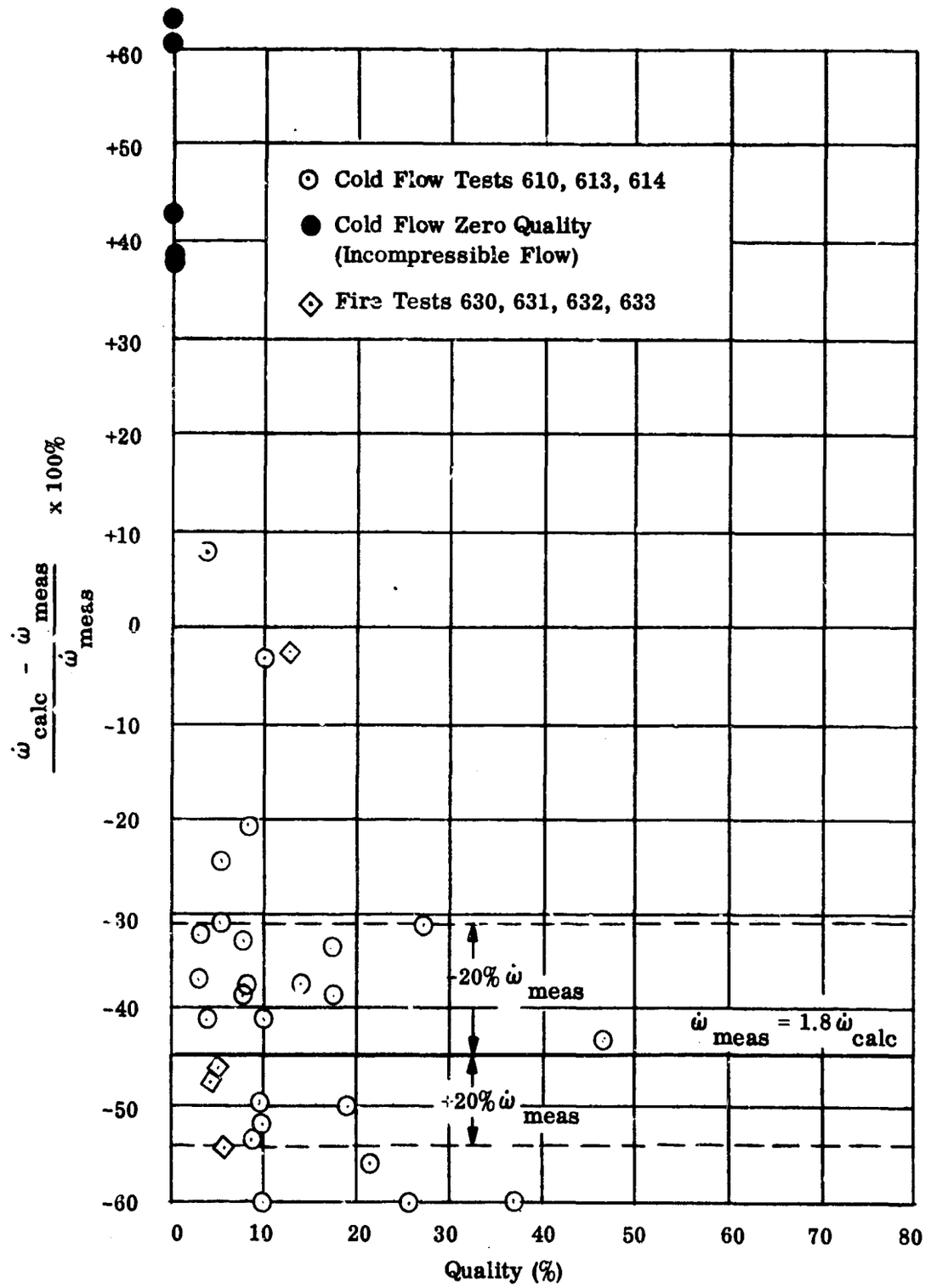


Figure 135. (U) Error in Flow Rate Prediction - Metastable Expansion From Initial Condition (Predicted by Method 1)

(U) where, $v_L (P_s) = C_1 + C_2 P + C_3 P^2$

the liquid specific volume as a function of saturation pressure, P, $ft^3/lb$

$$v_V = C_4 P^{C_5}$$

the vapor specific volume, $ft^3/lb$

$x_{te}$ = thermal equilibrium quality at any pressure during the expansion

Since the propellants are assumed to be in thermal equilibrium, representations of the specific volumes as functions of vapor pressure automatically satisfies their dependency on the saturation temperature. A closed form solution of equation (8) was not possible when vapor entropy was represented as a polynomial as shown in Table XVIII. Therefore, the solutions of the equation of motion (8) were performed graphically from a pressure-entropy-specific volume-quality plot after noting that relatively small increases in quality occurred between the initial condition at $P_o$ and at the critical pressure, P*. The average value of quality, $x_{te}$, was used to obtain the sonic velocity, a, from this equation. Iteration was performed using assumed values of P* until the sonic velocity obtained from equation (8) equaled that obtained from the sonic velocity definition (3). In equation (3), $\left(\frac{\partial P}{\partial \rho}\right)_{s=c}$ was obtained graphically.

(c) (U) Correlation with Test Results

(U) Calculation of flow rate for a limited number of test runs using this mass transfer expansion model resulted in flow rate prediction below that obtained from the metastable expansion model. Therefore, it was decided that further effort placed on this approach was not warranted. The reason for relative underprediction of flow rate using this model as opposed to the metastable expansion calculations is the fact that the mixture sonic velocity prediction was much lower since $\left(\frac{\partial P}{\partial \rho}\right)_{s=c}$ was lower, and the increase in specific volume of the mixture was higher because the average value of $x_{te}$ was greater than the initial quality, $x_2$. Therefore, the $\rho$ a introduced in the continuity equation was low and flow rate prediction was low.

(3) (U) Homogeneous, Nonequilibrium Flow

(a) (U) Assumptions

(U) Steady, one-dimensional inviscid flow is assumed as in the thermal equilibrium, homogeneous flow case. However, the expansion is reduced to an investigation within two regimes.

(U) At high pressure, the initial liquid mass is subcooled and its entropy and specific volume are taken as the initial saturation values. As the pressure is reduced, the liquid mass fraction is increased through vapor condensation, and the total entropy of the system remains constant.

(U) Below the pressure identical to the vapor pressure of the liquid, vaporization occurs as the pressure is further reduced and the quality increases while the liquid and vapor temperatures are identical. Also during this thermal equilibrium regime, the system entropy is assumed constant as the liquid and vapor temperatures identically decrease.

(b) (U) Final Development

(U) In the subcooled region, the liquid entropy at any pressure $P_i$, is approximated by the following equation.

$$(9)\quad \sum S_L = \frac{S_{LO}(1 - x_o) + (x_o - x_i) S_{Li}}{1 - x_i}$$

where, $\sum S_L$ = specific entropy of initial and condensed liquid

$S_{LO}$ = Initial liquid specific entropy assumed as saturation value at initial vapor pressure, $P_V$

$S_{Li}$ = specific entropy of liquid at pressure $P_i$

$x_o$ = vapor mass fraction at injector inlet, $x_2$

$x_i$ = vapor mass fraction at pressure $P_i$

For an assumed pressure, $P_i$ with $P_o > P_i > P_V$ the quality $x_i$ is assumed and iterated until this value satisfies equation (9) and the total system entropy relation (10).

$$(10)\quad x_i = \frac{S_o - \Sigma S_L}{S_{V_i} - \Sigma S_L}$$

where, $S_o$ = mixture specific entropy at the injector inlet

$S_{V_i}$ = vapor specific entropy at pressure, $P_i$

The liquid specific volume and mixture specific volume at the pressure $P_i$ are obtained when $x_i$ is found.

$$(11)\quad v_i = \Sigma v_L + x_i \left[ v_{V_i} - \Sigma v_L \right]$$

(U) (12) $$\sum v_L = \frac{v_{LO}(1 - x_o) + (x_o - x_i)\ v_{Li}}{1 - x_i}$$

where, $v_i$ = mixture specific volume

$v_{Vi}$ = vapor specific volume at assumed pressure, $P_i$

$v_L$ = specific volume of initial and condensed liquid

The acoustic velocity can therefore be obtained while evaluating the thermodynamic properties by finite reductions of $P_i$ below the initial value $P_o$. The physical definition of acoustic velocity, a, obtained from $a^2 = -144\ g_c v_i^2 \left(\frac{\partial P}{\partial v}\right)_{S_i = S_o}$ of equation (3) is found by approximately; $\left(\frac{\partial P}{\partial v}\right)_{S_i = S_o} \approx \left(\frac{(P_i - P_j)}{(v_i - v_j)}\right)_{S_i = S_o}$ from the statepoint i to statepoint j while the average value of quality, $\bar{x}_i$, is used during the pressure reduction. The integration of the momentum equation (2) is performed at each pressure value and the acoustic velocity, a, is found when equations (3) and (13) are satisfied. The pressure value at this condition is the critical pressure, P*.

$$(13)\quad -\frac{a^2}{2} = 144\ g_c \int_{P_o}^{P^*} v_i\, dP$$

where, $v_i$ is obtained from equation (11). Using polynomial representatives of the specific volumes of the phases and treating the liquid as incompressible, the integral of equation (13) may be approximated as:

$$(14)\quad \int_{P_o}^{P^*} v_i P = v_{LO}(1 - x_o)(P^* - P_o)$$

$$+ \frac{(x_o - x_i)}{2}\left\{P^*\left[C_1 + \frac{C_2}{2}P^* + \frac{C_3}{3}(P^*)^2\right]\right.$$

$$\left. - P_o\left[C_1 + \frac{C_2}{2}P_o + \frac{C_3}{3}(P_o)^2\right]\right\}$$

$$+ \left(\frac{x_o + x_i}{2}\right)\ \frac{C_4}{(1 + C_5)}\ \left[(P^*)^{1 + C_5} - (P_o)^{1 + C_5}\right]$$

(U) where, the constants are identical to those presented in Table XVIII.

Equation (14) is evaluated while the liquid is in the subcooled region. As the pressure is reduced below the vapor pressure of the liquid mass, the integral $\int_{P_o}^{P^*} v_i P$ is evaluated as in the thermal equilibrium case and the total integral becomes:

$$(15) \quad \int_{P_o}^{P^*} v_i P = \int_{P_o}^{P_{sat}} v_i P + \int_{P_{sat}}^{P^*} v_i dP$$

where, the first integral is the subcooled representation and the second integral is the thermal equilibrium form.

(c) (U) Correlation with Test Results

(U) Evaluation of the equations (13) and (15) was performed on a limited number of test points with statepoint predicted by Method 2 of Section 7, B, 3, b. No improvement was noted as compared to the homogeneous thermal equilibrium approach. However, even though condensation was predicted by the model during expansion, the $\rho$ a was still low and fluorine flow rate underprediction occurred.

(4) (U) Vapor Choking

(a) (U) Assumptions

(U) Separated flow with velocity slip between the vapor and liquid was investigated as a final approach to correlate theory with the test data. Oscillograph data showed stable operation during the cold flow test series. Had separated flow occurred, the phase distribution would have probably consisted of a liquid annulus and a vapor core. Calculations were made for a vapor choking model in its simplest form which neglects the momentum interchange between the two phases during the expansion. Momentum interchange was reflected in further calculations using the slip ratio $K_u = \frac{a}{u_L} = \left(\frac{v_{V^*}}{v_L}\right)^{1/2}$ at the point of choking, which was suggested from Fauske's work (Reference 2). Again, each approach assumed steady, one-dimensional inviscid flow with no quality change during the expansion.

(U) An area ratio between the vapor and liquid was calculated from the secondary equation.

$$(16)\quad \frac{A_L}{A_V} = \frac{(1 - x_2)}{x_2}\left(\frac{v_L}{v_V^*}\right)\left(\frac{a_V}{u_L}\right)_{choking}$$

where $A_L$ and $A_V$ are the flow areas of the liquid and vapor

$\frac{v_L}{v_V}$ is the specific volume ratio, liquid to vapor at the point of choking.

$a\sqrt{\gamma g_c}\,RTZ$, the sonic velocity of the vapor

≈ 500 fps

$u_L$ = liquid velocity at the point of choking

In the approach neglecting momentum interchange, the liquid velocity was found using the Bernoulli equation. In the other vapor choking method, the velocity ratio was calculated from the previously mentioned specific volume ratio. Then the vapor and liquid flow rates were evaluated at the vapor choking condition.

(b) (U) Correlation with Test Results

(U) Flow rate correlations of the vapor choking approach without momentum interchange are shown for the initial nonequilibrium propellant condition of Method 2 in Figure 136 and for the initial condition of Method 1 in Figure 137. For the former case, the theoretical flow rate must be multiplied by a factor of 1.82 to bring the majority of test points within ±20% of actual flow rate. However, for the initial condition predicted by Method 2, this multiple is only 1.33 which is the closest correlation of presented cases. The zero quality points overpredicted flow rate. Heat transfer to the fluorine within the injector during the fire tests compensates for the basic flow rate underprediction of this vapor choking model.

(U) Use of the slip ratio, $K_u = \left(\frac{v_V^*}{v_L}\right)^{1/2}$, resulted in flow rates which were less than those shown for the vapor choking calculations presented in Figure 137. However, use of a slip ratio based on the average specific volumes of the phases improved the correlation with cold flow data as shown in Figure 138.

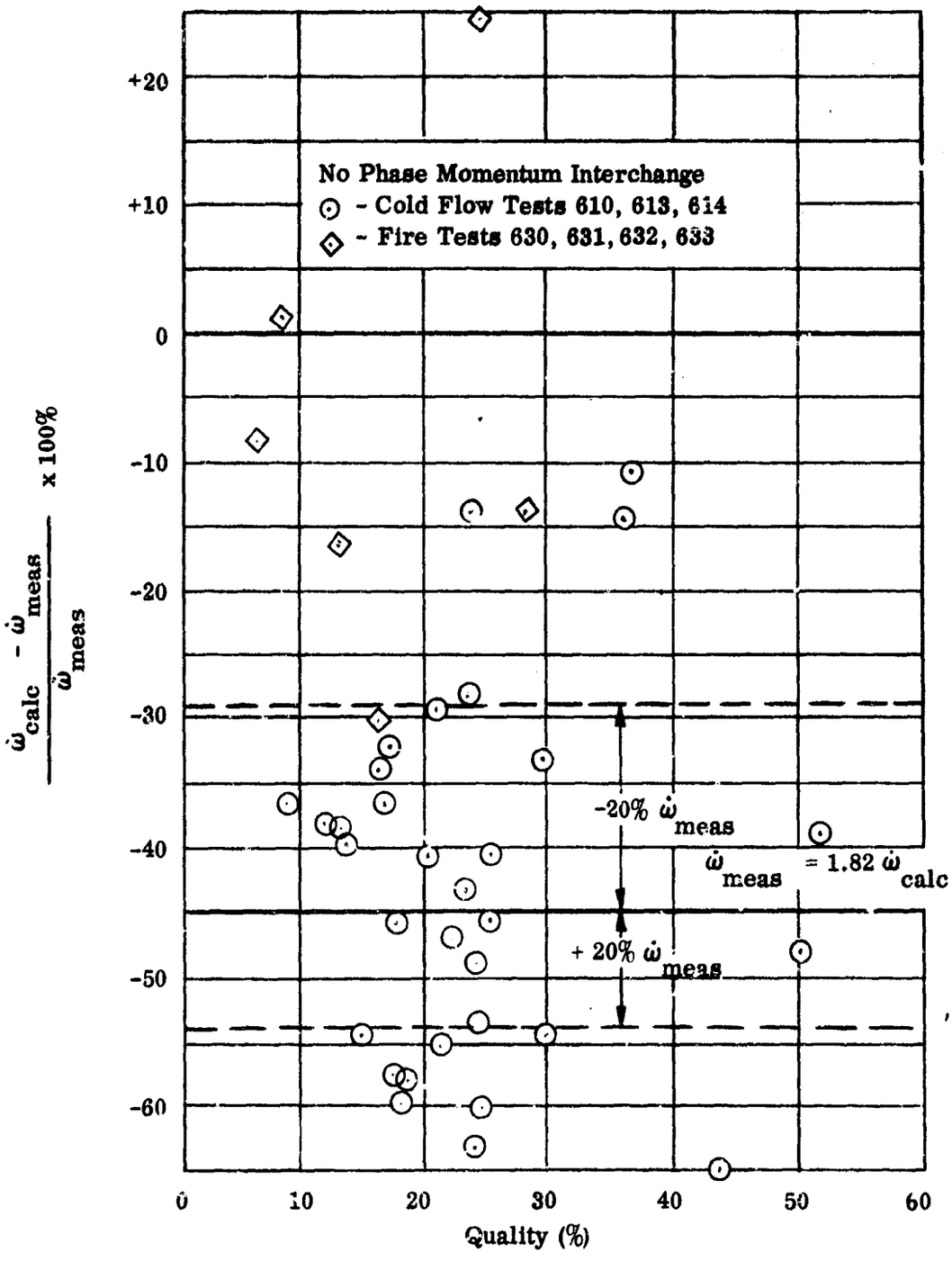


Figure 136. (U) Error in Flow Rate Prediction - Vapor Choking During Expansion From Initial Nonequilibrium Condition (Method 2)

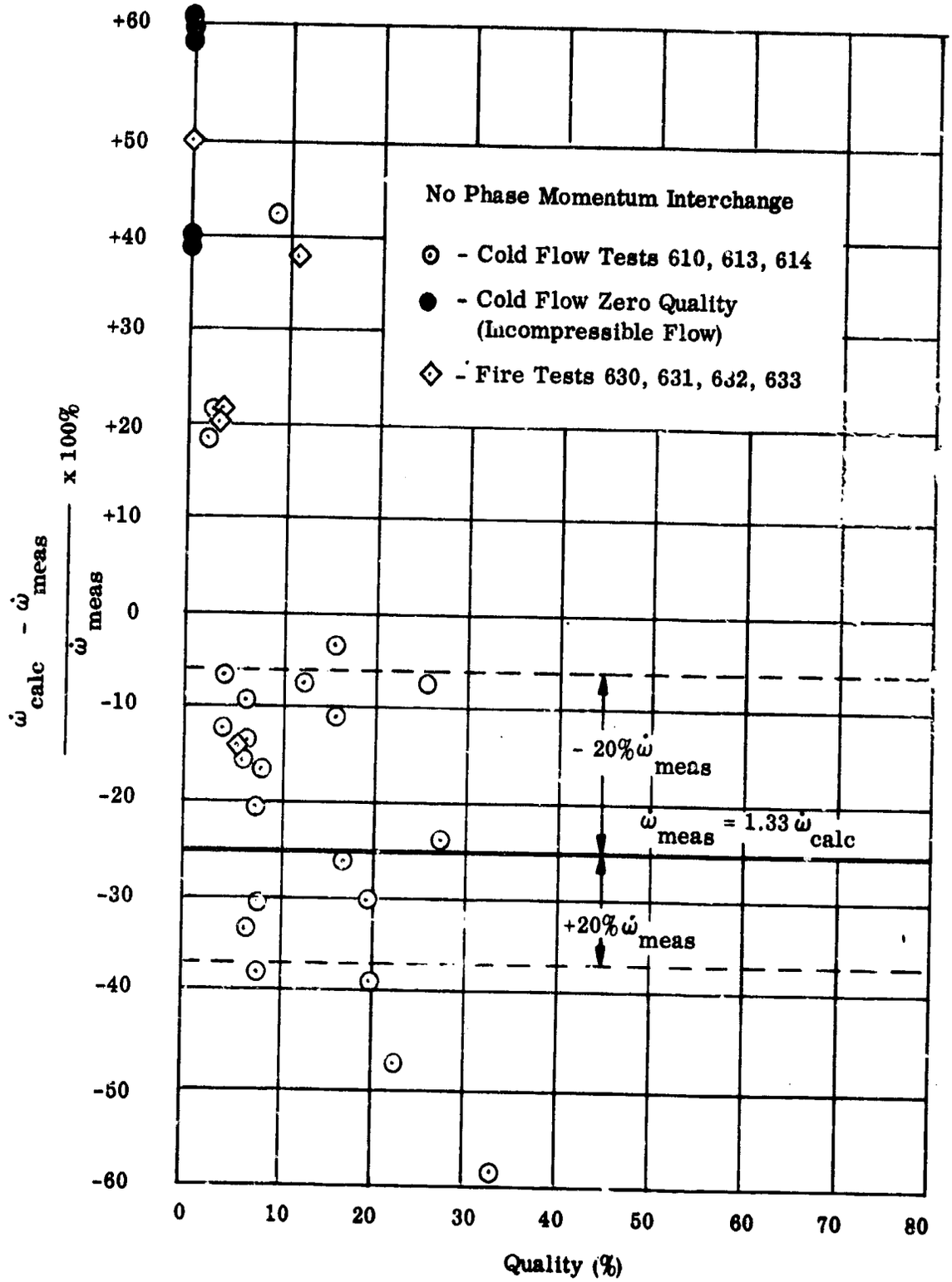


Figure 137. (U) Error in Flow Rate Prediction - Vapor Choking Expansion From Initial Condition (Predicted by Method 1)

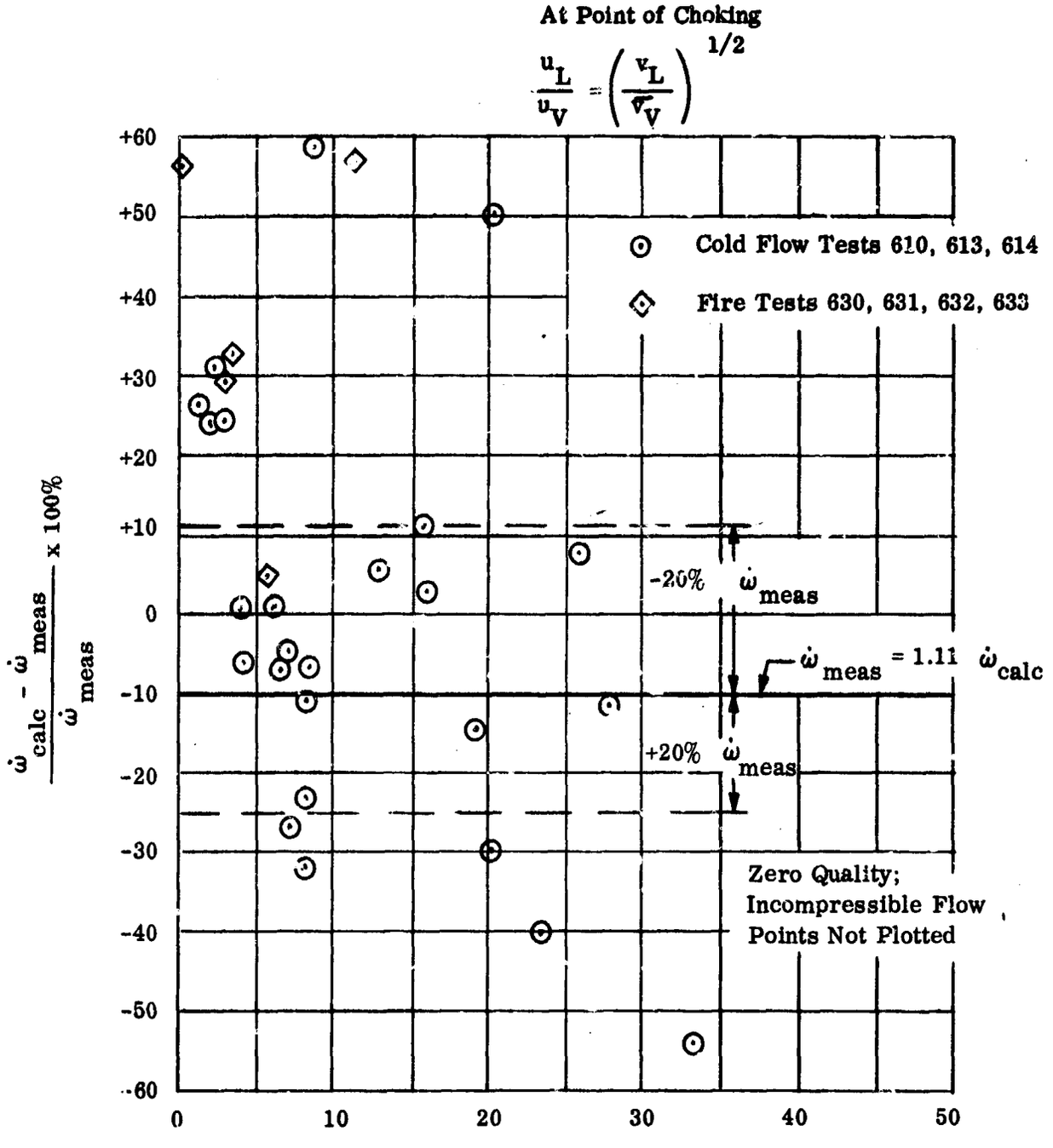


Figure 138. (U) Error in Flow Rate Prediction - Vapor Choking During Expansion From Initial Condition (Predicted by Method 1)

(5) (U) Other Methods

(U) Check calculations were made on a limited number of test points using the Fauske (Reference 2) theory. An analogy between the injector flow nozzle and a short tube was made and calculation of fluorine flow rate was made while using the back pressure at the injector. This approach was used to serve only as a limiting case since the local exit pressure of the stream was unknown. Fauske derived a representation for two-phase critical flow independent of acoustic velocity while defining critical flow as the condition where the mass flow rate per unit area does not increase with a reduction in back pressure. Also, at the critical flow condition, the pressure gradient at the exit has a finite maximum for a given flow rate and quality. The equation (5.11-8) of Reference 2 was evaluated for isentropic conditions. Underprediction of flow rate was evident and of the same order as that of the homogeneous thermal equilibrium approach.

(6) (U) Conclusions

(U) The compressible flow theories used in correlation of the test data generally underpredicted two-phase fluorine flow rate. The following multiples of calculated flow rate are required to correlate the majority of test points within ±20% of the measured flow rate:

| Choking Expansion Theory | Initial Propellant Condition Prediction | Semi-Empirical Constant |
|---|---|---|
| Metastable, homogeneous | Method 2 | 2.5 |
| Metastable, homogeneous | Method 1 | 1.8 |
| Homogeneous, heat and mass transfer | Thermal Equilibrium | ≈ 1.8 |
| Homogeneous, heat and mass transfer | Method 2 | ≈ 1.8 |
| Separated phase, no momentum interchange | Method 2 | 1.8 |
| Separated phase, no momentum interchange | Method 1 | 1.33 |
| Separated phases, slip ratio based on average specific volume ratio | Method 1 | 1.11 |

(U) Omission of the heat transfer to the propellant within the injector tends to compensate for the underprediction of the flow rates obtained from the isentropic compressible flow rate calculations. The thermal equilibrium calculation of propellant condition at the heat exchanger outlet results in less quality than that for the nonequilibrium approach of Method 2. Zero quality is predicted in some cases

(U) using the former assumption, and gross overprediction of flow rate results since the problem is reduced to incompressible flow. However, for nonzero initial quality cases, the injector inlet condition predicted by Method 1 generally results in less flow rate error than that of the nonequilibrium injector inlet condition of Method 2. Therefore, the actual quality experienced during the tests was probably less than that predicted by Method 2 and greater than that which would be predicted by assuming thermal equilibrium upstream of the injector. One possible reason for underprediction of flow rate for theoretical cases was due to the nonideal nozzle effect. Previous experimenters (References 3 and 4) have shown that in the flow of compressible fluids through orifices and fittings, critical flow is not attained with a back pressure identical to the critical pressure predicted by ideal nozzle theory. Rather, flow rate is further increased 10 to 15% with further reductions in back pressure.

(U) In regard to injector operation during fluorine cold flow and fire test, a stable injection system was demonstrated. The combustion efficiency during two-phase fluorine operation decreased at a faster rate than that of the liquid fluorine/BA-1014 runs. Aside from effects such as off-mixture ratio operation, the performance degradation is consistent with previous conclusions drawn from tests performed under Contract AF04(611)-8183 during experiments with injection of impinging streams. It is desired that the momentum relation between reacting streams be relatively constant over the throttling range. Since no mechanism was used to maintain a high fuel velocity during the tests, the velocity decrease of the subcooled fuel as chamber pressure was reduced could be expected to occur as that predicted from incompressible flow theory. This momentum ratio increases as chamber pressure is reduced as shown in Figure 139 . The relation is compared for calculations of fluorine velocity using the vapor choking model with the average specific volume slip ratio and the approach neglecting momentum transfer between the fluorine liquid and vapor phase. An empirical flow rate correction factor was applied to these throttling fire test fluorine injection velocities to obtain the oxidizer momentum. An increase in oxidizer to fuel momentum ratio is apparent as chamber pressure is reduced from 95 to 35 psia, and combustion efficiency decreased with the increase in momentum ratio.

(U) In summary, the concept of use of two-phase fluorine as a mechanism for deep throttling injectors has been demonstrated. As engine thrust is throttled, high injector pressure drops can be maintained for feed system stability. Furthermore, the injector feed pressure requirements at rated thrust are no higher than those required for a fixed area, fixed thrust injector. The only system control required with two-phase propellant injection is a single throttling valve for flow rate modulation of the initially subcooled propellant as thrust is controlled. In a system whereby the fuel injection velocity can be maintained, then two-phase fluorine injection could provide high combustion efficiency over a deep throttling range. In the $F_2$/BA-1014 engine, generation of fuel rich gases may be used to maintain fuel velocities at acceptable high levels. For the $F_2/H_2$ engine, advantage may be made of the high energy of the hydrogen as it is emitted from the regenerative cooled thrust chamber. These concepts had been outlined in Reference 5. Integration of the correct fuel injection technique with the two-phase fluorine injection concept can represent a potentionally high performance, simple and reliable, and stable method of deep throttling control for advanced space applications such as that of the Maneuvering Satellite Vehicle.

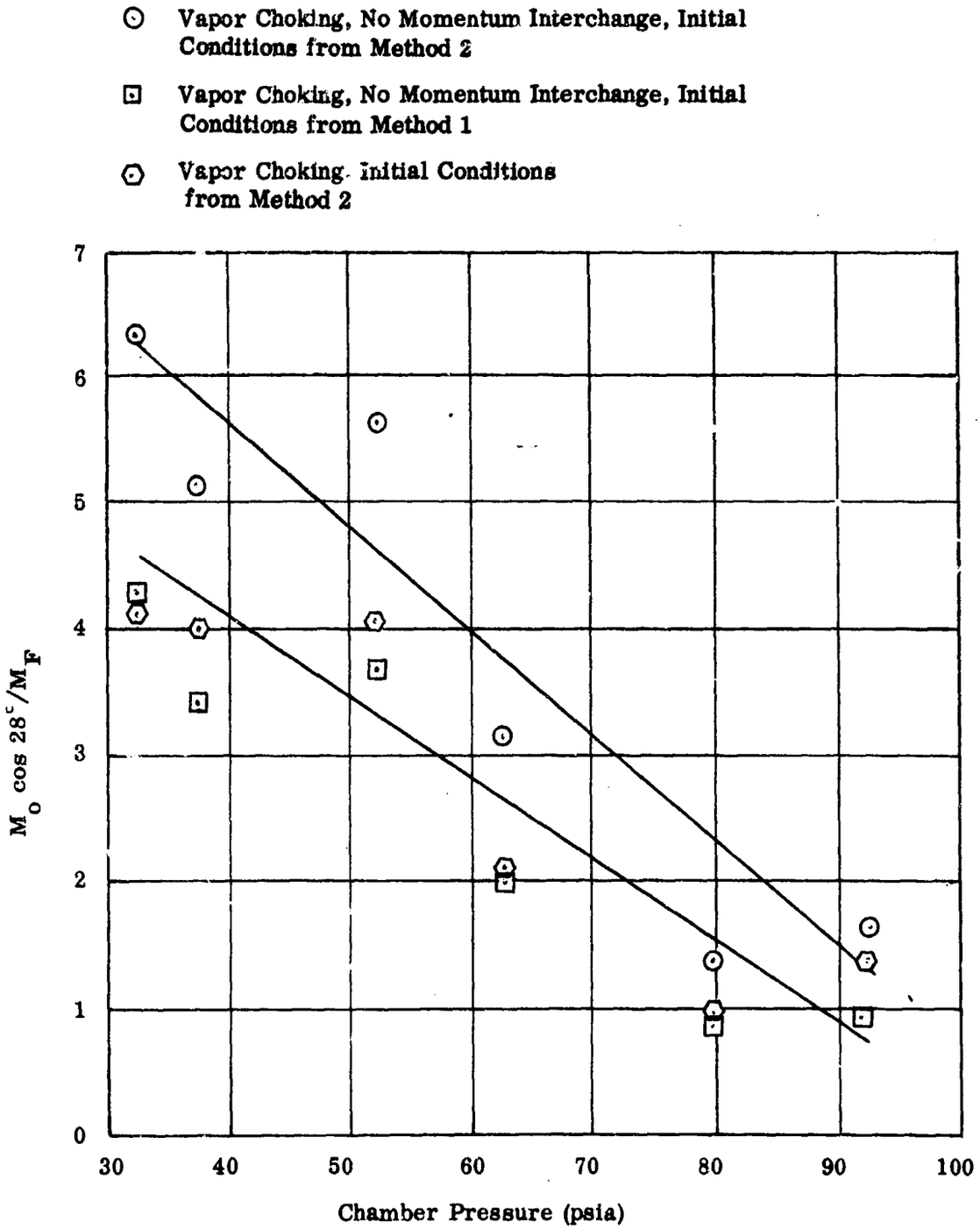


Figure 139 . (U) A Comparison of Momentum Ratio During Two-Phase Fluorine Fire Tests

## (U) REFERENCES

1. (U) "Compressibility Effects in Two Phase Flow,"
Tangren, R. F., Dodge, G. H., Seifert, H. S., Journal of Applied Physics, Volume 20, No. 7, 1949.

2. (U) "Contribution to the Theory of Two-Phase, One-Component Critical Flow,"
Fauske, H. K., Argonne National Laboratory, ANL-6633, October, 1962.

3. (U) "Critical Flow Through Sharp Edged Orifices,"
Perry, J. A., ASME (1949), pp 757-764.

4. (U) "Subcritical and Critical Flow Through Straight-Through Elbow and Tee AN Fittings and Sharp Edged Orifices,"
DuCoffe, H. L., Bennet, J. R., Ray, C. G., ASME (1958), pp 1349-1357.

5. (U) "Analysis of an Optimum Thrust Modulated Propulsion System for Use in a Space Maneuvering Vehicle,"
Volume I - Propulsion System Analysis, Report No. RPL-TDR-64-120, Contract AF04(611)-8183, October, 1964.

UNCLASSIFIED

Security Classification

**DOCUMENT CONTROL DATA - R&D**

*(Security classification of title, body of abstract and indexing annotation must be entered when the overall report is classified)*

| 1. ORIGINATING ACTIVITY (Corporate author) | 2a. REPORT SECURITY CLASSIFICATION |
|---|---|
| Bell Aerosystems Company<br>Buffalo, New York 14240 | CONFIDENTIAL |
| | 2b. GROUP |

3. REPORT TITLE

Maneuvering Satellite Propulsion System Demonstration

4. DESCRIPTIVE NOTES (Type of report and inclusive dates)

Final Report - Part III - May 1964 Through July 1965

5. AUTHOR(S) (Last name, first name, initial)

Germano, J., Chazen, M., Pearson, W.

| 6. REPORT DATE | 7a. TOTAL NO. OF PAGES | 7b. NO. OF REFS |
|---|---|---|
| September 1965 | 226 | 5 |

| 8a. CONTRACT OR GRANT NO. | 9a. ORIGINATOR'S REPORT NUMBER(S) |
|---|---|
| AF04(611)-8183 | AFRPL-TR-65-127 |
| b. PROJECT NO.<br>AF Program Structure No. 750G | |
| c.<br>BPSN No. 6299 | 9b. OTHER REPORT NO(S) (Any other numbers that may be assigned this report)<br>8173-933009 |
| d. Task No. 305803 | |

10. AVAILABILITY/LIMITATION NOTICES

Qualified users may obtain copies of this report from the Defense Documentation Center.

| 11. SUPPLEMENTARY NOTES | 12. SPONSORING MILITARY ACTIVITY |
|---|---|
| | Air Force Rocket Propulsion Laboratory<br>Research and Technology Division<br>Air Force Systems Command, USAF<br>Edwards, California |

13. ABSTRACT

This document presents the exploratory development work accomplished in the design, fabrication and testing of advanced rocket engine components for a high energy propellant space maneuvering vehicle. The exploratory development effort consisted of a series of critical experiments to determine operational capabilities of high temperature material and coating in fluorine rich and HF environments, the feasibility of a wide range throttling concept utilizing mixed phase propellants, and the feasibility of an advanced thrust chamber cooling concept.

DD FORM 1 JAN 64 1473

UNCLASSIFIED

Security Classification

| 14. KEY WORDS | LINK A | | LINK B | | LINK C | |
|---|---|---|---|---|---|---|
| | ROLE | WT | ROLE | WT | ROLE | WT |
| Maneuvering Satellite | | | | | | |
| High Energy Propellants | | | | | | |
| Materials | | | | | | |
| Coatings | | | | | | |
| Refractory Metals | | | | | | |
| Injectors | | | | | | |
| Adiabatic Thrust Chambers | | | | | | |
| Throttling Methods | | | | | | |
| Gas Generators | | | | | | |

## INSTRUCTIONS

1. ORIGINATING ACTIVITY: Enter the name and address of the contractor, subcontractor, grantee, Department of Defense activity or other organization *(corporate author)* issuing the report.

2a. REPORT SECURITY CLASSIFICATION: Enter the overall security classification of the report. Indicate whether "Restricted Data" is included. Marking is to be in accordance with appropriate security regulations.

2b. GROUP: Automatic downgrading is specified in DoD Directive 5200.10 and Armed Forces Industrial Manual. Enter the group number. Also, when applicable, show that optional markings have been used for Group 3 and Group 4 as authorized.

3. REPORT TITLE: Enter the complete report title in all capital letters. Titles in all cases should be unclassified. If a meaningful title cannot be selected without classification, show title classification in all capitals in parenthesis immediately following the title.

4. DESCRIPTIVE NOTES: If appropriate, enter the type of report, e.g., interim, progress, summary, annual, or final. Give the inclusive dates when a specific reporting period is covered.

5. AUTHOR(S): Enter the name(s) of author(s) as shown on or in the report. Enter last name, first name, middle initial. If military, show rank and branch of service. The name of the principal author is an absolute minimum requirement.

6. REPORT DATE: Enter the date of the report as day, month, year; or month, year. If more than one date appears on the report, use date of publication.

7a. TOTAL NUMBER OF PAGES: The total page count should follow normal pagination procedures, i.e., enter the number of pages containing information.

7b. NUMBER OF REFERENCES: Enter the total number of references cited in the report.

8a. CONTRACT OR GRANT NUMBER: If appropriate, enter the applicable number of the contract or grant under which the report was written.

8b, 8c, & 8d. PROJECT NUMBER: Enter the appropriate military department identification, such as project number, subproject number, system numbers, task number, etc.

9a. ORIGINATOR'S REPORT NUMBER(S): Enter the official report number by which the document will be identified and controlled by the originating activity. This number must be unique to this report.

9b. OTHER REPORT NUMBER(S): If the report has been assigned any other report numbers *(either by the originator or by the sponsor)*, also enter this number(s).

10. AVAILABILITY/LIMITATION NOTICES: Enter any limitations on further dissemination of the report, other than those imposed by security classification, using standard statements such as:

(1) "Qualified requesters may obtain copies of this report from DDC."

(2) "Foreign announcement and dissemination of this report by DDC is not authorized."

(3) "U. S. Government agencies may obtain copies of this report directly from DDC. Other qualified DDC users shall request through _____."

(4) "U. S. military agencies may obtain copies of this report directly from DDC. Other qualified users shall request through _____."

(5) "All distribution of this report is controlled. Qualified DDC users shall request through _____."

If the report has been furnished to the Office of Technical Services, Department of Commerce, for sale to the public, indicate this fact and enter the price, if known.

11. SUPPLEMENTARY NOTES: Use for additional explanatory notes.

12. SPONSORING MILITARY ACTIVITY: Enter the name of the departmental project office or laboratory sponsoring *(paying for)* the research and development. Include address.

13. ABSTRACT: Enter an abstract giving a brief and factual summary of the document indicative of the report, even though it may also appear elsewhere in the body of the technical report. If additional space is required, a continuation sheet shall be attached.

It is highly desirable that the abstract of classified reports be unclassified. Each paragraph of the abstract shall end with an indication of the military security classification of the information in the paragraph, represented as *(TS), (S), (C), or (U)*.

There is no limitation on the length of the abstract. However, the suggested length is from 150 to 225 words.

14. KEY WORDS: Key words are technically meaningful terms or short phrases that characterize a report and may be used as index entries for cataloging the report. Key words must be selected so that no security classification is required. Identifiers, such as equipment model designation, trade name, military project code name, geographic location, may be used as key words but will be followed by an indication of technical context. The assignment of links, rules, and weights is optional.